Université de Montréal

Improving the Use of G-CSF During Chemotherapy Using Physiological Mathematical Modelling: A Quantitative Systems Pharmacology Approach

par
Morgan Craig

Faculté de pharmacie

Thèse présentée à la Faculté des études supérieures
en vue de l'obtention du grade de Philosophiæ Doctor (Ph.D.)
en sciences pharmaceutiques

Décembre, 2015

© Morgan Craig, 2015.

Université de Montréal
Faculté des études supérieures

Cette thèse intitulée:

Improving the Use of G-CSF During Chemotherapy Using Physiological Mathematical Modelling: A Quantitative Systems Pharmacology Approach

présentée par:

Morgan Craig

a été évaluée par un jury composé des personnes suivantes:

Marc Servant,	président-rapporteur
Fahima Nekka,	directeur de recherche
Michael C. Mackey,	codirecteur
Leon Glass,	membre du jury
Piat van der Graaf,	examinateur externe

Thèse acceptée le: .....

Résumé

La diminution des doses administrées ou même la cessation complète d'un traitement chimiothérapeutique est souvent la conséquence de la réduction du nombre de neutrophiles, qui sont les globules blancs les plus fréquents dans le sang. Cette réduction dans le nombre absolu des neutrophiles, aussi connue sous le nom de myélosuppression, est précipitée par les effets létaux non spécifiques des médicaments anti-cancéreux, qui, parallèlement à leur effet thérapeutique, produisent aussi des effets toxiques sur les cellules saines. Dans le but d'atténuer cet impact myélosuppresseur, on administre aux patients un facteur de stimulation des colonies de granulocytes recombinant humain (rhG-CSF), une forme exogène du G-CSF, l'hormone responsable de la stimulation de la production des neutrophiles et de leurs libération dans la circulation sanguine. Bien que les bienfaits d'un traitement prophylactique avec le G-CSF pendant la chimiothérapie soient bien établis, les protocoles d'administration demeurent mal définis et sont fréquemment déterminés *ad libitum* par les cliniciens. Avec l'optique d'améliorer le dosage thérapeutique et rationaliser l'utilisation du rhG-CSF pendant le traitement chimiothérapeutique, nous avons développé un modèle physiologique du processus de granulopoïèse, qui incorpore les connaissances actuelles de pointe relatives à la production des neutrophiles des cellules souches hématopoïétiques dans la moelle osseuse. À ce modèle physiologique, nous avons intégré des modèles pharmacocinétiques/pharmacodynamiques (PK/PD) de deux médicaments : le PM00104 (Zalypsis®), un médicament anti-cancéreux, et le rhG-CSF (filgrastim). En se servant des principes fondamentaux sous-jacents à la physiologie, nous avons estimé les paramètres de manière exhaustive sans devoir recourir à l'ajustement des données, ce qui nous a permis de prédire des données cliniques provenant de 172 patients soumis au protocol CHOP14 (6 cycles de chimiothérapie avec une période de 14 jours où l'administration du rhG-CSF se fait du jour 4 au jour 13 post-chimiothérapie). En utilisant ce modèle physio-PK/PD, nous avons démontré que le nombre d'administrations du rhG-CSF pourrait être réduit de dix (pratique actuelle) à quatre ou même trois administrations, à condition de retarder le début du traitement prophylactique par le rhG-CSF. Dans un souci d'applicabilité clinique de notre approche de modélisation, nous avons investigué l'impact de la variabilité PK présente dans une population de patients, sur les prédictions

du modèle, en intégrant des modèles PK de population (Pop-PK) des deux médicaments. En considérant des cohortes de 500 patients *in silico* pour chacun des cinq scénarios de variabilité plausibles et en utilisant trois marqueurs cliniques, soient le temps au nadir des neutrophiles, la valeur du nadir, ainsi que l'aire sous la courbe concentration-effet, nous avons établi qu'il n'y avait aucune différence significative dans les prédictions du modèle entre le patient-type et la population. Ceci démontre la robustesse de l'approche que nous avons développée et qui s'apparente à une approche de pharmacologie quantitative des systèmes (QSP).

Motivés par l'utilisation du rhG-CSF dans le traitement d'autres maladies, comme des pathologies périodiques telles que la neutropénie cyclique, nous avons ensuite soumis l'étude du modèle au contexte des maladies dynamiques. En mettant en évidence la non validité du paradigme de la rétroaction des cytokines pour l'administration exogène des mimétiques du G-CSF, nous avons développé un modèle physiologique PK/PD novateur comprenant les concentrations libres et liées du G-CSF. Ce nouveau modèle PK a aussi nécessité des changements dans le modèle PD puisqu'il nous a permis de retracer les concentrations du G-CSF lié aux neutrophiles. Nous avons démontré que l'hypothèse sous-jacente de l'équilibre entre la concentration libre et liée, selon la loi d'action de masse, n'est plus valide pour le G-CSF aux concentrations endogènes et mènerait en fait à la surestimation de la clairance rénale du médicament. En procédant ainsi, nous avons réussi à reproduire des données cliniques obtenues dans diverses conditions (l'administration exogène du G-CSF, l'administration du PM00104, CHOP14). Nous avons aussi fourni une explication logique des mécanismes responsables de la réponse physiologique aux deux médicaments.

Finalement, afin de mettre en exergue l'approche intégrative en pharmacologie adoptée dans cette thèse, nous avons démontré sa valeur inestimable pour la mise en lumière et la reconstruction des systèmes vivants complexes, en faisant le parallèle avec d'autres disciplines scientifiques telles que la paléontologie et la forensique, où une approche semblable a largement fait ses preuves. Nous avons aussi discuté du potentiel de la pharmacologie quantitative des systèmes appliquées au développement du médicament et à la médecine translationnelle, en se servant du modèle physio-PK/PD que nous avons mis au point.

Mots clés: pharmacologie des systèmes, granulopoïèse, modélisation méchanistique, pharmacocinétiques/pharmacodynamiques physiologiques, biologie des systèmes.

Abstract

Dose-limitation or interruption of chemotherapeutic treatment is most often prompted by a decrease in circulating neutrophils, the most abundant white blood cell in the human body. Myelosuppression, or a reduction in absolute neutrophil counts (ANCs) by anti-cancer treatments, is precipitated by the nonspecific killing effect of chemotherapeutic drugs which have toxic effects on noncancerous cells. To mitigate this myelosuppressive effect, patients are frequently administered recombinant human granulocyte colony-stimulating factor (rhG-CSF), an exogenous form of the cytokine G-CSF, which stimulates neutrophil production and release into the blood stream. While the benefits of adjuvant treatment rhG-CSF during chemotherapy are well recognised, the protocols with which it is administered are not well defined and are frequently determined *ad libitum* by clinicians. To quantify and address the optimisation of the administration of rhG-CSF during chemotherapeutic treatment, we developed a physiological model of granulopoiesis which incorporates the contemporary understanding of the production of neutrophils from the hematopoietic stem cells in the bone marrow. To this physiological model, we incorporated mechanistic pharmacokinetic/pharmacodynamic (PK/PD) models of two drugs, PM00104 (Zalypsis®), a chemotherapeutic drug, and rhG-CSF (filgrastim). Through exhaustive parameter estimation using first principles and no data fitting, we successfully predicted clinical data from 172 patients for an average patient undergoing the CHOP14 protocol (6 cycles of 14-day periodic chemotherapy with rhG-CSF administered on days 4-13 post-chemotherapy). We then demonstrated that delaying the administration of rhG-CSF to 6 or 7 days post-chemotherapy allowed for a reduction in the number of filgrastim administrations from ten to four or even three while maintaining or improving the neutrophil nadir. We also investigated the effects of PK variability on the model's predictions by incorporating population PK (PopPK) models of both drugs. Using five different variability scenarios and cohorts of 500 *in silico* patients per scenario, we established that there are no statistically significant differences between a typical patient and the population in the model's predictions with respect to three crucial clinical endpoints, namely the time to ANC nadir, the ANC nadir, and the area under the concentration-effect curve. The model's robustness to PK variability allows for the scaling up from the individual to

population level.

Motivated by the use of rhG-CSF in other disease-states, namely periodic pathologies like cyclical neutropenia, we next endeavoured to contextualise the model within dynamic diseases. By bringing to light that the cytokine paradigm is broken when exogenous cytokine mimetics are administered, we developed a novel physiological PK model for G-CSF incorporating both unbound and bound concentrations. The updated PK model prompted changes to the PD model since we could now track the concentrations of bound G-CSF. We showed that the mass-action equilibrium hypopthesis for bound and unbound drugs is not valid and led to overestimations of the renal clearance of G-CSF. We also successfully reproduced clinical data in a variety of settings (exogenous G-CSF alone, PM00104 alone, CHOP14 protocol) and clarified the mechanisms underlying the body's response to both drugs. Lastly, we discussed the potential of quantitative systems pharmacology in both drug development and translational medicine by using the physiological PK/PD model we developed.

Keywords: quantitative systems pharmacology, granulopoiesis, mechanistic modelling, physiologic pharmacokinetics/pharmacodynamics, systems biology.

Contents

List of Tables

List of Figures

List of Appendices

List of Abbreviations

Abbreviation	Description
ABM	Agent-based model
AIDS	Acquired immunodeficiency syndrome
ALB	Albumin
ANC	Absolute neutrophil count
ARV	Antiretroviral treatments
ASCO	American Society of Clinical Oncology
AUC	Area under the curve
AUEC	Area under the effect curve
B	B-cell
BILI	Bilirubin
BMP-4	Bone morphogenetic protein 4
C/EBPα	CCAAT/enhancer-binding protein, alpha
C/EBPε	CCAAT-enhancer-binding proteins, epsilon
CCS	Canadian Cancer Society
CGP	Circulating granulocyte pool
CHOP	Chemotherapy regimen which includes Cyclophosphamide, Hydroxydaunorubicin, Oncovin and Prednisone/Prednisolone
CI	Confidence interval
CL	Clearance
CLP	Common lymphoid progenitor
CMP	Common myeloid progenitor
CN	Cyclical neutropenia
CRU	Competitive repopulating unit
DDE	Delay differential equation
DNA	Deoxyribonucleic acid
E.coli	*Escherichia coli*
ELANE	Neutrophil elastase gene

Abbreviation	Description
EORTC	European Organisation for Research and Treatment of Cancer
Eos	Eosinophil
EP	Erythroid progenitor
FDA	Food and Drug Administration
FN	Febrile neutropenia
G-CSF	Granulocyte colony-stimulating factor
G-CSFR	Granulocyte colony-stimulating factor receptor
GFI-1	Growth factor independent 1 transcription repressor
GM-CSF	Granulocyte-macrophage colony-stimulating factor
GMP	Granulocyte-macrophage progenitor
H_0	Null hypothesis
HIV	Human immunodeficiency virus
HoxB4	Homeobox protein B
HSC	Hematopoietic stem cell
IIV	Interindividual variability
IL	Interleukin
IOV	Interoccasion variability
kDa	Kilodaltons
LTRC	Long-term repopulating cell
MC	Monocyte
MEM	Mixed-effects model
MEP	Megakaryocyte erythroid progenitor
MKP	Megakaryocyte progenitor
MNP	Marginated neutrophil pool
MPP	Multipotent progenitor
MTT	Mean transit time
Nad	ANC nadir
NCA	Non-compartmental analysis
NCCN	National Comprehensive Cancer Network

Abbreviation	Description
Neu	Neutrophil
NIH	National Institutes of Health
NK	Natural killer cell
NSERC	Natural Sciences and Engineering Research Council
ODE	Ordinary differential equation
PBPC	Peripheral blood progenitor cells
PBPK	Physiologically-based pharmacokinetics
PDE	Partial differential equation
PK/PD	Pharmacokinetics/pharmacodynamics
PKPD	Pharmacokinetics/pharmacodynamics
PLT	Platelet
PopPK/PD	Population pharmacokinetics/pharmacodynamics
QSP	Quantitative systems pharmacology
RBC	Red blood cell/erythroid
rh	Recombinant human
RV	Random variable
SCN	Severe congenital neutropenia
T	T-cell
TBGP	Total blood granulocyte pool
TGF	Transforming (tumour) growth factor
TMDD	Target-mediated drug disposition
TNad	Time to ANC nadir
TNF	Tumour necrosis factor
Vd	Volume of distribution
WBC	White blood cell

Notation

Notation	Interpretation	Units
	Chapter 1	
C_{ave}	Average concentration etoposide	–
C_{24}	Etoposide concentration after 24 hours	–
R_1	Infusion rate before 28 hours	–
R_2	Infusion rate after 28 hours	–
$C_{e\,f\,f}$	Effective concentration	–
$E(t)$	Concentration-effect relationship	–
$WBC(t)$	WBC count over time	–
$Baseline$	Baseline WBC count	–
E_{dir}	Direct effect	–
E_{obs}	Observed effect	–
C	Drug concentration	–
γ_1	Hill coefficient	–
C_{50}	Half-maximal concentration	–
$AUCE_{dir}$	Area under the concentration-effect curve	–
$E_{dir\,max}$	Scaling factor	–
WBC_{pred}	Predicted WBC count	–
E_{max}	Maximal effect	–
P	Proliferating neutrophils	–
T_i	Transit compartment i	–
N	Circulating neutrophils	–
N_0	Baseline neutrophil count	–
γ	Hill coefficient	–
k_{tr}	Transit rate	–
k_{prol}	Rate of proliferation	–
k_{circ}	Rate of circulation	–
C_p	Plasma concentration of drug	–
DR	Concentration of drug-receptor complex	–

Abbreviation	Interpretation	Units
D_T	Tissue concentration	–
R_{max}	Total density of surface receptors	–
V_c	Volume of central compartment	–
k_{on}	Rate of receptor binding	–
k_{off}	Rate of receptor unbinding	–
k_m	Rate of internalisation	–
k_{syn}	Rate of synthesis	–
k_{deg}	Degradation rate	–
	Chapters 2 and 3	
Q^{homeo}	Concentration of HSCs at homeostasis	10^6 cells/kg
γ_S	HSC rate of apoptosis	days^{-1}
τ_S	Time for HSC re-entry	days
A_Q^{homeo}	HSC amplification at homeostasis	
κ_δ	HSC differentiation rate into other lineages	days^{-1}
β_Q^{homeo}	HSC rate of re-entry	days^{-1}
f_Q	Maximal HSC re-entry rate	days^{-1}
s_2	HSC re-entry Hill coefficient	
θ_2	Half-maximal HSC concentration	10^6 cells/kg
N_r^{homeo}	Homeostasis concentration of reservoir	10^9 cells/kg
N^{homeo}	Homeostatic concentration of TBNP	10^9 cells/kg
N_{circ}^{homeo}	Homeostatic concentration of circulating neutrophils	10^9 cells/kg
γ_N	Circulating neutrophil rate of removal	days^{-1}
τ_{NP}	Time for neutrophil proliferation	days
a_{NM}	Time for neutrophil maturation at homeostasis	days
τ_{Nr}	Time spent in marrow reserve	days
γ_{Nr}	Rate of removal from marrow reserve	days^{-1}
γ_{NM}	Rate of removal during maturation phase	days^{-1}
$\kappa_N(N^{homeo})$	HSC differentiation rate into neutrophil line	days^{-1}

Abbreviation	Interpretation	Units
A_N^{homeo}	Neutrophil amplification at homeostasis	
η_{NP}^{homeo}	Neutrophil proliferation rate	days^{-1}
f_N	Maximal rate of neutrophil differentiation	days^{-1}
s_1	Neutrophil differentiation Hill coefficient	
θ_1	Half maximal conc. neutrophil differentiation	$10^9\,\text{cells/kg}$
f_{trans}^{homeo}	Homeostatic rate of transit from marrow reserve	days^{-1}
k_{el_C}	Zalypsis®rate of elimination	days^{-1}
k_{12}	Rate of exchange	days^{-1}
k_{21}	Rate of exchange	days^{-1}
k_{13}	Rate of exchange	days^{-1}
k_{31}	Rate of exchange	days^{-1}
k_{24}	Rate of exchange	days^{-1}
k_{42}	Rate of exchange	days^{-1}
BSA	Average body surface area	m^2
G^{homeo}	G-CSF concentration at homeostasis	ng/mL
G_{prod}	Rate of G-CSF production	ng/mL/days
k_{ren}	Rate of G-CSF renal elimination	days^{-1}
χ	Normalisation factor	$\frac{\text{ng/mL}}{10^9\text{cells/kg}}$
k_{int}	G-CSF receptor-internalisation rate	days^{-1}
k_D	G-CSF dissociation constant	ng/mL
k_a	Subcutaneous filgrastim absorption rate	days^{-1}
F	Filgrastim bioavailable fraction	
V_d	Volume of distribution (filgrastim)	mL
γ_S^{homeo}	HSC apoptotic homeostatic rate	days^{-1}
γ_S^{min}	Minimal HSC apoptotic rate	days^{-1}
γ_S^{max}	Maximal HSC apoptotic rate	days^{-1}
h_S	Effect of chemotherapy on HSC apoptosis	
b_S	HSC apoptosis Michaelis-Menten parameter	ng/mL
h	Hill coefficient for Zalypsis®effect on proliferation	

Abbreviation	Interpretation	Units
EC_{50}	Zalypsis®half-concentration on proliferation	ng/mL
η_{NP}^{max}	Maximal rate of proliferation	days^{-1}
η_{NP}^{min}	Minimal rate of proliferation	days^{-1}
V_{max}	Maximal maturation velocity	
γ_{NM}^{min}	Minimal apoptosis rate out of maturing phase	days^{-1}
γ_{NM}^{max}	Minimal apoptosis rate out of maturing phase	days^{-1}
$trans^{max}$	Maximal rate of transfer from marrow reserve	days^{-1}
b_V	Michaelis-Menten parameter (maturation speed)	ng/mL
b_{NP}	Michaelis-Menten parameter (proliferation)	ng/mL
b_{NM}	Michaelis-Menten parameter (maturation)	ng/mL
b_G	Michaelis-Menten parameter (transit from pool)	ng/mL
Cl	PM001014 Clearance	L/hr
V_1	PM001014 Volume of central compartment	L
Q_2	PM001014 Transit rate (compartments 1 and 2)	L
V_2	PM001014 Volume of second compartment	L/hr
Q_3	PM001014 Transit rate (compartments 1 and 3)	L/hr
V_3	PM001014 Volume of third compartment	L
Q_4	PM001014 Transit rate (compartments 2 and 4)	L/hr
V_4	PM001014 Volume of fourth compartment	L
k_{el}	Rate of renal elimination filgrastim (Krzyzanski)	hr^{-1}
V_d	Volume of distribution filgrastim (Krzyzanski)	L
ξ	GCSFR concentration per neutrophil (Krzyzanski)	fg/cell
NB_0	Initial number of blood neutrophils (Krzyzanski)	cells/μL
SC_{50}	Concentration eliciting 50% of the maximal effect	ng/mL
S_{max_1}	Maximum effect (Krzyzanski)	
$P_{j,k}$	Individual jth PK parameter for the kth occasion	
η_j	IIV random variable	
τ_j	IOV random variable	
TNad$_{ref}$	Reference time to nadir	days

Abbreviation	Interpretation	Units
TNad_{test}	Test time to nadir	days
Nad_{ref}	Reference nadir value	10^9 cells/kg
Nad_{test}	Test nadir value	10^9 cells/kg
AUCE_{ref}	Reference AUCE value	$10^9 \frac{\text{days cells}}{\text{kg}}$
	Chapter 4	
γ_Q	HSC apoptosis rate	days^{-1}
τ_Q	Time for HSC re-entry	days
A_Q	HSC Amplification Factor	–
f_Q	Maximal HSC re-entry rate	days^{-1}
s_2	HSC re-entry Hill coefficient	–
θ_2	Half-effect HSC concentration	10^6 cells/kg
κ_δ	HSC differentiation rate to other lines	days^{-1}
κ^{min}	HSC-neutrophil minimal differentiation rate	days^{-1}
κ^*	HSC-neutrophil homeo differentiation rate	days^{-1}
G_2^*	Bound G-CSF concentration	ng/mL
s_1	HSC-neutrophil differentiation Hill coefficient	–
$\eta_{N_P}^*$	Neutrophil homeostasis effective proliferation rate	days^{-1}
b_{N_P}	Neutrophil proliferation M-M constant	ng/mL
$\eta_{N_P}^{min}$	Neutrophil minimal proliferation rate	days^{-1}
τ_{N_P}	Neutrophil proliferation time	days
V_{max}	Maximal neutrophil maturation velocity	–
b_V	Maturation velocity half-effect concentration	ng/mL
a_{N_M}	Homeostasis neutrophil maturation time	days
γ_{N_M}	Neutrophil death rate in maturation	days^{-1}
$\varphi_{N_R}^*$	Homeostasis Reservoir Release rate	days^{-1}
$\varphi_{N_R}^{max}$	Maximal Reservoir Release rate	days^{-1}
b_G	Reservoir Release half-effect concentration	ng/mL
γ_{N_R}	Neutrophil death rate in reservoir	days^{-1}

Abbreviation	Interpretation	Units
γ_N	Neutrophil Removal Rate from Circulation	days^{-1}
G_{prod}	Endogenous G-CSF production rate	ng/mL/day
V	Bound G-CSF conversion factor	$\frac{\text{ng/mL}}{10^9\text{cells/kg}}$
k_{ren}	G-CSF renal elimination rate	days^{-1}
k_{int}	G-CSF effective internalisation rate	days^{-1}
k_{12}	Unbound to bound G-CSF compartment	$\frac{\text{days}^{-1}}{\text{ng/mL}^{Pow}}$
k_{21}	Bound to unbound G-CSF compartment	$\frac{\text{days}^{-1}}{\text{ng/mL}^{Pow}}$
Pow	Effective G-CSF binding coefficient	
$\varphi_{N_R}^{ratio}$	$\varphi_{N_R}^{max}/\varphi_{N_R}^{*}$	
G_1^*	Free G-CSF	ng/mL
$G_{dat}^{SC}(t)$	Data SC G-CSF function	ng/mL
$G_{dat}^{IV}(t)$	Data IV G-CSF function	ng/mL
$G_1^{SC}(t)$	Simulated SC G-CSF function	ng/mL
$G_1^{IV}(t)$	Simulated IV G-CSF function	ng/mL
$\chi^{0.95}$	Scaling factor	
$N_{dat}^{375}(t)$	Data 375 μg neutrophil function	10^9cells/kg
$N_{dat}^{750}(t)$	Data 750 μg neutrophil function	10^9cells/kg
$N^{375}(t)$	Simulated 375 μg neutrophil function	10^9cells/kg
$N^{750}(t)$	Simulated 750 μg neutrophil function	10^9cells/kg
$N_{dat}^{ch_j}(t)$	Data neutrophil function for chemo subject j	10^9cells/kg
$N^{ch_j}(t)$	Simulated neutrophil function for chemo subject j	10^9cells/kg
Q^*	HSC homeostasis concentration	10^6cells/kg
$\beta(Q^*)$	HSC re-entry rate	days^{-1}
N^*	Homeostasis Total Blood Neutrophil Pool	10^9cells/kg
N_R^*	Homeostasis Neutrophil Reservoir Concentration	10^9cells/kg
N_P^*	Homeostasis Neutrophil Proliferation Concentration	10^9cells/kg
N_M^*	Homeostasis Neutrophil Maturation Concentration	10^9cells/kg
G_2^*	Homeostasis bound G-CSF concentration	ng/mL
$\tau_{N_R}^*$	Homoeostasis Neutrophil mean time in reservoir	days

Abbreviation	Interpretation	Units
$\tau^*_{N_C}$	Homoeostasis Neutrophil mean time in circulation	days
$\tau_{1/2}$	Circulating Neutrophil half-removal time	hours
A^*_N	Homeostasis neutrophil proliferation+maturation amplification	–
$\tilde{b}_V$	Scaled maturation half-effect concentration	ng/mL
$\varphi^{ratio}_{N_R}$	Ratio of maximal and homeostasis reservoir release rates	–
$\varphi_{N_R}(0)$	Minimal reservoir release rate	days^{-1}
θ	Ratio of rate cells leave proliferation at knockout to homeostasis	–
C_{ko}	Knockout total blood neutrophil pool fraction	–
μ	Ratio of minimal and homeostasis proliferation rates	–
V_d	Volume of distribution	mL
F	Bioavailable fraction	–
k_a	Subcutaneous rate of absorption	days^{-1}
k_{fp}	Rate of exchange from compartment f to p	days^{-1}
k_{sl_1p}	Rate of exchange from compartment sl_1 to p	days^{-1}
k_{pf}	Rate of exchange from compartment p to f	days^{-1}
k_{psl_1}	Rate of exchange from compartment p to sl_1	days^{-1}
k_{el_C}	Rate of elimination	days^{-1}
k_{sl_2f}	Rate of exchange from compartment sl_2 to f	days^{-1}
k_{fsl_2}	Rate of exchange from compartment f to sl_2	days^{-1}
BSA	Body surface area	m^2
h_Q	Effect of chemotherapy on $Q(t)$	–
EC_{50}	Half-maximal effect of chemotherapy on η_{N_P}	–
s_c	Chemotherapy effect Hill coefficient	–
$\eta^{inf}_{N_P}$	Rate of proliferation with an infinite chemotherapy dose	days^{-1}

To all of my family and friends who have contributed in no small way to where I am now, and especially for Gramma and Baba.

Acknowledgments

I want to begin by thanking my co-directors, Dr Fahima Nekka and Dr Michael Mackey, for their encouragement and support during my doctoral studies. I have been enormously lucky to work closely with both Fahima and Michael. Their input has always guided me and my research and their personal dedication to me as a student and a person has and will always be very much appreciated. I look forward to many more fruitful collaborations together.

I am grateful to the members of my thesis jury for all of their comments and questions after reading my dissertation and at my defence. I have an immense amount of respect for all of their work, so I am particularly touched by their reflections. Thank you to Dr Piet van der Graaf, Dr Leon Glass, Dr Marc Servant, and Dr Yan Burrell.

I am fortunate enough to have collaborated with exceptional researchers who have also been influential to my doctoral path. Thank you very much to Dr Tony Humphries for all of our discussions and for his guidance, which amounted to having a third co-director who helped at each step of the way. Thank you to Dr Jacques Bélair for his assistance in not only my research work, but also in my teaching experiences at l'Université de Montréal.

I would like to thank Dr Jun Li for all of his helpful suggestions and comments, and for all of our interesting conversations and debates. Thank you also to Dr Mario González-Sales for sharing his ideas with me and for our collaborations, and to Dr Joe Mahaffy for our ongoing collaborations together. I am grateful for the advice and guidance of Dr Nathalie Letarte and Dr David Dale who both provided very valuable insight about clinical issues related to my work. I am also very thankful to have worked with Dr Stéphanie Portet during my masters and to have her and Dr Jullien Arino's continued guidance during my PhD.

Thank you to my colleagues at l'Université de Montréal–Olivier, Leila, Sarem, Guillaume, Xiao, Steven, Abbass, Sara–and at McGill University–Grace, Gabriel, Tyler, Daniel–for all of our time spent together working (and sometimes not working as much). I've really enjoyed sharing this time with you all.

I'm particularly indebted to all of the UdeM staff at the Faculté de pharmacie and at la FESP for their support.

Of course, I owe so many thanks to my friends and family (and family who are friends and friends who are family) for every piece of advice, love, kindness, and support during my (long) time as a university student. My thesis is undoubtedly better because I had an outlet of support from them. To Rachel, Jenna, Haley, Braydon, Cam, Ty, Shoni, Sean, Stacey, Mike, Jenn, Krysta, Flo, Rebecca, Sumeep, Shannon, Leanne, Josh, Dave Paton, Laurena, Sylvie, Justin, Kameron, Jeff, Gwen, Ginny, Genna, Roberta, and Dave Landreth for every message, visit, and call. To all of the kids you guys have made who are cool people we get to visit. And to my family, near and far: Auntie Rhonda and Jayne, Uncle Paul and Carole, Deanna, Vanessa, and Ellis (for being here for my defence and also for hosting us on so many occasions in Toronto–having cousin friends is the best!), Sera, Shumit, Phoenix, and Cassis, Auntie Andrea and Uncle Brian, Josh and Kate, Auntie Donna and Uncle Tony, Jeni, Blake, Grant (and one who we haven't met yet), Nick, Sid, and Eddy, Kirby, Cory (and Charlie!), and Auntie Barbie (for being like my other mom)–thank you for loving me my whole life and helping me get here. Thanks to our close family friends the Burketts (Gary, Cindy, Kyle, Kira, Brittany, and Darcy), les Collette (Pauline et Denis), Gio, the Carberrys (Uncle Tom, Auntie Fran, Jamie, Katie, Patrick, and Quinn) and the Loewens (Peter, Paulette, Alex, and Andrew).

I'm very fortunate to have a wonderful family of (common) in-laws who have welcomed me into their gigantic family. Thanks to Hannah and Tom, Isaac and Jana, Joel and Bobbi, Josiah and Quelly, Gersh and Kat, Levi and Cassandra, and our gaggle of nieces and nephews. Lots of love to Judie and Bob for their continued love and support.

None of my accomplishments would be possible without my parents, Richard and Pam, and my sister and brother in-law, Ashleigh and Isaac. And of course our precious nephews Noah, Xavier, and Sebastian. They gave me room to grow into whatever interested me and they allowed me to be whatever and whoever I wanted to be (within reason...) and I can never show them enough appreciation. I love our overly cautious and hilarious family.

To my grandparents who are no longer with us, and especially for my Margaret who passed away during my PhD. I miss you very much and am glad I got to be your granddaughter.

Lastly, thank you to Jesse, the man I am so lucky to spend my life with. I can't say enough nice things about how I feel about you. Thanks for always sticking up for me and

for helping me with whatever (this thesis, my PhD, grabbing things from high shelves, bike repairs, and so much more). I look forward to many, many more adventures together.

Preface

This dissertation deals with the optimisation of the use of a cytokine which stimulates certain white blood cells after anti-cancer treatment. The motivation for this work was three-fold: from a clinical standpoint, the *ad libitum* administration of the exogenous form of this cytokine did not serve patients in the best way possible. Pharmacologically speaking, the concurrent administration of drugs presents an interesting yet complex opportunity to understand drug-drug interactions. Finally, in terms of systems biology, mathematical modellers have long been intrigued by the dynamics of the blood system and the complexity of related structures. Bridging these three major perspectives required a wholly interdisciplinary approach and has motivated several important ancillary studies.

In what follows, I will begin by situating the biological foundations of the blood and neutrophil system, including the cytokine of interest and its clinical use to treat neutrophil pathologies. Next, I will situate the continuously evolving pharmacometrics field by anchoring its history to the background of models for neutrophil development.

The publications are presented in the following order:

— Craig M, Humphries AR, Bélair J, Li J, Nekka F, Mackey MC. Neutrophil dynamics during concurrent chemotherapy and G-CSF administration: Mathematical modelling guides dose optimisation to minimise neutropenia. *Journal of Theoretical Biology, 385*, 77–89 (2015).

— Craig M, González-Sales M, Li J, Nekka F. Impact of Pharmacokinetic Variability on a Mechanistic Physiological Pharmacokinetic/Pharmacodynamic Model: A Case Study of Neutrophil Development, PM00104, and Filgrastim. In *Interdisciplinary Mathematical Research and Applications* (ed. B. Toni). Springer, New York. In press.

— Craig, M., Humphries, A.R., Mackey, M.C. A mathematical model of granulopoiesis incorporating the negative feedback dynamics and kinetics of G-CSF/neutrophil binding and internalisation. Under review (submitted to the *Bulletin of Mathemat-*

ical Biology December 21, 2015).

— Craig, M., González-Sales, M., Li, J., Nekka, F. Approaching pharmacometrics as a palaeontologist would: Recovering the links between drugs and the body through reconstruction. *CPT: Pharmacometrics and Systems Pharmacology*. In press.

Chapter 1

Introduction

1.1 Neutrophil Bone Marrow Development from the Hematopoietic Stem Cells

This section provides an overview of the development of circulating neutrophils to the total blood neutrophil pool from the hematopoietic stem cells. The focus is primarily systems level physiology, although certain signalling mechanisms and fundamentals will be discussed.

1.1.1 Hematopoietic Stem Cells: Pluripotent Regulators of Hematopoiesis

History is littered with coincidental and peculiar developments. While the first portion of the last century saw a nuclear arms race take hold, the focus on building atomic weapons led to several important scientific advances, extending even to the life sciences. One such breakthrough is the identification of cells capable of clonal repopulation [28]. Stem cells were first discovered by Till and McCulloch [128] after injecting bone marrow into mice spleens and observing clonal nodules in the excised organs. This pioneering work led to many subsequent discoveries on the physiology of these pluripotent cells and the identification of the various stem cell types. One such variety are those which generate the cells in the blood. Hematopoietic stem cells (HSCs) give rise to cells of all blood cell lineages and regulate hematopoiesis (the production of blood cells). HSCs produce about ten times human body weight in blood cells per lifetime [81] yet they comprise just 0.01-0.2% of the total bone marrow mononuclear cells in human beings [96]. The current understanding of the production of these hematopoietic cells is highlighted in Figure 1.1, although it should be noted that there exists several proposed models of hematopoiesis. Much remains unknown about the mechanisms instructing lineage potential [28] and the current paradigm of lineage determination has recently been called into question [95]. The HSC population is fairly stable and rarely divides [102], which is likely an evolutionary mechanism

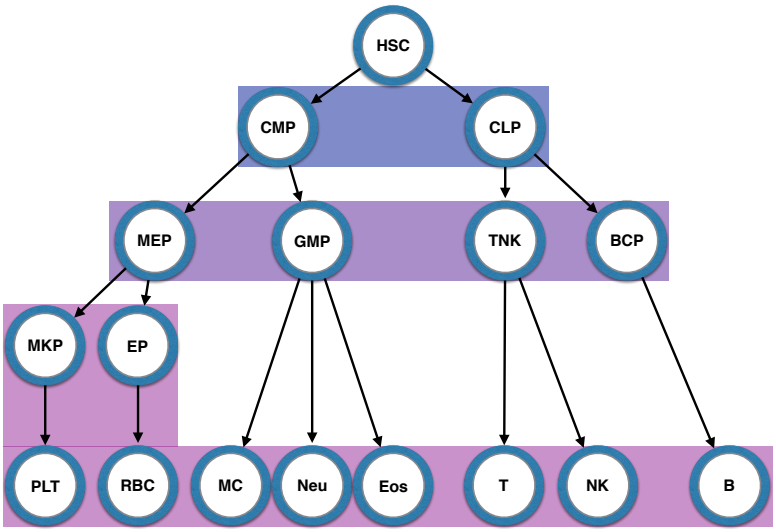

Figure 1.1 – In this classical model, the pluripotent hematopoietic stem cells give rise to the multitude of blood cells by first dividing into one of either of the primitive progenitor cells (common myeloid progenitors or common lymphoid progenitors). These primitive progenitor cells further differentiate into committed precursor cells (megakaryocyte erythroid progenitors, granulocyte-macrophage progenitors, T-cell natural killer cell progenitors, and B-cell progenitors), each of which further differentiate into the lineage committed cells (megakaryocyte progenitors and platelets, erythroid progenitors and red blood cells/erythroids, monocytes, neutrophils, and eosinophils, T-cells, natural killer cells, and B-cells). HSC: hematopoietic stem cell; CMP: common myeloid progenitor; CLP: common lymphoid progenitor; MEP: megakaryocyte erythroid progenitor; GMP: granulocyte-macrophage progenitor; TNK: T-cell natural killer cell progenitor; BCP: B-cell progenitor; MKP: megakaryocyte progenitor; EP: erythroid progenitor; PLT: platelet; RBC: red blood cell/erythroid; MC: monocyte; Neu: neutrophil; Eos: eosinophil; T: T-cell; NK: natural killer cell; B: B-cell. Background colours indicate the level of differentiation. Blue: primitive progenitor cells; purple: committed precursor cells; pink: lineage committed cells. Schematic adapted from [103].

as instabilities in the HSC population can lead to a variety of hematopoietic pathologies, including the class of cyclical blood disorders [16, 21, 35]. Recent studies [27, 28, 95, 102] have put forward different mechanisms for the division of HSCs and the maintenance of their populations which include the classical model and the model of asymmetrical division. In the classical model, hierarchical differentiation leads to lineage commitment of multipotent progenitors (MPPs) that will become mature, circulating blood cells. This classical model, first constructed using the blood system as a basis, has subsequently been proposed as a model for the structure of other stem cell populations [141]. Others maintain

that the HSCs are capable of asymmetrical division where, after division, one daughter cell remains an HSC while the other is committed to one of the hematopoietic lineages [102]. This self-renewal process would maintain a near constant HSC population and would account for the apparent robustness of HSC numbers. Further propositions include the idea that there are two reservoirs of HSCs: dormant and homeostatic [27]. In this hypothesis, the homeostatic HSCs divide about once a month and maintain the homeostatic concentrations of blood cells whereas the dormant population (which divide once every 145 days or so) would be called upon in times of emergency or stress. Durand and Charbord [27] posit, contrary to the asymmetrical model of HSC division, that homeostatic HSCs likely perform symmetric division but their fate is primarily determined asymmetrically.

The differing opinions on various aspect of HSC physiology are directly attributable to the difficulty we have in studying them. The direct identification of an HSC is complicated. Consequently, indirect measures are instead employed [81]. The identification and purification of HSCs relies on the up- or down-regulation of the expression of certain proteins on the cell's surface. HSCs belong to the class of long-term repopulating cells (LTRCs) and can therefore be detected in assays for LTRCs [28]. Two main methods are employed for this identification: the competitive repopulating unit (CRU) assay, which is employed *in vivo*, and the *in vitro* long-term culture-initiating cell or cobblestone area-forming cell assay. In the former case, cells from another source are supplied and CRU frequencies are measured after transplantation. In the latter method, adult bone marrow cells are cultured in presence of steroids and are then quantified using limited dilution assays [28].

Although much remains unsettled in terms of HSC biology and physiology, what we do understand has led to extraordinary advances in both basic science and medicine. HSCs have an undeniable potential given their importance in transplantations, hematological disorders, and gene therapy [81]. More broadly, the entire hematopoietic system is ideally situated for study by mathematical modelling not only because of what remains to be discovered about the HSC population and cellular particularities, but also as a result of the system in which they operate: a refined complex regulated by a variety of cytokines (cell signalling proteins) which work to maintain blood health for a lifetime. Next, we focus one important hematopoietic lineage predominately regulated by one particular cytokine.

1.1.2 Neutrophil Development and Biology

After commitment into the myeloid lineage, HSCs begin the process of becoming one of a number of terminally differentiated cells. One such blood cell is a neutrophil, the most abundant white blood cell in the body [134]. The neutrophils are implicated as first-line defenders in immune response and are therefore crucial to mammalian health. The development of neutrophils occurs only in the bone marrow, where they proliferate and mature in a process known as granulopoiesis [15]. As previously mentioned, the differentiation of HSCs into the various hematopoietic lineages is not fully elucidated. It is currently hypothesised that various signals, including HoxB4, Ikaros, the activated nuclear form of Notch1, cell cycle inhibitor P21, TGF/BMP-4 family members, TNFalpha receptor P55 signalling [144], PU.1, CCAAT enhancer binding protein (C/EBP)α, C/EBPε, and GFI-1 [15] all play a role in HSC self-regulation, while the various colony-stimulating factors (CSFs) and interleukins (ILs) mediate and instruct lineage commitment [144]. There is also likely a stochastic element to the differentiation of HSCs [122].

In the current understanding of hematopoietic blood cell production, HSCs initially differentiate into multipotent progenitors (MPPs) before branching off into two distinct progenitor types: common myeloid progenitors (CMPs) and common lymphoid progenitors (CLPs). The CLPs eventually lead to lymphoid cells that are primarily constituted by B-cells and T-cells, but also contain natural killer cells. CMPs will eventually form platelets, red blood cells, neutrophils, monocytes, eosinophils, basophils, and mast cells. Dendritic cells have origins in both the CMPs and the CLPs [60]. The formation of neutrophils from the CMP niche involves several transitional steps. First, CMPs differentiate into myeloblasts which are the common progenitor of all granulocytes (basophils, eosinophils, and neutrophils) and monocytes. The next transition involves the terminal differentiation into the neutrophil lineage. Myeloblasts become promyelocytes, myelocytes, metamyelocytes, and band neutrophils before they proliferate and mature into neutrophils (see Figure 1.1 in [78] and Figure 2 in [76]) [123]. These mature neutrophils are initially stored in the bone marrow prior to their release into the circulation [101].

Circulating neutrophils have a short half-life of approximately 7-10 hours [134] before their disappearance from the blood. A confounding factor in the reporting of neutrophil half-life is the significance of the marginated neutrophil pool (MNP). Athens [3], studying

70 male subjects from the Utah State Prison, reported the total blood granulocyte pool (TBGP) to have a mean of 65×10^7 cells/kg, while the circulating granulocyte pool (CGP) had a mean of 31.7×10^7 cells/kg, leaving a marginal granulocyte pool of 33.3×10^7 cells/kg. The MNP exists in several tissues and organs in addition to the capillaries. During neutrophil reinfusion, one-third of reintroduced cells were found in the liver and the bone marrow while approximately 15% migrated to the spleen. It is further known that the lungs harbour a significant amount of the TBNP. Higher rates of neutrophil margination in different ethnicities may explain why some ethnicities and races exhibit curiously low neutrophil counts while demonstrating no ill effects for the individual [134]. Further, the division between the circulating and marginated pools is in constant flux. Exercise and the release/administration of adrenaline tends to shift the size of the MGP to the CGP, which is likely a protective measure [3]. The transfer of neutrophils from the blood to the tissues/marginated pool is mediated by both integrins (receptors responsible for the cross-talk between cells and a cell to the extra cellular matrix) and selectins (cell adhesion molecules) [134].

After margination, neutrophil clearance is carried out by both the spleen and the liver, though some suggest that neutrophils which have trafficked back into bone marrow may be cleared from there [77, 101, 108, 127]. More recently, researchers have observed that there are very few neutrophils which complete this migration back into the marrow. However, others report that it appears that this trafficking contributes to 32% of neutrophil clearance, while the liver and the spleen contribute to 29% and 31% of clearance, respectively [1, 101]. Neutrophil removal is accomplished by the macrophages at the various sites of clearance [101] during which they release IL-23, setting off a cascade of cytokine secretion from IL-17 in the T cells thereby inducing increasing concentrations of granulocyte colony-stimulating factor (G-CSF) [134]. G-CSF is the cytokine which predominates in the homeostatic regulation of neutrophil production and its role and specificities will be discussed in Section 1.3 below.

1.2 Neutrophil Pathologies

As the neutrophils are implicated in immune responses, low absolute neutrophil counts (ANCs) contribute to an increased likelihood of acquiring infections. The most common

neutrophil disorder is neutropenia, or a lack of neutrophils in the blood. Due to individual fluctuations in neutrophil counts (anywhere from daily [56] to monthly [3]) small dips below baseline are not necessarily a cause for concern. For this reason, neutropenia is typically graded, where grade 1 corresponds to ANCs between 1.5 and 2 $\times 10^9$ cells/L, grade 2, or mild, to ANCs between 1 and 1.5 $\times 10^9$ cells/L, grade 3, or moderate, to ANCs between 0.5 and 1 $\times 10^9$ cells/L, and grade 4 (severe) to ANCs less than 0.5 $\times 10^9$ cells/L, though these ranges vary with age and race [68]. Neutropenia can be classified as acute (where the disorder is brought upon by an outside source whose removal restores ANCs) or as chronic, and chronic neutropenia is further subdivided into congenital, syndrome-associated, antibody-mediated, or idiopathic disorders [68].

Within the congenital disorders is severe chronic neutropenia, which itself encompasses two notable pathologies, namely cyclical neutropenia (CN) and severe congenital neutropenia (SCN). Cyclical neutropenia is a rare disease with an incidence of about one in one million where neutrophil counts oscillate with a period of 21 days, though some patients exhibit oscillations of over 40 days [21]. CN is a lifelong disease brought about by mutations on the neutrophil elastase (or ELANE) gene [21] which carries a high risk of infection during the times when neutrophil numbers are low (and vice versa) [68]. CN has been fairly extensively analysed by means of mathematical models (see [21] for an extensive review) because of the existence of an animal model which has presented a great potential for study. As with patients with CN, grey collies also exhibit oscillations in their neutrophil counts, although with a period of seven to 11 days [16]. This mathematical modelling of CN has been valuable. For example, the identification of the ELANE mutation by molecular biologists was reinforced by the modelling prediction that a disruption in the apoptosis of neutrophil progenitors caused the cycling [21]. Recently, there has been an increased focus on aiding the clinical prediction of CN. Dale's group at the University of Washington has submitted to the Food and Drug Administration (FDA) of the United States for the approval of an at-home blood sampling kit. This would aid in the diagnosis of CN by allowing patients to easily monitor their neutrophil counts, something which would also make rich data available to researchers [21]. Concurrently, the launch of an informal online prediction tool has made Lomb-Scargle periodogram analysis available to practitioners so they may more easily detect oscillations in suspected CN cases (visit the Cyclic neutrope-

nia website at http://cyclicneutropenia.org). Due to the oscillatory nature of the disorder, patients with CN may experience neutrophilia (high ANCs) whereas patients with SCN experience chronically low neutrophil counts, leaving them exposed to life threatening infections [68]. SCN is equally if not more rare than CN (affecting approximately 0.5 in a million) and patients with the disorder are more likely to develop acute myelogenous leukaemia or myelodysplasias. Some patients have been found to carry mutations on their G-CSF receptors, leaving them with a reduced or even no response to treatment with exogenous G-CSF [68, 136] (discussed further in Section 1.5.1). Researchers at the University of Washington established and maintain an international registry to track those affected by SCN and to keep a record of their prescribed treatments and outcomes (visit the Severe Chronic Neutropenia International Registry at https://depts.washington.edu/registry/).

Both CN and SCN are identified as rare diseases but neutropenia on the whole is not an uncommon condition since iatrogenic causes of neutropenia contribute significantly to the prevalence of the disorder. One such significant cause of acute neutropenia is brought about by myelosuppressive drugs such as those used in anti-cancer treatments. As will be discussed in Section 1.6.1, chemotherapeutic drugs work by disrupting cellular division to quell the uncontrolled growth of cancerous cells. Unfortunately this disruption affects cells which are particularly short-lived, such as the neutrophils, due to their continuous production in the bone marrow (approximately 1 billion neutrophils per kilogram of body weight are released into and disappear from the blood every day) [19, 90]. Patients undergoing anti-cancer treatment are particularly prone to febrile neutropenia (neutropenia with fevers), which leave them open to infection during an already challenging period [91]. In both the pathological or healthy case, the control of neutrophil production and blood counts is assured through a host of chemical signals of which G-CSF is the principle actor.

1.3 Regulation of Neutrophils by G-CSF

The blood system is regulated by a diverse set of cytokines (cell signalling proteins) whose role is to control and balance cell numbers in the blood. A broad set of signalling molecules are involved in regulating neutrophils counts, including IL-3, granulocyte-macrophage colony stimulating factor (GM-CSF), and IL-6, though none of these have proven to be the main drivers of granulopoiesis. In fact no defects in granulocytes were

observed when IL-3, GM-CSF, or IL-6 receptors were knocked out in mice [15]. Contrary to these results, in G-CSF(-/-) mice, only 20-30% of normal neutrophil counts are present and the mobilisation of neutrophils from the marrow into the circulation is impaired [72]. Absolute neutropenia in humans has also been observed with deficiencies in G-CSFRs, as is the case of an infant born with no neutrophils. She experienced SCN and was unresponsive to treatment with G-CSF due to a point mutation on the extracellular domain of the GCSFR [136]. These results suggest that G-CSF is indispensable for neutrophil regulation and it is considered the primary cytokine driving granulopoiesis [101].

Colony-stimulating factors were initially discovered in the 1960s. The first purification of human G-CSF occurred in 1983/1984 following its initial purification from mice in 1983 [90]. What would become the common recombinant human (rh) form of G-CSF was successfully expressed in *Escherichia coli* in 1986 [137]. Today, *E. coli* bacteria are still used to generate rhG-CSF for clinical uses.

Structurally, the G-CSF gene is a 174-amino acid protein with a molecular weight of 19,6 kDa and encodes a 204-amino acid protein structure (a signalling sequence at the end of the molecule accounts for the difference in the number of amino acids). Among mammals, a 99% similarity in G-CSF protein structures has been observed and humans share a 74% and a 65% similarity with the G-CSF structure of mice and rats, respectively [2]. G-CSF is formed by four alpha-helices, as shown in Figure 3 of Arvedson et al. [2] and is a part of the long-chain subfamily which includes proteins having an average length of 260 amino acids with helices 20 to 30 residues long [2].

The GCSFR binds to G-CSF with a primarily 2:2 stoichiometry [2, 69] although certain groups have reportedly been able to produce a 1:1 binding in laboratory conditions [69]. The current understanding of G-CSF/GCSFR interactions was visualised in Figure 5 of Layton et al. [69].

The action of G-CSF on the neutrophils occurs in several ways to modulate the concentration of neutrophils in the blood. G-CSF is a potent regulator of both neutrophil production (by various means) and of the release of neutrophils from the marrow into circulation [5, 101] but it does not seem to affect the clearance or removal of neutrophils [15]. The most immediate effect of an increase in G-CSF concentrations is emergency granulopoiesis, or the rapid mobilisation of neutrophils into the blood [39, 101]. During such

inflammatory events, the neutrophil transit from the marrow seems to also be mediated by IL-17, though the same is not true for the maintenance of homeostasis [101]. After the release of cells from the marrow reservoir, G-CSF acts upstream on proliferating and maturing cells to ensure the replenishment of the reserve by increasing cell proliferation, decreasing the speed of transit from the marrow, and ensuring the differentiation and maturation of neutrophils [78]. To wit, it has been demonstrated that neutrophil precursors are subject to higher rates of apoptosis (programmed cell death) in the absence of G-CSF [90].

The major impetus for G-CSF action on the neutrophils is binding to GCSFRs on the surface of the cells, whereby G-CSF is subsequently cleared from the blood. After saturation of this mechanism, G-CSF is cleared by the kidneys [78, 90]. This dual elimination route is an important mechanism of the pharmacokinetics and pharmacodynamics (PK/PD) of G-CSF and it has a notable effect on the half-life ($t_{1/2}$) of G-CSF in the blood, as G-CSF has a half-life of around 4.7 hours without neutrophils available for binding but just 2 hours when neutrophils are available [90]. In a simple model, this combination of nonlinear, saturable elimination with a linear clearance route (as is common for several types of small molecules, including ethanol and erythropoietin) also affects the volume of distribution, a theoretical amount relating the volume of occupancy of a drug in the body [139, 140]. Further, the two routes of elimination are relevant to the PKs of exogenous G-CSF administrations since the clearance of the drug will be increased as neutrophil counts rise, which requires multiple and repeated administration to combat this effect [90].

1.4 The Use of G-CSF in a Clinical Setting

After the replication of G-CSF in *E. coli*, the first rhG-CSF preparation began clinical trials in 1991, and a second derivative from hamster ovary was approved in 1993. rhG-CSF is available in various forms, including the most common forms known as filgrastim (NEUPOGEN®), lenograstim (Granocyte®), and KW-2228 (Nartograstim®) [90]. All three of these forms are biosimilar to the native G-CSF molecule, albeit with the addition/deletion of an N-terminal methionine and an O-linked carbohydrate on threonine (filgrastim), and an allowance for radioactive labelling (KW-2228) [90]. An additional form of rhG-CSF, known as pegfilgrastim (Neulasta®), which is formed by adding a polyethylene

glycol moiety to the N-terminal methionine of filgrastim, bypasses the linear elimination from the kidneys due to its increased size. As a result, although the molecule has a similar PD action as filgrastim from the binding to neutrophil receptors, it has a markedly increased exposure from the altered PKs.

The use of rhG-CSF in clinical practice has been approved for several applications. As alluded to in Section 1.2, the most significant use of G-CSF mimetics is for the treatment of neutropenia of various origins. A brief outline of the use of rhG-CSF in non-oncological settings follows, before addressing its administration in cancer treatment.

1.5 Non-oncological Treatment with rhG-CSF

1.5.1 Severe Congenital Neutropenia

One of the major successes of treatment with rhG-CSF has been for patients affected by SCN. Since these individuals have a mutation on the ELANE gene, they experience higher than normal rates of apoptosis in the early proliferating neutrophil progenitors [21]. Accordingly, as G-CSF is known to increase proliferation rates, rhG-CSF is administered daily to increase neutrophil counts [20]. Treatment of SCN with rhG-CSF has proven not entirely straightforward, however, as phase II clinical trials showed a high variability in the required effective dose and the time to the onset of treatment efficacy. Regardless, fairly immediate results of the treatment were observed in the reduction of the number of infections experienced by the participants [20].

1.5.2 Cyclical Neutropenia

One of the first clinical trials after the purification of rhG-CSF was for the treatment of CN by IV administration, which was quickly changed to subcutaneous administration after it was found to be equally as efficacious [20]. The treatment of CN with rhG-CSF has proven to be an effective means of controlling the disease, using daily or once-every-other-day administrations [22]. Those affected by CN undergoing treatment with rhG-CSF experience fewer periods of severe neutropenia and no longer experience the mouth ulcers, fevers, and serious infections related to the disorder [20]. Indeed, one patient has been treated nearly daily for 20 years with exogenous G-CSF and has experienced virtually no

significant side effects [21]. Despite these encouraging results, treatment with rhG-CSF has not been shown to eliminate neutropenic cycling all together [22], though it has been demonstrated to shorten the length of the cycling [21]. Mathematical modelling has been used to address this curiosity by studying the timing of G-CSF administrations for patients with CN [16, 21, 35]. The authors of one such study demonstrated that alternate-day administration of rhG-CSF was as effective as daily treatment [35], though this assertion has yet to be borne out in a clinical setting [21].

1.5.3 Stem Cell Transplantation

Myeloid growth factors, including rhG-CSF, are used during stem cell transplantation in two notable ways. The first is to increase the mobilisation of the peripheral blood progenitor cells (PBPCs) for stem cell collection, while they are also administered during autologous stem cell transplantation (removal, storage, and reinjection of one's own stem cells) to combat neutropenia during the procedure [22, 107]. When rhG-CSF is given repeatedly prior to autologous stem cell transplantation, PBPCs numbers are increased and there is improved neutrophil recovery and marrow engraftment [22].

1.5.4 Further Applications and Investigational Studies

Supplementary uses of rhG-CSF within hematological disorders include the treatment of Shwachman-Diamond Syndrome (mutations on the Shwachman-Blackfan-Diamond gene which disrupt cellular proliferation), acquired neutropenic disorders, including neonatal immune and autoimmune neutropenia (disruption of maternal antibodies leading to changes in antigen expression in infants), and chronic idiopathic neutropenia (benign neutropenia of childhood) [21, 90]. Although the mechanisms with which treatment with rhG-CSF improves outcomes for these disorders are not known, they are generally attributed to the pro-proliferative effects of the G-CSF [21]. Outside the scope of purely hematological pathologies, rhG-CSF is used to treat neutropenia in inflammatory diseases like rheumatoid arthritis and acquired large granular lymphocyte syndrome. Unfortunately in these instances, a common side effect of the treatment of neutropenia with rhG-CSF is an increase or worsening in arthritic pain. rhG-CSF is also used to effectively treat glycogen storage disease type 1b, a disorder affecting the cellular trafficking of glucose across

the membrane, certain infectious diseases (including bacterial pneumonia and meningitis, and sepsis) [73], and has been investigated for use after stroke, myocardial infarctions, peripheral vascular disease, liver disease, traumatic nerve damage, among others [90].

A major use of rhG-CSF beyond its application in treating hematological disorders is for the treatment of human immunodeficiency virus (HIV). With the advent of combination antiretroviral treatment (ARV), the prognosis of those affected by HIV has steadily improved [51, 124] implying there is a greater need to manage the now lifelong comorbidities associated with the infection. Early in the HIV/acquired immunodeficiency syndrome (AIDS) epidemic, neutropenic infections were identified as a critical concern for the care of patients whose HIV had progressed to AIDS [51]. Though recent progress in the management of HIV has markedly increased life expectancies for those with HIV, neutropenia remains present within the patient community due to ART resistance and non-compliance [51, 124]. Beyond the decreased number of circulating neutrophils associated with HIV, it is also known that the infection (and other viral infections) causes defects on the neutrophils themselves which affect their ability to perform chemotaxis, phagocytosis, the respiratory or oxidative burst, and their microbicidal capacity [51]. Neutropenia in patients with HIV is an ongoing concern due to the increased risk of bacterial infections and invasive aspergillosis for those with hematological malignancies [51]. Treatment with filgrastim during HIV has been shown to induce a 56% reduction in mortality in a retrospective study [24]. Regrettably, treatment with filgrastim during HIV infection has been known to cause disseminated intravascular coagulation, hepatitis, and pancreatitis in addition to the usual bone pain, fever, and other symptoms typically experienced by patients without HIV [51]. Ultimately, since the majority of HIV-affected individuals live in the developing world (some 23.5 million people out of the 34 million globally infected in Sub-Saharan Africa alone [130]), the most significant drawback to rhG-CSF treatment for HIV patients is drug costs [51], a concern echoed in other clinical settings.

1.6 Oncological Settings: Treating Cancer with Chemotherapy

Cancer, in its various presentations, is a public health concern across the globe. In Canada, the Canadian Cancer Society (CCS) estimates that 42% of women and 45% of men will face a cancer diagnosis during their lifetime [13]. In 2012, the number of new

incidences of cancer in Canada rose to 175 310 [12], while that number is estimated to reach 196 900 in 2015 [13]. A slim (51%) majority of these new cases are lung, breast, colorectal, and prostate cancers, though there are some 100 different types of cancer known to affect humans [13]. Cancer is a broad class of cellular growth disorders, where cells undergo increased division and unmitigated growth due to a disruption in the cell cycle [85]. This cycle is generally represented as four distinct phases: G_1, S, G_2, and M, however Burns and Tannock [10] wrote of the existence of the G_0 phase (a quiescent, resting phase, or extended G_1 phase) in 1970. Cells exiting the G_0 phase committed to divide will enter G_1 and the precursory mechanisms of cell division are commenced. Next, the cell enters the S phase, or DNA synthesis phase. Here, signals within the cell control the copying of the DNA inside the nucleus and 4N or tetraploid content is produced. Next, the cell rests in the G_2 phase before entering the mitotic M phase where cellular division occurs [85]. The mitotic phase comprises the separation of the cell's chromosomes, the cleavage of the cell by the microtubules, and the production of two daughter cells. Cancer/tumour kinetics disrupt this usually well-performed process in three important ways:

1. the time of the cell cycle is disrupted (cells divide faster),
2. the fraction of cells undergoing cellular division is increased,
3. the total number of cancerous cells increases.

These three factors determine the growth rate of cancerous tumours [85]. To address the overall uncontrolled growth of cancer cells, anti-cancer treatment in the form of radiotherapy or chemotherapy (or a combination thereof) is administered with the goal of disrupting this rapid cellular division. Herein, we focus on chemotherapeutic options.

1.6.1 Chemotherapy: Mechanism of Action and Hematological Toxicities

Current anti-cancer treatment with chemotherapy focuses on combination therapy, which aims to maximise the cellular killing effects of each drug while minimising their toxicities [85]. Chemotherapeutic drugs fall into several classes, among them alkylating agents, nitrosoureas, platinum agents, antimetabolites, antitumour antibiotics, anthracyclines, epipodophyllotoxins, vinca alkaloids, taxanes, and camptothecin analogs [86], all of which disrupt cellular division through various mechanisms of action.

The two most general means by which chemotherapeutic agents disrupt the uncontrolled growth of cells is by disturbing DNA synthesis (during the S phase) and by interfering with microtubule elongation and contraction, which leads to the inability of the cell to properly cleave. The former action is performed by drugs in the alkylating agents, nitrosoureas, platinum agents, antimetabolites, antitumour antibiotics, anthracyclines, epipodophyllotoxins, and camptothecin analogs classes. Vinca alkaloids and taxanes perform the latter action, although they disrupt the assembly of microtubules in opposite ways. Vinca alkaloids inhibit assembly by binding to the tubulin which forms the subunits of microtubules. Taxanes, an important class of anti-cancer drugs which include paclitaxel and docetaxel, *induce* microtubule polymerisation and result in increased cellular apoptosis.

Unfortunately, the nature of the cell-killing mechanism of chemotherapeutic agents and their efficacy *in vivo* lead to cytotoxic secondary effects which limit their use [34, 79]. Of particular concern is the myelosuppressive action of chemotherapy and the induction of acute neutropenia in patients receiving treatment. To account for the somewhat rapid disappearance of the circulating neutrophils due to their half-life of around 7 hours, the neutrophil precursors in the bone marrow must be steadily dividing to replenish blood neutrophil counts and so these latter cells undergo fairly rapid division. Consequently, during anti-cancer treatment, circulating neutrophil numbers can become significantly reduced, leading to either dose adaptation or complete cessation of treatment [106]. Further, febrile neutropenia from the chemotherapy's cytotoxicity leaves the patient susceptible to infections, which increases the risk for hospitalisation and complications from morbidities. Moreover, modern chemotherapy combinations are administered in periodic cycles, which is believed to progressively reduce the number of cancerous cells. However, this periodic administration worsens the myelosuppression due to the repeated exposure of the neutrophils to the cytotoxic drug. Accordingly, ANC counts and the response of the hematopoietic system to chemotherapy are often used as surrogates for the successfulness of the treatment [21].

1.7 The Use of rhG-CSF to Mitigate Myelosuppressive Chemotherapy

To address the onset of neutropenia in patients receiving chemotherapy, rhG-CSF is administered concurrently, frequently prophylactically. In 1991, the FDA approved the

use of rhG-CSF for patients undergoing myelosuppressive chemotherapy [106]. Currently, the American Society of Clinical Oncology (ASCO) recommends the use of G-CSF during chemotherapeutic treatment as a primary prophylactic measure when there is a 20% or more risk of febrile neutropenia [79, 106] and both ASCO and the National Comprehensive Cancer Network (NCCN) have also expanded this recommendation to patients with a risk between 10% and 20% based on clinical experience and trial reviews [106]. For primary prophylactic use, Canadian recommendations followed suit with those of ASCO, the NCCN, and the European Organisation for Research and Treatment of Cancer (EORTC). The Canadian guidelines call for treatment with CSFs when the risk of neutropenia exceeds 20%, there are previous comorbidities and/or neutropenic events, and when the risk of neutropenia is between 10% and 20% based on expected benefits considering a variety of factors (clinical, laboratory, patient risk, and disease factors) [63]. The factors determining the risk of neutropenia for a patient undergoing treatment with chemotherapy include advanced age, poor performance status, the presence of other complicating disease-statuses, and atypical baseline counts [79]. Older patients are regularly singled out as having a higher propensity for neutropenia and are, accordingly, labelled as high-risk by the EORTC [79]. Identifying those patients who present an increased chance of developing neutropenia has also been addressed by the regulatory cancer organisations. ASCO provides a worksheet for clinicians to evaluate their patients' likelihood of developing neutropenia [79]. The EORTC published the decision tree presented in Figure 1.2 to help guide clinicians in their expectation of risk [79]. Canadian recommendations combined those of the EORTC and ASCO, as seen in Figure 1.3 [63]. All told, regulatory agencies have put forward methods for standardising clinical decisions on the prophylactic use of rhG-CSF in oncological settings to appropriately triage patients for effective care during chemotherapeutic treatment. Differences in recommendations exist between the different organisations owing to the prevalent practices of their respective regions [79].

While ASCO, the NCCN, and the EORTA have put forward advice for systematic risk assessment, guidelines for treatment of neutropenia during chemotherapy and the timing of this treatment are more vague. Canadian recommendations based on recent meta-analyses indicate that filgrastim therapy should begin soon after chemotherapeutic administration and continue until the ANC nadir is observed to be raised above 1.5×10^9

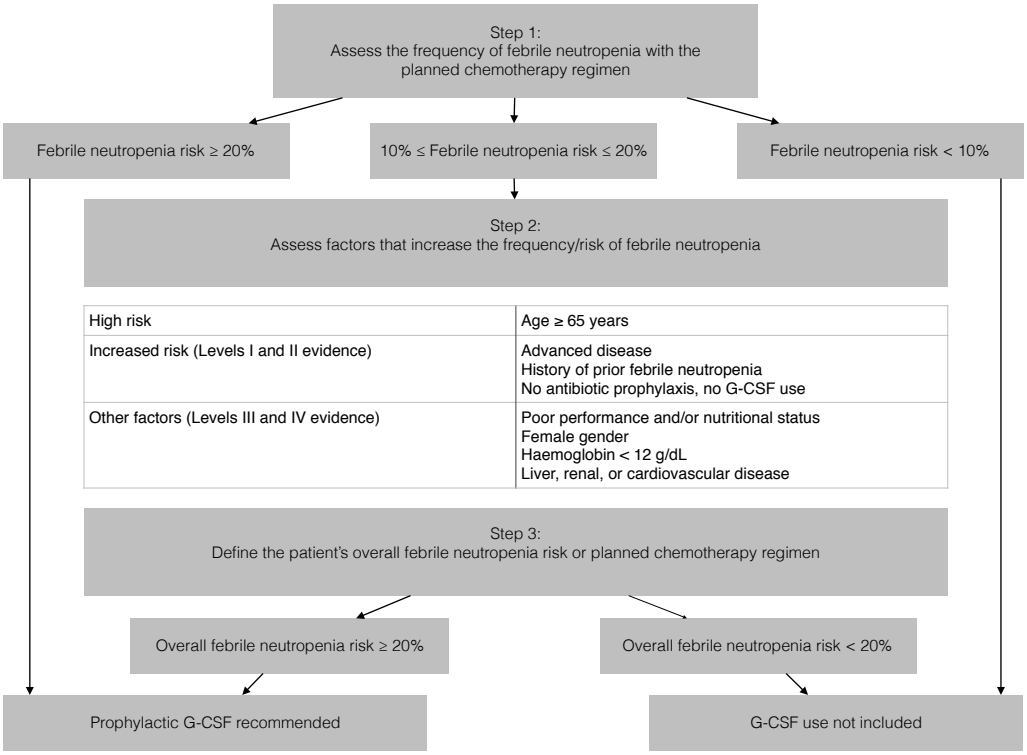

Figure 1.2 – The European Organisation for Research and Treatment of Cancer decision tree guidelines for the prophylactic use of G-CSF during chemotherapy. Adapted from [21].

cells/L, although this nadir value is also somewhat ill-defined and ANCs of 1-1.5$\times 10^9$ cells/L are recommended prior to treatment cessation. Treatment with rhG-CSF after chemotherapy is prescribed to continue until after the nadir has passed, necessitating some clinical intuition as ANCs are known to drop moderately between the time when rhG-CSF treatment is stopped and the next chemotherapy period begins. The duration and timing of the treatment with rhG-CSF depends on the time to the nadir and on the grade of the neutropenia [63]. The difficulties in making these determinations are further compounded due to the uncertainty of an individual's tolerance for chemotherapy.

1.8 An Interdisciplinary Approach to Guide the Clinical Practice

Mathematical modelling is well-positioned to respond to the need to predict the ANC nadir after chemotherapeutic administration. Predictions based on modelling work can help to standardise treatment protocols and take out the guesswork for clinicians, leading

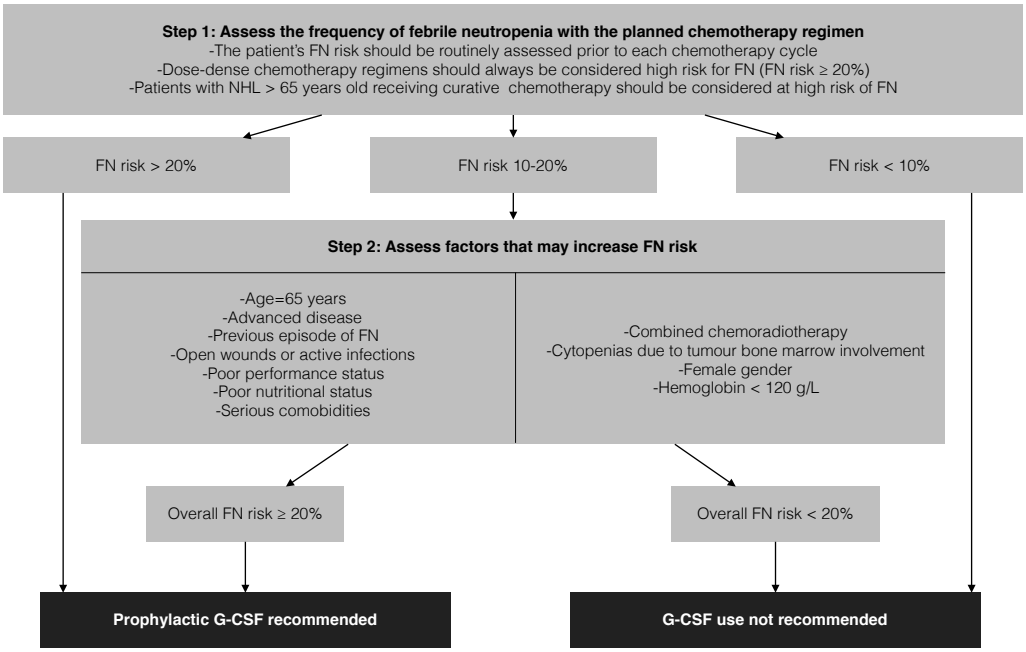

Figure 1.3 – The combined European Organisation for Research and Treatment of Cancer and American Society of Clinical Oncologists decision tree guidelines for the prophylactic use of G-CSF during chemotherapy. Adapted from [63].

to an increased evidence-based practice [21, 132].

The approach undertaken in this dissertation is one which is interdisciplinary and focussed on patient outcomes. It combines our most current understanding of granulopoiesis within an appropriate mathematical framework and incorporates key pharmacological considerations, all while maintaining a focus on clinical realism.

To situate the articles highlighted in Chapters 2 to 5, it is important to understand the historical evolution of the fields of pharmacometrics and pharmacology. The following sections will contextualise the broad swath of studies undertaken to respond to the need for guidance where myelosuppressive chemotherapy is concerned.

1.9 Early Studies of Myelosuppression and Statistical Approaches

Initial work to predict a neutrophil response during chemotherapy centred on more statistical approaches, as is consistent with the beginnings of the PK/PD field as a whole. Two important early works were authored by Karlsson et al. [58, 59], the latter of which

focussed mainly on a more generalised approach. In the work of [58], measures for the average concentration of etoposide (a topoisomerase inhibitor) contribute to an effect on the white blood cells (WBCs) by an Emax model (a saturating sigmoidal response function), as seen in Equations (1.1). Due to a statistical relationship between the average plasma concentration of etoposide, the albumin in the blood, and bilirubin (blood proteins), a correlated function of the effective concentration was used as the driver of the WBC response:

$$\begin{aligned} C_{ave} &= \frac{C_{24}\left(28 + 44\frac{R_1}{R_2}\right)}{72} \\ C_{eff} &= C_{ave}\frac{3.7}{ALB}(1 + \theta_{BILI}(BILI - 0.5)) \\ E(t) &= \frac{E_{max}(t)C_{ave}^{\gamma}}{C_{ave}^{\gamma} + C_{50}^{\gamma}} \\ WBC(t) &= Baseline(1 - E(t)), \end{aligned} \tag{1.1}$$

where C_{ave} is the average concentration of etoposide, C_{24} is the concentration of etoposide 24 hours after the beginning of infusion, R_1 and R_2 are the rates of infusion before and after 28 hours, C_{eff} is the effective concentration, ALB is the covariate for albumin, $BILI$ is the covariate for bilirubin, $E(t)$ is the modelled concentration-effect relationship, E_{max} is the maximal effect, γ is the steepness of the Emax curve, C_{50} is the concentration of etoposide which generates half of the maximal effect, $WBC(t)$ is the modelled WBC count over time, and $Baseline$ is the baseline WBC before drug infusion. The authors of [59] undertook a similar statistical relationship analysis to predict WBC counts during treatment with paclitaxel, although here the drug served as an example for a more generalised model, the principle equations of which are presented in Equations (1.2) below.

$$\begin{aligned} E_{dir} &= \frac{C^{\gamma_1}}{C^{\gamma_1} + C_{50}^{\gamma_1}} \\ E_{obs} &= \frac{E_{obs\ max}AUC_{dir}^{\gamma_2}}{AUCE_{dir\ 50}^{\gamma_2} + AUCE_{dir}^{\gamma_2}} \\ WBC_{pred}(t) &= Baseline\left(1 - \frac{E_{max}(t)AUC_{dir}^{\gamma_2}}{AUCE_{dir\ 50}^{\gamma_2} + AUCE_{dir}^{\gamma_2}}\right), \end{aligned} \tag{1.2}$$

where E_{dir} is the direct (unobserved) effect of the chemotherapeutic drug, E_{obs} is the observed effect, C is the concentration of the drug, γ_1 determines the slope of the sigmoidal effect, C_{50} is the concentration of the drug eliciting 50% of the maximal effect, $AUCE_{dir}$ is the area under the E_{dir}-time curve, $E_{dir\,max}$ is a scaling factor set to 1, $AUCE_{dir\,50}$ is the AUCE which gives 50% of the maximal effect, γ_2 determines the slope of the sigmoidal effect, $WBC_{pred}(t)$ is the predicted WBC count over time, and E_{max} is the maximal effect over time.

Both models lack a physiological impetus and are mainly determined by statistical analyses [36]. Though these studies appeared in the mid-to-late 1990s, the development of increasingly refined models for the prediction of neutrophil counts parallels the maturation of the PK/PD modelling field and modelling trends in PK/PD over time.

Though the earliest PK study can be traced back to 1919 in the work of Widmark [4, 138], it wasn't until the late 1960s that PK/PD modelling truly began expanding [4, 18] with the pioneering studies from the Sheiner lab. The pharmacokinetics outlined in [115] are simple one-compartment models, but what was important in this work was the computational framework that would later serve as the basis for the gold-standard software in the field (see Section 1.13). In 1979, Sheiner readapted this model to account for the time delay in the effects of d-tubocurarine, a neuromuscular blocking drug in producing paralysis [118] based on work developed by Segre [4, 114]. This model included a hypothetical effects compartment in which drug concentrations related directly to a drug's pharmacological actions. This pioneering model quickly became standard in the field and compartmental analysis developed into the dominant modelling philosophy [42].

Although compartmental methods took off, the ease with which summary parameters can be obtained through non-compartmental analysis (NCA) meant that this latter methodology remains a straightforward initial means to obtain parameter estimates [42]. NCA, also known perhaps somewhat anomalously model-independent, makes no illusions as to its empirical nature, having been developed from the statistical moment closure techniques of Yamaoka [4, 42, 142]. NCA rests primarily on the assumption of a kinetically homogenous central compartment from which clearance takes place and is frequently relied upon to predict drug exposure in the form of the area under the (concentration) curve, or AUC [42]. As in the WBC models of [58] and [59], no explicit physiology is accounted

for, which can be viewed as advantageous by some (more generalisable, less assumptive, directly related to observed behaviours [42]) while others would argue this to be a defect of the method [71, 94].

NCAs are usually concerned with the estimation of a few key PK parameters: clearance (CL), volume of distribution (Vd), and AUCE and may also deal with the concept of mean residence time (the time a drug remains in the system). Due to the assumption of a single central compartment, one of the main properties of a NC system is the terminal, mono-exponential phase in the concentration-time evolution [42]. For this reason, NCA can be viewed as a generalisation of equivalent compartmental models. If one is primarily concerned with physiological inference, however, NCA is not an appropriate framework due to the broad hypotheses underlying the approach [42]. Though the initial models of myelosuppression weren't necessarily realised with NCA, they were overwhelmingly performed using similar empirical methods, frequently relying upon clinical data of neutrophil numbers, time above a toxicity threshold, or exposure in the form of AUC [29, 30, 38, 88, 129]. These statistical approaches were not generalisable and lacked insight into the origins of neutropenia. Parallel to the push in the PK/PD field toward incorporating more and more physiological mechanisms into models, the next major development in PKPD modelling applied to forecasting the neutrophil response to chemotherapy was to approach the problem with an increased emphasis on the inner-workings of the blood system.

1.10 The Friberg Model and Semi-mechanistic Approaches

Perhaps the most well-known and well-used model of myelosuppression during chemotherapy in the PK/PD literature is the Friberg model developed at Uppsala University in the lab of Karlsson [36]. Prompted by the idea of separating physiological parameters from PK ones, the authors of [36] concentrated on developing a model which could be applicable across drugs but which remained system-related and interpretable. As previously mentioned, the model was the result of an earlier call for increasingly mechanistic PK/PD models of leukocyte behaviour during chemotherapy.

In 1998, Minami et al. [89] published an indirect PD model of the surviving fraction of leukocytes after chemotherapy. In this compartmental PD model, each of the two partitions represented a separate region occupied by the neutrophils, namely the bone marrow

and the blood. A fractional inhibition dependent on drug exposure relayed the effects of chemotherapy on the system and the addition of the bone marrow compartment indirectly accounted for the time delay between drug administration and observable effects [89]. This division of the body into central (blood/plasma) and 'other' (tissues, bone marrow) mimics the principle modelling strategy of the PK field in compartmental modelling and also represents a step forward from the previous direct effect PD measures [25].

As introduced in Section 1.9, one of the fundamental modelling approaches to drug disposition has been, and continues to be, compartmental analysis. In this approach, tissue systems are grouped together to form compartments in a rational way to represent the kinetics of drug concentrations in the blood [40]. The relationships between these compartments are modelled with ordinary differential equations (ODEs), frequently linear ODEs, which correspond to mono- (one compartment) or poly-exponential solutions. This decaying solution type is supported by the presence of linear relationships in the log(concentration) vs time space, indicating an exponential relationship in the concentration vs time space. ODEs are well understood and characterised mathematical objects and similarly well-defined simulation techniques exist for their numerical analysis [42]. As such, compartmental modelling approaches evolved in step with advances in ODE theory and numerical techniques [18]. The indirect PD model of [89], with its compartmental division of physiological space, was a step forward towards more physiologically driven PD models of myelosuppression [36]. A schematic comparison of direct vs indirect PD models is given in [25] and is adapted here in Figure 1.4.

Following the work of [89], the Karlsson group continued incorporating physiological elements into PD models but within specific drug contexts [37, 38]. However, these studies began incorporating transit compartments into the PD model as a means of accounting for the observed delays between the administration of each drug (2'-deoxy-2'-methylidenecyidine and 5-flourouracil, respectively) and their myelosuppressive effects. Building upon this semi-physiological construction, Friberg et al. then generalised this approach in [36].

In Friberg's seminal work, the development of neutrophils in the bone marrow is comprised of a proliferative compartment (cells undergoing division), followed by a certain number of transit compartments before reaching the circulation. The transit compartments represent the maturation phase and inherently account for the observed delays in

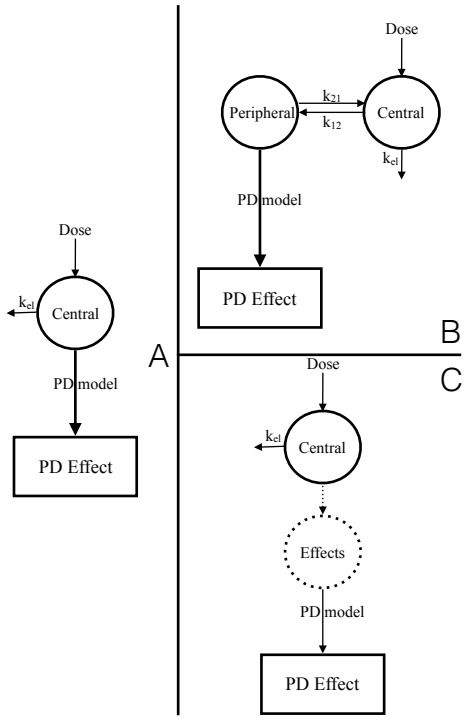

Figure 1.4 – Comparison of direct and two indirect pharmacodynamic effect models. A) In a direct model, concentrations in the central compartment drive the PD effect. B) Indirect model where concentrations in the peripheral compartment produce the effect. C) Indirect model with a hypothetical effects compartment is responsible for the PDs. Adapted from [25].

chemotherapeutic cytotoxicity. The sum of the time spent in passage between these compartments is referred to as the mean transit time (MTT). Since chemotherapy acts to interrupt cell division, the effect of the drug is modelled as an effect on the rate of self-renewal in the proliferative compartment. Last, due to the effects of G-CSF to replenish circulating neutrophil counts, a negative feedback control from the circulating compartment to the proliferative compartment was added. See Figure 1.5 for a generalisation of the model presented in [36].

Friberg et al. originally presented a myelosuppressive model with three transit compartments accounting for the delay between proliferation and circulation. However, since the number of transit compartments is estimated from data, a more general model is represented by n transit compartments, as in Equations (1.3).

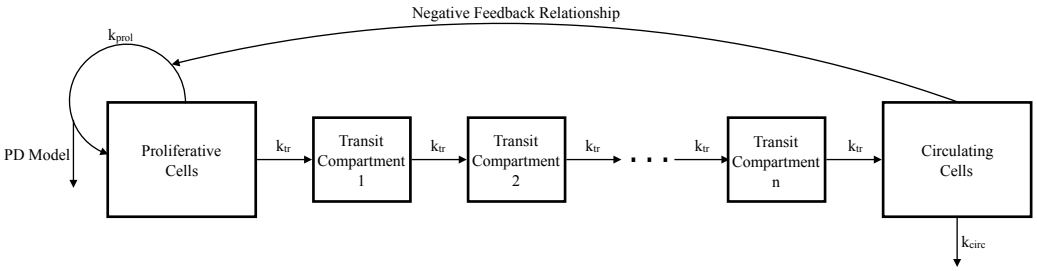

Figure 1.5 – Schematic representation of the general semi-mechanistic model of neutrophil development developed by Friberg. Proliferative cells self-renew at rate k_{prol} or begin the transition to the circulation by exiting with rate k_{tr} (the rate of transit). The delay between the time cells leave proliferation to when they enter the circulation is called the mean transit time and is equally divided between n transit compartment, each connected by the rate of transit. Once cells enter the circulation, they die with rate k_{circ}. The number of circulating cells has a negative feedback on the proliferation rate of the proliferative cells. The myelosuppressive action of the drug is assumed to also effect k_{prol}. Figure adapted from [36].

$$
\begin{aligned}
\frac{dP}{dt} &= k_{prol}P(1 - E_{drug})\left(\frac{N_0}{N}\right)^{\gamma} - k_{tr}P \\
\frac{dT_1}{dt} &= k_{tr}P - k_{tr}T_1 \\
\frac{dT_2}{dt} &= k_{tr}T_1 - k_{tr}T_2 \\
&\cdots \\
\frac{dT_n}{dt} &= k_{tr}T_{n-1} - k_{tr}T_n \\
\frac{dN}{dt} &= k_{tr}T_n - k_{circ}N,
\end{aligned}
\tag{1.3}
$$

where P are the proliferative cells, k_{prol} is the rate of proliferation, E_{drug} is the PD model of the myelosuppressive action of the drug, N_0 is the baseline neutrophil count, N is the current number of circulating cells, γ modulates the effect of the feedback from the circulating compartment to the proliferative compartment, k_{tr} is the rate of transit, T_i $(i = 1, \ldots, n)$ is the i^{th} transit compartment, and k_{circ} is the rate of exit from the circulating compartment.

As with compartmental PK models, the model in [36] quickly became adopted in a

great deal of studies of myelosuppression after its publication, in its original form or with slight adaptations (see [14, 31, 45, 53, 55, 97, 98, 100] for a representative sample). It remains perhaps the most well-known neutrophil model in the pharmaceutical sciences community. Given the growing shift towards entirely physiological models in the field to better inform the drug development cycle [23, 25, 40, 133], researchers are increasingly recognising the limitations of the approach [8, 64, 113, 132]. One of the major criticisms of the transit compartment model is the dependence upon data which determines its structure. As with the corresponding compartmental PK models, basing the structural form of a model entirely on clinical data instead of assimilating a priori physiological knowledge at the outset requires researchers only demonstrate that the model is a good fit to data in relation to a statistical objective. This does not mean that the physiology is well-represented within the model and limits the generalisability of its predictions [42, 94]. To respond to these limitations, modellers began branching into two different methodologies somewhat in parallel.

1.11 Physiologically-Based PK/PD Studies and Target-Mediated Drug Disposition Models

The realisation that the prevailing compartmental models were in need of more physiological basis paved the way for physiologically-based pharmacokinetic models, or PBPK models [94]. Since the cytotoxicity of anti-cancer agents is driven first by the concentration of drug reaching the proliferating neutrophil precursors, this formalism was a natural fit for those seeking to increase the physiological realism of models of myelosuppression [97]. PBPK models relate drug kinetics to a physiologically-informed compartment structure, as opposed to the lumping together of physiological systems that is customary in traditional compartmental models. Typically, these numerous physiological compartments represent the various organ systems in the body and are linked by the rate of blood perfusion to the system [94]. Parameter estimation in PBPK modelling still incorporates clinical data but less emphasis is made on constructing the model from data. Instead, the model is constructed from hypotheses governing the inclusion/exclusion of certain corporal systems before making use of available clinical and preclinical data. Generally, the major organs like the heart, liver, kidneys (if the drug is renally excreted), and fat tissues (for lipophilic

drugs) are included by default. Other systems associated with the particular compound of interest are also incorporated, as are tissues that are known to be implicated in the drug's kinetics. If there is clinical data available for an organ or tissue that has yet to be included, they may also be modelled [104]. At this stage, any available data for the rates of exchange between compartments, compartment volume, tissue permeability etc. is used for parameter estimation keeping in mind the targeted population, the intended pharmacological use of the drug of interest, and allometric data [94]. To this end, several authors have put forward broad reviews of typical parameter values for PBPK models [9, 11, 104].

Groups based in optimal control particularly took to this approach when they set forth to model myelosuppression and toxicity following anti-cancer treatment. The interest of the control theorists in PBPK/PD modelling of drug toxicity is not unforeseen. Though PBPK/PD models do integrate more detailed physiology, the mathematical objects with which they do so are no more sophisticated or complicated than the ODEs used in traditional compartmental modelling. Further, there is more emphasis on the prior method for parameter estimation [99] and less reliance on statistical fitting in the PBPK methodology. Accordingly, PBPK/PD models are ideal candidates for analysing in an optimal control setting. Such studies have been put forward in [14, 46, 53], and [97]. These models incorporated not only the classical PBPK/PD approach but also integrated the diverse range of cell types and kinetics involved in the WBC and inflammatory response [14]. Further, optimal control served to determine dosing schedules for chemotherapeutic drugs which would minimise the neutropenic risk to the patient [46].

Though it is clear that PBPK/PD models of neutropenia have extra compartments incorporating a more complex understanding of physiology, limitations remain. One conspicuous shortcoming of PBPK and PBPK/PD modelling is the static nature of the approach [4]. The compartmentalisation with exchange rates between the various organs and tissues does not allow for any reorganisation or dynamic dependence to changing conditions, implying that PBPK and PBPK/PD are appropriate when systems are stationary during observation, which is not necessarily the case in studies of myelosuppression [54]. The haematological system, and the neutrophil lineage in particular, is a compelling dynamic system [21] which suggests that PBPK/PD modelling of cytotoxicity is not the most nat-

ural framework for analysis of these systems. Given the natural association between such models and optimal control systems, PBPK/PD remains a valid methodology given one's specific interests.

Concurrent to the development of PBPK/PD models of myelosuppression, advances were being made on target-mediated drug disposition (TMDD) models [83]. TMDD models are used to describe the interaction of ligands demonstrating a high affinity binding to their targets [26]. The principle ideas of ligand-receptor binding date back to the development of fundamental chemical principles [26] though the inspiration for the work of [83] traces perhaps more directly back to the work of [74]. The major hypothesis behind TMDD is that an important proportion of the drug will become bound to its receptor. Contrary to the assumption of compartmental models, where it is assumed that the binding of an agent has an inconsequential effect on the PKs of the drug, TMDD models do not presuppose this hypothesis [84]. A general TMDD model as presented in [83] is provided in Equations (1.4) below. Let C_p be the concentration of the drug in the central compartment and consider the exogenous administration of a drug be modelled by $I(t)$. Considering the interactions of the drug with the tissues and receptors, let D_T be the tissue compartment, DR be the concentration of the drug-receptor complex, and R_{max} be the total density of surface receptors. Then a general TMDD model can be expressed as

$$\begin{aligned}
\frac{dC_p}{dt} &= I(t) - (k_{el} + k_{pt})C_p + k_{tp}\left(\frac{D_T}{V_c}\right) - k_{on}(R_{max} - DR)C_p + k_{off}DR \\
\frac{dD_T}{dt} &= k_{pt}C_pV_c - k_{tp}D_T \\
\frac{dDR}{dt} &= k_{on}(R_{max} - DR)C_p - (k_{off} + k_m)DR \\
\frac{dR_{max}}{dt} &= k_{syn} - k_mD_R - k_{deg}(R_{max} - DR),
\end{aligned} \tag{1.4}$$

where k_{el} is the rate of elimination from the central compartment, k_{tp} is the rate of distribution, V_c is the volume in the central compartment, k_{off} is the rate of dissociation, k_{on} is the rate of association, k_{pt} is the rate unbound drug binds to nonspecific tissues, k_{syn} is the zero-order production constant, k_m is the rate of internalisation and degradation of the complex, and k_{deg} is the degradation rate of unbound receptors.

Krzyzanski, who has worked extensively on TMDD models for exogenous cytokine

mimetics, applied the idea of TMDD to drugs that altered cell behaviours in [66]. Therein, several key cell cycle behaviours were introduced, including senescence (biological aging) and the PDs were predicated on indirect link models, like that of [89]. This general model was later applied specifically to the case of rhG-CSF in the form of filgrastim [67]. Krzyzanski has also applied lifespan models to hematopoietic stem cell modelling, which is described in Section 1.12.1.

Since TMDD models are conceived with ligand-receptor dynamics forming their basis, crucial features specific to cytokines like G-CSF are easily incorporated. As seen in Section 1.3, the major means of elimination of G-CSF is through receptor internalisation on the GCSFR of the neutrophils. Further as the action of G-CSF is initiated by the association of the molecule to its receptor, it cannot be assumed that its binding has little effect on its PKs. As such, TMDD is well-suited as a model for G-CSF kinetics. In [67], an adaptation of the Friberg model [36] and the general TMDD model are combined to account for the kinetics of neutrophil development and the contribution of the neutrophils to the clearance of G-CSF (see Figure 1 in [67]). In such TMDD models, it is not uncommon that PD effects are modelled using Michaelis-Menten dynamics [87] which, together with the Hill function [52], account for our fundamental understanding of how enzyme kinetics and ligand binding occur.

The increased realism achieved through by accounting for ligand/receptor dynamics in the TMDD models does not overcome the use of the semi-mechanistic model of granulopoiesis. As discussed in Section 1.10, the reliance on clinical data to determine the appropriate number of transit compartments limits the scope of application of this class of models. Further, the rate of transit between compartments is typically taken to be constant (see, for example, [45, 67, 135] among others) which is not physiologically realistic (since G-CSF modulates the rate of proliferation and maturation within the bone marrow [34]). The shortcomings in terms of the explicit physiological mechanisms of the TMDD models leave room for the continued refinement of granulopoiesis models. Parallel to the development of the models discussed thus far is the establishment of more traditional systems biology approaches to hematological modelling, as will be broached in the following section.

1.12 Systems Biology Approaches and Quantitative Systems Pharmacology Developments

The importance of interdisciplinary approaches is increasingly recognised but it is clear that this has not always been the case. Unfortunately the mathematical biology and the pharmaceutical sciences communities have developed fairly independently without much exchange of ideas [133]. This is particularly evidenced by the lateral efforts of the mathematical biology community to model hematopoiesis and granulopoiesis in particular, which failed to inform the similar undertakings in the PK/PD community. Mathematicians tend to seek out models which are capable of explaining many situations at once [64], something which is not at all possible with an empirical or statistical fitting modelling approach and are further interested in investigating dynamic presentations of hematopoietic diseases (including cyclical neutropenia). For example, cyclical hematopoietic diseases were addressed as early as the late 1960s by many [125]. Morley in particular was interested by cyclical neutropenia [92], a fascination later picked up by Mackey [80], who would become a pivotal figure in the field [21]. As is customary, models of hematopoiesis arising in the mathematical biology literature took a systems approach [133]. Models were constructed using first principles with physiological hypothesis at the basis. Parameter estimation using the prior method (although it should be noted that this term is not widely used in the mathematical biology community) were undertaken and did not frequently include any parameter fitting, contrary to the methods being concurrently developed in the pharmaceutical sciences community. The mathematics community, however, did not have extensive exposure to PK/PD modelling implying that relevant drug kinetic and drug effect models were largely absent until more recently [21].

In 1975, Rubinow published a model of neutrophil production in humans [105]. This model is comprised of two proliferative and three maturation compartments and included feedback control mechanisms to regulate blood neutrophil counts. The interest was not only in reproducing some quantitative measurements of the granulocytes but in also studying the dynamical properties of the model. Outside of the work of the Mackey lab, the details of which will follow, the Segal Lab of Computational Biology in Rehovot, Israel also contributed heavily to mechanistic modelling of granulocytes [119–121]. The abstraction by the authors of [121], in particular, contributed to the understanding of the physiological

mechanisms regulating neutrophils and their control by G-CSF concentrations. Another group in Israel led by Agur have also been instrumental in the construction of sophisticated models of neutrophil development [131, 132]. In [132], Vainstein et al. put forward a model which accounted for the major physiological developments in the bone marrow and also incorporated accepted PK models of G-CSF. This is perhaps the first instance of the fusing of systems biology and PK/PD modelling in the story of granulopoiesis modelling. This model later served as the basis for the development of proprietary software destined to individualise chemotherapy treatment (PrediCare suite of products, visit the Optimata web site at http://www.optimata.com). They also determined that delaying the first administration of G-CSF after treatment with chemotherapy improves the neutropenic status of the patient [131]. The latter group was not the only one to combine mathematical biological approaches with traditional PK/PD ones. The Löffler group in Leipzig, Germany has also published extensively in this area. In 1994, Schmit et al. (including Löffler) published a study on the origins of cyclic neutropenia [111]. Two years later, the group successfully delineated the effects of G-CSF and GM-CSF scheduling on the dynamics of granulopoiesis using mathematical modelling [112]. More recent work has focused on modelling the effects of chemotherapy and G-CSF on the granulocytes [109, 113] and on extending these models to the hematopoietic system as a whole [110]. The common element in the granulopoiesis modelling of this group is the compartmentalisation of the neutrophil progenitors in the bone marrow, similar to that of [36], however much more detail into the biology of these early cells is included. Further, the PD effects of both the myelosuppressive drug and G-CSF are included at the specific level of action (on each compartment of proliferating cells, for example). A typical model is presented in Figure 1 of [113]. In this paper, a dose-dependent effect on the bioavailability of subcutaneous rhG-CSF was discerned and is an example of how systems biological modelling can inform the drug development cycle. Though this group tends to use ODE modelling for the hematopoietic system, they also recently examined a novel modelling philosophy combining agent-based models (ABMs) with the traditional ODE structure [64]. ABMs are rooted in a chemical reactions formalism [41] and have become increasingly used to model systems which do not satisfy the general hypotheses of ODE models (homogenous mixing, probable reactions). In [64], the ABM is employed to model the HSCs and is

compared to a corresponding ODE model. Their results show that the ABM improved the modelling of the proliferative stem cells. Whether this novel approach proves itself to be fruitful is still undetermined.

The work of the Mackey group at McGill University in Montreal, Canada spans the longest period of the systems biology groups working on granulopoiesis. Much of Mackey's work has been centred on understanding cyclical neutropenia [16, 35, 47–50, 70] but more recent work has focused on both the exogenous administration of G-CSF and the reaction of the system to chemotherapeutic treatment [8, 17, 34]. What is notable in the work of this group is the progressive approach to model construction. Although differences in the models across these studies are present, most if not all retain certain physiological components. This consistency is directly attributable to the first principles modelling philosophy where models are built by mapping what is known of the physiology mathematically as opposed to determining the structure from data. Key findings about the timing of G-CSF administration are attributable to the work of this group. For example, the authors of [35] demonstrated that once every-other-day as opposed to daily G-CSF treatment was as effective for avoiding neutropenia in patients with cyclical neutropenia. Similar to the findings of [131] in the same year, the authors of [8] found that delaying the first administration of G-CSF post-chemotherapy was more successful for staving off neutropenia than administering G-CSF the day of anti-cancer treatment. As seen in Chapter 2, this delayed treatment protocol was again found to be optimal when more refined PK/PD models of G-CSF and a chemotherapeutic drug were incorporated into the model [17]. As alluded to, until recently, the PK models used within this group, specifically in [34] and [8] did not make use of current studies from the pharmaceutical sciences literature and were accordingly limited in scope. The models of this group were equivalently less known to those working in PK/PD on account of the mathematical objects used in these studies, briefly introduced in the following section.

1.12.1 Delay Differential Equations, Age-Structured Models, and Lifespan Models in Hematopoiesis

The physiological models used by Mackey and associated authors are based on delay differential equations (DDEs) and are not typically familiar for those working in traditional

PK/PD modelling. DDEs are infinite dimensional functional-state extensions of ODEs which inherently incorporate time delays as the current solution depends on the past [62]. A general DDE takes the form

$$\frac{dx(t)}{dt} = f(x(t), x(t-\tau)), \tag{1.5}$$

where $f(x, x(t-\tau))$ is a function depending on the current state and a past state, and $\tau > 0$ is a time delay [93]. One of the most famous DDEs is possibly the logistic growth equation

$$\frac{dN}{dt} = rN(t)\left[1 - \frac{N(t-T)}{K}\right],$$

$(r, K, T > 0)$ as the logistic map (the difference equation reformulation of the above equation) leads to period doubling bifurcations and chaos for increasing r. Mackey and Glass are also well-known for their similarly chaos-producing eponymous Mackey-Glass equation

$$\frac{dx}{dt} = \beta\frac{x(t-\tau)}{1 + x^n(t-\tau)} - \gamma x, \tag{1.6}$$

for $\gamma, \beta, n > 0$, which arose from modelling of respiration and hematopoietic cells [43, 44, 93]. In population biology, delay equations are particularly useful for modelling birth processes which exhibit time lags [93]. For example, as discussed in [82], a general equation for a DDE modelling a time-delayed birth process subject to a population-dependent destruction rate is

$$\frac{dx(t)}{dt} = -\gamma x(t) + F(x(t-\tau)), \tag{1.7}$$

where γ is this constant destruction rate, $F(x(t-\tau))$ is a production rate which depends on past behaviour, and $\tau > 0$ is the birth process delay in the system. The construction of DDEs for populations exhibiting age structures (like those of hematopoietic cells, animals with age-dependent reproduction rates, diseases with age-dependent infection rates etc. [75]) typically begins from age-structured partial differential equations (PDEs). These PDEs are then integrated along characteristics from a_1 to a_2, where a_1 is the earliest age of each stage and a_2 is the oldest age of the corresponding stage, producing the DDE. A

detailed derivation can be found in the appendix of [33] and also in [75]. An application of this process is available in [7] and a derivation specific to the model studied in this dissertation is provided in Chapter 4.

Models using DDEs are more flexible than the semi-mechanistic approach and the delays in their systems are more explicitly expressed which makes them a natural counterpart to the usual transit compartment model [62]. Indeed, in general (as described in [62]), letting

$$y_n(t) = x_1(t) + \dots x_n(t)$$

be the total sum of a transit compartment model with n compartments and a fixed MTT of n/k, then

$$\lim_{n\to\infty} y_n(t) = y(t),$$

where $y(t)$ is the solution to the simple DDE

$$\frac{dy(t)}{dt} = k_{in}(t) - k_{in}y(t-T), \tag{1.8}$$

where k_{in} it the production, or birth rate, and T is the MTT. The above equation is referred to as a lifespan model [62] and, as mentioned, has been used to study hematopoietic cell populations by Krzyzanski [65]. This model for populations with specific lifespans, similar to that of equation (1.7), is useful to account for the birth and death process of the population of interest but does not necessarily incorporate all of the physiological details of the age-structured hematopoietic cell lines. Nonetheless, it is a good first introduction to DDE modellers and has gained exposure within the PK/PD community [65].

One recognisable difference in systems biological approaches to modelling hematopoiesis versus those from pharmaceutical sciences is the absence of any estimation of variability in the classic PK/PD sense. An introduction to population PK/PD (PopPK/PD) modelling is given in the following section, where PopPK/PD approaches to models of myelosuppression are also introduced.

1.13 Population Pharmacokinetics/Pharmacodynamics and their Application to Myelosuppression

PopPK/PD was first introduced by Sheiner in 1972 [18, 115] and later refined in 1977 in a paper that would transform and mould the PK/PD modelling field [116, 117]. Broadly speaking, population approaches are a means of quantifying the differences between individuals in a population while simultaneously characterising this same population. In particular, the PopPK/PD technique is used to discern the individual differences present in the drug concentration and the effects produced from the individual concentration with reference to the studied population [126]. The method described by [115] and [116] used mixed effects regression model for the analysis of a population to be able to delineate both interindividual and intraindividual variability within the population [143]. Mixed effects modelling (MEMing) is a statistical model which accounts for average (fixed) effects and random effects. These random effects are used in PopPK/PD modelling to account not only for explained (interindividual/intraindividual variability) but unexplained variability [143]. Later the introduction of interoccasion variability (the random change in parameters between study occasions) was also included [57]. As detailed in Chapter 3, in general, a population model with both interindividual and interoccasion variability (IIV and IOV, respectively) has parameters which take the form

$$P_{j,k} = P^* e^{\eta_j \tau_k}, \tag{1.9}$$

where $P_{j,k}$ is the j^{th} PK parameter estimate for the k^{th} occasion and P^* is the average (or fixed) value of the population for this parameter P. The random variable (RV) representing IIV is η_j and it is independent and normally distributed, as is τ_k, the RV accounting for the IOV. Both RVs have zero mean and a variance of ω_p^2 and π_p^2, respectively. PopPK/PD models have been used to provide parameter estimates from clinical data since their introduction [18, 126, 143]. Beyond the methodological acceptance gained by this approach, a contributing factor to the adoption of the MEMing approach was the introduction in 1984 of NONMEM, a black box software to perform model determination and parameter estimation for population models [6, 18]. The rise of NONMEM and its recognition as the gold standard software used in pharmacometrics and the pharmaceutical sciences [61] paved the

way for the inclusion of PK/PD modelling in the FDA approval requirements for new drugs [32]. The existence of software packages that perform similar analyses should however also be noted here and include Monolix, Phoenix® WinNonlin®, and ADAPT from the University of Southern California (Monolix software website (http://www.lixoft.eu), WinNonlin® software website (http://pharsight.com/products/prod_winnonlin_trial.php), and ADAPT software website (https://bmsr.usc.edu/software/adapt/)).

Studies of myelosuppression and neutrophil dynamics from the pharmacometrics community have generally included MEMs into their analyses. The Friberg model of [36] incorporated population analysis from its initial publication and similarly for subsequent studies using this model [31, 45, 55, 98, 100, 135]. The TMDD and lifespan model studies of Krzyzanski [65, 67] also incorporated population parameter estimation as did the more physiologically oriented work of Vainas [131]. As noted in [94], the inclusion of variability and population models to the class of physiologically-based models is notoriously complex and remains a problem to solve. In line with this observation, the physiologically-based work of Parker and his collaborators[14, 46, 53, 97] were entirely deterministic. The Mackey group, which is firmly rooted in systems biological approaches to neutrophil modelling has also not included PopPK/PD into their approach. However, owing to their interest in neutrophil pathologies, recognition of individual variability has been addressed [16, 35]. Further, as seen in Chapter 3, there may be some flexibility as to the inclusion of PopPK/PD analysis in systems pharmacological approaches within certain frameworks.

1.14 Objectives

As mentioned in the Preface, this dissertation was motivated by an interest in improving clinical protocols of G-CSF administration for patients undergoing anti-cancer treatment. As put forward in the previous introductory sections, this is a multifaceted problem which has been addressed by a number of groups. The chief goal of this work is to answer to the needs of patients. However, to persuade clinicians and researchers of our findings, one also must respond to a number of methodological questions.

In the first portion of this dissertation (Chapter 2), the optimisation of G-CSF regimens in an oncological setting is carried out by the development and numerical analysis of the physiological model of neutrophil production which serves as the basis of this thesis.

Therein, we develop a combined physiological and PK/PD approach, demonstrate the model's predictive ability by comparison to clinical data, and optimise administration protocols for a specific treatment regimen.

Chapter 3 outlines the inclusion of IIV and IOV into the PK models of both the chemotherapeutic drug of interest (PM00104) but also filgrastim. In this section, we show that the physiological model is robust to PK variability.

Chapter 4 details the development of the DDE physiological model from an age-structured PDE model and describes the methods used for parameter estimation at homeostasis and in dynamic situations, like the exogenous administration of G-CSF. This article also develops a novel PK model for G-CSF using physiology as the basis.

The penultimate section of this dissertation (Chapter 5) examines the methodological implications of Chapters 2 through 4 and situates physiological modelling in the context of systems pharmacology. Finally, Chapter (6) presents conclusions and future perspectives.

References

[1] J.L. Abkowitz, A.E. Robinson, S. Kale, M.W. Long, and J. Chen. Mobilization of hematopoietic stem cells during homeostasis and after cytokine exposure. *Blood*, 102:1249–1253, 2003.

[2] T.L. Arvedson and M.J. Giffin. Structural biology of G-CSF and its receptor. In G. Molineux, T. Arvedson, and M. Foote, editors, *Twenty Years of G-CSF Clinical and Nonclinical Discoveries*. McGraw-Hill Companies, Inc., 2012.

[3] J.W. Athens, O.P. Haab, S.O. Raab, A.M. Mauer, H. Ashenbrucker, G.E. Cartwright, and M.M. Wintrobe. Leukokinetic studies. IV. The total blood, circulating, and marginal granulocyte pools and the granulocyte turnover rate in normal subjects. *Journal of Theoretical Biology*, 40:989–995, 1961.

[4] A.J. Atkinson, Jr and R.L. Lalonde. Introduction of quantitative methods in pharmacology and clinical pharmacology: A historical overview. *Clinical Pharmacology and Therapeutics*, 82:3–6, 2007.

[5] S. Basu, G. Hodgson, M. Katz, and A.R. Dunn. Evaluation of role of G-CSF in the production, survival, and release of neutrophils from bone marrow into circulation. *Blood*, 100:854–861, 2002.

[6] S. Beal and L.B. Sheiner. NONMEM I users guide. Technical report, Division of Clinical Pharmacology, University of California at San Fransisco, 1984.

[7] S. Bernard, J. Bélair, and M.C. Mackey. Oscillations in cyclical neutropenia: New evidence based on mathematical modeling. *Journal of Clinical Investigation*, 228: 1–16, 2015.

[8] G. Brooks, G.P. Langlois, J. Lei, and M.C. Mackey. Neutrophil dynamics after chemotherapy and G-CSF: The role of pharmacokinetics in shaping the response. *Journal of Theoretical Biology*, 315:97–109, 2012.

[9] R.P. Brown, M.D. Delp, S.L. Lindstedt, L.R. Rhomberg, and R.P. Beliles. Physiological parameter values for physiologically based pharmacokinetic models. *Toxicology Industrial Health*, 13:407–484, 1997.

[10] F. Burns and I. Tannock. On the existence of a G_0 phase in the cell cycle. *Cell Tissue Kinetics*, 3:321–334, 1970.

[11] W.A. Calder, editor. *Size, Function, and Life History*. Harvard University Press, London, 1984.

[12] Statistics Canada. New cases and Age-standardized Rate for Primary Cancer (Based on the May 2015 (CCR Tabulation File), by Cancer Type and Sex, Canada, Provinces and Territories, Annual, CANSIM (Database). Technical report, Statistics Canada, 2012.

[13] Canadian Cancer Society. Canadian Cancer Society's Advisory Committee on Cancer Statistics. Technical report, Canadian Cancer Society, Toronto, ON, 2015.

[14] Ho. *Modeling neutrophil dynamics in sepsis and cancer treatment*, Savannah, Georgia, USA, 2012. Chemical Process Control 8.

[15] M.J. Christopher and D.C. Link. Regulation of neutrophil homeostasis. *Current Opinion in Hematology*, 14:3–8, 2007.

[16] C. Colijn and M.C. Mackey. A mathematical model of hematopoiesis: II. Cyclical neutropenia. *Journal of Theoretical Biology*, 237:133–146, 2005.

[17] M. Craig, A.R. Humphries, J. Bélair, J. Li, F. Nekka, and M.C. Mackey. Neutrophil dynamics during concurrent chemotherapy and G-CSF administration: Mathematical modelling guides dose optimisation to minimise neutropenia. *Journal of Theoretical Biology*, 385:77–89, 2015.

[18] C. Csajka and D. Verotta. Pharmacokinetic–pharmacodynamic modelling: History and perspectives. *Journal of Pharmacokinetics and Pharmacodynamics*, 33:227–279, 2006.

[19] D.C. Dale. Neutropenia. In E. Beutler, M.A. Lichtman, B.S. Colelr, and T.J. Kipps, editors, *Williams Hematology*, volume 5. McGraw-Hill Companies, Inc., 1995.

[20] D.C. Dale and A.A. Bolyard. rHuG-CSF for the treatment of severe chronic neutropenia. In G. Molineux, T. Arvedson, and M. Foote, editors, *Twenty years of G-CSF Clinical and Nonclinical Discoveries*. McGraw-Hill Companies, Inc., 2012.

[21] D.C. Dale and M.C. Mackey. Understanding, treating and avoiding hematological disease: Better medicine through mathematics? *Bulletin of Mathematical Biology*, 77:739–757, 2015.

[22] D.C. Dale and K. Welte. Cyclic and chronic neutropenia. In G.H. Lyman and D.C. Dale, editors, *Hematopoietic Growth Factors in Oncology*. Springer, 2011.

[23] M. Danhof, E.C.M. de Lange, O.E. Della Pasqua, B.A. Ploeger, and R.A. Voskuyl. Mechanism-based pharmacokinetic-pharmacodynamic (PK-PD) modeling in translational drug research. *Trends in Pharmacogical Sciences*, 29:186–191, 2008.

[24] M. Davidson, Y.-I. Min, J.T. Holbrook, et al. Use of filgrastim as adjuvant therapy in patients with AIDS-related cytomegalovirus retinitis. *AIDS*, 16:757–765, 2002.

[25] H. Derendorf and B. Meibohm. Modeling of pharmacokinetic/pharmacodynamic (PK/PD) relationships: Concepts and perspectives. *Pharmaceutical Research*, 16: 176–185, 1999.

[26] P. Dua, E. Hawkins, and P.H. van der Graaf. A tutorial on target-mediated drug disposition (TMDD). *Clinical Pharmacology and Therapeutics: Pharmacometrics and Systems Pharmacology*, 4:324–337, 2015.

[27] C. Durand and P. Charbord. *Stem Cell Biology and Regenerative Medicine*, volume 3. River Publishers, Aalborg, Denmark, 2010.

[28] C.J. Eaves. Hematopoietic stem cells: Concepts, definition, and the new reality. *Blood*, 125:2605–2613, 2015.

[29] M.J. Egorin, D.A. Van Echo, M.Y. Whitacre, A. Forrest, L.M. Sigman, K.L. Engisch, and J. Aisner. Human pharmacokinetics, excretion, and metabolism of the

anthracycline antibiotic menogaril (7-OMEN,NSC 269148) and their correlation with clinical toxicities. *Cancer Research*, 46:1514–1520, 1986.

[30] C.L. Erickson-Miller, R.D. May, J. Tomaszewski, B. Osborn, M.J. Murphy, J.G. Page, and R.E. Parchment. Differential toxicity of camptothecin, toptecan, and 9-aminocamptothecin to human, canine, and murine myeloid progenitors (CFU-GM) *in vitro*. *Cancer Chemotherapy and Pharmacology*, 39:467–472, 1992.

[31] N.D. Evans, R.J. Dimelow, and J.W.T. Yates. Modelling of tumour growth and cytotoxic effect of docetaxel in xenografts. *Computer Methods and Programs in Biomedicine*, 114:e3–e13, 2014.

[32] FDA. Guidance for Industry, Exposure-response Relationships – Study Design, Data analysis, and Regulatory Applications. Technical report, U.S. Department of Health and Human Services, Food and Drug Administration, Center for Drug Evaluation and Research, Center for Biologics Evaluation and Research, Rockville, MD, USA, April 2003.

[33] C. Foley and M.C. Mackey. Dynamic hematological disease: A review. *Journal of Mathematical Biology*, 58:285–322, 2009.

[34] C. Foley and M.C. Mackey. Mathematical model for G-CSF administration after chemotherapy. *Journal of Theoretical Biology*, 257:27–44, 2009.

[35] C. Foley, S. Bernard, and M.C. Mackey. Cost-effective G-CSF therapy strategies for cyclical neutropenia: Mathematical modelling based hypotheses. *Journal of Theoretical Biology*, 238:756–763, 2006.

[36] L.E. Friberg and M.O. Karlsson. Mechanistic models for myelosuppression. *Investigational New Drugs*, 21:183–194, 2003.

[37] L.E. Friberg, C.J. Brindley, M.E. Karlsson, and A.J. Devlin. Models of schedule demandent haematological toxicity of 2'-deoxy-2'-methylidenecytidine (DMDC). *European Journal of Clinical Pharmacology*, 56:567–574, 2000.

[38] L.E. Friberg, A. Freijs, M. Sandström, and M.O. Karlsson. Semiphysiological model for the time course of leukocytes after varying schedule of 5-fluorouracil in rats. *Journal of Pharmacology and Experimental Therapeutics*, 295:734–740, 2000.

[39] R.C. Furze and S.M. Rankin. Neutrophil mobilization and clearance in the bone marrow. *Immunology*, 125:281–288, 2008.

[40] L.E. Gerlowski and R.K. Jain. Physiologically based pharmacokinetic modeling: Principles and applications. *Journal of Pharmaceutical Sciences*, 72:1103–1125, 1983.

[41] D.T. Gillespie. Exact stochastic simulation of coupled chemical reactions. *The Journal of Physical Chemistry*, 81:2340–2361, 1977.

[42] W.R. Gillespie. Noncompartmental versus compartmental modelling in clinical pharmacokinetics. *Clinical Pharmacokinetics*, 20:253–262, 1991.

[43] L. Glass and M.C. Mackey. Oscillation and chaos in physiological control systems. *Science*, 197:287–289, 1977.

[44] L. Glass and M.C. Mackey. Pathological conditions resulting from instabilities in physiological control systems. *Annals of the New York Academy of Sciences*, 316: 214–235, 1979.

[45] M. González-Sales, B. Valenzuela, C. Pérez-Ruixo, C. Fernández Teruel, B. Miguel-Lillo, Soto Matos A., et al. Population pharmacokinetic-pharmacodynamic analysis of neutropenia in cancer patients receiving PM00104 (Zalypsis®). *Clinical Pharmacokinetics*, 51:751–764, 2012.

[46] J.M. Harrold and R.S. Parker. Clinically relevant cancer chemotherapy dose scheduling via mixed-integer optimization. *Computers and Chemical Engineering*, 33:2042–2054, 2009.

[47] C. Haurie, M.C. Mackey, and D.C. Dale. Cyclical neutropenia and other periodic hematological diseases: A review of mechanisms and mathematical models. *Blood*, 92:2629–2640, 1998.

[48] C. Haurie, D.C. Dale, and M.C. Mackey. Occurrence of periodic oscillations in the differential blood counts of congenital, idiopthic, and cyclical neutropenic patients before and during treatment with G-CSF. *Experimental Hematology*, 27:401–409, 1999.

[49] C. Haurie, D.C. Dale, R. Rudnicki, and M.C. Mackey. Modeling complex neutrophil dynamics in the grey collie. *Journal of Theoretical Biology*, 204:504–519, 2000.

[50] T. Hearn, C. Haurie, and M.C. Mackey. Cyclical neutropenia and the peripherial control of white blood cell production. *Journal of Theoretical Biology*, 192:167–181, 1998.

[51] V. Hemmige, W.C. Liles, and D.L. Pitrak. Use of filgrastim (r-metHuG-CSF) in human immunodeficiency virus infection. In G. Molineux, T. Arvedson, and M. Foote, editors, *Twenty years of G-CSF Clinical and Nonclinical Discoveries*. McGraw-Hill Companies, Inc., 2012.

[52] A.V. Hill. The possible effects of the aggregation of the molecules of haemoglobin on its dissociation curves. *The Journal of Physiology: Proceedings of the Physiological Society*, 40:i–vii (suppl), 1910.

[53] T. Ho, G. Clermont, and R.S. Parker. A model of neutrophil dynamics in response to inflammatory and cancer chemotherapy challenges. *Computers and Chemical Engineering*, 51:187–193, 2013.

[54] N.H.G. Holford and K.E. Peace. Methodologic aspects of a population pharmacodynamic model for cognitive effects in Alzheimer patients treated with tacrine. *Proceedings of the National Academy of Science of the United States of America*, 89: 11466–11470, 1992.

[55] D. Jayachandran, A.E. Rundell, R.E. Hannemann, T.A. Vik, and D. Ramkrishna. Optimal chemotherapy for leukemia: A model-based strategy for individualized treatment. *PLoS ONE*, 9:e109623, 2014.

[56] B. Jilma, N. Hergovich, P. Stohlawetz, H.-G. Erichler, P. Bauer, and O.F. Wagner.

Circadian variation of granulocyte colony stimulating factor levels in man. *British Journal of Haematology*, 106:368–370, 1999.

[57] M.O. Karlsson and L.B. Sheiner. The importance of modeling interoccasion variability in population pharmacokinetic analyses. *Journal of Pharmacokinetics and Biopharmaceutics*, 21:735–750, 1993.

[58] M.O. Karlsson, R.E. Port, M.J. Ratain, and L.B. Sheiner. A population model for the leukopenic effect of etoposide. *Clinical Pharmacology and Therapeutics*, 57: 325–334, 1995.

[59] V. Karlsson, M.O. Molnar, J. Bergh, A. Reijs, and R. Larsson. A general model for time-dissociated pharmacokinetic-pharmacodynamic relation exemplified by paclitaxel myelosuppression. *Clinical Pharmacology and Therapeutics*, 63:11–25, 1998.

[60] K. Kaushansky. Hematopoietic stem cells, progenitors, and cytokines. In K. Kaushansky, M.A. Lichtman, E. Beutler, T.J. Kipps, U. Sligsohn, and J.T. Prchal, editors, *Williams Hematology*, volume 8. McGraw-Hill Companies, Inc., 2010.

[61] R.J. Keizer, M.O. Karlsson, and A. Hooker. Modeling and simulation workbench for NONMEM: Tutorial on Xpose. *CPT Pharmacometrics and Systems Pharmacology*, 2:e50, 2013.

[62] G. Koch, W. Krzyzanski, J.J. Pérez-Ruixo, and J. Schropp. Modeling of delays in PKPD: Classical approaches and a tutorial for delay differential equations. *Journal of Pharmacokinetics and Pharmacodynamics*, 41:291–318, 2014.

[63] C.T. Kouroukis, S. Chia, S. Verma, D. Robson, C. Desbiens, C. Cripps, and J. Mikhael. Canadian supportive care recommendations for the management of neutropenia in patients with cancer. *Current Oncology*, 28:9–23, 2008.

[64] A. Krinner, I. Roeder, M. Loeffler, and M. Scholz. Merging concepts - coupling an agent-based model of hematopoietic stem cells with an ODE model of granulopoiesis. *BMC Systems Biology*, 7:117, 2013.

[65] W. Krzyzanski and J.J. Pérez-Ruixo. Lifespan based indirect response models. *Journal of Pharmacokinetics and Pharmacodynamics*, 39:109–123, 2012.

[66] W. Krzyzanski, R. Ramakrishnan, and W.J. Jusko. Basic pharmacodynamic models for agents that alter production of natural cells. *Journal of Pharmacokinetics and Biopharmaceutics*, 27:467–489, 1999.

[67] W. Krzyzanski, P. Wiczling, P. Lowe, E. Pigeolet, M. Fink, A. Berghout, and S. Balser. Population modeling of filgrastim PK-PD in healthy adults following intravenous and subcutaneous administrations. *Journal of Clinical Pharmacology*, 9 Suppl:101S–112S, 2010.

[68] R. Lakshman and A. Finn. Neutrophil disorders and their management. *Journal of Clinical Pathology.*, 54:7–19, 2001.

[69] J.E. Layton and N.E. Hall. The interaction of G-CSF with its receptor. *Frontiers in Bioscience*, 31:177–199, 2006.

[70] J. Lei and M.C. Mackey. Multistability in an age-structured model of hematopoiesis: Cyclical neutropenia. *Journal of Theoretical Biology*, 270:143–153, 2011.

[71] T.A. Leil. A Bayesian perspective on estimation of variability and uncertainty in mechanism-based models. *Clinical Pharmacology and Therapeutics: Pharmacometrics and Systems Pharmacology*, 3:e121, 2014.

[72] G.J. Leischke, D. Grail, G. Hodgson, D. Metcalf, E. Stanley, C. Cheers, K.J. Fowler, S. Basu, Y.F. Zhan, and A.R. Dunn. Mice lacking granulocyte colony-stimulating factor have chronic neutropenia, granulocyte and macrophage progenitor cell deficiency, and impaired neutrophil mobilization. *Blood*, 84:1737–1746, 1994.

[73] L. Leone and M. Cruciani. Use of rHuG-CSF in infectious diseases. In G. Molineux, T. Arvedson, and M. Foote, editors, *Twenty years of G-CSF Clinical and Nonclinical Discoveries*. McGraw-Hill Companies, Inc., 2012.

[74] G. Levy. Pharmacologic targeted mediated drug disposition. *Clinical Pharmacology and Therapeutics*, 56:248–252, 1994.

[75] J. Li and F. Brauer. Continuous-time age-structured models in population dynamics and epidemiology. In F. Brauer, P. van den Driessche, and J. Wu, editors, *Mathematical Epidemiology*. Springer-Verlag, Berlin/Heidelberg, Germany, 2008.

[76] D.C. Link. Discovery of G-CSF and early clinical studies. In G. Molineux, T. Arvedson, and M. Foote, editors, *Twenty years of G-CSF Clinical and Nonclinical Discoveries*. McGraw-Hill Companies, Inc., 2012.

[77] K. Lovas, E. Knudsen, P.O. Iversen, and H.B. Benestad. Sequestration patterns of transfused rat neutrophilic granulocytes under normal and inflammatory condistions. *European Journal of Haematology*, 56:221–229, 1996.

[78] G.H. Lyman and D.C. Dale. Introduction to the hematopoietic growth factors. In G.H. Lyman and D.C. Dale, editors, *Hematopoietic Growth Factors in Oncology*. Springer, 2011.

[79] G.H. Lyman and J.M. Kleiner. Summary and comparison of myeloid growth factor guidelines in patients receiving cancer chemotherapy. In G.H. Lyman and D.C. Dale, editors, *Hematopoietic Growth Factors in Oncology*. Springer, 2011.

[80] M.C. Mackey. A unified hypothesis for the origin of aplastic anemia and periodic haematopoiesis. *Blood*, 51:941–956, 1978.

[81] M.C. Mackey. Cell kinetic status of haematopoietic stem cells. *Cell Proliferation*, 34:71–83, 2001.

[82] M.C. Mackey and I.G. Nechaeva. Noise and stability in differential delay equations. *Journal of Dynamics and Differential Equations*, 6:395–426, 1994.

[83] D.E. Mager and W.J. Jusko. General pharmacokinetic model for drugs exhibiting target-mediated drug disposition. *Journal of Pharmacokinetics and Pharmacodynamics*, 28:507–532, 2001.

[84] D.E. Mager and W. Krzyzanski. Quasi-equilibrium pharmacokinetic model for drugs exhibiting target-mediated drug disposition. *Pharmaceutical Research*, 22:1589–1596, 2005.

[85] V. Maholtra and M.C. Perry. Models of anti-cancer therapy. Classical chemotherapy: Mechanism, toxicities, and the therapeutic window. *Cancer Biology and Therapy*, 2:S2–S4, 2003.

[86] T.R. Medler, T. Cotechini, and L.M. Coussens. Immune response to cancer therapy: Mounting an effective antitumor respons and mechanisms of resistance. *Trends in Cancer*, 1:66–76, 2015.

[87] L. Michaelis and M.L. Menten. Die kinetik der invertinwirkung. *Biochemische Zeitschrift*, 49:333–369, 1913.

[88] R. Mick and M.J. Ratain. Modeling interpatient pharmacodynamic variability of etoposide. *Journal of the National Cancer Institute*, 83:1560–1564, 1991.

[89] H. Minami, Y. Saski, N. Saijo, T. Ohtsu, H. Fujii, T. Igarashi, and K. Itoh. Indirect-response model for the time course of leukopenia with anticancer drugs. *Clinical Pharmacology and Therapeutics*, 64:511–521, 1998.

[90] G.. Molineux. Granulocyte colony-stimulating factors. In G.H. Lyman and D.C. Dale, editors, *Hematopoietic Growth Factors in Oncology*. Springer, 2011.

[91] G. Molineux, T. Arvedson, and M. Foote. *Twenty years of G-CSF Clinical and Nonclinical Discoveries*. Springer Basel AG, Basel, Switzerland, 2012.

[92] A. Morley, E.A. King-Smith, and F. Stohlman. The oscillatory nature of hemopoiesis. In F. Stohlman, editor, *Hemopoietic Cellular Proliferation*. Grune and Stratton, New York, USA, 1969.

[93] J.M. Murray, editor. *Mathematical Biology I: An Introduction*, volume 3. Springer Science, USA, 2002.

[94] I. Nestorov. Whole body pharmacokinetic models. *Clinical Pharmacokinetics*, 42: 883–908, 2003.

[95] F. Notta, S. Zandi, N. Takayama, S. Dobson, O.I. Gan, G. Wilson, K.B. Kaufmann, J. McLeod, E. Laurenti, C.F. Dunant, J.D. McPherson, L.D. Stein, Y. Dror, and J.E. Dick. Distinct routes of lineage development reshape the human blood hierarchy across ontogeny. *Science Express*, 223:283–298, 2003.

[96] W.W. Pang, E.A. Price, D. Sahoo, I. Beerman, W.J. Maloney, D.J. Rossi, et al. Human bone marrow hematopoietic stem cells are increased in frequency and myeloid-biased with age. *Proceedings of the National Academy of Sciences of the United States of America*, 108:20012–20017, 2011.

[97] R.S. Parker. Modeling for anti-cancer chemotherapy design. *Journal of Process Control*, 17:576–582, 2007.

[98] M.L. Pastor, C.M. Laffont, L. Gladieff, E. Chatelut, and D. Concordet. Model-based approach to early predict prolonged high grade neutropenia in carboplatin-treated patients and guide G-CSF prophylactic treatment. *Pharmaceutical Research*, 32: 654–664, 2015.

[99] P. Ploeger, B.A. van der Graaf and M. Danhof. Incorporating receptor theory in mechanism-based pharmacokinetic-pharmacodynamic (PK-PD) modeling. *Drug Metabolism and Pharmacokinetics*, 24:3–15, 2009.

[100] A.L. Quartino, L.E. Friberg, and M.O. Karlsson. A simultaneous analysis of the time-course of leukocytes and neutrophils following docetaxel administration using a semi-mechanisitic myelosuppression model. *Investigational New Drugs*, 30:833–845, 2012.

[101] S.M. Rankin. The bone marrow: A site of neutrophil clearance. *Journal of Leukocyte Biology*, 88:241–251, 2010.

[102] C. Riether, C.M. Schürch, and A.F. Ochsenbein. Regulation of hematopoietic and leukemic stem cells by the immune system. *Cell Death and Differentiation*, 22: 187–198, 2015.

[103] L. Robb. Cytokine receptors and hematopoietic differentiation. *Oncogene*, 26:6715–6723, 2007.

[104] M. Rowland, C. Peck, and G. Tucker. Physiologically-based pharmacokinetics in drug development and regulatory science. *Annual Reviews in Pharmacological Toxicology*, 51:45–73, 2011.

[105] S. Rubinow and J. Lebowitz. A mathematical model of neutrophil production and control in normal man. *Journal of Mathematical Biology*, 1:187–225, 1975.

[106] S. Saraf and H. Ozer. Practice guidelines for the use of rHuG-CSF in an oncology setting. In G. Molineux, T. Arvedson, and M. Foote, editors, *Twenty Years of G-CSF Clinical and Nonclinical Discoveries*. McGraw-Hill Companies, Inc., 2012.

[107] S. Sarrazin and M. Sieweke. Integration of cytokine and transcription factor signals in hematopoietic stem cell commitment. *Seminars in Immunology*, 23:326–334, 2011.

[108] S.H. Saverymuttu, A.M. Peters, A. Keshavarzian, H.J. Reavy, and J.P. Lavender. The kinetics of 111Indium distribution following injection of 111Indium labeled autologous granulocytes in man. *British Journal of Haematology*, 61:1675–1685, 1985.

[109] S. Schirm, C. Engel, M. Loeffler, and M. Scholz. Modelling chemotherapy effects on granulopoiesis. *BMC Systems Biology*, 8:138, 2014.

[110] S. Schirm, C. Engel, M. Loeffler, and M Scholz. A combined model of human erythropoiesis and granulopoiesis under growth factor and chemotherapy treatment. *Theoretical Biology and Medical Modelling*, 11:24, 2014.

[111] S. Schmitz, H. Franke, M. Löffler, H.E. Wichmann, and V. Diehl. Reduced variance of bone-marrow transit time of granulopoiesis-A possible pathomechanism of human cyclic neutropenia. *Cell Proliferation*, 27:655–667, 1994.

[112] S. Schmitz, H. Franke, M. Löffler, H.E. Wichmann, and V. Diehl. Model analysis of the contrasting effects of GM-CSF and G-CSF treatment on peripheral blood neutrophils observed in three patients with childhood-onset cyclic neutropenia. *British Journal of Haematology*, 95:616–625, 1996.

[113] M. Scholz, S. Schirm, M. Wetzler, C. Engel, and M. Loeffler. Pharmacokinetic and -dynamic modelling of G-CSF derivatives in humans. *Theoretical Biology and Medical Modelling*, 9:1497–1502, 2012.

[114] G. Segre. Kinetics of interaction between drugs and biological systems. *Il Farmaco; Edizione Scientifica*, 23:907–918, 1968.

[115] L. Sheiner, B. Rosenberg, and K. Melmon. Modeling of individual pharmacokinetics for computer-aided drug dosage. *Computers and Biomedical Research*, 5:441–459, 1972.

[116] L.B. Sheiner, B. Rosenberg, and V.V. Marathe. Estimation of population characteristics of pharmacokinetic parameters from routine clinical data. *Journal of Pharmacokinetics and Biopharmaceutics*, 5:445–479, 1977.

[117] L.B. Sheiner, S. Beal, B. Rosenberg, and V.V. Marathe. Forecasting individual pharmacokinetics. *Clinical Pharmacology and Therapeutics*, 26:294–305, 1979.

[118] L.B. Sheiner, D.R. Stanski, S. Vozeh, R.D. Miller, and J. Ham. Simultaneous modeling of pharmacokinetics and pharmacodynamics: Application to d-tubocurarine. *Clinical Pharmacology and Therapeutics*, 53:358–371, 1979.

[119] E. Shochat and V. Rom-Kedar. Novel strategies for granulocyte colony-stimulating factor treatment of severe prolonged neutropenia suggested by mathematical modeling. *Clinical Cancer Research*, 14:6354–6363, 2008.

[120] E. Shochat, S.M. Stemmer, and L.A. Segel. Human haematopoiesis in steady state and following intense perturbations. *Bulletin of Mathematical Biology*, 64:861–886, 2002.

[121] E. Shochat, V. Rom-Kedar, and L.A. Segel. G-CSF control of neutrophils dynamics in the blood. *Bulletin of Mathematical Biology*, 69:2299–2338, 2007.

[122] C.W. Smith. Regulation of neutrophil homeostasis. In K. Kaushansky, M.A. Lichtman, E. Beutler, T.J. Kipps, U. Sligsohn, and J.T. Prchal, editors, *Williams Hematology*, volume 8. McGraw-Hill Companies, Inc., 2010.

[123] C.W. Smith. Production, distribution, and fate of neutrophils. In K. Kaushansky, M.A. Lichtman, J.T. Prchal, M.M. Levi, O.W. Press, L.J. Burns, and M. Caligiuri, editors, *Williams Hematology*, volume 9. McGraw-Hill Companies, Inc., 2016.

[124] K.M. Stadeli and D.D. Richman. Rates of emergence of HIV drug resistance in resource-limited settings: A systematic review. *Antiretroviral Therapy*, 18:115–123, 2013.

[125] F. Stohlman. *Hemopoietic Cellular Proliferation*. Grune and Stratton, New York, USA, 1969.

[126] S.E. Tett, N.H.G. Holford, and A.J. McLachlan. Population pharmacokinetics and pharmacodynamics: An underutilized resource. *Drug Information Journal*, 32:693–710, 1998.

[127] M.L. Thakur, J.P. Lavender, R.N. Arnot, D.J. Silverster, and A.W. Segal. Indium-111-labeled autologues leukocytes in man. *Journal of Nuclear Medicine*, 18:1014–1021, 1977.

[128] J.E. Till and E. McCullogh. A direct measurement of the radiation sensitivity of normal mouse bone marrow cells. *Radiation Research*, 14:213–222, 1961.

[129] D.G. Tubergen, C.F. Stewart, C.B. Pratt, W.C. Zamboni, N. Winick, V.M. Santan, Z.A. Dryer, J. Kurtzberg, B. Bell, H. Grier, and T.J. Viettei. Phase I trial and pharmacokinetic (PK) and pharmacodynamics (PD) study of toptecan using a five-day course in children with refractory solid tumors: A Pediatric Oncology Group Study. *Journal of Pediatric Hematology/Oncology*, 18:352–361, 1996.

[130] UNAIDS. Global Report: UNAIDS Report on the Global AIDS Epidemic. Technical report, The Joint United Nations Programme on HIV/AIDS, Geneva, Switzerland, 2012.

[131] O. Vainas, S. Ariad, O. Amir, W. Mermershtain, V. Vainstein, M. Kleiman, O. Inbar, R. Ben-Av, A. Mukherjee, S. Chan, and Z. Agur. Personalising docetaxel and G-CSF schedules in cancer patients by a clinically validated computational model. *British Journal of Cancer*, 107:814–822, 2012.

[132] V. Vainstein, Y. Ginosar, M. Shoham, D.O. Ranmar, A. Ianovski, and Z. Agur. The complex effect of granulocyte colony-stimulating factor on human granulopoiesis analyzed by a new physiologically-based mathematical model. *Journal of Theoretical Biology*, 235:311–327, 2005.

[133] P. van der Graaf and N. Benson. Systems pharmacology: Bridging systems biology

and pharmacokinetics-pharmacodynamics (PKPD) in drug discovery and development. *Pharmaceutical Research*, 28:1460–1464, 2011.

[134] S. von Vietinghoff and K. Ley. Homeostatic regulation of blood neutrophil counts. *Journal of Immunology*, 181:5183–5188, 2008.

[135] B. Wang, T.M. Ludden, E.N. Cheung, G.G. Schwab, and L.K. Roskos. Population pharmacokinetic-pharmacodynamic modeling of filgrastim (r-metHuG-CSF) in healthy volunteers. *Journal of Pharmacokinetics and Pharmacodynamics*, 28:321–342, 2001.

[136] A.C. Ward, Y.M. van Aesch, J. Gits, A.. Schelen, J.P. de Koning, D. van Leeuwen, M.H. Freedman, and I.P. Touw. Novel point mutation in the extracellular domain of the granulocyte colony-stimulating factor (G-CSF) receptor in a case of severe congenital neutropenia hyporesponsive to G-CSF treatment. *Journal of Experimental Medicine*, 190:497–507, 1999.

[137] K. Welte. Discovery of G-CSF and early clinical studies. In G. Molineux, T. Arvedson, and M. Foote, editors, *Twenty Years of G-CSF Clinical and Nonclinical Discoveries*. McGraw-Hill Companies, Inc., 2012.

[138] E.M.P. Widmark. Studies in the concentration of indifferent narcotics in blood and tissues. *Acta Medica Scandinavica*, 52:205–225, 1919.

[139] X. Wu, J. Li, and F. Nekka. Closed form solutions and dominant elimination pathways of simultaneous first-order and Michaelis-Menten kinetics. *Journal of Pharmacokinetics and Pharmacodynamics*, 42:151–161, 2015.

[140] X. Wu, F. Nekka, and J. Li. Steady-state volume of distribution of some two compartmental models with immediate linear and saturated eliminations., Under review.

[141] R. Yamamoto, Y. Morita, J. Ooehara, S. Hamanaka, M. Onodera, K.L. Rudolph, H. Ema, and H. Nakauchi. Clonal analysis unveils self-renewing lineage-restricted progenitors generated directly from hematopoietic stem cells. *Cell*, 154:1112–1126, 2013.

[142] K. Yamaoka, T. Nakagawa, and T. Uno. Statistical moments in pharmacokinetics. *Journal of Pharmacokinetics and Biopharmaceuticals*, 6:547–558, 1978.

[143] L. Yuh, S. Beal, M. Davidian, F. Harrison, A. Hester, K. Kowalski, E. Vonesh, and R. Wolfinger. Population pharmacokinetic/pharmacodynamics methodology and applications: A bibliography. *Biometrics*, 50:566–575, 1994.

[144] J. Zhu and S.G. Emerson. Hematopoietic cytokines, transcription factors and lineage commitment. *Oncogene*, 21:3295–3313, 2002.

The focus of the following article was the improvement of rhG-CSF regimens during anti-cancer treatment. For this, we developed a physiological DDE model of granulopoiesis and incorporated PK/PD models of filgrastim and Zalypsis®, a chemotherapeutic drug. Using no statistical parameter fitting, we successfully reproduced clinical data of 172 patients undergoing CHOP14 chemotherapy treatment, which prescribes 10 filgrastim administrations per cycle. We then optimised dosing regimens by demonstrating that delaying filgrastim administration post-chemotherapy improves the ANC nadir for an average patient. This work was published in the *Journal of Theoretical Biology* (Craig, M., Humphries, A.R., Nekka, F., Bélair, J., Li, J., and Mackey, M.C. (2015). *Journal of Theoretical Biology, 385*. 77–89).

As the earliest study in this thesis, some clarification should be given for specific passages which were not necessarily fully elaborated due to space constraints. Specifically "a downside of using transit compartment models to study neutrophil dynamics is the dependency of the parameters on the data upon which they are constructed" could be expanded upon. Here the intention is to impress upon the reader that given the quality of the data collected for any particular study, the parameter estimates could widely vary (as mentioned following this passage in the text). The point can be made that without a physiological guidance as to a range of possible values, statistical techniques may only rely on minimisation of the objective function [29]. Although there may be widely accepted approaches (for example, least squares or maximum likelihood optimisation [29]), the question remains as to the appropriate definition of the objective function and the suitable tolerance of its minimisation. Further, the assertion that "the resulting physiological models, which do not generally depend on specific patient datasets for their parameter estimation, are flexible across pathologies and across clinical scenarios," highlights what differentiates first-principles modelling approaches from more traditional ones often applied in PK/PD modelling. Systems approaches can more easily be applied to different scenarios (be they drug regimens or diseases) because of their generic nature and their dependency on the physiology which determines their structure. Since the underlying nature of the system does not generally undergo structural changes, physiological models can be implemented in the study of new diseases without changes to their framework but to their parameter values, which can again be ascertained by the prior method of estimation. Nonetheless, it

is paramount that models in translational research remain capable of characterising and quantifying data, which is where the traditional PK/PD approaches continue to play a role. The conclusions drawn in Chapter 5 serve as an elaboration of the point raised in this passage, namely that traditional empirical approaches in pharmacology need to be developed in tandem with mechanistic and physiologically driven modelling approaches to ensure a well-rounded pharmacometric stratagem is applied to decision-making in drug development and the betterment of patient outcomes.

Chapter 2

Neutrophil Dynamics During Concurrent Chemotherapy and G-CSF Administration: Mathematical Modelling Guides Dose Optimisation to Minimise Neutropenia

Morgan Craig[1,2], Antony R. Humphries[2,3], Fahima Nekka[1,2], Jacques Bélair[2,4], Jun Li[1,2], Michael C. Mackey[2,5]

[1]Faculté de Pharmacie, Université de Montréal, Montréal, QC, Canada H3T 1J4, [2]Centre for Applied Mathematics in Bioscience and Medicine (CAMBAM), McGill University, Montreal, QC, Canada H3G 1Y6, [3]Department of Mathematics and Statistics, McGill University, Montreal, QC, Canada H3A 0B9, [4] Département de mathématiques et de statistique, Université de Montréal, Montréal, QC, Canada H3T 1J4, [5] Departments of Physiology and Physics, McGill University, Montreal, QC, Canada H3G 1Y6

Keywords

myelopoiesis; physiological mathematical modelling; pharmacokinetics; pharmacodynamics

Abstract

The choice of chemotherapy regimens is often constrained by the patient's tolerance to the side effects of chemotherapeutic agents. This dose-limiting issue is a major concern in dose regimen design, which is typically focused on maximising drug benefits. Chemotherapy-induced neutropenia is one of the most prevalent toxic effects patients experience and frequently threatens the efficient use of chemotherapy. In response, granulocyte colony-stimulating factor (G-CSF) is co-administered during chemotherapy to stimulate

neutrophil production, increase neutrophil counts, and hopefully avoid neutropenia. Its clinical use is, however, largely dictated by trial and error processes. Based on up-to-date knowledge and rational considerations, we develop a physiologically realistic model to mathematically characterise the neutrophil production in the bone marrow which we then integrate with pharmacokinetic and pharmacodynamic (PKPD) models of a chemotherapeutic agent and an exogenous form of G-CSF (recombinant human G-CSF, or rhG-CSF). In this work, model parameters represent the average values for a general patient and are extracted from the literature or estimated from available data. The dose effect predicted by the model is confirmed through previously published data. Using our model, we were able to determine clinically relevant dosing regimens that advantageously reduce the number of rhG-CSF administrations compared to original studies while significantly improving the neutropenia status. More particularly, we determine that it could be beneficial to delay the first administration of rhG-CSF to day seven post chemotherapy and reduce the number of administrations from ten to three or four for a patient undergoing 14-day periodic chemotherapy.

2.1 Introduction

Mammalian hematopoiesis is an ideal system in which to study the control of cellular proliferation and differentiation. This is because of the rapid division of hematopoietic precursor cells and the morphologically well characterised stages that these cells go through in their progression to mature and functional white cells, red cells and platelets. Just as experimentalists have exploited these characteristics in their laboratory studies, so have biomathematicians utilised this system to sharpen their modelling tools to understand hematological dynamics drawing on a spectrum of clinically interesting diseases in their quest to understand the nature of hematopoietic control [12, 17]. These dynamics include a variety of periodic hematological diseases [12] as well as the observed response of the normal hematopoietic system to periodic perturbation as a side effect of chemotherapy [3, 44].

Chemotherapy is widely used to reduce the spread of malignant cells by interrupting their growth and eventual proliferation. Unfortunately the nonselective nature of chemotherapeutic drugs also disrupts development in non-malignant cell lines, including

the blood cells. Neutropenia, a condition characterised by a diminished number of neutrophils, is a common dose-limiting side effect of chemotherapy. In this acute condition, the production of neutrophils in the bone marrow is disrupted. In a healthy individual, circulating neutrophils are created from the commitment of a hematopoietic stem cell (HSC), which undergoes division, maturation, and remain in a reservoir within the bone marrow before being released into the systemic circulation. Patients with low neutrophil counts are susceptible to infection, and to stimulate the production of neutrophils post-chemotherapy, recombinant human granulocyte colony-stimulating factor (rhG-CSF) is administered.

In this paper, we adopt a phenomenological physiological modelling approach to granulopoiesis. Herein, we extend our previous modelling of the regulation of neutrophil dynamics [3, 12, 44] in three significantly novel ways. First, we take into account the sequestering of mature neutrophils into a reservoir in the bone marrow before their release into circulation, which is crucial for the rapid mobilisation of the neutrophils into the plasma. Second, we account for the marginated pool of neutrophils in the blood, leading to increased accuracy in the parameter estimation and a greater correspondence between the parameters and the physiology. Finally, we include a physiologically realistic representation of the action of a recently developed chemotherapeutic drug (Zalypsis®), and extend our previous models for the effects of rhG-CSF. These extensions to previous work on neutrophil dynamics, combined with our determination of relevant model parameters from the physiological and clinical literature, have led to a model that is physiologically realistic and comprehensive.

A number of authors have previously addressed the issue of post-chemotherapy neutropenia through mathematical models, with or without the administration of rhG-CSF (see [3, 11, 13, 18, 23, 37, 42] among others). Within these, a range of methodologies is used to study the dynamics of neutrophils, including the similarly named but conceptually divergent physiological modelling and physiologically-based modelling, both of which are described below.

Physiological modelling techniques arise frequently in systems biology, where the system of interest is modelled using an appropriate framework (a variety of differential equation approaches, difference equations etc.) and parameters are identified from a variety of data sources. Accordingly, the importance of physiological models in pharmacometric

applications has increased over the past fifteen years [24]. Typically, these models are constructed using a set of hypotheses (first principles) related to the mechanisms of the system of interest before parameter estimation occurs. In the case of hematopoiesis, delay differential equation (DDE) models are a natural representation as a result of the presence of delays in the system, and a variety of authors have applied this approach to model neutrophil development including Brooks et al. [3], Foley and Mackey [11], Vainas et al. [41], and Vainstein et al. [42]. The resulting physiological models, which do not generally depend on specific patient datasets for their parameter estimation, are flexible across pathologies and across clinical scenarios [6, 12, 24]. Additionally, we have also recently shown that this class of mechanistic models demonstrate a robustness to PK variability, thereby underlining their rational construction and establishing their utility in clinical settings by extending their applicability to the population level [7].

Physiologically-based pharmacokinetic (PBPK) models aim to track drug disposition in the body by tracking the complex drug transport interactions in a physiologically-realistic way [29]. While traditional pharmacokinetic (PK) modelling is based on the optimisation to patient data, generally using mixed effects modelling (MEM) statistical techniques, PBPK uses a mix of both empirical (as in the traditional case) and mechanistic knowledge of the physiological system to predict drug concentrations. The resulting PBPK models use a system of ordinary differential equations to relate the flow of blood (and therefore drug concentrations) using mass-balance. It is generally recognised that PBPK models provide more insight into the physiological origin of drug disposition than traditional empirical models but the implementation of variability, especially population-level variability, persists in being an important consideration [29]. Notwithstanding the increased level of anatomical detail present in PBPK models, the problem of relating the drug's concentration to its effect persists. While PBPK models incorporate more detailed physiological considerations by describing the drug disposition process to closely mimic the true corporal processes, physiological models generally target the dynamic evolution of cells and their interaction with the drug. In the case of hematopoiesis, models for the pharmacodynamic (PD) effects of chemotherapy and/or G-CSF on the neutrophil system are generally based on the semi-mechanistic model of Friberg and Karlsson [13]. Therein, the developmental stages of the marrow neutrophils are modelled using transit compartments and the de-

lays present in the system are estimated using MEM. Several authors have since adapted and extended this model and incorporated PBPK approaches to optimise chemotherapy treatment using optimal control theory [16], and even to study separate pathologies, notably sepsis [5, 40]. These models take a range of signalling pathways and cell populations (stromal cells, T-cells) into consideration and provide more physiological accuracy than traditional PK approaches. A downside of using transit compartment models to study neutrophil dynamics is the dependency of the parameters on the data upon which they are constructed. For example, the mean transit time of the neutrophils in the marrow estimated by MEM techniques varies greatly [13, 15, 35], while irradiation studies of neutrophil development in the bone marrow reveal much more consistent neutrophil transit times [9, 34]. Further, phenomenological insight into the origins of given effects, like the increased speed of maturation, and the correspondence of the model's parameters to a physiological meaning can be absent, implying that more traditional PKPD models are not able to predict long-term drug effects [41].

By adopting a physiological approach in this work, we reproduce recently published data on the temporal neutrophil response in a population of 172 patients receiving periodic chemotherapy every 14 days *without any model fitting to the data*. Furthermore, using this extended model for neutrophil regulation we have examined the response of the model to the administration of rhG-CSF following simulated chemotherapy. We predict that a significant reduction (from 10 to 3 or 4) in the number of days of administration of rhG-CSF will still result in a clinically satisfactory outcome. If this prediction is borne out in a clinical setting it will have a significant impact on the cost of post-chemotherapy treatment, as well as decreasing patient inconvenience.

This paper is structured as follows: Section 2.2.1 provides the motivation and details the construction of the myelopoiesis model by updating our group's previously published works ([3, 6] and [11]). Section 2.2.2 develops the pharmacokinetic models for both the chemotherapeutic drug Zalypsis®and rhG-CSF (filgrastim) which have been adapted from previously developed models (particularly [15] and [21]). The hematopoietic effect of both drugs is modelled in Section 2.2.3.1. Results are presented in Section 2.3, where the model is first validated against published data on a population of 172 patients receiving chemotherapy (Section 2.3.2.1) and then used to examine dose optimisation (Sec-

tion 2.3.2.2). The paper concludes with a discussion of our findings in Section 4.7. Details on the estimation of model parameter from the physiological and clinical literature are to be found in the Appendix.

2.2 The Model

2.2.1 Development of a Physiological Model of Granulopoiesis

In the following, the reader may find it useful to refer to the schematic representation of neutrophil production in Figure 3.1. The production of a single neutrophil from an HSC in the bone marrow can be summarised into five distinct steps: differentiation, proliferation, maturation, sequestration, and exit, whether by random loss or through entry into the blood stream/tissues. Once in circulation, neutrophils die at random through apoptosis. The physiological model we present here is an extension of previously proposed models ([3, 11] and [23]), with the notable addition of a neutrophil reservoir that holds newly mature neutrophils in the bone marrow so the body may react rapidly in response to falling neutrophil blood counts or infection [14, 36]. Our model also differs from the models in [3, 11] and [23] by accounting for the difference in the sizes of the total blood neutrophil pool and the circulating neutrophil pool due to margination.

The production of circulating neutrophils begins with the hematopoietic stem cells (HSCs, population Q in units of 10^6 cells/kg). The HSCs are generally considered to be in the quiescent stage, though they may enter the proliferative stage at rate β (days^{-1}) which occupies a period of τ_S (days), differentiate into the neutrophil line at a rate $\kappa_N(N)$ (units days^{-1}), or enter the erythroid or platelet lineages at a rate of κ_δ (days^{-1}). The HSCs undergo apoptosis at rate γ_S (days^{-1}) during their proliferative phase and their total amplification during their proliferative phase is given by $A_Q(t)$. Once committed to the neutrophil lineage, cells divide at rate η_{NP} (days^{-1}) before entering a maturing phase with variable aging velocity $V_N(t)$ where they remain for a period of $\tau_{NM}(t)$ days. Upon beginning the maturation process, neutrophil precursors grow in volume but are no longer proliferating and experience random cell death at a rate of γ_{NM} (days^{-1}). The total amplification of committed precursors is $A_N(t)$. Once mature, cells do not exit the bone marrow directly but are sequestered into a reservoir pool (population N_r in units of 10^9 cells/kg) and a steady stream of reserved, mature neutrophils transition into the blood with rate

$f_{trans}(G(t))$ (in units of days^{-1}) which depends on the circulating concentration of G-CSF ($G(t)$ in ng/mL). Indeed, in the case of reduced circulating numbers or infection, G-CSF concentrations rise and mature neutrophils are rapidly mobilised from the reserve pool. Cells that do not reach the blood exit the reservoir pool at a rate γ_{Nr} (days^{-1}). Neutrophils in the blood may be circulating or marginated. We let N (in units of 10^9 cells/kg) be the size of the total blood neutrophil pool (TBNP) which is composed of both the circulating neutrophil pool (CNP) and the marginated neutrophil pool (MNP). We assume free exchange and identical kinetics in the CNP and MNP, and also that the ratio of their sizes is constant over time. Neutrophils (population N in units of 10^9 cells/kg) are then removed from the TBNP at a rate of γ_N days^{-1}. This implies that the average lifespan of a neutrophil within the TBNP is $1/\gamma_N$. Overall, the time from the entrance of a stem cell into the neutrophil line to the exit of progeny into the blood is $\tau_N = \tau_{NP} + \tau_{NM}(t)$ (days).

The entire process of granulopoiesis is regulated by G-CSF, which stimulates entry into the neutrophil lineage, promotes proliferation, speeds up maturation, and increases mobilisation from the reservoir pool. The circulating neutrophils and the concentration of G-CSF are under constant feedback control so the concentration of G-CSF is increased when neutrophil counts decrease, thereby stimulating the production of more neutrophils to be released into the circulation which, in turn, reduces G-CSF levels.

In our model, the production of neutrophils is described by a system of three differential equations describing the temporal evolution of hematopoietic stem cells ($Q(t)$), the mature neutrophil reservoir pool in the marrow ($N_r(t)$), and the total blood neutrophil pool ($N(t)$). Two of these differential equations involve delays and so the model is described by a system of delay differential equations (DDEs). The equations are derived from an age-structured partial differential equation (PDE) model with appropriate boundary conditions. Careful attention must be paid here to the derivation of the DDEs from the PDEs due to the dependency of the maturation speed upon G-CSF, implying that we are dealing with an age-structured model with variable aging rate and threshold maturation condition. A detailed derivation can be found in [8] and explanations of all of the parameters can be found in Table 2.I.

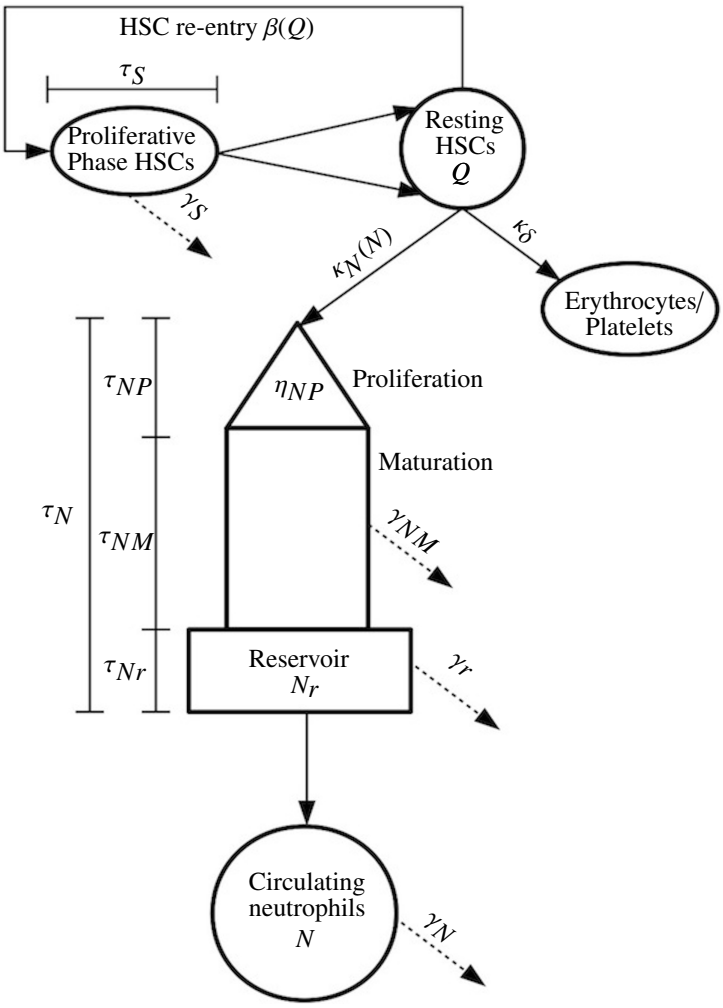

Figure 2.1 – Schematic representation of the production of circulating neutrophils in the bone marrow. Stem cells (Q) undergo the usual cell cycle and mitosis (at rate $\beta(Q)$) where they die at rate γ_S or return to the quiescent stage. They then remain at rest until differentiation into the neutrophil lineage (at rate $\kappa_N(N)$) or other blood lines at rate κ_δ. After entering the neutrophil lineage, a period of successive divisions (proliferation) at rate η_{NP} is followed by a maturing phase with velocity V_N. The mature neutrophils then reach the neutrophil reservoir (N_r) in the bone marrow. Mature reserved cells are maintained within the bone marrow for rapid mobilisation if needed [14]; the rate of transfer from the pool into the circulation (f_{trans}) is determined by G-CSF concentrations in the central compartment (plasma). Mature reserved neutrophils that do not reach the circulation die from the reservoir at rate γ_{Nr}. Circulating neutrophils N disappear from the circulation by apoptosis at rate γ_N. The time for the hematopoietic stem cell proliferative phase cycle is τ_S. The process of the development of a neutrophil takes time τ_N from their entry into the neutrophil line to their appearance in the blood, which includes the time for proliferation (τ_{NP}), maturation (τ_{NM}), and marrow sequestration (τ_{Nr}).

The model's equations are given by

$$\frac{dQ(t)}{dt} = -\left(\kappa_N(N(t)) + \kappa_\delta + \beta(Q(t))\right) Q(t) + A_Q(t)\beta\left(Q(t-\tau_S)\right) Q(t-\tau_S) \quad (2.1)$$

$$\frac{dN_r(t)}{dt} = A_N(t)\kappa_N(N(t-\tau_N))Q(t-\tau_N)\left(\frac{V_N(G(t))}{V_N(G(t-\tau_{NM}(t)))}\right) - \Big(\gamma_{Nr} + f_{trans}(G(t))\Big) N_r(t) \quad (2.2)$$

$$\frac{dN(t)}{dt} = f_{trans}(G(t))N_r(t) - \gamma_N N(t). \quad (2.3)$$

The remaining terms of Equations (3.1)–(3.3) will be defined later in this section. Herein, the initial condition of the above equations is taken to be homeostasis ($Q(t) = Q^{homeo}$, $N_r(t) = N_r^{homeo}$, $N(t) = N^{homeo}$, for all $t \leqslant t_0$, where t_0 marks the beginning of treatment). In our model $N(t)$ represents the total blood neutrophil pool (TBNP). If we are interested in only circulating neutrophil numbers for comparison with clinical measurements, we simply multiply $N(t)$ by the fraction of circulating cells. This calculation is detailed in Appendix A.

Neutrophils are relatively large and have long transit times through smaller capillaries, particularly in the lungs and spleen, which largely results in their nonuniform distribution in the blood, and the difference in the size of the circulating neutrophil pool (CNP) as measured from blood samples, and the TBNP. In the models of [3, 11] and [23] the quantity $N(t)$ was taken to directly represent the CNP, but like us they modelled the total production of neutrophils in the bone marrow. However, since the size of the CNP is significantly smaller than the TBNP, the models in [3, 11] and [23] required very large apoptosis rates in the maturation phase of the neutrophils. Essentially, in those models the neutrophils that should have been destined for the marginated neutrophil pool (MNP) in the blood were instead removed from the maturation phase by apoptosis, since those models contained no MNP for those cells to enter. By letting $N(t)$ represent the total blood neutrophil pool in the current model we avoid the necessity of artificially elevated apoptosis rates in the maturation phase and mature neutrophil reservoir pool.

In the current model above, we have that

$$\beta(Q) = f_Q \frac{\theta_2^{s_2}}{\theta_2^{s_2} + Q^{s_2}} \tag{2.4}$$

$$\kappa_N(N) = f_N \frac{\theta_1^{s_1}}{\theta_1^{s_1} + N^{s_1}}, \tag{2.5}$$

and the previously mentioned amplification rates of the stem cells ($A_Q(t)$) and of the neutrophils ($A_N(t)$) are defined as

$$A_Q(t) = 2 \exp\left[-\int_{t-\tau_S}^{t} \gamma_S(s) ds\right] \tag{2.6}$$

$$A_N(t) = \exp\left[\int_{t-\tau_N(t)}^{t-\tau_N(t)+\tau_{NP}} \eta_{NP}(s) ds - \int_{t-\tau_N(t)+\tau_{NP}}^{t} \gamma_{NM}(s) ds\right]. \tag{2.7}$$

Numerical implementation of the amplification rates of Equations (4.7) and (4.14) is obtained by differentiating the integral expressions to obtain the following DDEs

$$\frac{dA_Q}{dt} = A_Q(t)\left[\gamma_S(t-\tau_S) - \gamma_S(t)\right], \tag{2.8}$$

$$\frac{dA_N}{dt} = A_N(t)\left[\left(1 - \frac{d\tau_N(t)}{dt}\right)\right. \tag{2.9}$$

$$\times \left.\left(\eta_{NP}(t-\tau_N(t)+\tau_{NP}) + \gamma_{NM}(t-\tau_N(t)+\tau_{NP}) - \eta_{NP}(t-\tau_N(t))\right) - \gamma_{NM}(t)\right],$$

where $d\tau_N(t)/dt$ is defined by Equation (3.20) detailed below (the temporal-evolution of the maturing phase delay depends on the speed of maturation). The initial conditions of Equation (4.39) and Equation (4.15) are the homeostatic value of the amplification rates (i.e. A_Q^{homeo} and A_N^{homeo}).

2.2.2 Pharmacokinetic Modelling

2.2.2.1 Zalypsis®Pharmacokinetics

Zalypsis®is a cytotoxic agent whose mechanism of action is thought to disrupt the cell cycle and inhibit transcription through binding to cells' DNA [30]. It has been shown to

have a significant killing action in several tumour sites *in vivo* while demonstrating strong suppression of proliferation *in vitro* [30]. The population pharmacokinetic (PopPK) study of [30] determined that a four-compartment model significantly improved the fit of the mixed effect model when compared to a three-compartment model, implying that the drug is highly distributed in the tissues. It was further determined that Zalypsis®has but one principal channel of elimination from the central compartment. This same study also concluded that no covariates were linked to the pharmacokinetics of Zalypsis®, meaning that the physical parameters selected for investigation were not found to influence interindividual variability in the model.

Using the commonly relied-upon transit compartment model of the neutrophil lineage of [13], it has been reported that a power function effects model was sufficient to reproduce the neutropenic effects of Zalypsis®*in vivo* [15]. The same study also identified two equivalently optimal dosing regimens for the administration of Zalypsis®, having determined that the incidence and severity of the drug's neutropenic effects were both dose- and frequency-dependent. Owing to this dose-dependency, a more frequent dosing schedule per chemotherapy cycle was determined to be possible providing the total dose remained unchanged over a full chemotherapy treatment cycle of 12 weeks. For the phase II clinical trial, the authors reported that a 2.0 mg/m^2 dose administered over a 1-h infusion three times per 28 day cycle (on days 1, 8, and 15) produced similar neutropenic effects as a 4.0 mg/m^2 dose infused over 1-h once every 21 days [15].

As previously mentioned, a four-compartment Pop-PK model of Zalypsis®was found to best fit the available data and was subsequently accepted for PopPK and PopPKPD analyses ([15, 30]). These four compartments represent drug molecules that distribute to and from the plasma into fast-exchange and slow-exchange tissues before inevitably being cleared from the blood. Accordingly, we adapt this four-compartment model in this work. The PK model is given by the following system of ODEs

$$\frac{dC_p}{dt} = \frac{Dose_{Zal}}{\Delta_t} + k_{21}C_{\text{fast}} + k_{31}C_{\text{slow}_1} - (k_{12} + k_{13} + k_{el_C})C_p \quad (2.10)$$

$$\frac{dC_{\text{fast}}}{dt} = k_{12}C_p + k_{42}C_{\text{slow}_2} - (k_{21} + k_{24})C_{\text{fast}} \quad (2.11)$$

$$\frac{dC_{\text{slow}_1}}{dt} = k_{13}C_p - k_{31}C_{\text{slow}_1} \quad (2.12)$$

$$\frac{dC_{\text{slow}_2}}{dt} = k_{24}C_{\text{fast}} - k_{42}C_{\text{slow}_2}, \quad (2.13)$$

where C_p is the systemic concentration of Zalypsis®(traditionally referred to as the central or first compartment), C_{fast} is the concentration of Zalypsis®in the fast-exchange tissues (second compartment), and C_{slow_1} and C_{slow_2} are the concentrations in the slow-exchange tissues (third and fourth compartments, respectively), k_{ij} are constants expressing the rate of transfer between the i^{th} and j^{th} compartments, and k_{el_C} is the rate of elimination from the central compartment. As is typical in PK studies, this rate of elimination can be expressed as $k_{el} = \frac{Cl}{V_1}$, or the rate of clearance Cl over the volume of the central compartment V_1. The rate of IV infusion of Zalypsis®is the division of the IV dose ($Dose_{Zal}$) by the duration of the infusion Δ_t (typically one hour).

2.2.2.2 G-CSF Pharmacokinetics

Filgrastim is a commercially-available form of rhG-CSF which is used in diverse applications including as an adjuvant to promote neutrophil production during chemotherapy. It acts as endogenous G-CSF but is an unglycosylated molecule which is cleared quickly (half-life of around 3.5 hours) by the kidneys [1]. Its clinical administration is mainly subcutaneous and it is available in two formats (300 μg and 480 μg), implying that administered doses calculated per body weight are rounded to the nearest size to minimise waste [1, 26]. Current dosing protocols state that the administration of filgrastim should begin one day post-chemotherapy and continue until neutrophil counts reach 10 000 mm^{-3} [1], though its clinical use can vary based on institutional practices and may be administered for between 7 to 10 days post-chemotherapy [26].

We express the changes in concentration of circulating G-CSF by accounting for G-CSF concentrations entering the blood stream ($G(t)^{in}$) and G-CSF concentrations exiting the

blood stream ($G(t)^{out}$) per unit time

$$\frac{dG(t)}{dt} = \frac{dG(t)^{in}}{dt} - \frac{dG(t)^{out}}{dt},$$

where

$$G(t)^{in} = G(t)^{endo} + G(t)^{admin}$$
$$G(t)^{out} = R^{ren} + R^{int}.$$

The endogenous production rate of G-CSF is believed to be constant [10, 19], implying that

$$G(t)^{endo} = G_{prod},$$

where G_{prod} (in ng/mL/day) is the zero-order rate of endogenous production. In oncological settings, rhG-CSF is administered subcutaneously and several authors have proposed models for fractionated absorption after subcutaneous administration (see, for example, [28] and [33]). We selected the model of [21], which neglects a subcutaneous pool compartment in favour of a decreasing exponential rate of diffusion from the subcutaneous tissue, because it did not introduce additional compartments to the filgrastim model:

$$G(t)^{admin} = \frac{k_a F(Dose_{GCSF})}{V_d} e^{-k_a t_{inj}}. \tag{2.14}$$

Through the term $e^{-k_a t_{inj}}$ (t_{inj} being the time since the subcutaneous injection), the amount of rhG-CSF absorbed from the subcutaneous pool decreases with increasing time. Here F is the bioavailable fraction, $Dose_{GCSF}$ is the administered dose (ng), k_a is the absorption constant (days^{-1}), and V_d is the volume of distribution (mL).

The removal of G-CSF from the body is accomplished through two mechanisms: by renal elimination and through binding and internalisation by the neutrophils [3, 22]. We account for the renal elimination with

$$R^{ren} = k_{ren} G(t),$$

where k_{ren} is the first-order rate constant of renal elimination. The internalisation of G-CSF by the neutrophils is modelled using the Hill equation for receptor-complex formation. Since G-CSF binds to neutrophil receptor sites with a 2:2 stoichiometry [22], the Hill coefficient for the receptor dynamics is taken to be 2. We then have

$$R^{int} = k_{int}\frac{G^2(t)}{G^2(t) + K_D^2}N(t), \tag{2.15}$$

where k_{int} is the rate of internalisation and K_D is the usual dissociation constant. Hence

$$G(t)^{in} = G_{prod} + \frac{k_a F(Dose_{GCSF})}{V_d}e^{-k_a t_{inj}}$$
$$G(t)^{out} = k_{ren}G(t) + k_{int}\frac{G^2(t)}{G^2(t) + K_D^2}N(t)$$

and, finally, the model for the pharmacokinetics of G-CSF is given by

$$\frac{dG(t)}{dt} = \frac{k_a F(Dose_{GCSF})}{V_d}e^{-k_a t_{inj}} + G_{prod} - k_{ren}G(t) - \chi k_{int}\frac{G(t)^2}{G(t)^2 + K_D^2}N(t), \tag{2.16}$$

where $\chi = G^{homeo}/N^{homeo}$ (with G^{homeo} the homeostatic concentration of G-CSF and similarly for N^{homeo}) is a normalisation factor necessary to obtain the equilibrium at homeostatic conditions (absence of rhG-CSF administration–refer to Appendix A).

2.2.3 Determination of Pharmacodynamic Models for Drug Effects

Generally speaking, the usual empirical Michaelis-Menten and Hill equations serve to model most PD effects in this section.

2.2.3.1 Myelosuppressive Effects of Chemotherapy

Since chemotherapy usually acts to disrupt cellular division, we assume that the systemic concentration of the chemotherapeutic agent affects only proliferating cells. This implies that the death rate of the proliferating stem cells will increase during administration of chemotherapy. To our knowledge, no studies report the direct effects of chemotherapy on the hematopoietic stem cells, so we retain, for simplicity, a linear model for the PDs of

Zalypsis®on the population Q [3]. Accordingly, we model the increase in the death rate for the stem cells during chemotherapy as

$$\gamma_S^{chemo}(C_p(t)) \quad = \quad \gamma_S^{homeo} + h_S C_p, \tag{2.17}$$

where γ_S^{chemo} relates the effect of chemotherapy on the rate of apoptosis in the proliferative HSCs through the increase of γ_S^{homeo} (the homeostatic rate of apoptosis of the proliferative HSCs) by the effect h_S of the plasma concentration of the chemo-agent.

Concurrently, the rate of proliferation of the neutrophils in the bone marrow will decrease during exposure to chemotherapeutic agents. To model this effect, we modified the usual I_{max} (inhibitory Michaelis-Menten) PD model given by

$$E = \frac{E_{max} C_p^h}{EC_{50}^h + C_p^h}$$

to incorporate the two main assumptions on the effects of chemotherapy on the neutrophil proliferation rate. In the above equation, E is the observed effect, E_{max} is the maximal observed effect, C_p is the plasma concentration of the drug, EC_{50} is the concentration of drug inducing 50% of the maximal effect, and h is the usual Hill coefficient which determines the slope of the concentration-effects curve.

For our purposes, we consider that neutrophil proliferation would be completely halted when the plasma concentration of the chemotherapeutic agent is at a maximum (at supra-therapeutic levels, so $C_p^\infty \gg EC_{50}$, , where C_p^∞ is an intolerably high dose of continuous chemotherapy). This implies that $\eta_{NP}^{chemo}(C_p^\infty) = 0$. Further, when no chemotherapy is given ($C_p(t) = 0$), the proliferation rate remains at the steady state homeostatic rate, so that $\eta_{NP}^{chemo}(0) = \eta_{NP}^{homeo}$, where η_{NP}^{homeo} is the homeostatic rate of neutrophil proliferation. Together, these conditions imply that the above Imax model is instead expressed as

$$\eta_{NP}^{chemo}(C_p(t)) \quad = \quad \eta_{NP}^{homeo} \frac{(EC_{50})^h}{(EC_{50})^h + (C_p(t))^h}. \tag{2.18}$$

2.2.3.2 Myelostimulative Effects of G-CSF

Following [12, 39, 43], G-CSF reduces cell death rates in the HSCs and the random loss rates of the maturing neutrophils (decreasing γ_S and γ_{NM}, respectively) while also increasing the rate of proliferation of the marrow neutrophils (increasing η_{NP}). In what follows, the b_i, $i = S, N, NP, V$ are parameters relating the half-maximal concentration of G-CSF (see Appendix C for details on the estimation of these parameters). We consider the death rate out of the neutrophil marrow reservoir γ_{Nr} to be constant for simplicity. The rate of loss of the HSCs is given by

$$\gamma_S(G(t), C_p(t))) = \gamma_S^{min} - \frac{(\gamma_S^{min} - \gamma_S^{chemo})b_S}{G(t) - G^{homeo} + b_s}, \tag{2.19}$$

and is subject to the simultaneous effects of the chemotherapy and G-CSF in the stem cell compartment acting as an indirect feedback loop from the circulating neutrophil numbers. Here, γ_S^{min} is the minimal rate of apoptosis in the HSCs proliferative phase. The effects of G-CSF on cells committed to the neutrophil lineage are expressed as

$$\begin{aligned} \eta_{NP}(G(t), C_p(t)) &= \eta_{NP}^{chemo}(C_p(t)) \\ &\quad + \frac{(\eta_{NP}^{max} - \eta_{NP}^{chemo}(C_p(t)))(G(t) - G^{homeo})}{G(t) - G^{homeo} + b_{NP}} \end{aligned} \tag{2.20}$$

$$\gamma_{NM}(G(t)) = \gamma_{NM}^{min} - \frac{(\gamma_{NM}^{min} - \gamma_{NM}^{homeo})b_{NM}}{G(t) - G^{homeo} + b_{NM}}, \tag{2.21}$$

where η_{NP}^{max} is the maximal proliferation rate of the neutrophils and γ_{NM}^{min} is the minimal rate of random cell loss of the maturing neutrophils. As is the case for the HSCs, the proliferation rate $\eta_{NP}(G(t), C_p(t))$ is subject to the simultaneous effects of chemotherapy and G-CSF. Additionally, it is known that visibly immature neutrophils appear in the circulation after exogenous G-CSF administration [36]. Since our system is a DDE model with variable aging rate, we express this effect by a dependency of the maturation time on G-CSF (decreasing $\tau_{NM}(t)$), which implies an increase in the speed of maturation (increasing $V_N(t)$) modelled by

$$V_N(G(t)) \quad = \quad 1 + (V_{max} - 1)\frac{G(t) - G^{homeo}}{G(t) - G^{homeo} + b_V}, \tag{2.22}$$

where V_{max} is the maximal aging velocity of the maturing neutrophils (see Appendix C). The maturation time $\tau_{NM}(t)$ is defined by the threshold condition

$$\int_{t-\tau_{NM}(t)}^{t} V_N(G(s))ds \quad = \quad a_{NM}, \tag{2.23}$$

where a_{NM} is a constant equal to the maturation time at homeostasis. Differentiating Equation (2.23) gives

$$\frac{d\tau_N(t)}{dt} = \frac{d\tau_{NM}(t)}{dt} \quad = \quad 1 - \frac{V_N(G(t))}{V_N(G(t - \tau_{NM}(t)))}. \tag{2.24}$$

Finally, the concentration of G-CSF determines the mobilisation of mature neutrophils in the marrow reserve into the circulation. The functional form of this effect was previously proposed in [37] and has been generalised here to be

$$f_{trans}(G(t)) \quad = \quad trans^{homeo}\frac{trans^{ratio}(G(t) - G^{homeo}) + b_G}{G(t) - G^{homeo} + b_G}. \tag{2.25}$$

The parameter $trans^{homeo}$ relates the homeostatic rate of transit from the neutrophil bone marrow reservoir into the circulation. This rate of exit can, under changing G-CSF concentrations, be either increased or decreased by an empirically determined ratio $trans^{ratio} = \frac{trans^{max}}{trans^{homeo}}$, so more neutrophils exit the reservoir into the circulation under higher G-CSF concentrations.

2.3 Results

Parameter values, their interpretation, units as well as sources of references are reported in Table 2.I. Parameter estimation can be found in the Appendices.

Parameter	*Interpretation*	*Value*	*Unit*	*Reference*
Stem cells				
Q^{homeo}	Concentration of HSCs at homeostasis	1.1	10^6 cells/kg	[23]
γ_S	HSC rate of apoptosis	0.1	days^{-1}	[3]
τ_S	Time for HSC re-entry	2.8	days	[3]
A_Q^{homeo}	HSC amplification at homeostasis	1.5116		* Eq. (4.39)
κ_δ	HSC differentiation rate into other lineages	0.0140	days^{-1}	* Eq. (3.1)
β_Q^{homeo}	HSC rate of re-entry	0.043	days^{-1}	[25]
f_Q	Maximal HSC re-entry rate	8	days^{-1}	**
s_2	HSC re-entry Hill coefficient	2		**
θ_2	Half-maximal HSC concentration	0.0809	10^6 cells/kg	* Eq. (3.4)
Neutrophils				
N_r^{homeo}	Homeo.conc. of reservoir	2.26	10^9 cells/kg	[9]
N^{homeo}	Homeo. conc.of TBNP	0.3761	10^9 cells/kg	[9]
N_{circ}^{homeo}	Homeo. conc. of circulating neutrophils	0.22	10^9 cells/kg	[9]
γ_N	Circulating neutrophil rate of removal	2.1875	days^{-1}	*
τ_{NP}	Time for neutrophil proliferation	7.3074	days	*
a_{NM}	Time for neutrophil maturation at homostasis	3.9	days	** [34]
τ_{Nr}	Time spent in marrow reserve	2.7	days	**
γ_{Nr}	Rate of removal from marrow reserve	0.0064	days^{-1}	* Eq. (2.28)
γ_{NM}	Rate of removal during maturation phase	0.1577	days^{-1}	* Eq. (3.2)
$\kappa_N(N^{homeo})$	HSC differentiation rate into neutrophil line	0.0073	days^{-1}	** Eq. (2.26)
A_N^{homeo}	Neutrophil amplification at homeostasis	103 780		* Eq. (4.15)
η_{NP}^{homeo}	Neutrophil proliferation rate	1.6647	days^{-1}	*
f_N	Maximal rate of neutrophil differentiation	0.0088	days^{-1}	**
s_1	Neutrophil differentiation Hill coefficient	2		[22]
θ_1	Half maximal conc. neutrophil differentiation	0.8409	10^9 cells/kg	* Eq. (3.5)
f_{trans}^{homeo}	Homeostatic rate of transit from marrow reserve	0.3640	days^{-1}	* Eq. (3.5)
Zalypsis®				
k_{el_C}	Zalypsis® rate of elimination	132.0734	days^{-1}	[30]
k_{12}	Rate of exchange	90.2752	days^{-1}	[30]
k_{21}	Rate of exchange	18.2222	days^{-1}	[30]
k_{13}	Rate of exchange	8.2936	days^{-1}	[30]
k_{31}	Rate of exchange	0.6990	days^{-1}	[30]
k_{24}	Rate of exchange	9.2296	days^{-1}	[30]
k_{42}	Rate of exchange	62.5607	days^{-1}	[30]
BSA	Average body surface area	1.723	m^2	[30]
G-CSF				
G^{homeo}	G-CSF concentration at homeostasis	0.0246	ng/mL	[21]
G_{prod}	Rate of G-CSF production	0.2535	ng/mL/days	* Eq. (3.15)
k_{ren}	Rate of G-CSF renal elimination	10.3	days^{-1}	[37]
χ	Normalisation factor	0.0654	(ng/mL)/(10^9cells/kg)	**
k_{int}	G-CSF receptor-internalisation rate	114.48	days^{-1}	[37]
k_D	G-CSF dissociation constant	1.44	ng/mL	[21]
k_a	Subcutaneous filgrastim absorption rate	13.5	days^{-1}	[37]
F	Filgrastim bioavailable fraction	0.6020		[21]

(=Calculated, **=Estimated) Continued on next page*

Table 2.I – *Continued from previous page*

Parameter	*Interpretation*	*Value*	*Unit*	*Reference*
V_d	Volume of distribution (filgrastim)	1788	mL	* Appendix B
PD parameters				
Chemotherapy				
γ_S^{homeo}	HSC apoptotic homeostatic rate	0.1	days^{-1}	[3]
γ_S^{min}	Minimal HSC apoptotic rate	0.1	days^{-1}	[3]
γ_S^{max}	Maximal HSC apoptotic rate	0.4	days^{-1}	[3]
h_S	Effect of chemotherapy on HSC apoptosis	0.1		**
b_S	HSC apoptosis Michaelis-Menten parameter	11.2679	ng/mL	* Eq. (2.31)
h	Hill coefficient for Zalypsis® effect on proliferation	3		[35]
EC_{50}	Zalypsis® half-concentration on proliferation	2.3056	ng/mL	[35]
G-CSF				
η_{NP}^{max}	Maximal rate of proliferation	2.544	days^{-1}	[3]
η_{NP}^{min}	Minimal rate of proliferation	0.4	days^{-1}	[3]
V_{max}	Maximal maturation velocity	10		* [34]
γ_{NM}^{min}	Minimal apoptosis rate out of maturing phase	0.12	days^{-1}	[3]
γ_{NM}^{max}	Minimal apoptosis rate out of maturing phase	0.67	days^{-1}	[3]
$trans^{max}$	Maximal rate of transfer from marrow reserve	1.456	days^{-1}	[39]
b_V	Michaelis-Menten parameter (maturation speed)	3.5	ng/mL	* [34]
b_{NP}	Michaelis-Menten parameter (proliferation)	11.2679	ng/mL	* Eq. (2.31)
b_{NM}	Michaelis-Menten parameter (maturation)	11.2679	ng/mL	* Eq. (2.31)
b_G	Michaelis-Menten parameter (transit from pool)	11.2679	ng/mL	* Eq. (2.31)

Table 2.I – Table of parameter values used for an average patient undergoing chemotherapy with filgrastim support.

2.3.1 Numerical Simulations

The mathematical modelling of hematopoiesis, Zalypsis®, and filgrastim was supplemented by numerical simulation. All models were simulated using the *ddesd* solver in Matlab [27], which is an adaptive Runge-Kutta solver for DDEs with state-dependent delays. Since our model's delays are explicitly physiological and not artificially imposed by the modelling structure, defining several parameters in our model required extrapolation from published neutrophil studies, particularly [4] and [9]. Some digitisation was carried out using Matlab [27] to facilitate the estimation.

2.3.2 The Use of Physiological Models

The regulation of myelopoiesis is a dynamical system which implies that any periodic administration of a perturbation (for our purposes, chemotherapy) can induce oscillations where there were none previously. Additionally, in a phenomenon known as reso-

nance [3], the cyclical administration of myelosuppressive chemo-agents can worsen the neutrophil nadir when administered during specific periods in the oscillating cycle. We therefore sought to study how a periodic chemotherapeutic regimen affects neutrophil counts and how the timing of the administration of filgrastim post-chemotherapy influences the patient's neutropenic status. This combines previous work addressing the effects of period-shortening in poly-chemotherapy ([31, 32]; Section 2.3.2.1–see below) and dose optimisation to minimise neutropenia during treatment with Zalypsis®[15].

2.3.2.1 Verifying the Model's Predictions

CHOP21, an established treatment for lymphoma, involves the concomitant administration of cyclophosphamide, doxorubicin, vincristine, and prednisone given over 21-day cycles, with G-CSF administration determined *ad libitum* by the individual patient's neutrophil count. Investigations into period-condensing in the CHOP protocol (14-day instead of 21-day) have concluded that a shorter cycle length leads to better survival rates in younger patients (less than 60 years old) and less toxicity in older patients [31, 32]. The CHOP14 14-day protocol calls for G-CSF administration (300 μg/day or 480 μg/day depending on the patient's body weight) to begin 4 days post-chemotherapy and to continue until day 13 post-chemotherapy (for a total of 10 days). Recent work on model development for granulopoiesis has made available extensive data sets from the initial CHOP14 studies [20]. Reported are patients' absolute neutrophil count (ANC) in quartiles for a 6-cycle CHOP treatment, thereby giving an idea of the variability in patients' response to chemotherapy with pre-defined G-CSF support.

Our first focus was to compare our model's predictions using a previously optimised dose of Zalypsis®for a 21-day cycle (4 mg/m^2) to the CHOP14 protocol in a manner analogous to the investigations of [32] and [31]. While it may seem counterintuitive to compare mono- and polytherapies, it is important to note that in the context of our fully mechanistic model, myelosuppressive drugs will have similar effects on the renewal rate of the HSCs ($\beta(Q)$) and on the proliferation rate of the neutrophils ($\eta(G(t), C_p(t))$) since chemotherapeutic drugs are explicitly administered for their ability to disrupt cellular division. Moreover, we were limited by the availability of data in the literature and, as such, made use of the data sets at our disposal (accessed through [20]). Accordingly,

we simulated six 14-day period administrations of 4 mg/m^2 of Zalypsis®with 10 daily administrations of 300 μg of subcutaneous filgrastim beginning on the fourth day post-chemotherapy, as was prescribed for the CHOP14 study. We then compared the model prediction to the CHOP14 data of $N = 172$ patients (data was available in quartiles), which is highlighted in Figure 2.2. It should be noted here that no model fitting was undertaken from clinical data. The parameter estimation herein was performed through published PK models for Zalypsis®or filgrastim or from physiological studies of neutrophil production. In this work, our intention was to reproduce the major characteristics of the system's dynamics under the CHOP14 protocol. As our simulated result falls within the interquartile ranges from [31, 32] through simple comparison, it is apparent that the model sufficiently reproduces the neutrophils' behaviour to the level of anticipated detail.

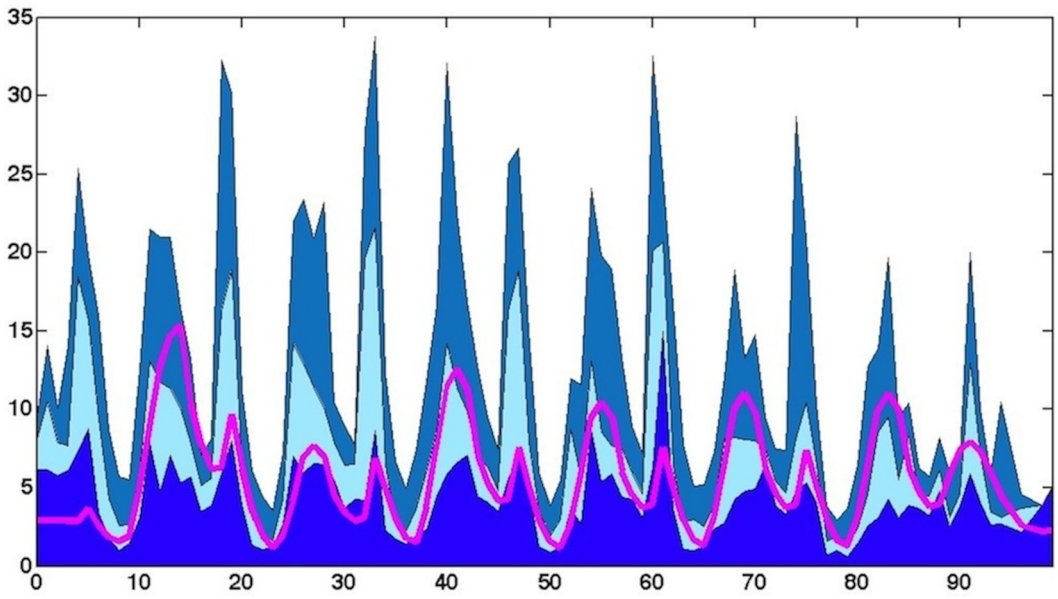

Figure 2.2 – Model predictions (pink) compared to CHOP14 protocol described in [31, 32] (data from $N = 172$ patients arranged in quartiles from [20]–shaded regions). x-axis: time (days); y-axis: ANC (10^9 cells/L). The CHOP14 protocol outlined in [31] is compared to the model's prediction. Data from the CHOP14 study available from [20] is divided into quartiles (shaded regions). The simulation results (in pink) shows the model's solution for the typical patient (sampled at clinical sampling points-once daily for 100 days) and compares positively to the study's findings. Note that no model fitting was performed to obtain the prediction.

2.3.2.2 Applying the Model to G-CSF Dose Optimisation

As previously mentioned, the utility of fully mechanistic models is related to their ability to explain and unravel how the underlying physiological mechanisms dictate a drug's effects and efficacy. In parallel, physiological models should afford predictive abilities and help guide dosing decisions. In that vein, our main focus was to optimise the use of G-CSF during anti-cancer treatment. This was achieved by reducing the number of doses administered during each chemotherapy period in comparison to the CHOP14 protocol, thereby minimising the cost and the burden to patients. No optimisation of chemotherapy dose amount or period was undertaken. In this work, dose optimisation refers to the minimisation of the undesirable neutropenic effect of chemotherapeutic treatment. Accordingly, we used the accepted classifications of the grade of severity of neutropenia to minimise toxicity (Grade 1: ANCs between 1500 and 2000 cells/mm^3, Grade 2 (Mild): ANCs between 1000 and 1500 cells/mm^3, Grade 3 (Moderate): ANCs between 500 and 1000 cells/mm^3, and Grade 4 (Severe): ANCS less than 500 cells/mm^3).

As the model captures the dynamics of the published CHOP14 data (as shown in Figure 2.2), we used the CHOP14 chemotherapy protocol (6 cycles of chemotherapy administered 14 days apart with 10 administrations of 300 μg of filgrastim beginning 4 days post-chemotherapy) as a baseline reference case. To establish optimal dosing regimens, we simulated a baseline standard by administering 4 mg/m^2 dose of Zalypsis®(previously determined to be an optimal dose for Zalypsis®[15]) every 14 days for 6 cycles in total. Next we ran simulations in the $(t_{post-chemo}, n_{admins}, p_{admins})$-space by varying both start day ($t_{post-chemo}$), the number of filgrastim administrations (n_{admins}), and the period between filgrastim doses (p_{admins}–up to a maximum of 3 days to minimise the impact of the filgrastim period upon adherence). We then progressively ranked each $(t_{post-chemo}, n_{admins}, p_{admins})$-triplet against the reference by visual predictive check looking for improvement in the ANC nadir with regards to the neutropenic grade experienced by the average patient during anti-cancer treatment. To ensure clinical relevancy, optimal regimens were labelled as those which reduce the number of administrations of filgrastim over each chemotherapy cycle while simultaneously maintaining or, even better, increasing the ANC nadir observed in the complete CHOP14 study.

Our results indicate that the number of administrations of G-CSF post-chemotherapy

plays a dominant role on therapeutic outcomes. Indeed, our predictions indicate that the timing of the first administration of G-CSF post-chemotherapy becomes less important when the number of administrations are increased within each chemotherapy cycle (Figures 2.3 and 2.4). This supports the current clinical dosing scheme of G-CSF in oncological settings which begins one-day post-chemotherapy and continues daily for seven to ten days, depending on the ANC status of the patient [1]. Our results further indicate that administering the first dose of filgrastim seven days post-chemotherapy improves the neutropenic status of the average patient. This is to be expected based on the time it takes to produce and release a mature neutrophil after proliferation has been disturbed by chemotherapy ($\tau_{NM}(t) + \tau_{Nr}$) and supports the findings' of previous modelling work on G-CSF timing [3, 41]. Indeed, starting G-CSF one week after the chemotherapy dose, we demonstrate that as few as three or four daily administrations of G-CSF are sufficient to completely avoid moderate neutropenia (three administrations) or nadirs characteristic of neutropenia altogether (four administrations). Figure 2.5 reveals that these dosing regimens are optimal in comparison with the CHOP14 protocol, implying a reduction of six to seven G-CSF doses *per chemotherapy cycle*. Such dosing regimens could lead to significant cost reductions and alleviate the physical and hematopoietic burdens on patients undergoing chemotherapy. We determined that daily dosing of filgrastim is preferable over extending the period between administrations: increasing the time between administrations allowed for more severe reductions in ANC (not shown) and would not support patient adherence. This last result is again attributable to the underlying physiology of neutrophil production, as exogenous G-CSF stimulates the release of reserved marrow neutrophils, which in turn increases ANC (an increase which then triggers a decrease in G-CSF concentrations through saturated internalisation and renal elimination). ANC then returns to homeostatic levels after briefly fluctuating above and below the baseline value. When administration periods were increased past one day, ANCs had time to rise and fall between rhG-CSF doses. Once daily administrations of rhG-CSF staved off the rapid decline after peak ANCs because of the frequent dosing and therefore prevented worsening nadirs.

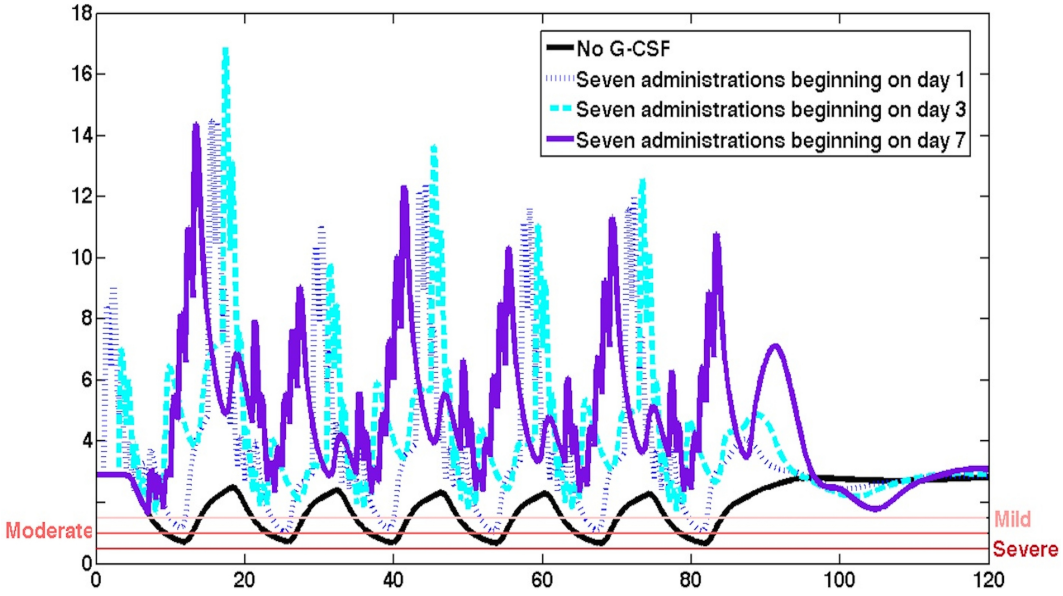

Figure 2.3 – The effect of the day of administration of G-CSF post-chemotherapy. x-axis: time (days); y-axis: ANC (10^9 cells/L). Horizontal lines indicate thresholds for mild (1000 cells/μL $\leqslant$ ANC $\leqslant$ 1500 cells/μL), moderate (500 cells/μL $\leqslant$ ANC $\leqslant$ 1000 cells/μL), and severe (ANC $\leqslant$ 500 cells/μL) neutropenia and these classifications were used to identify optimal regimens. As the number of administrations of filgrastim post-chemotherapy increase, the importance of the first day of administration diminishes. Six cycles of chemotherapy with 14-day periods are compared for different filgrastim protocols. Seven administrations of filgrastim beginning on day 7 achieve results similar to seven administrations beginning on day 3. A regimen where seven administrations of filgrastim begin 1 day post-chemotherapy is not sufficient to avoid neutropenia.

2.4 Discussion

In this paper, we have extended an age-structured model for myelopoiesis [3] by the addition of a neutrophil reservoir in the bone marrow that is known to play a role in the rapid mobilisation of neutrophils into the blood during infection or falling circulating neutrophil numbers [14, 36]. We also accounted for the marginated neutrophil pool in the blood. The fully mechanistic physiological model of neutrophil production is then integrated with up-to-date PKPD models for a chemotherapeutic-drug and an adjuvant [21, 30] to characterise the hematopoietic response to periodic chemotherapy with a supportive agent. Parameter estimation was performed in a progressive and logical fashion by establishing the pivotal mechanisms of myelopoiesis from the relevant literature from both physiological studies and PKPD analyses. Proceeding in this manner leads to an im-

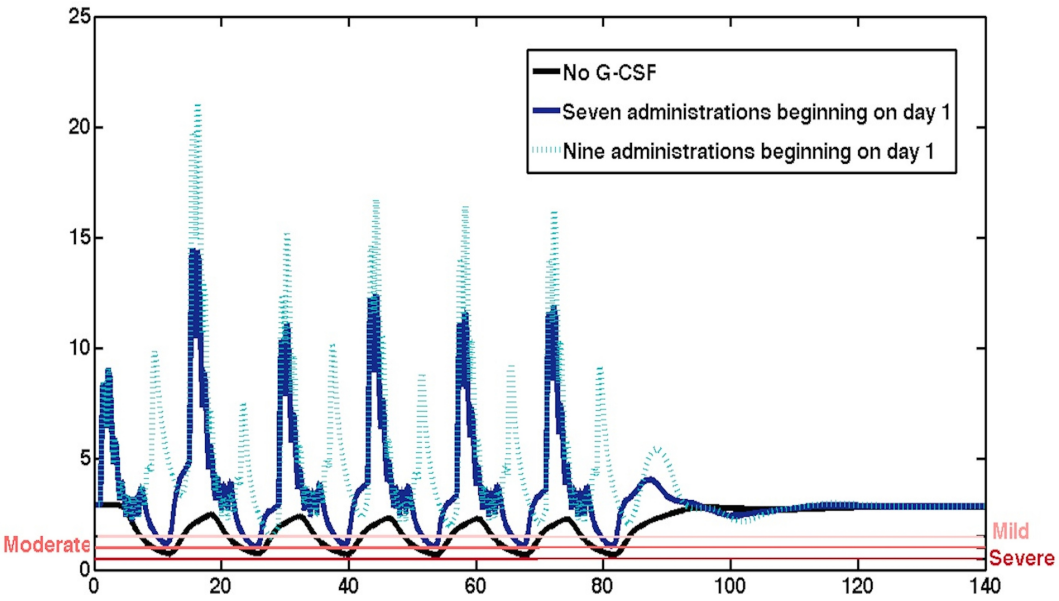

Figure 2.4 – Effect of fixing the starting day post-chemotherapy while increasing the number of G-CSF administrations. x-axis: time (days); y-axis: ANC (10^9 cells/L). Horizontal lines indicate thresholds for mild, moderate, and severe neutropenia as in Figure 2.3. These classifications were used to identify optimal regimens. Six cycles of chemotherapy with 14-day periods are compared for different filgrastim protocols. Increasing the number of filgrastim administrations from 7 to 9 allows filgrastim dosing to begin 1 day post-chemotherapy while avoiding neutropenia, which is not the case in the 7 administration regimen, as shown in Figure 2.3.

proved strategy for parameter identification, one that is capable of evolving in-step with experimental work and physiological knowledge of neutrophil production. Utilising these parameter values directly, the model successfully reproduced the neutrophil data from the CHOP14 studies of 14-day periodic chemotherapy with filgrastim support [31, 32].

We also determined improved dosing regimens for 14-day periodic chemotherapy with the filgrastim adjuvant. We began by studying the optimal timing of the first rhG-CSF dose after the administration of chemotherapy and established that delaying the first dose of filgrastim improved the patient's neutropenic status (Figure 2.3). This lead us to the determination that the number of filgrastim administrations could be significantly reduced (from 10 to three or four) by delaying its first dose post-chemotherapy (Figure 2.5). This is a novel result which is simultaneously capable of improving the patient's neutropenic status by raising the neutrophil nadir, of alleviating the patient's drug burden, and of reducing the costs associated with filgrastim support during chemotherapy. It is therefore

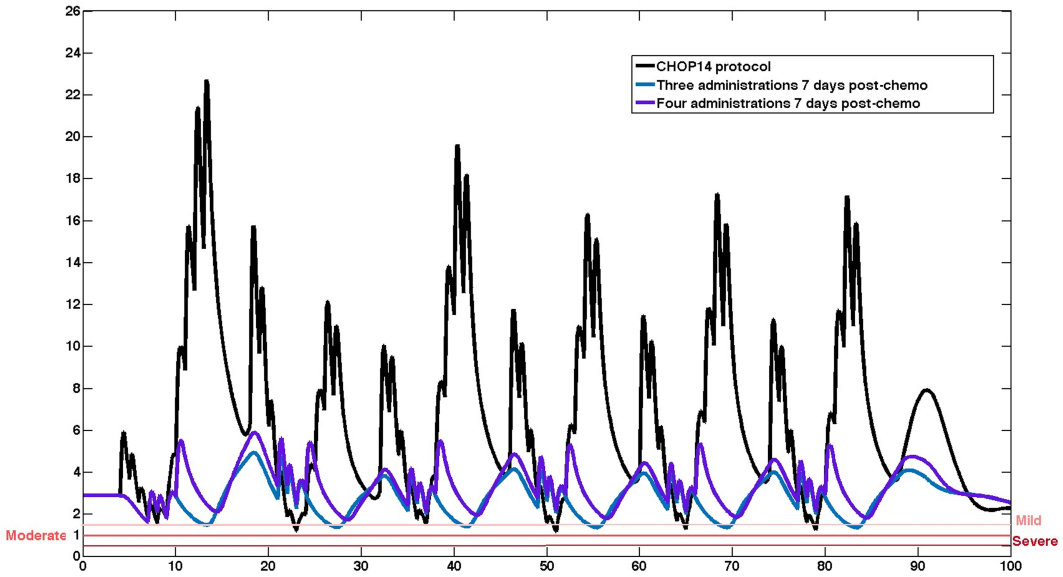

Figure 2.5 – Optimal dosing regimens compared to the CHOP14 protocol. x-axis: time (days); y-axis: ANC (10^9 cells/L). Horizontal lines indicate thresholds for mild, moderate, and severe neutropenia as in Figure 2.3. These classifications were used to identify optimal regimens. Model predictions for 6 chemotherapy cycles with 14-day periods. The CHOP14 protocol which studied 10 administrations of filgrastim beginning four days post-chemotherapy is compared to regimens where filgrastim administrations begin seven days post-chemotherapy, with three or four administrations per cycle. Delaying the first administration of filgrastim allows for a reduction in the number of administrations per cycle while showing improvement in the neutropenic status for the average patient.

an important observation for the clinical practice and one which bears further investigation through collaboration with clinicians.

Inspired by the results in this paper, we are interested in applying the model to the case of cyclical neutropenia, with the aim of depicting the influence of G-CSF on oscillatory dynamical hematopoietic diseases. Future work will also include a full characterisation of the impact of PK variability in the PD response. Through sensitivity analysis, this depiction will help us discern the principle mechanisms of neutrophil production. Indeed, the rational construction of the myelopoiesis model affords us the ability to delineate the role of individual variables on the predicted behaviour, a particularly salient advantage of physiological models. Moreover, owing to this careful construction, the hematopoietic model is applicable across pathologies without major parameter re-estimation. Outlining which processes significantly impact on myelopoiesis and portraying how these processes affect neutrophil production is inherent to the physiological modelling paradigm. This

work highlights that hypothesis-driven mathematical modelling contributes considerably to the problem of attenuating chemotherapy-induced neutropenia in the PKPD scope and beyond. Indeed, the mechanistic model we have developed provides predictive ability in addition to hypothesis elimination, meaning it can both confirm previous results and repudiate unconfirmed concepts, which has broad implications for patients, clinicians, and researchers alike.

Acknowledgments

This work was supported by the Natural Sciences and Engineering Research Council (NSERC, Canada) PGS-D program (MC), four NSERC Discovery Grants (ARH, JB, MM, FN), and the NSERC Industrial Research Chair in Pharmacometrics (FN), jointly supported by Novartis, Pfizer and inVentiv Health Clinics. We wish to thank Université de Montréal, McGill University, and our colleagues J. Lei (Tsinghua University, China), N. Letarte (Centre hospitalier de l'Université de Montréal), G. Brooks, G. Provencher Langlois, and L. Ferraton for their insight and support during this project.

Conflicts of Interest/Disclosure

The authors have no conflict of interest to declare. All authors have approved this manuscript.

Author Contributions

This work makes up a portion of the doctoral thesis of MC. Construction of physiological models: MC ARH JB MM. Construction of PKPD models: MC FN JL. Numerical simulation implementation: MC ARH. Data analysis: MC ARH. Wrote the paper: MC FN JL MM ARH.

References

[1] Limited Amgen Manufacturing. Neupogen-filgrastim monograph, 2007.

[2] S. Bernard, J. Bélair, and M.C. Mackey. Oscillations in cyclical neutropenia: New evidence based on mathematical modeling. *Journal of Theoretical Biology*, 223:283–298, 2003.

[3] G. Brooks, G.P. Langlois, J. Lei, and M.C. Mackey. Neutrophil dynamics after chemotherapy and G-CSF: The role of pharmacokinetics in shaping the response. *Journal of Theoretical Biology*, 315:97–109, 2012.

[4] G.E. Cartwright, J.W. Athens, and M.M. Wintrobe. Analytical review: The kinetics of granulopoiesis in normal man. *Blood*, 24:800–803, 1964.

[5] Ho. *Modeling neutrophil dynamics in sepsis and cancer treatment*, Savannah, Georgia, USA, 2012. Chemical Process Control 8.

[6] C. Colijn and M.C. Mackey. A mathematical model of hematopoiesis: II. Cyclical neutropenia. *Journal of Theoretical Biology*, 237:133–146, 2005.

[7] M. Craig, A.R. Humphries, J. Bélair, J. Li, F. Nekka, and M.C. Mackey. Neutrophil dynamics during concurrent chemotherapy and G-CSF administration: Mathematical modelling guides dose optimisation to minimise neutropenia. *Journal of Theoretical Biology*, 385:77–89, 2015.

[8] M. Craig, A.R. Humphries, and M.C. Mackey. A mathematical model of granulopoiesis incorporating the negative feedback dynamics and kinetics of G-CSF/neutrophil binding and internalisation, In preparation.

[9] J.T. Dancey, K.A. Deubelbeiss, L.A. Harker, and C.A. Finch. Neutrophil kinetics in man. *The Journal of Clinical Investigation*, 58:705–715, 1976.

[10] M. de Haas, C.E. van der Schoot, J. Calafat, C.E. Hack, J.H. Nuijens, D. Roos, et al. Granulocyte colony-stimulating factor administration to healthy volunteers: Analysis of the immediate activating effects on circulating neutrophils. *Blood*, 84:3885–3894, 1994.

[11] C. Foley and M.C. Mackey. Mathematical model for G-CSF administration after chemotherapy. *Journal of Theoretical Biology*, 257:27–44, 2009.

[12] C. Foley, S. Bernard, and M.C. Mackey. Cost-effective G-CSF therapy strategies for cyclical neutropenia: Mathematical modelling based hypotheses. *Journal of Theoretical Biology*, 238:756–763, 2006.

[13] L.E. Friberg and M.O. Karlsson. Mechanistic models for myelosuppression. *Investigational New Drugs*, 21:183–194, 2003.

[14] R.C. Furze and S.M. Rankin. Neutrophil mobilization and clearance in the bone marrow. *Immunology*, 125:281–288, 2008.

[15] M. González-Sales, B. Valenzuela, C. Pérez-Ruixo, C. Fernández Teruel, B. Miguel-Lillo, Soto Matos A., et al. Population pharmacokinetic-pharmacodynamic analysis of neutropenia in cancer patients receiving PM00104 (Zalypsis®). *Clinical Pharmacokinetics*, 51:751–764, 2012.

[16] J.M. Harrold and R.S. Parker. Clinically relevant cancer chemotherapy dose scheduling via mixed-integer optimization. *Computers and Chemical Engineering*, 33:2042–2054, 2009.

[17] C. Haurie, M.C. Mackey, and D.C. Dale. Cyclical neutropenia and other periodic hematological diseases: A review of mechanisms and mathematical models. *Blood*, 92:2629–2640, 1998.

[18] T. Ho, G. Clermont, and R.S. Parker. A model of neutrophil dynamics in response to inflammatory and cancer chemotherapy challenges. *Computers and Chemical Engineering*, 51:187–193, 2013.

[19] E. Johnston, J. Crawford, S. Blackwell, T. Bjurstrom, P. Lockbaum, L. Roskos, et al. Randomized dose escalation study of SD/01 compared with daily filgrastim in patients receiving chemotherapy. *Journal of Clinical Oncology*, 18:2522–2528, 2000.

[20] A. Krinner, I. Roeder, M. Loeffler, and M. Scholz. Merging concepts - coupling an agent-based model of hematopoietic stem cells with an ODE model of granulopoiesis. *BMC Systems Biology*, 7:117, 2013.

[21] W. Krzyzanski, P. Wiczling, P. Lowe, E. Pigeolet, M. Fink, A. Berghout, and S. Balser. Population modeling of filgrastim PK-PD in healthy adults following intravenous and subcutaneous administrations. *Journal of Clinical Pharmacology*, 9 Suppl:101S–112S, 2010.

[22] J.E. Layton and N.E. Hall. The interaction of G-CSF with its receptor. *Frontiers in Bioscience*, 31:177–199, 2006.

[23] J. Lei and M.C. Mackey. Multistability in an age-structured model of hematopoiesis: Cyclical neutropenia. *Journal of Theoretical Biology*, 270:143–153, 2011.

[24] T.A. Leil. A Bayesian perspective on estimation of variability and uncertainty in mechanism-based models. *Clinical Pharmacology and Therapeutics: Pharmacometrics and Systems Pharmacology*, 3:e121, 2014.

[25] M.C. Mackey. Cell kinetic status of hematopoietic stem cells. *Cell Proliferation*, 34: 71–83, 2001.

[26] Y. Madarnas, A. Eisen, R. Myers, and A.E. Haynes. The Prophylactic Use of Filgrastim in Patients with Breast Cancer. Program in Evidence-based Care MCED-CCO Special Advice Report. Technical report, Cancer Care Ontario, Toronto, ON, Canada, 2009 Oct 1-Archives 2013 May.

[27] Mathworks. *MATLAB 2013a*. Mathworks, Natick, Massachusetts, 2013.

[28] D.N. McLennan, C.J.H. Porter, G.A. Edwards, S.W. Martin, A.C. Heatherington, and S.A. Charman. Lymphatic absorption is the primary contributor to the systemic availability of epoetin alfa following subcutaneous administration to sheep. *The Journal of Pharmacology and Experimental Therapeutics*, 313:345–35, 2005.

[29] I. Nestorov. Whole body pharmacokinetic models. *Clinical Pharmacokinetics*, 42: 883–908, 2003.

[30] C. Pérez-Ruixo, B. Valenzuela, C. Fernández Teruel, M. González-Sales, B. Miguel-Lillo, A. Soto-Matos, et al. Population pharmacokinetics of PM00104 (Zalypsis®) in cancer patients. *Cancer Chemotherapy and Pharmacology*, 69:15–24, 2012.

[31] M. Pfreundschuh, L. Trümper, M. Kloess, R. Schmits, A.C. Feller, C. Rudolph, et al. Two-weekly or 3-weekly CHOP chemotherapy with our without etoposide for the treatment of young patients with good prognosis (normal LDH) aggressive lymphomas: Results of the NHL-B1 trial of the DSHNHL. *Blood*, 104:626–633, 2004.

[32] M. Pfreundschuh, L. Trümper, M. Kloess, R. Schmits, A.C. Feller, C. Rudolph, et al. Two-weekly or 3-weekly CHOP chemotherapy with our without etoposide for the treatment of elderly patients with aggressive lymphomas: Results of the NHL-B2 trial of the DSHNHL. *Blood*, 104:634–641, 2004.

[33] C.J.H. Porter and S.A. Charman. Lymphatic transport of proteins after subcutaneous administration. *Journal of Pharmaceutical Sciences*, 89:297–310, 2000.

[34] T.H. Price, G.S. Chatta, and D.C. Dale. Effect of recombinant granulocyte colony-stimulating factor on neutrophil kinetics in normal young and elderly humans. *Blood*, 88:335–340, 1996.

[35] A.L. Quartino, L.E. Friberg, and M.O. Karlsson. A simultaneous analysis of the time-course of leukocytes and neutrophils following docetaxel administration using a semi-mechanisitic myelosuppression model. *Investigational New Drugs*, 30:833–845, 2012.

[36] S.M. Rankin. The bone marrow: A site of neutrophil clearance. *Journal of Leukocyte Biology*, 88:241–251, 2010.

[37] M. Scholz, S. Schirm, M. Wetzler, C. Engel, and M. Loeffler. Pharmacokinetic and -dynamic modelling of G-CSF derivatives in humans. *Theoretical Biology and Medical Modelling*, 9:1497–1502, 2012.

[38] E. Shochat and V. Rom-Kedar. Novel strategies for granulocyte colony-stimulating factor treatment of severe prolonged neutropenia suggested by mathematical modeling. *Clinical Cancer Research*, 14:6354–6363, 2008.

[39] E. Shochat, V. Rom-Kedar, and L.A. Segel. G-CSF control of neutrophils dynamics in the blood. *Bulletin of Mathematical Biology*, 69:2299–2338, 2007.

[40] S.O.K. Song, J. Hogg, Z.Y. Peng, R.S. Parker, J.A. Kellum, and G. Clermont. Ensemble models of neutrophil trafficking in severe sepsis. *PLoS Computational Biology*, 8:e1002422, 2012.

[41] O. Vainas, S. Ariad, O. Amir, W. Mermershtain, V. Vainstein, M. Kleiman, O. Inbar, R. Ben-Av, A. Mukherjee, S. Chan, and Z. Agur. Personalising docetaxel and G-CSF schedules in cancer patients by a clinically validated computational model. *British Journal of Cancer*, 107:814–822, 2012.

[42] V. Vainstein, Y. Ginosar, M. Shoham, D.O. Ranmar, A. Ianovski, and Z. Agur. The complex effect of granulocyte colony-stimulating factor on human granulopoiesis analyzed by a new physiologically-based mathematical model. *Journal of Theoretical Biology*, 235:311–327, 2005.

[43] B. Wang, T.M. Ludden, E.N. Cheung, G.G. Schwab, and L.K. Roskos. Population pharmacokinetic-pharmacodynamic modeling of filgrastim (r-metHuG-CSF) in healthy volunteers. *Journal of Pharmacokinetics and Pharmacodynamics*, 28:321–342, 2001.

[44] C. Zhuge, J. Lei, and M.C. Mackey. Neutrophil dynamics in response to chemotherapy and G-CSF. *Journal of Theoretical Biology*, 293:111–120, 2012.

2.5 Appendices

2.5.1 Appendix A: Homeostatic Hematopoietic Parameter Estimation

There are two main points to address in the parameter estimation for the physiological variables. The first issue is interpreting appropriate values from laboratory and clinical studies while the second is assuring that homeostatic levels are consistent when the equations are at steady states. A thorough explanation of the homeostatic parameter values is available in [8]; we will briefly summarise the parameter identification for the hematopoietic values in the absence of chemotherapy and G-CSF and then describe the estimation of parameter values in the PKPD model with both drugs.

We begin with the stem cell line. From [2] and [23], we take $Q^{homeo} = 1.1 \times 10^6$ cells/L and set the rate of apoptosis in the stem cell pool to be $\gamma_S = 0.1\,\text{days}^{-1}$ as in [3]. From Equation (4.7) at homeostasis, we have

$$A_Q^{homeo} = 2\exp(-\tau_S\gamma_S) = 1.512.$$

Using an average from the mouse data in [25], we calculate the re-entry rate in the stem cell compartment to be

$$\beta(Q^{homeo}) = \frac{0.02 + 0.053 + 0.057}{3} = 0.043\,\text{days}^{-1}.$$

Clinically determining the rate of differentiation into the neutrophil lineage is difficult and we are not aware of any data estimating this value. Consequently, we use the equilibrium requirement for Equation (3.1) which gives

$$\kappa_{tot} = (A_Q^{homeo} - 1)\beta(Q^{homeo}) = 0.0220\,\text{days}^{-1}, \tag{2.26}$$

where $\kappa_{tot} = \kappa_N(N^{homeo}) + \kappa_\delta$. From this total differentiation rate, we can roughly estimate the differentiation into the neutrophil line as $\frac{1}{3}\kappa_{tot}$, since for our purposes, we consider the hematopoietic stem cells to differentiate into three distinct lineages (neutrophils, red blood cells, and platelets). This implies that $\kappa_N(N^{homeo}) = 0.0073\,\text{days}^{-1}$. From Equation (3.4), we have

$$\beta(Q^{homeo}) = \frac{f_Q}{1 + \left(\frac{Q^{homeo}}{\theta_2}\right)^{s_2}}. \tag{2.27}$$

We take $s_2 = 2$ and $f_Q = 8\,\text{days}^{-1}$, which within the Hill function interpretation can be interpreted to mean that the number of molecules capable of binding to any given stem cell to initiate re-entry is two while the maximal rate of re-entry is $8\,\text{days}^{-1}$ [6]. Rearranging Equation (2.27), we get

$$\theta_2 = \left[\frac{(Q^{homeo})^{s_2}\beta(Q^{homeo})}{f_Q - \beta(Q^{homeo})}\right]^{\frac{1}{s_2}} = 0.0809 \times 10^6 \,\text{cells/kg}.$$

Turning now to the neutrophil line, from [9], we take the size of the reservoir and total blood neutrophils (respectively) as

$$N_r^{homeo} = 2.26 \times 10^9 \,\text{cells/kg}$$
$$N^{homeo} = 0.22/0.585 \times 10^9 \,\text{cells/kg}.$$

The factor 0.585 accounts for the reported average recovery rate in [9] and implies that the baseline circulating neutrophil count is 0.22×10^9 cells/kg. From the usual half-life equation for an exponential decay,

$$\gamma_N = \frac{\ln 2}{t_{\frac{1}{2}}} = \frac{35}{16} = 2.1875 \,\text{days}^{-1},$$

by rounding the half-life value from [9] of $t_{\frac{1}{2}} = 7.6$ days. At homeostasis, the rate of entry into the reservoir will equal the rate of exit from the pool, giving

$$f_{trans}(G^{homeo})N_r^{homeo} = \gamma_N N^{homeo}$$

or, equivalently,

$$f_{trans}(G^{homeo}) = trans_N^{homeo} = \frac{\gamma_N N^{homeo}}{N_r^{homeo}} = \frac{2.1875 \times 0.4}{2.26} = 0.387.$$

We take $a_{NM} = 3.9$ days which implies, by the constraints detailed in [8], that τ_{Nr}^{homeo} is within the interval $(2.4432, 2.589)$. Accordingly, we select $\tau_{Nr} = 2.5$ days. The average time a neutrophil spends in the reservoir is given by

$$\tau_{Nr}^{homeo} = \frac{1}{f_{trans}(G^{homeo}) + \gamma_{Nr}}. \tag{2.28}$$

Thus the average transit time of a neutrophil in the marrow reservoir is the reciprocal of the means with which it exits the reservoir: by transiting into the circulation ($f_{trans}(G^{homeo})$) or through random cell death (γ_{Nr}). Rearranging Equation (2.28), we have then that the rate of random cell loss from the marrow reserve is

$$\begin{aligned}\gamma_{Nr} &= \frac{1}{\tau_{Nr}^{homeo}} - f_{trans}(G^{homeo}) \\ &= \frac{1}{2.5} - 0.387 = 0.0064\,\text{days}^{-1}.\end{aligned}$$

From the age-structured PDE model structure, we determined that $A_N^{homeo} = 103777.178$ and $\eta_{NP}^{homeo} = 1.665\,\text{days}^{-1}$. These values correspond to approximately 17.55 effective divisions within the proliferative phase. We have also calculated τ_{NP} to be equal to 7.307 days, implying there is one effective division every 10 hours in the proliferative stage [8]. Finally, we can determine the parameters relating to the differentiation rate from the HSCs to the neutrophils. Recall that by Equation (2.26), we have set $\kappa_N(N^{homeo}) = \frac{1}{3}\kappa_{tot} = 0.0073\,\text{days}^{-1}$. From this estimate, we calculate the parameters of Equation (3.5) in a manner similar to Equation (3.4). From [22], we set $s_1 = 2$ on account of the 2:2 stoichiometry between G-CSF and its receptor. We have observed bifurcation from a steady homeostatic equilibrium to a steady limit cycle solution with increases to f_N, which indicates a switch from a hematopoietically normal individual to one exhibiting a pathology similar to cyclical neutropenia. To ensure solutions remain stable at homeostasis, we take $f_N = 1.2\kappa_N(N^*)$. θ_1 is then estimated by

$$\theta_1 = \left[\frac{(N^{homeo})^{s_1}\kappa_N(N^{homeo})}{f_N - \kappa_N(N^{homeo})}\right]^{-s_1} = 0.8409 \times 10^9\,\text{cells/kg}.$$

2.5.2 Appendix B: PK-related Parameter Estimation

All Zalypsis®parameters are taken directly from [30] and reported in Table 2.I. An effort was made for G-CSF PK parameter consistency with a number of studies namely

[37, 38, 42] and particularly [21]. The endogenous concentration of G-CSF at homeostasis is estimated from [21] as the mean of the observed baseline values in that study, therefore for our purposes, $G^{homeo} = 0.0246\,\text{ng/mL}$. In terms of endogenous production and elimination, we estimated $G_{prod} = 0.2535\,\text{ng/(mL days)}$, which is a consequence of the homeostatic condition of Equation (3.15). The renal clearance rate k_{ren} is taken from the parameter estimation performed in [37] and is estimated as $k_{ren} = 10.3\,\text{days}^{-1}$. Particular attention should be paid when estimating the rate of internalisation of G-CSF by the neutrophils. [21] measured a value of $0.105\,\text{hours}^{-1}$, while it is estimated in [37] that the maximum Michaelis-Menten elimination to occur at a rate of $4.77\,\text{hours}^{-1}$, and a literature value of 0.015 pM/hour is reported in [42]. [21] note that their estimate is lower than anticipated. We therefore opted to estimate the rate of internalisation from [37], giving $k_{int} = 114.48\,\text{days}^{-1}$. It is worth noting, however, that model predictions were not significantly different when we used the internalisation rate reported in [21] (not shown). A quasi-equilibrium assumption is used in [21] to calculate the dissociation constant k_D given by $\frac{(C)(R)}{RC} = \frac{k_{on}}{k_{off}} = k_D$, where C is the concentration of G-CSF, R the concentration of G-CSFR receptors, and RC the concentration of receptor complexes in the same manner as in our model by using the law of mass-action (see derivation in [11]). Accordingly we took the dissociation constant they reported and set $k_D = 1.44\,\text{ng/mL}$.

The subcutaneous absorption rate of filgrastim is reported as $0.161\,\text{hours}^{-1}$ in [37] and as $0.651\,\text{hours}^{-1}$ in [21]. As we readapted the latter's absorption model we selected a k_a similar to the value reported therein, namely $k_a = 0.5625\,\text{hours}^{-1} = 13.5\,\text{days}^{-1}$. The bioavailability of filgrastim was found to be dose-dependent in [37]. We estimated $F = 0.602$ from [21], which turns out to be higher than the value found in Figure 3 of [37] who report a value close to $F = 0.3$ based on their model simulations accounting for losses in the subcutaneous tissues. Future work should address this discrepancy through a sensitivity analysis of our model. Finally, the volume of distribution V_d of filgrastim is set at 1788 mL, between the values used in [37] (1.156 L) and [21] (2.42 L) since both studies utilise V_d in the central compartment only.

2.5.3 Appendix C: PD-related Parameter Estimation

The parameter estimation of the previous section deals solely with the model at homeostasis for a healthy individual. We now turn to the estimation of parameters related directly to the PD effects of Zalypsis®and filgrastim (the rhG-CSF drug studied). In the absence of data reporting effect versus concentration curves for the mechanism of interest, we derived a theoretical measure for the EC50 values of the Michaelis-Menten equations. In a typical study of saturating effects, we allow for 5% variation in the C_{min} values (starting point) and 15% in the end points C_{max} (saturating concentration). We can equivalently vertically translate the dose-response curve to allow for 0% variation in the start point (implying $C = 0$ gives $E = 0$) and 20% variation in the target endpoint (or that $C = C_{max}$ implies $E > 0.8E_{max}$). In this latter case, the dose-response curve is described by

$$E = \frac{E_{max}C}{EC_{50} + C}. \tag{2.29}$$

Let x be the observed effect, which is some fraction of the maximal effect E_{max} so that we report the measured effect as xE_{max}. Then at $C = C_{max}$ we have from Equation (2.29)

$$\begin{aligned} xE_{max} = \frac{E_{max}C_{max}}{EC_{50} + C_{max}} &\iff x = \frac{C_{max}}{EC_{50} + C_{max}} \\ \iff xEC_{50} = C_{max}(1 - x) &\iff EC_{50} = C_{max}\left(\frac{1}{x} - 1\right). \end{aligned}$$

Further, suppose that a uniform distribution characterises the variability at the end point, meaning that the probability of reaching $0.8E_{max}$ is equal for each observed dose-response curve. Then by the last equivalency above, we calculate that

$$EC_{50} = C_{max}\left(\frac{1}{0.8} - 1\right) = \frac{C_{max}}{4}. \tag{2.30}$$

Practically this indicates that the half-maximal concentration occurs at after the first 25% (quartile) of concentrations in the case of a uniform distribution between dose-response curves. Using this theoretical relationship, we were able to calculate EC50s in absence of clinical data. For our purposes, we express Equation (2.30) as

$$EC_{50} = C_{min} + \frac{(C_{max} - C_{min})}{4}. \tag{2.31}$$

From the PK model and clinical studies, we are able to measure $C_{min} = G^{homeo}$ and C_{max} and then give an estimate for the half-maximal concentrations which is independent of the target effect. This has the potential to be an important method for the determination of EC50 concentrations when only the PK models are reported. One is also able to attribute other probability distributions at the end points if there is one that is preferable over others. Using Equation (2.31) in conjunction with Equation (3.15), we calculated

$$b_S = b_{NP} = b_{NM} = b_G = C_{min} + \frac{(C_{max} - C_{min})}{4} = 11.2679\,\text{days}^{-1},$$

for the half-maximal concentrations of Equations (3.16), (4.9), (3.18), and (3.21). The remaining half-maximal concentration parameter relates the effect of G-CSF on the maturation velocity of the marrow neutrophils (Equations (4.10) to (3.20)). For this determination, we make use of the data reported in Figure 3 in [34] which reports the time-evolution of the appearance of irradiated cells in the circulation after 5 successive days of G-CSF dosing (with daily blood samples and ANC analysis). Assuming the 300 μg dose induced the maximal observed effect, we determined that $V_{max} = 10$ by first calculating the difference that [34] measured for the total production time at the high dose compared to the reported baseline for the whole production time. This difference was then subtracted from our baseline neutrophil maturation time estimation of $a_{NM} = 3.9$. Assuming that the renal elimination is the dominant method of G-CSF excretion during exogenous administration, we can neglect the internalisation elimination and calculate a closed-form solution from

$$\frac{dG_{estimate}}{dt} = \frac{k_a F(Dose_{GCSF})}{V_d} e^{-k_a t_{inj}} + G_{prod} - k_{ren} G(t)$$

to obtain

$$G_{estimate}(t) = \frac{\frac{k_a F(Dose_{GCSF})}{V_d} e^{-k_{ren}t - t(k_a - k_{ren})}}{k_{ren} - k_a} + \frac{G_{prod}}{k_{ren}} + e^{-k_{ren}t} \frac{G^{homeo} - \frac{k_a F(Dose_{GCSF})}{V_d}}{k_{ren} - k_a - \frac{G_{prod}}{k_{ren}}}. \tag{2.32}$$

Then, the 30 μg dose is used to find b_V making use of Matlab's $fzero$ function [27] to

solve for b_V from Equation (2.23) (τ_{NM} is determined from the data curve of [34] and a_{NM} is again taken to be 3.9 days). This gave $b_V = 3.5\,\mathrm{ng/mL}$.

Finally, [39] cite a range of $(8-16)\times b_N^{min}$ for their B_N^{max}, which accounts for the maximal birth rate. We take our similar parameter under the cited range since the additional processes of proliferation and maturation accounted for in our model contribute to the 'birth' of neutrophils in our study. With this in mind, we take $trans^{max}$ to be 4 times the homeostatic transition rate, or $trans^{max} = 4trans^{homeo}$.

The analyses of the previous chapter pertained particularly to an average patient owing to the parameter estimation undertaken therein. Accordingly, we sought to demonstrate the applicability of our predictions by answering to the impact PK variability has on the model's outcomes. The following chapter outlines the inclusion of PopPK models for both filgrastim (from [14]) and PM001014, or Zalypsis ® (from [19]). IIV and IOV were included according to their previously estimated values and *in silico* variability scenarios were performed. A total of five such combinations were analysed in terms of three pertinent clinical endpoints: the time to ANC nadir, the nadir's value, and the area under the concentration-effect curve (AUCE). Our results indicate that PK variability's impact on the model's prediction was not statistically significant and, as such, the physiological model is robust to PK variability. This work is accepted for publication (Craig, M., González-Sales, M., Li, J., Nekka, F. (2015-to appear). In: *Interdisciplinary Mathematical Research and Applications*. Springer PROMS. B. Toni (ed.)).

For clarity, a magnification of Figure 3.7 is provided at the end of this chapter.

Chapter 3

Impact of Pharmacokinetic Variability on a Mechanistic Physiological Pharmacokinetic/Pharmacodynamic Model: A Case Study of Neutrophil Development, PM00104, and Filgrastim

Morgan Craig[1], Mario González-Sales[1,2], Jun Li[1], Fahima Nekka[1]

[1]Faculté de Pharmacie, Université de Montréal, Montréal, QC, Canada H3T 1J4 [2] InVentiv Health Clinical, 5260 Boulevard Décarie, Montréal, QC H3X 2H9

Abstract

Interindividual variability (IIV) is considered a crucial factor for the general use of mathematical modelling in physiology. However, mechanistic models of physiological systems are commonly built for an average patient, raising the question of their applicability at the population level. Using our previously developed physiological model of neutrophil regulation, which accounts for the detailed hematopoietic mechanisms as well as the pharmacokinetics (PKs) of a chemotherapeutic agent (PM00104) and a granulostimulant (filgrastim), we incorporated the reported population pharmacokinetic (PopPK) models of each drug to investigate the impact of PK variability on fully mechanistic models. A variety of scenarios, including multiple doses of PM00104, were simulated for cohorts of 500 *in silico* patients to analyse the model's predictability in terms of several pharmacological indicators, such as the time to neutrophil nadir, the value of the nadir, and the area under the effect curve. Our results indicate the robustness of our model's predictions in all considered scenarios. Based on our findings, we conclude that for drugs with short-lived PKs in comparison to

their pharmacodynamics (PDs), models that "sufficiently" account for physiological mechanisms inherently assimilate PK deviations, making the further inclusion of PK variability unnecessary.

3.1 Introduction

One of the most important considerations in modern pharmacometrics is the determination of the dose-response relationship. This can be obtained through data-driven models [13, 14, 19] but can also be achieved through techniques stemming from mathematical biology using physiologically-driven mechanistic modelling [2, 4, 5, 9, 10, 12]. While both approaches use mathematics to describe the disposition of drugs in the body, each handles the problem from a unique vantage point. On one hand, data-driven models are based on various components: the structural model (typically compartmental), a set of statistical models (with assumptions for probabilistic distributions around model parameters as well as error structure), and covariate models (when relevant). To this end, population pharmacokinetic/pharmacodynamic (Pop-PK/PD) modelling is the most representative approach and is now widely used in drug research and development. Even so, the construction of data-driven models highly depends on the available data and the required statistical optimisation procedures. The poor quality of data can induce model misspecification and hamper the generalisability of the models outside of the context in which they were built.

On the other hand, mechanistic models of human processes tackle the problem using the so-called bottom-up strategy. These models are constructed directly from the system being studied by applying the available physiological knowledge to drive their predictions. During this process, a number of hypotheses are generated and translated using various mathematical techniques. Generally, the model parameters are derived or estimated from experimentally determined values available from a diverse cross-section of fields (physiological, chemical, physical, etc.), and utilise patients' average values [3]. Physiological models are used to explore a variety of complex situations. For example, the model of neutrophil development studied herein can be applied in oncological settings or in the study of hereditary disorders like cyclical neutropenia. Mechanistic models are useful for explaining an observed effect in relation to its components as a result of their physiologically-detailed construction. However, constructing a physiological model can be time-consuming and re-

quires advanced mathematical knowledge to ensure the models' validity. This complexity makes this approach more popular in academia but work still needs to be done to expand its use in routine data analysis.

Since physiological models are frequently developed for an average patient, an investigation of the impact of PK variability on their predictions is crucial to extend their applicability to patient populations. Considering the complexity of these models, testing their robustness by simulating credible scenarios of patient variability will determine their suitability for general use. For instance, it is pertinent to know whether drug regimens identified for an average patient through these models can be extended to the population level. We have previously published a physiological model of myelopoiesis [5], with integrated PK models of both PM00104 [19] and filgrastim (adjuvant recombinant human granulocyte colony-stimulating factor (G-CSF), used to increase neutrophil counts to prevent and/or recover from neutropenia) [14], which studied the impact of the time of administration of supportive filgrastim during chemotherapy. Using published or well-derived parameters from the literature for an average patient, our model successfully predicted clinical data and identified beneficial regimens. Therein, we determined that delaying the administration of rhG-CSF after PM00104 by 7 days mitigated the neutropenic impact of anti-cancer treatment, resulting in a reduction from 10 administrations per cycle to 3 or 4 and a reduction in the burden to the patient [5]. The current study will address the extendibility of this regimen to a population by investigating the impact of PK interindividual variability (IIV), and of the reported interoccasion variability (IOV) of PM00104, on relevant indicators, such as the time to neutrophil nadir and the nadir level.

From a systems pharmacology point of view, the PKs of the previously mentioned drugs are short-lived in comparison to their PDs. Indeed, the PK half-lives of both PM00104 and filgrastim are on the order of hours (24 and from 6-10, respectively) whereas it can take several days to observe their effects on cells in circulation due to the production time of neutrophils in the bone marrow (up to 14 days) [5, 19]. In the current work, we focused on the impact that IIV components of the data-driven models of [14, 19] can have on our physiological model [5]. Based on numerical simulations, the sensitivity of the physiological model to the impact of IIV variability was quantified and statistically analysed. Using a variety of scenarios that cover a large number of clinical situations, our

physiological PK/PD model, though developed for an average patient, proved to be robust in terms of PK IIV when clinically relevant PD criteria are tested, advocating its general applicability to a large population.

3.2 A Hypothesis-driven Physiological/PK/PD Model of Granulopoiesis During Chemotherapy With Supportive Adjuvant

A mechanistic physiological model of myelopoiesis was constructed [5] by extending the previous work of [2, 4, 9, 10] through the addition of neutrophil reservoir pools in the bone marrow and other tissues, and then subsequently incorporating comprehensive PK/PD models for PM00104 (Zalypsis®), a chemotherapeutic drug, and filgrastim (rhG-CSF), a supportive adjuvant, to determine dosing schemes that provide the most benefit (least harm) for patients. The physiological model translates the physiological mechanisms of neutrophil production mathematically using delay differential equations (DDEs) to characterise the cellular transition delays.

The neutrophil model is a three-dimensional set of delay differential equations with variable aging rate and general delays obtained from an age-structured partial differential equation model with appropriate boundary conditions. A schematic diagram of the model is given in Figure 3.1. Beginning in a quiescent state, a hematopoietic stem cell (HSC-population $Q(t)$ in units 10^6 cells/kg), which is capable of self-renewal at rate $\beta(Q)$ (in units days^{-1}) and which is subject to apoptosis at rate γ_S (in units days^{-1}), undergoes differentiation into one of three blood cell lines. In this model, we consider any differentiation into the erythrocyte or platelet lineages to occur at rate κ_δ (in units days^{-1}) whereas differentiation into the neutrophil line occurs at rate $\kappa_N(N)$ (in units days^{-1}). Note that while κ_δ is taken herein to be constant, the rate of entry of the HSCs into the neutrophil lineage depends on the concentration of circulating neutrophils (population $N(t)$ in units 10^9 cells/kg). Once committed to the neutrophil line, cells undergo proliferation-a period of successive divisions-at a rate of η_{NP} (in units days^{-1}) for a total of τ_{NP} days. Cells then cease division and mature at a velocity of V_N (in units days^{-1}) for a total of $\tau_{NM}(t)$ days. During this maturation period, cells are subject to random cell death at a rate of γ_{NM} (in units days^{-1}). Newly mature neutrophils are then sequestered within the bone marrow in the mature neutrophil reservoir (population $N_r(t)$ in units 10^9 cells/kg). These

reserved cells are mobilised from the bone marrow into circulation at a rate of $trans_N$ (in units days^{-1}) or, failing to reach the circulation, die from the reservoir at rate γ_r (in units days^{-1}). The mature pool is a crucial aspect of the neutrophil lineage, as it contains ten times the number of circulating neutrophils and is necessary for the rapid restocking of the blood neutrophils in case of falling ANCs or infection [11, 22]. Cells reaching the circulation subsequently disappear from the blood at a rate of γ_N (in units days^{-1}). Beginning with a quiescent hematopoietic stem cell (HSC) differentiating into the neutrophil lineage, we model the proliferation and maturation of neutrophilic cells in the bone marrow. The mature neutrophils then settle into the marrow reservoir before appearing in circulation (release from the reservoir can be steady, or homeostatic, or rapid mobilisation in the case of emergency). Once a mature neutrophil reaches the circulation, it disappears fairly rapidly (half-life of around 7 hours) through apoptosis or margination into the tissues. Equations (3.1) – (3.3) below highlight the primary model equations.

$$\frac{dQ(t)}{dt} = -\left(\kappa_N(N(t)) + \kappa_\delta + \beta(Q(t))\right) Q(t) + A_Q(t)\beta\left(Q(t-\tau_S)\right) Q(t-\tau_S) \tag{3.1}$$

$$\frac{dN_r(t)}{dt} = A_N(t)\kappa_N(N(t-\tau_N))Q(t-\tau_N)\left(\frac{V_N(G(t))}{V_N(G(t-\tau_{NM}(t))}\right) \tag{3.2}$$

$$\frac{dN(t)}{dt} = f_{trans}(G(t))N_r(t) - \gamma_N N(t). \tag{3.3}$$

Delays are indicated by $t-\tau$, where τ is a physiologically present delay in the system (time of HSC self-renewal, time of proliferation, time of maturation, time of residence in the marrow reservoir, and the total time it takes to produce a neutrophil from differentiation to appearance in the circulation). Equations (3.1) – (3.3) are subject to the initial condition of homeostasis ($Q(t) = Q^{homeo}$, $N_r(t) = N_r^{homeo}$, $N(t) = N^{homeo}$, for all $t \leqslant t_0$, where t_0 marks the beginning of treatment). In [5], parameter estimation for an average patient was carried out in an consistent way using data available in the literature. Typical values of the PK models of PM00104 and G-CSF were adapted from [19] and [14], respectively. In this study, IIV and IOV components of the PK parameters were added where necessary. All parameter values in the current work were kept as in [5] and any exceptions will be indicated explicitly below. Particular attention was paid to capturing the dominant processes implicated in the development of a circulating neutrophil within the bone marrow.

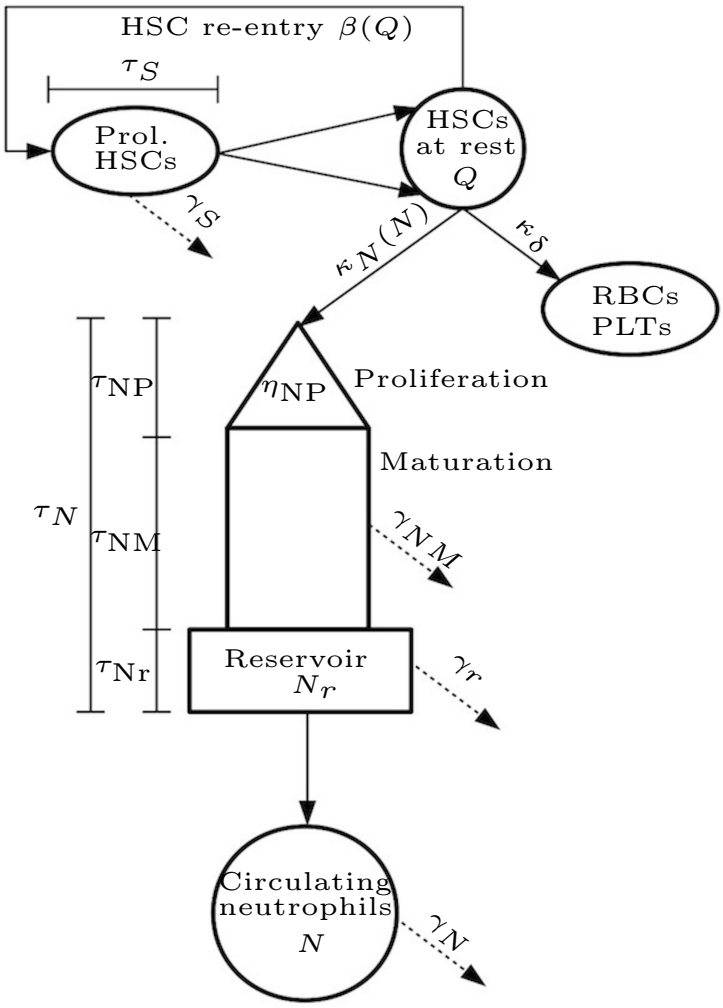

Figure 3.1 – Schematic representation of the production of circulating neutrophils in the bone marrow. Stem cells (Q) undergo the usual cell cycle and mitosis (at rate $\beta(Q)$) where they die at rate γ_S or return to the quiescent stage. They then remain at rest until differentiation into the neutrophil lineage (at rate $\kappa_N(N)$) or other blood lines (red blood cells-RBCs or platelets-PLTs) at rate κ_δ. After entering the neutrophil lineage, a period of successive divisions (proliferation) at rate η_{NP} is followed by a maturing phase with velocity V_N. The mature neutrophils then reach the neutrophil reservoir (N_r) in the bone marrow. Mature reserved cells are maintained within the bone marrow for rapid mobilisation if needed [11]; the rate of transfer from the pool into the circulation (f_{trans}) is determined by G-CSF concentrations in the central compartment (plasma). Mature reserved neutrophils that do not reach the circulation die from the reservoir at rate γ_{Nr}. Circulating neutrophils N disappear from the circulation by apoptosis at rate γ_N. The time for the hematopoietic stem cell proliferative phase cycle is τ_S. The process of the development of a neutrophil takes time τ_N from their entry into the neutrophil line to their appearance in the blood, which includes the time for proliferation (τ_{NP}), maturation (τ_{NM}), and marrow sequestration (τ_{Nr}). Figure from [5]

As in our previous work, multiplying $N(t)$ by the fraction of circulating cells is necessary for comparison to data since $N(t)$ herein represents the total blood neutrophil pool (TBNP). The HSC's feedback rate and amplification rates of both the HSCs and the blood neutrophils are modelled as

$$\beta(Q) = f_Q \frac{\theta_2^{s_2}}{(\theta_2^{s_2} + Q^{s_2})} \tag{3.4}$$

$$\kappa_N(N) = f_N \frac{\theta_1^{s_1}}{(\theta_1^{s_1} + N^{s_1})} \tag{3.5}$$

$$A_Q(t) = 2 \exp\left[-\int_{t-\tau_S}^{t} \gamma_S(s)ds\right] \tag{3.6}$$

$$A_N(t) = \exp\left[\int_{t-\tau_N(t)}^{t-\tau_N(t)+\tau_{NP}} \eta_{NP}(s)ds - \int_{t-\tau_N(t)+\tau_{NP}}^{t} \gamma_{NM}(s)ds\right]. \tag{3.7}$$

The entire process of neutrophil development is regulated by the concentration of G-CSF, $G(t)$ in units ng/ml), which acts in negative feedback with the blood neutrophil numbers in that its concentration falls when neutrophil numbers increase and vice versa. G-CSF acts the whole length of the neutrophil development cycle to maintain neutrophil counts at homeostatic levels. It is implicated in the recruitment of HSCs into the neutrophil line, in the regulation of the rates of proliferation and maturation, and controls the release of mature neutrophils from the bone marrow reservoir into circulation [9]. Details on the PD effects modelled herein are given in Figure 3.2 and in the following sections.

3.3 Pharmacokinetics and Pharmacodynamics of PM00104

The pharmacokinetics of PM00104 were characterised using a catenary four compartment disposition model with linear elimination [19]. The differential equations describing the system were as follows

$$\frac{dA_1}{dt} = -\left(\frac{CL}{V_1} + \frac{Q_2}{V_1} + \frac{Q_3}{V_1}\right) A_1 + \frac{Q_2}{V_2} A_2 + \frac{Q_3}{V_3} A_3 \tag{3.8}$$

$$\frac{dA_2}{dt} = -\frac{Q_2}{V_2} A_2 - \frac{Q_4}{V_2} A_2 + \frac{Q_2}{V_1} A_1 + \frac{A_4}{V_4} A_4 \tag{3.9}$$

$$\frac{dA_3}{dt} = -\frac{Q_3}{V_3} A_3 + \frac{Q_3}{V_1} A_1 \tag{3.10}$$

$$\frac{dA_4}{dt} = -\frac{Q_4}{V_4} A_4 + \frac{Q_4}{V_2} A_2, \tag{3.11}$$

where A_1, A_2, A_3 and A_4 represent the amount of PM00104 in compartments 1, 2, 3, and 4, CL represents the clearance (in units L/hr), Q_2 is the inter-compartmental clearance between compartments 1 and 2 (in units L/hr), Q_3 is the intercompartmental clearance between compartments 1 and 3 (in units L/hr), Q_4, is the intercompartmental clearance between compartments 2 and 4 (in units L/hr), V_1 is the volume of distribution in the central compartment (in units L), V_2 is the volume of distribution in compartment 2 (in units L), V_3 is the volume of distribution in compartment 3 (in units L), and V_4 is the volume of distribution in compartment 4 (in units L). Concentrations in each compartment are given by dividing the amount of the drug A_j $(j = 1, \ldots, 4)$ by the volume in the respective compartment V_j $(j = 1, \ldots, 4)$.

The above model and results of [13] and [19] were incorporated into [5] in a physiologically-consistent way. Since the main function of a chemotherapeutic agent is to quell the uncontrolled division of cells by reducing/destroying their ability to replicate. In the blood system, the effects of this reproductive cessation are assumed to be twofold: first, the HSCs experience an increase in the rate of cell death in the proliferative phase (effectively reducing their proliferative capabilities) and second, the rate at which the neutrophils undergo successive divisions is greatly reduced. These two effects are modelled, respectively, as

$$\gamma_S^{chemo}(C_p(t)) \quad = \quad \gamma_S^{homeo} + h_S C_p, \tag{3.12}$$

where C_p is the concentration of PM00104 in the first, or plasmatic, compartment, γ_S^{chemo}

is the rate of apoptosis of the proliferative HSCs during chemotherapy, γ_S^{homeo} is their rate of apoptosis at homeostasis. Due in large part to the absence of data relating the effects of chemotherapy on the HSCs, we took a linear effect from chemotherapy upon γ_S, modulated by the effects parameter h_S, and

$$\eta_{NP}^{chemo}(C_p(t)) \quad = \quad \eta_{NP}^{homeo}\left(\frac{(EC_{50})^h}{(EC_{50})^h + (C_p(t))^h}\right). \tag{3.13}$$

Here η_{NP}^{chemo} is the rate of neutrophil proliferation during chemotherapeutic treatment, η_{NP}^{homeo} is the homeostatic rate of proliferation, EC_{50} is the usual half-effects constant, and h is the Hill coefficient of the effect.

3.4 Pharmacokinetic and Pharmacodynamic Model of G-CSF

As previously alluded to, G-CSF is an endogenous cytokine which stimulates the production of neutrophils. It is also used in an exogenous form as a prophylactic to help patients with low neutrophil counts rescue their circulating ANCs [9]. In terms of its PK properties, G-CSF is believed to have a constant production rate [14] and to have two modes of elimination, namely an nonsaturable process from renal elimination, and a saturable process driven by internalisation by the neutrophils [15]. Accordingly, as in [5], we model the endogenous concentration of G-CSF as:

$$\frac{dG}{dt} = G_{prod} - k_{ren}G - \chi k_{int}\frac{G^2}{G^2 + k_d^2}N, \tag{3.14}$$

where G_{prod} is the endogenous constant production rate of G-CSF (in units ng/ml/day, k_{ren} is the rate of renal elimination (in units days^{-1}), k_{int} is the rate of internalisation by the neutrophils (in units days^{-1}), k_d is the usual dissociation constant (in units ng/mL), and χ is a scaling factor to correct for the units of Equation (3.14). The choice of Hill coefficient is due to the 2:2 stoichiometry of G-CSF binding to its G-CSFR receptor on the neutrophils [16]. When G-CSF is given exogenously, primarily in subcutaneous form, we model its administration as in [5], and originally in [14] as

$$\frac{dG}{dt} = \frac{F(Dose)k_a}{V_d}e^{-k_a t} + G_{prod} - k_{ren}G - \chi k_{int}\frac{G^2}{G^2 + k_d^2}N, \tag{3.15}$$

where F is the bioavailable fraction, $Dose$ is the administered subcutaneous dose (in ng), k_a is the rate of absorption from the subcutaneous pool (in units days^{-1}), and V_d is the volume of distribution (in units mL).

The pharmacodynamic action of G-CSF is multifaceted. From the beginning of a neutrophil as a stem cell, G-CSF reduces the rate of cell death in the proliferating HSC compartment (decreasing γ_S), increases the rate of neutrophil proliferation in the bone marrow (increases η_{NP}), increases the speed of neutrophil maturation (increases $V_N(N)$ or, equivalently, decreases τ_{NM} [22]), decreases neutrophil death out of the marrow maturation compartment (decreases γ_{NM}), and modulates the rate of transfer between the mature neutrophil reservoir and the circulation in function of the ANC (modulates f_{trans}) [2, 9, 14, 21]. These effects are modelled as follows, with b_i, $i = S, N, NP, V$ the parameters relating the half-maximal concentration of G-CSF. In the HSC compartment,

$$\gamma_S(G(t), C_p(t))) \quad = \quad \gamma_S^{min} - \frac{(\gamma_S^{min} - \gamma_S^{chemo})b_S}{G(t) - G^{homeo} + b_s}, \tag{3.16}$$

where γ_S^{min} is the minimal rate of apoptosis in the HSCs proliferative phase. Note that the rate of cell death of the HSCs is dependent both on the concentration of G-CSF and on the concentration of the chemotherapeutic agent. The details of the latter dependency are given in Equation (3.18) below.

Neutrophils undergoing proliferation are also subject to the effects of chemotherapeutic drugs (Equation (3.13) and details above) and to the concentration of G-CSF

$$\begin{aligned} \eta_{NP}(G(t), C_p(t)) &= \eta_{NP}^{chemo}(C_p(t)) \\ &\quad + \frac{(\eta_{NP}^{max} - \eta_{NP}^{chemo}(C_p(t)))(G(t) - G^{homeo})}{G(t) - G^{homeo} + b_{NP}} \end{aligned} \tag{3.17}$$

$$\gamma_{NM}(G(t)) = \gamma_{NM}^{min} - \frac{(\gamma_{NM}^{min} - \gamma_{NM}^{homeo})b_{NM}}{G(t) - G^{homeo} + b_{NM}}. \tag{3.18}$$

Here η_{NP}^{max} is the maximal proliferation rate of the neutrophils and γ_{NM}^{min} is the minimal

rate of random cell loss of the maturing neutrophils.

When G-CSF concentrations are high, the speed with which the neutrophils in the marrow age increases, thereby decreasing the time they spend maturing. These simultaneous effects are given by

$$V_N(G(t)) \quad = \quad 1 + (V_{max} - 1)\frac{G(t) - G^{homeo}}{G(t) - G^{homeo} + b_V}, \tag{3.19}$$

where V_{max} is the maximal aging velocity of the maturing neutrophils, and

$$\frac{d\tau_N(t)}{dt} = \frac{d\tau_{NM}(t)}{dt} \quad = \quad 1 - \frac{V_N(G(t))}{V_N(G(t - \tau_{NM}(t)))}. \tag{3.20}$$

The details of the derivation of Equation (3.20) are given in full in [5].

Finally, the recruitment of a reserved neutrophil to the blood given as

$$f_{trans}(G(t)) \quad = \quad trans^{homeo}\frac{trans^{ratio}(G(t) - G^{homeo}) + b_G}{G(t) - G^{homeo} + b_G}, \tag{3.21}$$

where $trans^{homeo}$ relates the homeostatic rate of transit from the neutrophil bone marrow reservoir into the circulation, and $trans^{ratio} = \frac{trans^{max}}{trans^{homeo}}$, is an empirically determined ratio modulating the fraction of neutrophils released from the reservoir [23, 26].

3.5 Incorporating Variability Into the Physiological PK/PD Model

By incorporating the PK variability reported for PM00104 and filgrastim in [19] and [14] into our average patient model [5], we now study the impact of PK variability on our model's predictions. In the case of PM00104, the fixed effects were assumed to follow a lognormal distribution according to the following equation:

$$P_{j,k} = P^* e^{\eta_j \tau_k}, \tag{3.22}$$

where $P_{j,k}$ is the individual j^{th} PK parameter for the k^{th} occasion, P^* is the typical value of the parameter of interest, and η_j and τ_k are independent and normally distributed

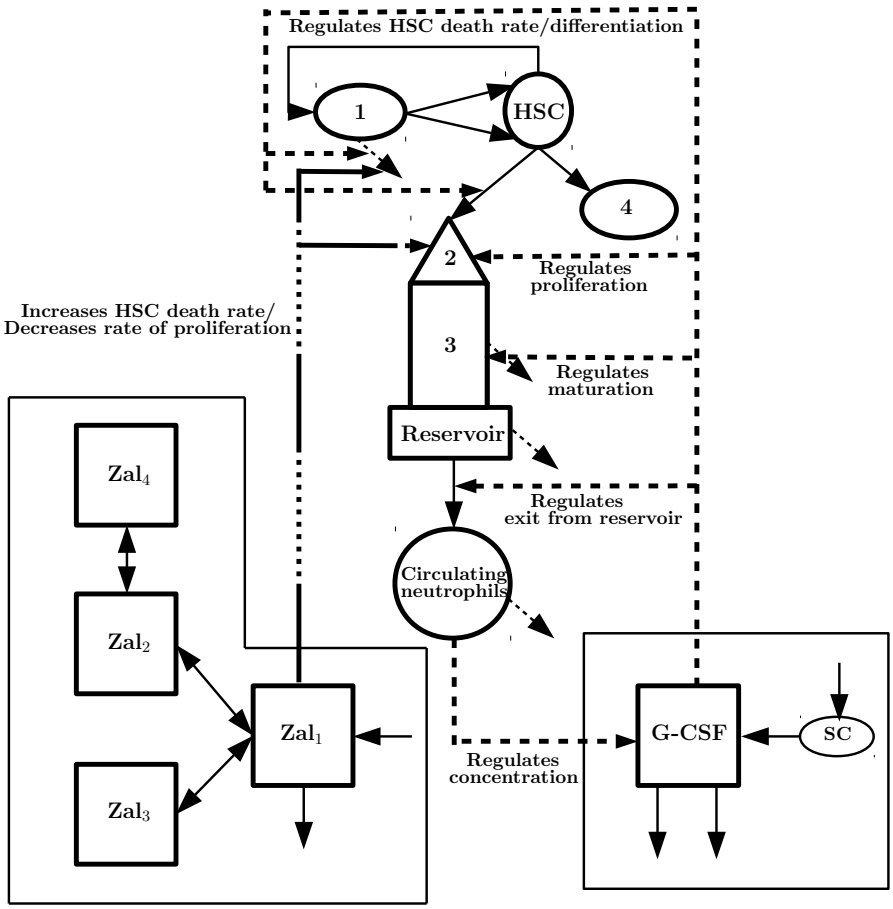

Figure 3.2 – Schematic representation of the effects of PM00104 (solid/dotted lines) and G-CSF (dashed). Model summary as in Figure 3.1 in Section 3.2. PM00104 (Zal) acts to disrupt cellular division resulting in a higher rate of death out of the hematopoietic stem cell (HSC) compartment, and a decrease in the rate of neutrophil proliferation in the bone marrow. G-CSF acts throughout the neutrophil lineage to stabilise the numbers of circulating neutrophils by regulating their exit out of the marrow reservoir, their proliferation, and their maturation. Concurrently, it acts upon the HSCs by regulating their differentiation into the neutrophil lineage and their death rate (to stabilise their population numbers). The complete model is taken from [5]. HSC: hematopoietic stem cells at rest, 1: dividing HSCs, 2: proliferating marrow neutrophils, 3: maturing marrow neutrophils, 4: other blood cell lines, Reservoir: mature marrow neutrophil reservoir, Zal_1: central compartment of PM00104, Zal_2: second compartment of PM00104, Zal_3: third compartment of PM00104, Zal_4: fourth compartment of PM00104, G-CSF: granulocyte colony-stimulating factor, SC: subcutaneous pool

interindividual and interoccasion (IOV) random variables with zero-mean and variance ω_p^2 and π_p^2, respectively. The magnitude of the IIV and the IOV were expressed as coefficient of variation (CV). The parameter estimates and their associated precisions, measured as percentage of relative standard error (%RSE), are presented in Table 3.I.

Parameter (Units)	**Interpretation**	**Estimate**	**%RSE**
Fixed Effect		θ	
Cl (L/hr)	Clearance	43.7	3.43
V_1 (L)	Volume of central compartment	32.7	12.4
Q_2 (L)	Transit rate (compartments 1 and 2)	123	5.76
V_2 (L)	Volume of second compartment	162	8.33
Q_3 (L/hr)	Transit rate (compartments 1 and 3)	11.3	13.2
V_3 (L)	Volume of third compartment	388	11.8
Q_4 (L/hr)	Transit rate (compartments 2 and 4)	62.3	9.00
V_4 (L)	Volume of fourth compartment	239	9.00
Interindividual variability		CV%	
Cl	IIV of Cl	34.1	24.6
V_1	IIV of V_1	82.5	37.7
V_2	IIV in V_2	65.1	41.8
Q_3	IIV of Q_3	87.7	31.2
V_3	IIV of V_3	52.0	25.2
(Cl, V_2)	Correlation between Cl and V_2	0.555	78.6
(Cl, Q_3)	Correlation between Cl and Q_3	0.572	33.6
(V_2, Q_3)	Correlation between V_2 and Q_3	0.522	84.0
Interoccasion variability		CV%	
Cl	IOV of Cl	14.1	96.0

Table 3.I – Summary of the PopPK model parameters of PM00104 reported in [19]. Interindividual variability (IIV), correlations between interindividual random effects, and interoccasion variability (IOV) were reported as percentage of coefficient of variation (CV)

The filgrastim model used in this study is given by Equation (3.15) in Section 3.4. Table 3.II summarises the estimated model parameters of filgrastim and their associated precisions, expressed as %RSE.

As we were primarily concerned with PK variability, and owing to the differences in the current model's PD effects (Equations (S20)-(S25)), the IIV reported by the SC_{50}, S_{max_1}, and NB_0 parameters were not considered in the present analysis.

Parameter (Units)	Interpretation	Estimate	%RSE
Fixed Effect		θ	
k_{el} (hr^{-1})	Rate of renal elimination	0.152	16.6
V_d (L)	Volume of distribution	2.42	6.8
ξ (fg/cell)	Proportionality constant ([GCSFR] per neutrophil)	0.181	45.5
NB_0 (cells/μL)	Initial number of blood neutrophils	1.55	17.9
SC_{50} (ng/mL)	Serum concentration eliciting 50% of the maximal effect	3.15	21.0
S_{max_1}	Maximum effect	34.7	36.0
Interindividual variability		ω^2	
k_{el}	IIV of k_{el}	0.194	33.1
V_d	IIV of V_d	0.138	25.9
ξ	IIV of ξ	5.87×10^{-2}	65.6
SC_{50}	IIV of SC_{50}	0.764	25.0
S_{max_1}	IIV of S_{max_1}	1.88×10^{-4}	133
NB_0	IIV of NB_0	0.109	29.1

Table 3.II – Summary of the PopPK/PD model parameters of filgrastim, adapted from [14]. Interindividual variability (IIV) was reported as variances. Only those values which were found to be impacted by IIV are reported

3.6 Quantification of the Impact of IIV Using Computer Simulation

To rigorously quantify the impact of IIV on the physiological granulopoiesis model, *in silico* simulations of 500 patients were performed. All simulations were carried out in Matlab 2013a [17]. The physiological model of neutrophil production, consisting of a three-dimensional system of delay-differential equations (DDEs), and the associated PK/PD models were previously implemented using the *ddesd* solver in Matlab as described in [5]. To incorporate the IIV of the PK models provided in Tables 3.I and 3.II, each parameter value subject to a random effect was sampled from a normal or multivariate normal distribution and a simulation was performed for these values. This sampling technique was performed 500 times to simulate 500 patients in each scenario. Parameter values were sampled using the *normrnd* and *mvnrnd* functions in Matlab. The following variability scenarios were covered:

(a) 6.892 mg (1 hour infusion) PM00104 alone with variability.

(b) 350 mg filgrastim alone with variability.

(c) 6.892 mg (1 hour infusion) PM00104 with variability and 350 mg filgrastim without

variability.

(d) 6.892 mg (1 hour infusion) PM00104 without variability and 350 mg filgrastim with variability.

(e) 6.892 mg (1 hour infusion) PM00104 and 350 mg filgrastim, both with variability.

The additional considered scenario without any variability was previously treated in [5] and serves as a reference in the present analysis.

3.6.1 Statistical Analyses

For each variability scenario, a hypothesis test was carried out in Matlab using the *ttest* function; one-sample Student t-tests about the mean time to nadir (TNad), mean ANC nadir (Nad), and mean area under the effect curve (AUEC) were performed. These three metrics were chosen as evaluation criteria for the determination of optimal regimens, as previously carried out in [5, 25]. Further, the 95% asymptotic confidence interval (CI) of the mean differences between the model with (*test*) and without (*reference*) variability were computed to check the narrowness of the CI. The mean difference is then judged significant if 0 is outside of CI, implying the null hypothesis (H_0) cannot be rejected. Finally, in a manner analogous to a bioequivalence trial, the ratios of the *test* to the *reference* for the mean TNad, mean Nad, and AUEC were computed. Accordingly, if the ratio was within the range of 80% to 125% [8], both models were considered equivalent implying no difference was observed in terms of this indicator.

3.7 Results

3.7.1 No Statistically Significant Differences in Time to Nadir Between the Model With and Without Variability

Visually, the five simulated scenarios produced TNads close to the mean for most, if not all, of the 500 *in silico* patients (Figure 3.7). Indeed, no significant difference in the time to nadir was found when testing for differences in the means between the test and reference models. While the mean TNad varies owing to the particular drug combination being tested, all five of the scenarios examined herein produced no difference to the time to the nadir onset and the asymptotic 95% CI of the difference in each case was narrow

and always included H_0 (see Table 3.III). Further, all ratios of the test model (with IIV) to the reference model (without IIV) were within the 80% and 125% range in every scenario. Consequently, the test models can be considered equivalent to the reference model (see Table 3.III).

Scenario	**Mean TNad$_{ref}$ (days)**	**Mean TNad$_{test}$ (days)**	**Ratio**	**95% CI of difference**
(a)	11.47	11.47	100.0%	$10^{-4}\times$([-1.77, 1.77])
(b)	6.26	5.77	92.1%	$10^{-2}\times$([-3.90, 3.90])
(c)	6.79	6.56	96.7%	$10^{-4}\times$([-4.93, 4.93])
(d)	6.79	6.57	96.8%	$10^{-3}\times$([-7.30, 7.30])
(e)	6.79	6.58	96.9%	$10^{-2}\times$([-2.07, 2.07])

Table 3.III – Results of the test for significance in the time to nadir of each of the studied scenarios: (a) PM00104 alone with variability, (b) Filgrastim alone with variability, (c) PM00104 with variability with filgrastim without variability, (d) PM00104 without variability and filgrastim with variability, (e) PM00104 and filgrastim, both with variability. Ratios computed as (test/reference)×100. In all cases, differences were determined to be statistically insignificant at the $\alpha = 5\%$ level (all p-values were 1). TNad$_{ref}$: time to nadir of the reference model, TNad$_{test}$: time to nadir of the test model, CI: confidence interval

3.7.2 No Statistically Significant Differences in the Value of the Nadir Between the Models With or Without Variability

On the other hand, and similar to the time to nadir, both visually (Figure 3.4) and statistically speaking, no significant differences were found in the nadir values. In all scenarios, the asymptotic 95% CI of the difference remains narrow, indicating small standard errors, as seen in Table 3.IV. In addition, the calculated ratios of the nadir value of the test models versus the reference model were within the interval of 80% to 125% and, accordingly, the models with variability were equivalent to the reference model.

3.7.3 No Statistically Significant Differences in the Area Under the Effects-time Curve Between the Model With or Without Variability

Furthermore, no statistically significant differences in the AUECs were found. While the previous tests of the time to nadir and the nadir value decomposed the results into one direction at a time (x and y, respectively), the AUEC metric provides insight into the

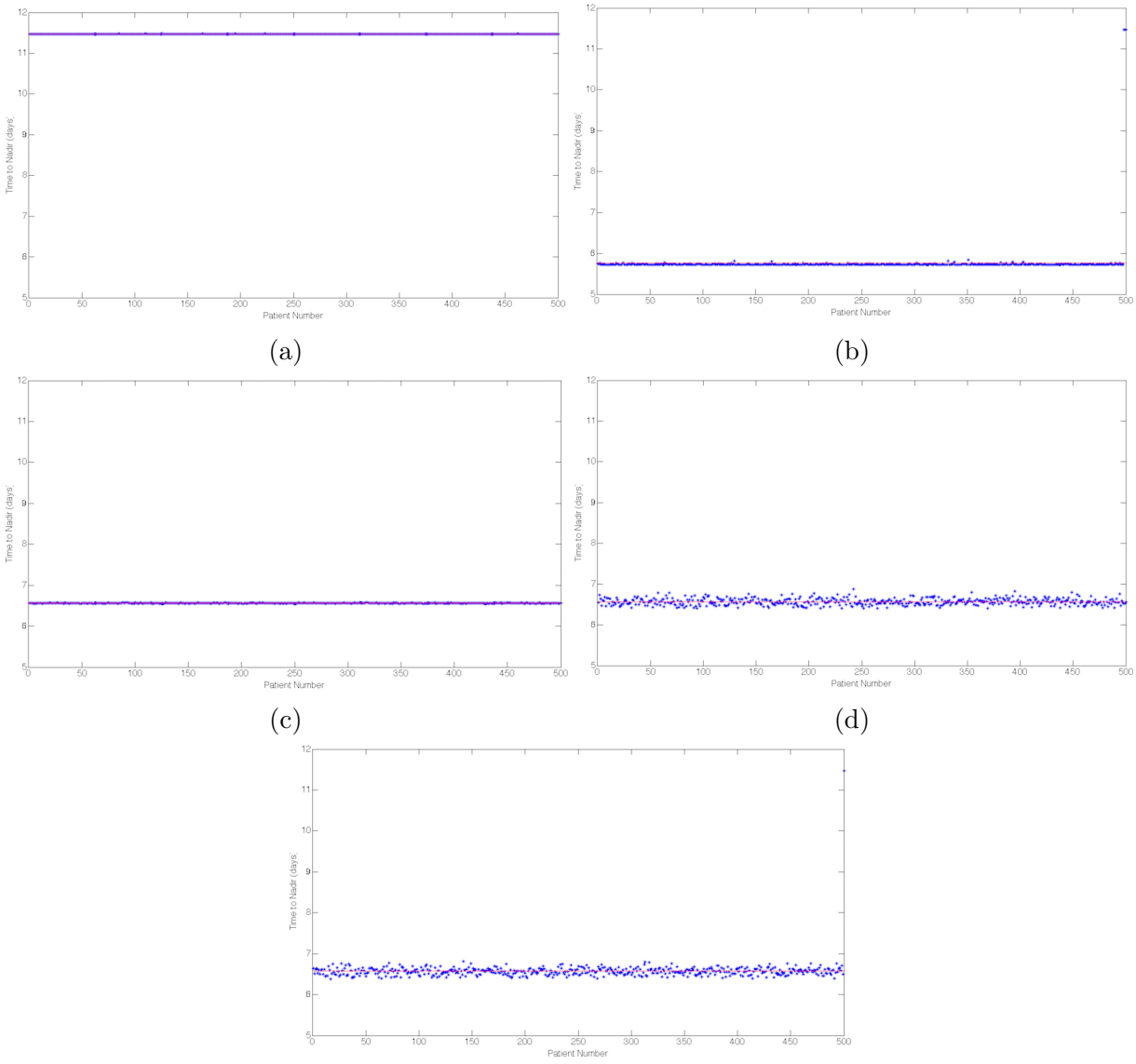

Figure 3.3 – Time to nadir results of each *in silico* patient in each scenario: (a) PM00104 alone with variability, (b) Filgrastim alone with variability, (c) PM00104 with variability with filgrastim without variability, (d) PM00104 without variability and filgrastim with variability, (e) PM00104 and filgrastim, both with variability. Solid horizontal lines represent the mean of each scenario

Scenario	Mean Nad_{ref} of (10^9 cells/L)	Mean Nad_{test} (10^9 cells/L)	Ratio	95% CI of difference
(a)	4.08	4.08	100.7%	$10^{-3}\times$([-1.60, 1.60])
(b)	6.88	6.35	92.4%	$10^{-2}\times$([-4.72, 4.72])
(c)	4.04	4.14	102.3%	$10^{-4}\times$([-8.04, 8.04])
(d)	4.04	4.10	101.5%	$10^{-2}\times$([-1.20, 1.20])
(e)	4.04	4.11	101.7%	$10^{-2}\times$([-1.28, 1.28])

Table 3.IV – Results of the test for significance in the nadir value of each of the studied scenarios: (a) PM00104 alone with variability, (b) Filgrastim alone with variability, (c) PM00104 with variability with filgrastim without variability, (d) PM00104 without variability and filgrastim with variability, (e) PM00104 and filgrastim, both with variability. Ratios computed as (test/reference)×100. In all cases, differences were determined to be statistically insignificant at the $\alpha = 5\%$ level (all p-values were 1). Nad_{ref}: nadir of the reference model, Nad_{test}: nadir of the test model, CI: confidence interval

simultaneous xy-behaviour of the predictions. Further, as we are no longer simply looking a single nadir point but over the entire 50 simulated days, this last measure synthesises the full temporal nature of the simulated solutions. In the case of the AUECs, as in the previous two tests, all the asymptotic 95% CI of the difference included 0. Finally, all ratios were within the 80% and 125% range and can therefore be considered equivalent (Table 3.V). Figure 3.5 reveals the consistency of the statistical analysis of the AUEC values. That being said, in each scenario involving the full variability model for filgrastim, AUEC values are less uniform. Indeed, because the AUEC investigation shifts the focus to the full time-course studied, the longer-term effects of G-CSF serving to replenish the neutrophil reservoir, such as increased speed of maturation (V_N), increased rate of neutrophil proliferation (η_{NP}), and increased rate of differentiation from the HSCs (κ_N), can be seen.

3.7.4 Full Time Courses of Neutrophil Counts

The full time courses of each patient's ANCs over 50 days were simulated and the results presented in Figure 3.6. Each subfigure corresponds to one of the five different scenarios used to discern the influence of IIV on the prediction. As is consistent with the previously presented results, variability in filgrastim leads to larger variations in the ANC compared to variability in PM00104, which does not cause deviations on the same scale due to its limited involvement in neutrophil development. PM00104 disrupts cellular transcription

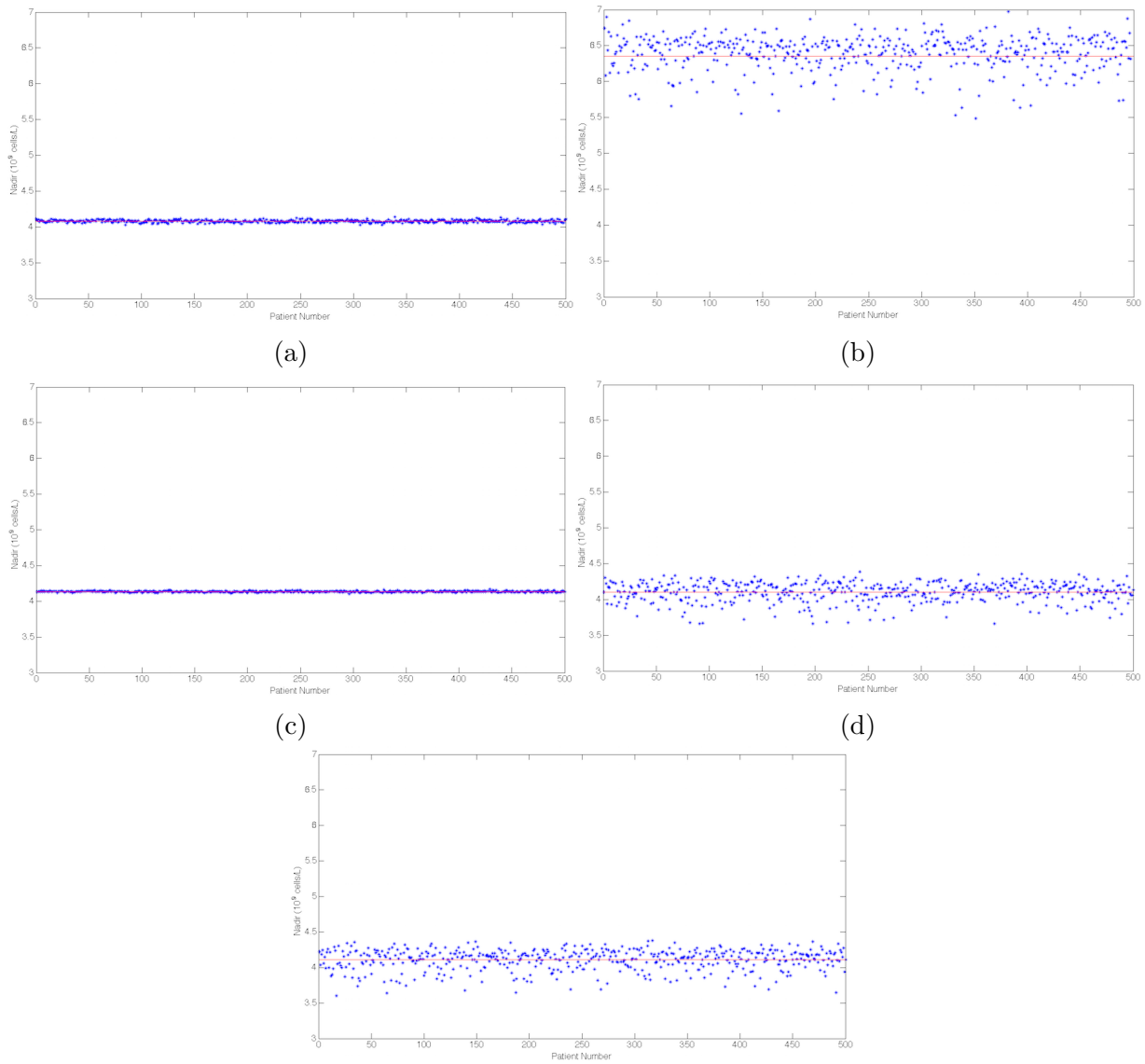

Figure 3.4 – Nadir value per *in silico* patient in each scenario: (a) PM00104 alone with variability, (b) Filgrastim alone with variability, (c) PM00104 with variability with filgrastim without variability, (d) PM00104 without variability and filgrastim with variability, (e) PM00104 and filgrastim, both with variability. Solid horizontal lines represent the mean of each scenario

in a variety of ways, leading to apoptosis through the arrest of the S-phase [20]. We therefore consider that those cells that are no longer dividing, notably neutrophils that have finished proliferation (postmitotic–maturing neutrophils, neutrophils in the marrow reservoir, and circulating and/or marginated neutrophils), are no longer subject to its effects.

Scenario	Mean $AUEC_{ref}$ ($(10^9$ cells/L) days)	Mean $AUEC_{test}$ ($(10^9$ cells/L) days)	Ratio	95% CI of difference
(a)	404.30	404.30	100.0%	$10^{-2}\times$([-1.74, 1.74])
(b)	501.25	478.80	95.5%	$10^{-1}\times$([-6.91, 6.91])
(c)	432.73	428.52	99.0%	$10^{-2}\times$([-2.39, 2.39])
(d)	432.73	429.92	99.4%	$10^{-1}\times$([-4.07, 4.07])
(e)	432.73	429.68	99.3%	$10^{-1}\times$([-4.08, 4.08])

Table 3.V – Results of the test for significance in the area under the effects curve (AUEC) of each of the studied scenarios: (a) PM00104 alone with variability, (b) Filgrastim alone with variability, (c) PM00104 with variability with filgrastim without variability, (d) PM00104 without variability and filgrastim with variability, (e) PM00104 and filgrastim, both with variability. Ratios computed as (test/reference)$\times$100. In all cases, differences were determined to be statistically insignificant at the $\alpha = 5\%$ level (all p-values were 1). $AUEC_{ref}$: area under the effect-time curve of the reference model, $AUEC_{test}$: area under the effect-time curve of the test model, CI: confidence interval

Accordingly, since these non-dividing cells constitute the bulk of the neutrophils in the lineage (postmitotic neutrophils are estimated to be about 77% of the marrow neutrophils [6]), the PDs of PM00104 will have a more limited role on neutrophils developing in the marrow.

3.7.5 Assessing the Impact of PK Variability on Regimens Identified by the Physiological Model

The value of the neutrophil nadir following the administration of PM00104 was previously used in [5] to determine those regimens which best mitigated neutropenia and which reduced the number of administrations of filgrastim per 21-day periodic cycle over six cycles. Although the nadir is not affected by the PK IIV, as shown for the single dose scenario reported above, the presence of interoccasion variability (IOV) was reported for PM00104 [19], which may have an impact on dosing regimen decisions. Hence, to extend our findings to the optimal regimens we previously reported, we investigated the impact of IOV on the physiological model by simulating three cycles of 21-day periodic administration of 6.892 mg (1 hour infusion) of PM00104 with both IIV and IOV models as in [19] for another group of in silico patients. However, no significant impact on the modelÕs predictions could be observed with this additional source of variability (not shown). Since all clinical markers used in this study are in fact not affected by the presence of PK IIV,

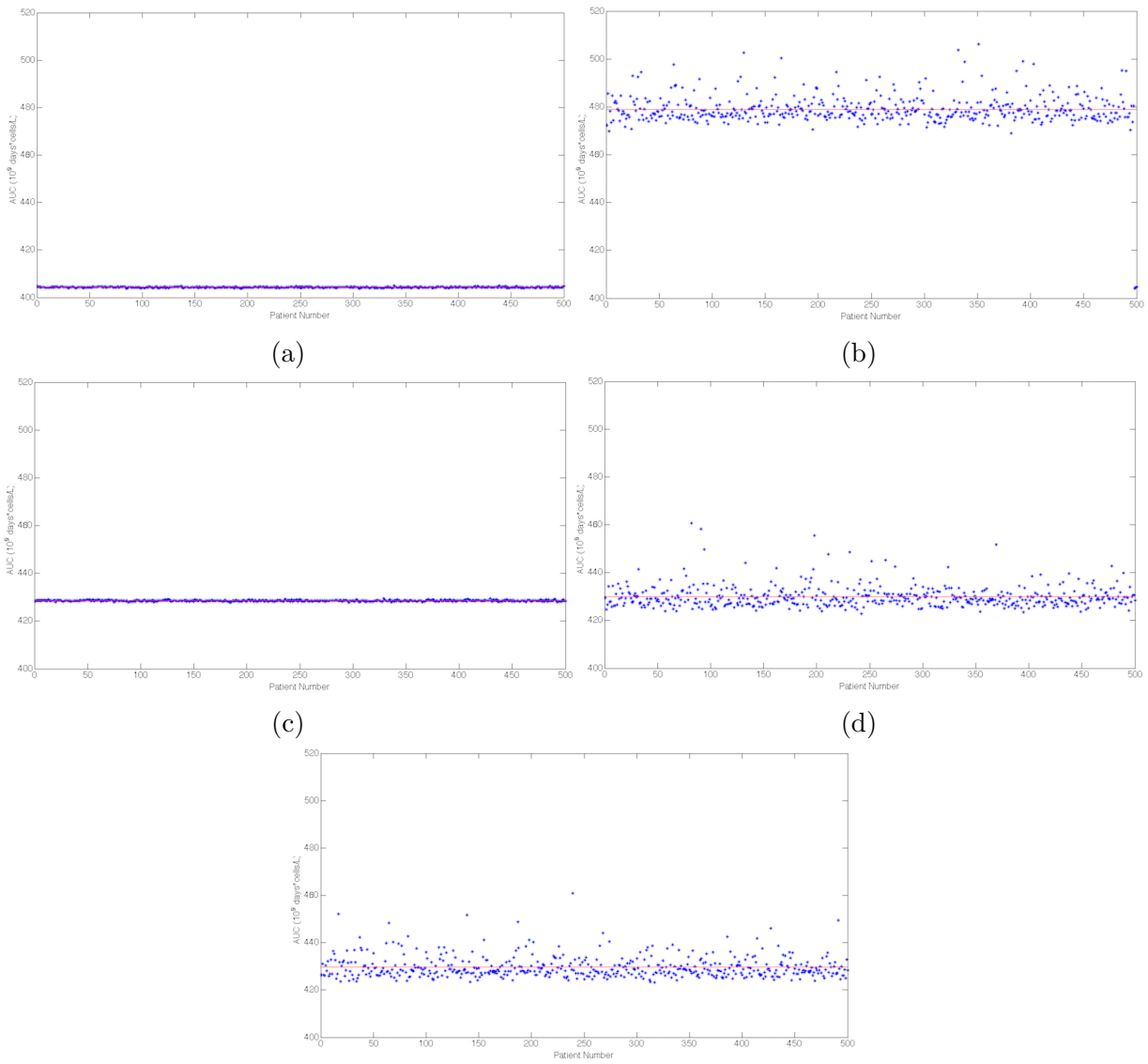

Figure 3.5 – Area under the effects curve (AUEC) results per *in silico* patient in each scenario: (a) PM00104 alone with variability, (b) Filgrastim alone with variability, (c) PM00104 with variability with filgrastim without variability, (d) PM00104 without variability and filgrastim with variability, (e) PM00104 and filgrastim, both with variability. Solid horizontal lines represent the mean of each scenario

and IOV did not have significant impact on the prediction of nadir, it is reasonable for us to extend the regimens identified for the average patient using the physiological model to the population as reported in [19]. Consequently, in line with the findings of [5], it may be prudent to delay the first administration of filgrastim after the administration of

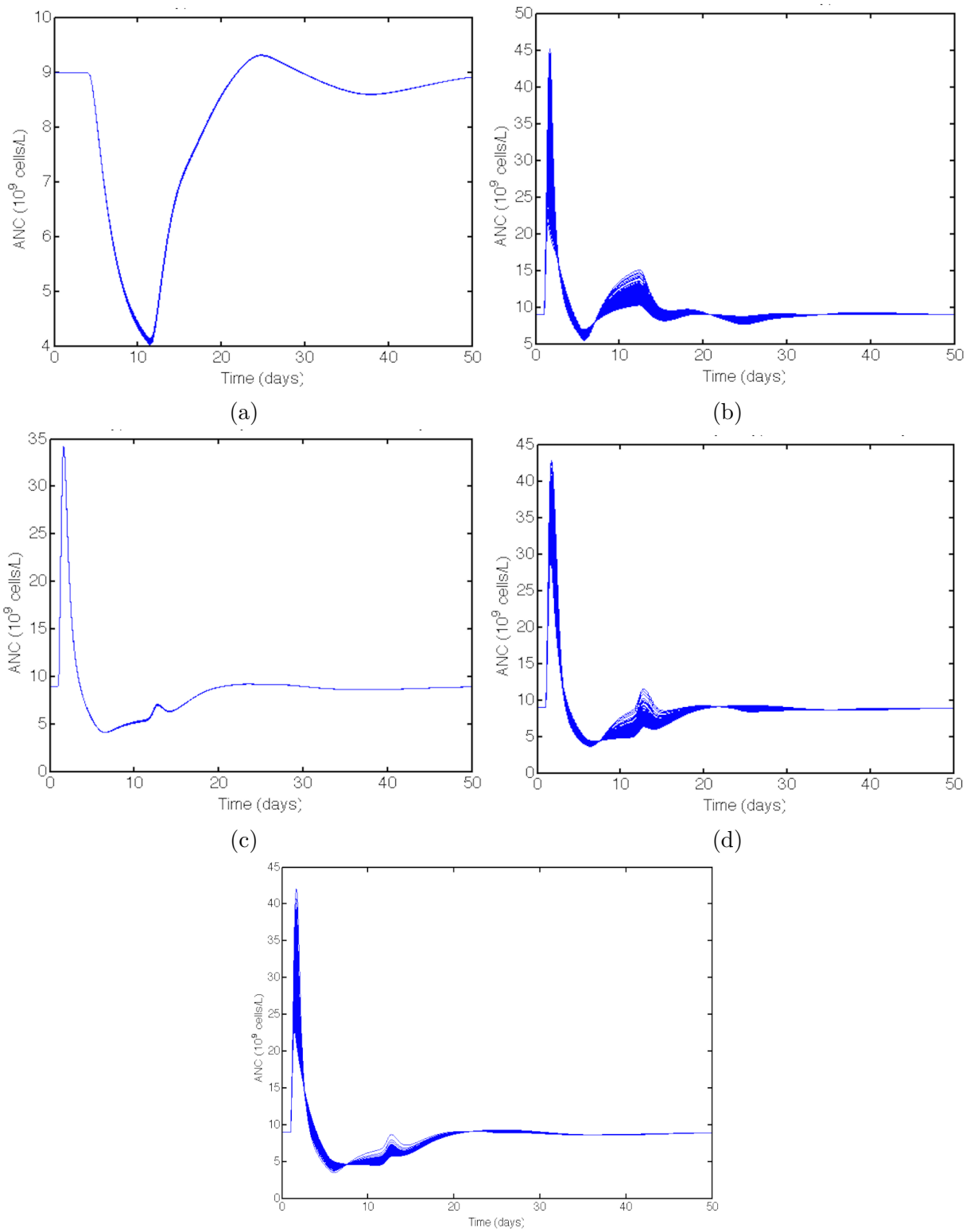

Figure 3.6 – Absolute neutrophil counts of each *in silico* patient in the five studied scenarios: (a) PM00104 alone with variability, (b) Filgrastim alone with variability, (c) PM00104 with variability with filgrastim without variability, (d) PM00104 without variability and filgrastim with variability, (e) PM00104 and filgrastim, both with variability

chemotherapy to lessen the impact of the anti-cancer drug(s) on the neutrophil lineage.

3.8 Discussion

Physiological modelling is increasingly in-demand as a means to deepen our understanding of the mechanisms underlying drug fate and effects and to allow for an increased incorporation of physiology beyond the more popular data-driven physiologically-based models. Although the most widespread model evaluation criteria are based on the goodness of fit of the model to data, this approach can overlook subtle mechanisms behind the physiological system that may be essential to explain outcomes. When these mechanisms become the key to ensuring the model's generalisability, concerns could be raised about the transferability of the model's findings and its applicability to a variety of situations. To bridge this gap, it is natural to root the model in contemporary scientific theories since their development inevitably leads to a deeper understanding of the principle processes of the systems under study. Physiological PK/PD models use rigorous mathematical expressions to characterise processes on the causal path between xenobiotics, the body, and pathologies, and are intended to improve our capacity for extrapolation and prediction [7]. As a result of the complexity of this tri-relationship, these kinds of models frequently use an average representation to reconstruct the entire process. While one can admit that this average portrayal greatly serves to demystify the physiological mechanisms being studied in addition to their interactions with drugs and diseases, its application to a population can be challenged by the presence of different sources of variability. The robustness of these physiological PK/PD models to IIV, a pervasive concern in PopPK/PD, has to be investigated to ensure clinical applicability.

This is precisely the objective of the current study; herein, we were concerned by the impact of IIV on the predictive quality of a physiological PK/PD model that we previously developed to study the production of neutrophils for use in chemotherapeutic contexts [5]. This model was predicated upon detailed hematopoietic mechanisms and incorporated the pharmacokinetics of a chemotherapeutic agent (PM00104) and a granulostimulant (filgrastim) to successfully reproduce the behaviour of this lineage with respect to a variety of oncological protocols. In this study, we have added the reported IIV of the PopPK models of the two previously considered drugs, PM00104 [19] and filgrastim [14], to investigate

the impact of IIV on this model. Five variability scenarios were considered to assess the impact of IIV for each separate drug model in addition to combinations thereof. First, single doses of PM00104 and filgrastim were administered alone to two separate cohorts of 500 *in silico* patients using each drug's respective variability model. Second, both drugs were administered together to two other sets of 500 *in silico* patients taking into account just the fixed effects of one drug, and the fixed and random effects of the other. Last, the variability models of both drugs were applied together to another set of 500 patients to evaluate the full impact of the IIV of both drugs. In all situations, no significant impact of IIV was observed on any chosen clinical indicator, namely the time to ANC nadir, the mean ANC value of the nadir, and the mean AUEC, nor did IOV significantly impact the predictions. These findings confirm the applicability of the physiological PK/PD neutrophil model beyond the case of an average patient. For example, on the basis of our current findings, the administration regimen previously judged to be optimal to avoid moderate to severe neutropenia during 21-day periodic administration of PM00104 over 6 cycles (G-CSF given on days 7 through 10 following the administration of PM00104) can now be extended beyond the average patient to a population of patients [5]. We attribute the robustness of the model's predictions to pharmacokinetic IIV to the fact that both drugs (PM00104 and filgrastim) have short elimination half-lives in comparison to the lifespan of the neutrophils they affect, a factor inherently incorporated into the physiological model. Since the physiological PK/PD model was built to reproduce the sequential events leading to the formation of neutrophils (recruitment of HSCs into the neutrophil line, proliferation, maturation, and release of mature neutrophils into circulation) and specifically identifies where each drug has an effect on the appearance of a neutrophil in the blood stream, the model is able to directly relate each drug's concentration in the plasma with the chain of events it will induce over the course of a neutrophil's lifespan. Thus, because both PM00104 and filgrastim have shorter PK timespans than their PDs, the magnitude of their IIV is also shorter lived and these differences will only marginally influence the effects on the physiology.

The results presented in this work provide evidence that physiological modelling is a valuable alternative to the widely used data-driven modelling approach. Once their general applicability has been proved, as it is the case for the present model, physiological

models can even transcend the means for which they are intended, thereby justifying the effort required for their construction. A large number of physiological models have been developed for which a combination with PK/PD models can be envisaged. It would be advisable to systematically submit these models to a "variability screening test" to guarantee their general applicability prior to any clinical validation. Designing such standard tests remains a challenge that has to be addressed. Indeed, the National Institutes of Health (NIH) in the United States has identified quantitative systems pharmacology (QSP) as ideally situated to develop quantitative and predictive methods able to identify the impact of individual variability [24]. Fortunately, systems biologists and pharmacologists have access to a variety of databases [1] which facilitate both the formation/instatement and the evolution of standardised variability screening tests. Ultimately, a concerted and coordinated effort between industry, academia, and regulatory agencies, as exemplified by the partnership between the NIH and the Food and Drug Administration (FDA), is required to ensure that variability is addressed when performing QSP approaches.

In conclusion, this study not only substantiates and situates the use of physiological modelling in pharmacometrics, it provides incentives to continue to improve our understanding of the underlying physiological mechanisms of a given system. In a broader sense, this work testifies to the necessity of building bridges between diverse actors from different backgrounds (pharmaceutical scientists, clinicians, biomathematicians, statisticians, engineers, etc.) in the pharmacometrics community to best serve patients and their needs.

References

[1] J.P.F. Bai and D.R. Abernathy. Systems pharmacology to predict drug toxicity: Integration across levels of biological organization. *Annual Review of Pharmacology and Toxicity*, 53:451–473, 2013.

[2] G. Brooks, G.P. Langlois, J. Lei, and M.C. Mackey. Neutrophil dynamics after chemotherapy and G-CSF: The role of pharmacokinetics in shaping the response. *Journal of Theoretical Biology*, 315:97–109, 2012.

[3] R.P. Brown, M.D. Delp, S.L. Lindstedt, L.R. Rhomberg, and R.P. Beliles. Physiological parameter values for physiologically based pharmacokinetic models. *Toxicology Industrial Health*, 13:407–484, 1997.

[4] C. Colijn and M.C. Mackey. A mathematical model of hematopoiesis: II. Cyclical neutropenia. *Journal of Theoretical Biology*, 237:133–146, 2005.

[5] M. Craig, A.R. Humphries, J. Bélair, J. Li, F. Nekka, and M.C. Mackey. Neutrophil dynamics during concurrent chemotherapy and G-CSF administration: Mathematical modelling guides dose optimisation to minimise neutropenia. *Journal of Theoretical Biology*, 385:77–89, 2015.

[6] J.T. Dancey, K.A. Deubelbeiss, L.A. Harker, and C.A. Finch. Neutrophil kinetics in man. *The Journal of Clinical Investigation*, 58:705–715, 1976.

[7] M. Danhof, E. DeLange, O. Della Pasqua, B. Ploeger, and R. Voskuyl. Mechanism-based pharmacokinetic-pharmacodynamic (PKPD) modeling in translational drug research. *Trends in Pharmacological Sciences*, 29:186–191, 2008.

[8] FDA. Guidance for Industry, Exposure-response Relationships – Study Design, Data analysis, and Regulatory Applications. Technical report, U.S. Department of Health and Human Services, Food and Drug Administration, Center for Drug Evaluation and Research, Center for Biologics Evaluation and Research, Rockville, MD, USA, April 2003.

[9] C. Foley and M.C. Mackey. Mathematical model for G-CSF administration after chemotherapy. *Journal of Theoretical Biology*, 257:27–44, 2009.

[10] C. Foley, S. Bernard, and M.C. Mackey. Cost-effective G-CSF therapy strategies for cyclical neutropenia: Mathematical modelling based hypotheses. *Journal of Theoretical Biology*, 238:756–763, 2006.

[11] R.C. Furze and S.M. Rankin. Neutrophil mobilization and clearance in the bone marrow. *Immunology*, 125:281–288, 2008.

[12] H. Gobburu, J.and Agersø, W. Jusko, and L. Ynddal. Pharmacokinetic-pharmacodynamic modeling of ipamorelin, a growth hormone releasing peptide, in human volunteers. *Pharmaceutical Research*, 16:1412–1416, 1999.

[13] M. González-Sales, B. Valenzuela, C. Pérez-Ruixo, C. Fernández Teruel, B. Miguel-Lillo, Soto Matos A., et al. Population pharmacokinetic-pharmacodynamic analysis of neutropenia in cancer patients receiving PM00104 (Zalypsis®). *Clinical Pharmacokinetics*, 51:751–764, 2012.

[14] W. Krzyzanski, P. Wiczling, P. Lowe, E. Pigeolet, M. Fink, A. Berghout, and S. Balser. Population modeling of filgrastim PK-PD in healthy adults following intravenous and subcutaneous administrations. *Journal of Clinical Pharmacology*, 9 Suppl:101S–112S, 2010.

[15] T. Kuwabara, Y. Kato, S. Kobayashi, H. Suzuki, and Y. Sugiyama. Nonlinear pharmacokinetics of a recombinant human granulocyte colony-stimulating factor derivative (Nartograstim): Species differences among rats, monkeys and humans. *Journal of Pharmacology and Experimental Therapeutics*, 271:1535–1543, 1994.

[16] J.E. Layton and N.E. Hall. The interaction of G-CSF with its receptor. *Frontiers in Bioscience*, 31:177–199, 2006.

[17] Mathworks. *MATLAB 2013a*. Mathworks, Natick, Massachusetts, 2013.

[18] I. Nestorov. Whole body pharmacokinetic models. *Clinical Pharmacokinetics*, 42: 883–908, 2003.

[19] C. Pérez-Ruixo, B. Valenzuela, C. Fernández Teruel, M. González-Sales, B. Miguel-Lillo, A. Soto-Matos, et al. Population pharmacokinetics of PM00104 (Zalypsis®) in cancer patients. *Cancer Chemotherapy and Pharmacology*, 69:15–24, 2012.

[20] B. Petek and R. Jones. PM00104 (Zalypsis®): A marine derived alkylating agent. *Molecules*, 19:12328–12335, 2014.

[21] T.H. Price, G.S. Chatta, and D.C. Dale. Effect of recombinant granulocyte colony-stimulating factor on neutrophil kinetics in normal young and elderly humans. *Blood*, 88:335–340, 1996.

[22] S.M. Rankin. The bone marrow: A site of neutrophil clearance. *Journal of Leukocyte Biology*, 88:241–251, 2010.

[23] M. Scholz, S. Schirm, M. Wetzler, C. Engel, and M. Loeffler. Pharmacokinetic and -dynamic modelling of G-CSF derivatives in humans. *Theoretical Biology and Medical Modelling*, 9:1497–1502, 2012.

[24] D.R. Sorger, S.R.B. Allerheiligen, R.B. Abernethy, K.L.R. Altman, A.C. Brouwer, A. Califano, D.Z. D'Argenio, R. Iyengar, W.J. Jusko, R. Lalonde, D.A. Lauffenburger, B. Shoichet, J.L. Stevens, P. Subramaniam, S. van der Graaf, and P. Vincini. Quantitative and Systems Pharmacology in the Post-genomic era: New Approaches to Discovering Drugs and Understanding Therapeutic Mechanisms. An NIH white paper by the QSP Workshop Group. Technical report, National Institutes of Health of the United States of America, Bethesda, Maryland, USA, 2011.

[25] O. Vainas, S. Ariad, O. Amir, W. Mermershtain, V. Vainstein, M. Kleiman, O. Inbar, R. Ben-Av, A. Mukherjee, S. Chan, and Z. Agur. Personalising docetaxel and G-CSF schedules in cancer patients by a clinically validated computational model. *British Journal of Cancer*, 107:814–822, 2012.

[26] B. Wang, T.M. Ludden, E.N. Cheung, G.G. Schwab, and L.K. Roskos. Population pharmacokinetic-pharmacodynamic modeling of filgrastim (r-metHuG-CSF) in healthy volunteers. *Journal of Pharmacokinetics and Pharmacodynamics*, 28:321–342, 2001.

3.9 Appendix

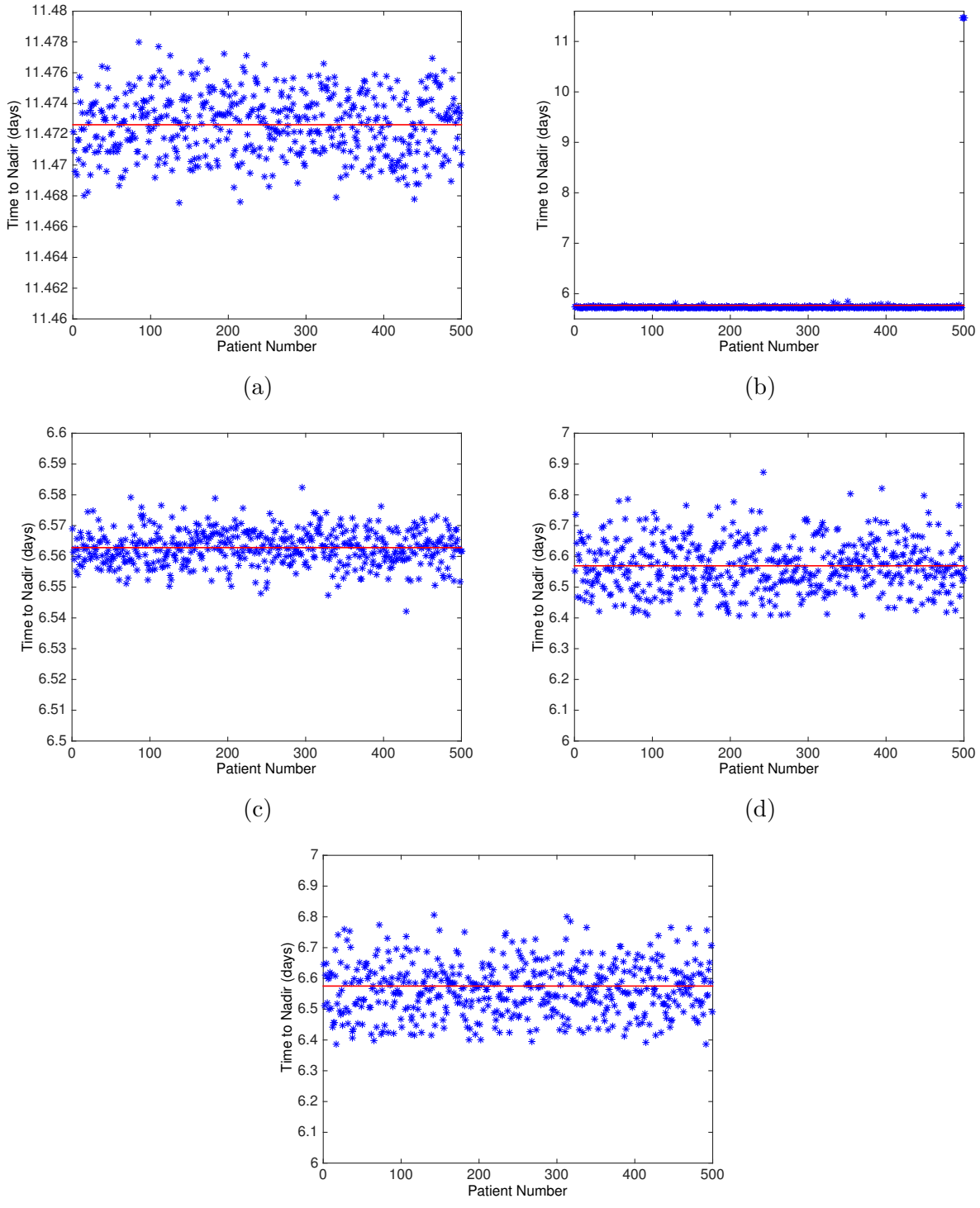

Figure 3.7 – Magnification of the time to nadir results of each *in silico* patient in each scenario: (a) PM00104 alone with variability, (b) Filgrastim alone with variability, (c) PM00104 with variability with filgrastim without variability, (d) PM00104 without variability and filgrastim with variability, (e) PM00104 and filgrastim, both with variability. Solid horizontal lines represent the mean of each scenario

Following the work in the preceding chapters, we endeavoured to apply our physiological model to the study of cyclical neutropenia (CN) and the optimisation of the use of rhG-CSF for patients with the disease. However, as CN is an inherently dynamic disease characterised by sustained oscillations in neutrophil numbers, we first needed to refine the physiological and PD models to account for the high neutrophil counts with high G-CSF concentrations observed during treatment with exogenous G-CSF. The work presented in this chapter grew out of the failure of the single unbound G-CSF model to account for data for the single administration in the log-scale. In this work, we develop a novel PK model for G-CSF which accounts for both unbound and bound concentrations and modify the PD model accordingly. We also demonstrate the derivation of the DDEs used in our model of granulopoiesis from an age-structured PDE model. Several intricate fitting procedures are then employed to estimate the parameters not available in the literature or unobtainable through model constraints. A comparison with the CHOP14 data presented in Chapter 2 is again included. This work is significant in that it demonstrates that the mass-action equilibrium hypothesis for endogenous hormones given exogenously in mimetic form is not satisfied at homeostasis. This suggests that this hypothesis should be revisited in other pharmacokinetic studies. The article is under review by the *Bulletin of Mathematical Biology* (submitted December 21, 2015; BMAB-D-16-00010).

Chapter 4

A Mathematical Model of Granulopoiesis Incorporating the Negative Feedback Dynamics and Kinetics of G-CSF/Neutrophil Binding and Internalisation

M. Craig[1], A.R. Humphries[2], M.C. Mackey[3]

[1]Faculté de Pharmacie, Université de Montréal, Montréal, QC, Canada H3T 1J4, [2] McGill University, Department of Mathematics and Statistics, Montréal, QC, Canada, H3A 0B9, [3]McGill University, Departments of Physics and Physiology, Montréal, QC, Canada, H3G 1Y6

Abstract

We develop a physiological model of granulopoiesis which includes explicit modelling of the kinetics of the cytokine granulocyte colony-stimulating factor (G-CSF) incorporating both the freely circulating concentration and the concentration of the cytokine bound to mature neutrophils. G-CSF concentrations are used to directly regulate neutrophil production, with the rate of differentiation of stem cells to neutrophil precursors, the effective proliferation rate in mitosis, the maturation time, and the release rate from the mature marrow reservoir into circulation all dependent on the level of G-CSF in the system. The dependence of the maturation time on the cytokine concentration introduces a state-dependent delay into our differential equation model, and we show how this is derived from an age-structured partial differential equation model of the mitosis and maturation, and also detail the derivation of the rest of our model. The model and its estimated param-

eters successfully predict the neutrophil and G-CSF responses to a variety of treatment scenarios, including the combined administration of chemotherapy and exogenous G-CSF. This concomitant treatment was reproduced *without any additional fitting* to characterise drug-drug interactions.

Keywords

granulopoiesis; mathematical modelling; state-dependent delay differential equations; physiologically constructed pharmacokinetics; G-CSF; bound and unbound drug concentrations

4.1 Introduction

We present a new model of granulopoiesis, in which the production of neutrophils is governed by a negative feedback loop between the neutrophils and granulocyte colony stimulating factor (G-CSF). G-CSF is the principal cytokine known to regulate neutrophil production and in our model it is used to moderate differentiation of stem cells, apoptosis of proliferating neutrophil precursors, the speed at which neutrophils mature and the rate that mature neutrophils are released from the marrow reservoir. To facilitate this, we derive not only new functions for the pharmacodynamic effects of G-CSF, but also a new model of the G-CSF kinetics which incorporates cytokine binding and internalisation by the neutrophils. We dispense with the mass action law assumption made in some previous models and directly model the concentration of both circulating G-CSF and G-CSF bound to neutrophils. This improved kinetic model furnishes us with G-CSF concentrations which are considerably more accurate than our previous models so we are able to use them to directly drive the pharmacodynamic effects and finally form a fully closed cytokine-neutrophil feedback loop.

At homeostasis the dominant removal mechanism for G-CSF is internalisation by neutrophils after it binds to receptors on these cells [32]. This gives rise to a negative feedback mechanism on the G-CSF pharmacokinetics (PKs) whereby large concentrations of neutrophils result in G-CSF being removed from circulation, in turn leading to low concentrations of circulating G-CSF. On the other hand if neutrophil concentrations are reduced then G-CSF is not cleared from circulation as quickly and circulating concentrations increase as a result. The feedback loop is completed by the pharmacodynamic (PD) effects

of the G-CSF: elevated (depressed) G-CSF levels lead to increased (decreased) neutrophil production. Due to this feedback, using the simple paradigm that neutrophil concentration is a cipher for the cytokine concentration (with one low when the other is high), it is possible to derive granulopoiesis models without explicitly modelling the cytokines. This is particularly useful because it is not universally agreed where or how the multitude of identified cytokines all act.

The mathematical modelling of granulopoiesis has a long and rich history [4, 5, 9, 11, 18, 20, 25, 27, 28, 53, 54, 56, 57, 61, 65, 66, 68, 72] but one of the earliest and most complete treatments is that of Rubinow [49] which incorporates a number of features that we retain in our model, including active proliferation, maturation, a marrow reservoir and free exchange between the circulating and marginal blood neutrophil pools. Rubinow's model, however, predates the discovery and characterisation of G-CSF and so it uses neutrophil concentrations as a cipher for the cytokine and its effects. Subsequent physiological models have also all incorporated at least some elements of this cytokine paradigm in their modelling. Some authors have been principally interested in neutrophil pathologies, including cyclical neutropenia, chronic myeloid leukemia, and myelosuppression during chemotherapy, while others have primarily studied the effects of G-CSF mimetics. Many models of cyclic neutropenia, including [9, 18, 25, 33] and [55] acknowledge the role of G-CSF in neutrophil production and pathologies but rely on the cytokine paradigm to drive the pharmacodynamic responses. A number of modelling approaches have been proposed, including compartmental ODE models [21, 22, 30, 46, 53, 69], delay differential equations (DDEs) incorporating statistical distributions to model delays [65, 66], and DDEs derived from age-structured partial differential equation (PDE) models, like the one developed in this work [5, 11, 20].

In recent years, synthetic forms of G-CSF have been developed and are administered to patients for a variety of reasons, including to treat cyclical neutropenia or as an adjuvant during chemotherapy [12, 13, 40]. However, the administration of exogenous G-CSF breaks the cytokine paradigm and it is possible for neutrophil and G-CSF concentrations to both be elevated at the same time. This breakdown of the natural feedback relationship can cause physiological models that use the paradigm to mischaracterise the elimination dynamics of G-CSF. For example, both [30] and [11] overestimate the renal clearance of

G-CSF so much as to essentially eliminate the contribution of neutrophil-mediated internalisation, even though they each include this nonlinear clearance in their models. If elevated neutrophil concentrations are used to drive the system dynamics on the assumption that corresponding G-CSF concentrations are reduced when they are in fact elevated, the modelled effects will act in the opposite sense to the physiology. As a consequence, the model will either develop instabilities and/or give a poor fit to observed dynamics.

The mischaracterisation of G-CSF elimination dynamics was the impetus for the current work. Consequently, we will not use the neutrophil concentration as a cipher for the G-CSF concentration, but will model both the G-CSF pharmacokinetics and pharmacodynamics (PK/PD) in detail. For this, we develop a novel pharmacokinetic model of G-CSF which includes both unbound and bound blood concentrations. The G-CSF concentrations given by this kinetic model are then used to drive the pharmacodynamic effects of the cytokine, in a fully formed negative feedback loop.

We begin by summarising the granulopoiesis model in Section 4.2. Its development is then extensively detailed in Section 4.3, beginning from the stem cells in Section 4.3.1. The novel pharmacokinetic G-CSF model incorporating bound and unbound blood concentrations is motivated and developed in Section 4.3.2. There we show how the hypothesis of an equilibrium between bound and unbound concentrations is not satisfied for G-CSF, necessitating the inclusion of more complex kinetics in its pharmacokinetic model. Next, the derivation of the DDE granulopoiesis model is given in Section 4.3.3 and the pharmacodynamic model of G-CSF is developed in Section 4.3.4. Models of the exogenous drugs considered in our study are detailed in Section 4.3.5. Having laid the foundations of our model, the various methods of parameter estimation and fitting used for our analyses are subsequently explained in Section 4.4. These approaches include model-specific constraints, as seen in Sections 4.4.1 and 4.4.3, while fitting procedures from published data are described in Sections 4.4.2, 4.4.4, and 4.4.5. The resulting parameters are then summarised in Section 4.5. Finally in Section 4.6 we put our model to the acid test of *predicting (not fitting)* the population neutrophil response in a group of patients undergoing simultaneous chemotherapy and G-CSF administration [42, 43] and obtain excellent agreement between the model predicted behaviour and the clinical data. We conclude with a short discussion in Section 4.7.

4.2 Model Summary

Here we define the variables and summarise the equations that define our granulopoiesis model. A detailed derivation is contained in Section 4.3. Figure 4.1 shows a schematic diagram describing the main elements of the hematopoietic system that we model.

The hematopoietic stem cell (HSC), neutrophil and G-CSF model is a set of five differential equations including constant and state-dependent delays. Let $Q(t)$ be the concentration of HSCs at time t, $N_R(t)$ be the concentration of mature neutrophils in the marrow reservoir, and $N(t)$ be the concentration of the total blood neutrophil pool (TBNP) at time t (which includes both circulating and marginated neutrophils). Further, let $G_1(t)$ be the concentration of unbound, circulating G-CSF and $G_2(t)$ be the concentration of G-CSF bound to receptors on mature neutrophils (in the reservoir or in the blood neutrophil pool).

The production of neutrophils from the HSCs is modelled by

$$\begin{aligned}
\tfrac{d}{dt}Q(t) &= -\big(\kappa(G_1(t)) + \kappa_\delta + \beta(Q(t))\big)Q(t) \\
&\qquad + A_Q(t)\beta\left(Q(t-\tau_Q)\right)Q(t-\tau_Q) && (4.1)\\
\tfrac{d}{dt}N_R(t) &= A_N(t)\kappa(G_1(t-\tau_N(t)))Q(t-\tau_N(t))\frac{V_{N_M}(G_1(t))}{V_{N_M}(G_1(t-\tau_{N_M}(t)))} \\
&\qquad - \big(\gamma_{N_R} + \varphi_{N_R}(G_1(t))\big)N_R(t) && (4.2)\\
\tfrac{d}{dt}N(t) &= \varphi_{N_R}(G_{BF}(t))N_R(t) - \gamma_N N(t), && (4.3)
\end{aligned}$$

with the concentrations of G-CSF (unbound and bound to neutrophil G-CSF receptors) given by

$$\begin{aligned}
\tfrac{d}{dt}G_1(t) &= I_G(t) + G_{prod} - k_{ren}G_1(t) \\
&\qquad - k_{12}([N_R(t)+N(t)]V - G_2(t))G_1(t)^{Pow} + k_{21}G_2(t) && (4.4)\\
\tfrac{d}{dt}G_2(t) &= -k_{int}G_2(t) + k_{12}\big([N_R(t)+N(t)]V - G_2(t)\big)G_1(t)^{Pow} - k_{21}G_2(t), && (4.5)
\end{aligned}$$

where $I_G(t)$ indicates input of exogenous G-CSF, which we assume is filgrastim (the most common bio-similar exogenous form of G-CSF). Filgrastim has very similar PK/PD properties to endogenous G-CSF, so we will not distinguish between the two types of G-CSF

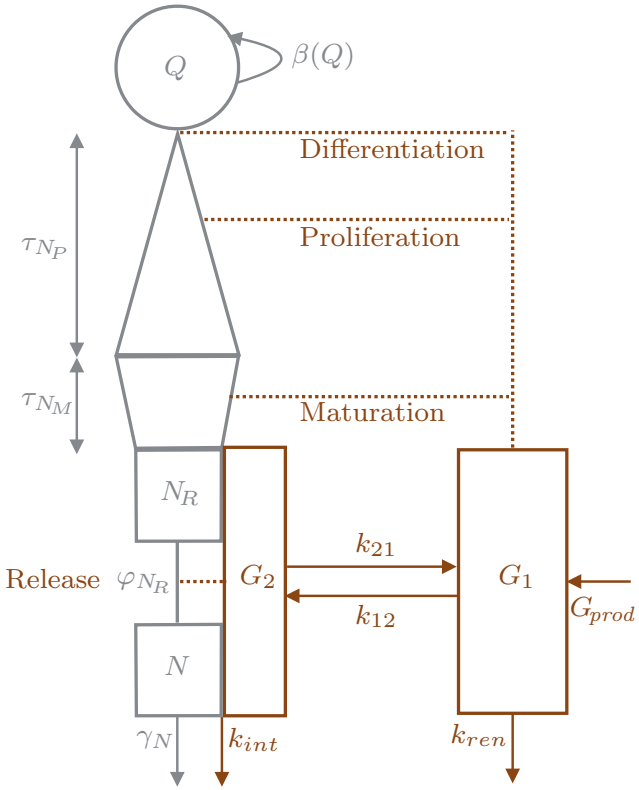

Figure 4.1 – Schematic representation of the production of circulating neutrophils in the bone marrow and the interaction of the system with G-CSF. Hematopoietic stem cells (HSCs-Q) enter the neutrophil lineage, the other blood lines, or are removed from the HSC pool. Differentiated HSCs then undergo successive divisions during the proliferative phase. Cells then mature before being stored in the marrow reservoir, or dying off during maturation. Neutrophils remain in the reservoir until they are removed randomly or enter the circulation, where they disappear rapidly from the blood. Freely circulating G-CSF may bind to receptors on the neutrophils. The concentration of bound G-CSF drives its pharmacodynamic effects. The concentration of G-CSF bound to mature neutrophils, G_2, determines the rate of release from the marrow reservoir. The concentration of G-CSF bound to neutrophil precursors, assumed proportional to G_1 the concentration of freely circulating G-CSF, determines the rate of differentiation from the HSCs, the speed of maturation, and the rate of proliferation. For all four effects, speed and rates increase with increasing G-CSF concentration.

in our model.

The derivation of these equations is given in Section 4.3. In Section 4.3.3, particular attention is paid to the derivation of the state-dependent delay terms in (4.2) from an age-structured partial differential equation (PDE) model of the mitosis and maturation with variable aging rate of the neutrophil precursors. The G-CSF equations (4.4),(4.5) are explained in detail in Section 4.3.2.

In the stem cell equation (4.1), as explained in Section 4.3.1, we have

$$\beta(Q) = f_Q \frac{\theta_2^{s_2}}{\theta_2^{s_2} + Q^{s_2}}, \tag{4.6}$$

$$A_Q(t) = A_Q^* = 2e^{-\gamma_Q \tau_Q}. \tag{4.7}$$

Only in the case of administration of chemotherapy is the stem cell amplification factor $A_Q(t)$ non-constant. During chemotherapeutic treatment $A_Q(t)$ will be modified by replacing (4.7) with (4.38) as discussed in Section 4.3.5. Stem cells commit to differentiate to neutrophil precursors at a rate given by

$$\kappa(G_1) = \kappa^* + (\kappa^* - \kappa^{min}) \left[\frac{G_1^{s_1} - (G_1^*)^{s_1}}{G_1^{s_1} + (G_1^*)^{s_1}} \right]. \tag{4.8}$$

Here, and throughout, the superscript * denotes the homeostasis value of a quantity. The rationale for using (4.8) to describe the pharmacodynamic effect of the G-CSF on the differentiation of the HSCs, along with the other G_1-dependent functions is explained in Section 4.3.4.

After entering the neutrophil lineage, cells undergo mitosis at a variable rate ($\eta_{N_P}(G_1(t))$) given by

$$\eta_{N_P}(G_1(t)) = \eta_{N_P}^* + (\eta_{N_P}^* - \eta_{N_P}^{min}) \frac{b_{N_P}}{G_1^*} \left(\frac{G_1(t) - G_1^*}{G_1(t) + b_{N_P}} \right) \tag{4.9}$$

for a proliferation time τ_{N_P}, considered to be constant. Cells subsequently mature at a variable aging rate given by

$$V_{N_M}(G_1(t)) = 1 + (V_{max} - 1) \frac{G_1(t) - G_1^*}{G_1(t) - G_1^* + b_V}, \tag{4.10}$$

until they reach age a_{N_M} so the time $\tau_{N_M}(t)$ it takes for a neutrophil maturing at time t to

mature satisfies the integral relationship

$$\int_{t-\tau_{N_M}(t)}^{t} V_{N_M}(G_1(s))ds = a_{N_M}. \tag{4.11}$$

At homeostasis, $V_{N_M}(G_1^*) = 1$, and thus a_{N_M} is the homeostatic maturation time. The total time it takes a neutrophil to be produced (from HSC differentiation to release into the reservoir pool) is

$$\tau_N(t) = \tau_{N_P} + \tau_{N_M}(t), \tag{4.12}$$

and we can differentiate equation (4.11) to obtain the following DDE for both τ_N and τ_{N_M}

$$\tfrac{d}{dt}\tau_N(t) = \tfrac{d}{dt}\tau_{N_M}(t) = 1 - \frac{V_{N_M}(G_1(t))}{V_{N_M}(G_1(t-\tau_{N_M}(t)))}. \tag{4.13}$$

Maturing neutrophils are assumed to die at a constant rate given by γ_{N_M}. The amplification factor $A_N(t)$ between differentiation from HSCs to maturation that appears in (4.2) is then given by

$$A_N(t) = \exp\left[\int_{t-\tau_N(t)}^{t-\tau_{N_M}(t)} \eta_{N_P}(G_1(s))ds - \gamma_{N_M}\tau_{N_M}(t)\right] \tag{4.14}$$

as derived in Section 4.3.3. Numerical implementation of the neutrophil amplification rate is obtained by differentiating the integral expressions in (4.14) using Leibniz's Rule to obtain

$$\begin{aligned}\tfrac{d}{dt}A_N(t) = A_N(t)\Big[\big(1 - \tfrac{d}{dt}\tau_{N_M}(t)\big)\big(\eta_{N_P}(G_1(t-\tau_{N_M}(t))) - \eta_{N_P}(G_1(t-\tau_N(t)))\big) \\ - \gamma_{N_M}\tfrac{d}{dt}\tau_{N_M}(t)\Big].\end{aligned} \tag{4.15}$$

After maturation neutrophils are sequestered into the marrow neutrophil reservoir. Mature neutrophils exit the reservoir either by dying with constant rate γ_{N_R}, or by being released into circulation with a rate φ_{N_R} depending on the fraction $G_{BF}(t)$ of neutrophil receptors that are bound by G-CSF. We define

$$G_{BF}(t) = \frac{G_2(t)}{V[N_R(t) + N(t)]} \in [0,1], \qquad G_{BF}^* = \frac{G_2^*}{V[N_R^* + N^*]}, \tag{4.16}$$

and let

$$\varphi_{N_R}(G_{BF}(t)) = \varphi^*_{N_R} + (\varphi^{max}_{N_R} - \varphi^*_{N_R})\frac{G_{BF}(t) - G^*_{BF}}{G_{BF}(t) - G^*_{BF} + b_G}. \tag{4.17}$$

Neutrophils are removed from circulation with constant rate γ_N.

In equations (4.1)–(4.5) we use units of 10^9 cells per kilogram (of body mass) for the reservoir and circulating neutrophils, and 10^6cell/kg for the stem cells. The scaling factors ensure that computations are performed with numbers of similar magnitude which improves numerical stability. Circulating and bound G-CSF concentrations are measured in standard units of nanograms per millilitre of blood. The differing units for neutrophils and G-CSF are only problematical in equations (4.4),(4.5) where quantities in both units appear; see Section 4.4.2 for the derivation of the conversion factor V.

Its also important to note that $N(t)$ measures the total blood neutrophil pool, including both the circulating and marginated neutrophils. To convert $N(t)$ to an absolute neutrophil count/circulating neutrophil numbers $N_C(t)$ (or *vice versa*) there is a conversion factor; see (4.93).

4.3 Model Development

Here we describe the development of our granulopoiesis model leading to the equations presented in Section 4.2. The equation for the stem cells (4.1) is described briefly in Section 4.3.1. The size of the mature neutrophil reservoir is described by (4.2). The first term on the right-hand side of this equation gives the rate that mature neutrophils enter the reservoir. This term is derived from an age-structured PDE model described in Section 4.3.3 below. Neutrophils are assumed to leave the reservoir either by dying at rate γ_{N_R} or by entering into circulation at rate φ_{N_R}, and are removed from circulation at a constant rate γ_N. In Section 4.3.2 we describe our new G-CSF model (4.4),(4.5) of the unbound freely circulating G-CSF (G_1), and the G-CSF bound to receptors on the neutrophils (G_2). This model allows us to model the pharmacodynamic effects of the G-CSF directly as detailed in Section 4.3.4. Finally, Section 4.3.5 outlines our models for the exogenous drugs we will consider in later sections.

4.3.1 Stem Cells

Equation (4.1) for the stem cell dynamics was previously used in [5, 8, 9, 11, 20, 33, 35, 45]. In particular, see [4] for a detailed derivation. Here, we remove the dependence of γ_Q upon G-CSF as the HSC population is relatively stable and infrequently dividing [16, 48] and, to our knowledge, no direct evidence of G-CSF's action upon HSC apoptosis currently exists. Craig [11] uses

$$A_Q(t) = 2\exp\left[-\int_{t-\tau_Q}^{t}\gamma_Q(s)ds\right], \tag{4.18}$$

and in the absence of chemotherapy we take the apoptotic rate γ_Q to be constant so this becomes (4.7).

4.3.2 A physiologically constructed pharmacokinetic G-CSF model

A new pharmacokinetic model of G-CSF, already stated in (4.4),(4.5) is used to model the concentrations of both unbound and bound G-CSF. We do not distinguish between endogenous and exogenous G-CSF in the model, which constrains us to only consider biosimilar forms of exogenous G-CSF. Accordingly, we focus on filgrastim, the most widely-available form of exogenous G-CSF. However, other less common forms of biosimilar exogenous G-CSF are available and include lenograstim and Nartograstim® [40]. The pegylated form of rhG-CSF has greatly reduced renal clearance relative to endogenous G-CSF, which would require a different model, so we will not consider it in this work.

In equations (4.4),(4.5) G_1 is the concentration of freely circulating G-CSF and G_2 is the concentration of G-CSF which is bound to receptors on the neutrophils. Since the bone marrow is well perfused. G-CSF can bind to mature neutrophils in the marrow reservoir as well as neutrophils in circulation. In the model k_{ren} denotes the nonsaturable removal rate of circulating G-CSF (mainly renal). k_{int} denotes the removal rate of bound-G-CSF, which we refer to as the effective internalisation rate. This term models the removal of bound G-CSF both by internalisation after binding and through the removal of the neutrophil itself from circulation (along with its bound G-CSF molecules). k_{12} is the rate of binding of free G-CSF to the neutrophils, and Pow is the effective binding coefficient. The G-CSF receptor has a 2:2 stoichiometry in *in vitro* studies [32], so a simple chemical reaction

model would suggest $Pow = 2$. However, the number of ligands binding to a receptor only provides an upper bound on the corresponding Hill coefficient [51]. Accordingly, we use an effective binding coefficient $Pow \in [1, 2]$.

In this model the bound G-CSF concentration is saturable, with $V[N_R(t) + N(t)]$ being the capacity of this compartment. $G_2 = V[N_R(t)+N(t)]$ would indicate that every receptor on every neutrophil in the reservoir and circulation was bound to two G-CSF molecules. Thus the removal rate of neutrophils by internalisation is saturable. G-CSF also binds to immature neutrophils and precursors, which will be important for the pharmacodynamics, but since these cells are fewer in number and/or have fewer receptors than the mature neutrophils we neglect this effect on the pharmacokinetics. Finally, k_{21} is the rate of unbinding (transformation from bound G-CSF to circulating G-CSF), and $I_G(t)$ denotes exogenous administration of G-CSF, discussed in Section 4.3.5.

If we were to assume that there is no net transfer between the bound and circulating G-CSF then letting $\tilde{N}(t) = [N_R(t) + N(t)]$, equations (4.4),(4.5) imply

$$k_{12}(V\tilde{N}(t) - G_2)G_1^{Pow} - k_{21}G_2 \approx 0. \tag{4.19}$$

Rearranging (4.19) we obtain

$$G_2(t) \approx \frac{[G_1(t)]^{Pow}}{[G_1(t)]^{Pow} + k_{21}/k_{12}} V\tilde{N}(t).$$

Now, adding (4.4) and (4.5)

$$\frac{d}{dt}(G_1 + G_2) \approx I_G(t) + G_{prod} - k_{ren}G_1 - k_{int}G_2,$$

and assuming that $G_1 \gg G_2$ and that $\frac{d}{dt}(G_1 + G_2) \approx \frac{d}{dt}G_1$, and finally replacing the $\approx$ by an equality we have

$$\frac{d}{dt}G_1 = I_G(t) + G_{prod} - k_{ren}G_1 - k_{int}V\tilde{N}(t)\frac{[G_1(t)]^{Pow}}{[G_1(t)]^{Pow} + k_{21}/k_{12}}. \tag{4.20}$$

Equations similar to (4.20) have been used to model G-CSF pharmacokinetics in many papers including [5, 11, 20, 29, 30, 69], but usually with $\tilde{N}(t) = N(t)$ the concentration of circulating neutrophils, as opposed to $\tilde{N}(t) = [N_R(t) + N(t)]$ as (4.4),(4.5) suggest.

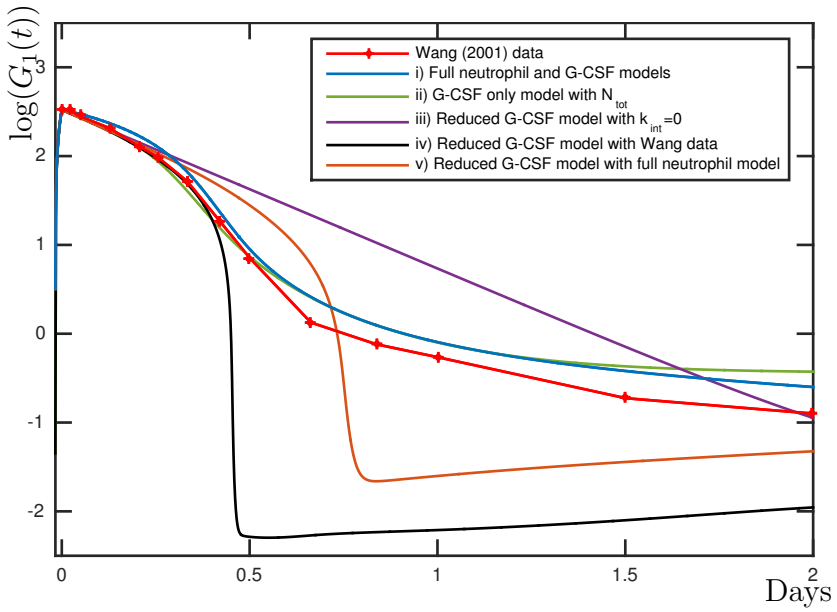

Figure 4.2 – Data from Wang [69] for G-CSF concentrations after a 750 μg 25 minute IV infusion and five different simulations: (i) the full neutrophil and G-CSF model (4.1)–(4.5) (ii) the G-CSF only model (4.68),(4.69), (iii) the reduced G-CSF model (4.20) with $k_{int} = 0$, (iv) the reduced G-CSF model (4.20) with $k_{int} = 30$ and $\tilde{N}(t) = N(t)$ and neutrophil concentrations taken from the Wang [69] and (v) the full neutrophil model (4.1)–(4.3) and the reduced G-CSF model (4.20) with $k_{int} = 25$ and $\tilde{N}(t) = [N_R(t) + N(t)]$. In ii) $N_{tot} = 4.1457$ and G_2^* and G_{prod} are determined by Equations (4.74) and (4.76), respectively. In (ii), (iv) and (v) $k_{ren} = 4.12$ and G_{prod} is determined by (4.20). All other parameters take values specified in the third columns of Tables 4.I and 4.II.

The usual derivation of (4.20) is from the law of mass action, but this is equivalent to the assumption (4.19) that the bound and circulating G-CSF are in quasi-equilibrium. However, the equilibrium hypothesis (4.19) cannot hold at homeostasis, since if (4.19) holds and $k_{int} > 0$ then $\frac{d}{dt}G_2 < 0$ which is contradictory. Clinical evidence [52, 64] suggests that at homeostasis, binding and internalisation is the dominant removal mechanism for G-CSF, so not only does (4.19) not hold but the net transfer from unbound to bound G-CSF should be more than $0.5 \times G_{prod}$. Another important situation where (4.19) will fail is during exogenous administration of G-CSF, which will initially increase the concentration of unbound G-CSF (often by orders of magnitude).

Figure 4.2 illustrates some of the issues involved in modelling the kinetics of G-CSF. This figure shows data from a 750 μg intravenous (IV) infusion digitised from Figure 6 of Wang [69], along with a number of simulations of the protocol using different G-CSF kinetic mod-

els. The data in Figure 4.2 seems to have at least two different slopes, suggesting that the G-CSF time course could be approximated by the sum of two exponentials. This naturally leads to two compartment pharmacokinetic models [15]. Such a two-compartment G-CSF model was previously considered by Kuwabara [31] for Nartograstim®. Consistent with general two-compartment models in pharmacology, the two compartments corresponded to the blood and the tissues, and generic saturable and nonsaturable removal of the G-CSF both occurred from the blood compartment. This differs from our model where elimination occurs from the two compartments (which instead represent unbound and bound G-CSF concentrations), both of which are subject to linear elimination. By contrast, in our model one compartment is saturable with nonsaturable elimination (the bound G-CSF), which corresponds to known G-CSF removal mechanisms. The assignment of elimination to the first or second compartments also has significant effects on the estimation of corresponding pharmacokinetic parameters so the mischaracterisation of these elimination dynamics could have significant effects on the model's predictions and behaviours [73].

The circulating G-CSF concentration time course for a simulation of our full model (4.1)–(4.5) tracks the measured G-CSF data very closely in Figure 4.2. It slightly overestimates the G-CSF, but note that the data points are average values from a number of subjects and we will see in Section 4.4.2 that our G-CSF concentrations are well within the data range for several of administration protocols.

Also shown in Figure 4.2 is a simulation of a simplified version of the G-CSF equations (4.4),(4.5) where the time dependent neutrophil term $[N_R(t) + N(t)]$ is replaced by a constant N_{tot}, so the G-CSF kinetic equations become independent of the neutrophil dynamics. The resulting equations are stated as (4.68),(4.69) in Section 4.4.2 where they are used to determine the pharmacokinetic parameters that appear in (4.4),(4.5). The constant N_{tot} can be thought of as a time average of the term $[N_R(t) + N(t)]$. As seen in Figure 4.2, this stand-alone simplified G-CSF model gives G-CSF concentrations very close to those of the full model, which justifies using it to determine the kinetic parameters.

Three different simulations of the single G-CSF equation (4.20) are also shown in Figure 4.2 to illustrate the difficulties in dealing with reduced models. One simulation has $k_{int} = 0$ so that the elimination of G-CSF is purely renal and it is clear that the nuances of the G-CSF kinetics are lost.

A simulation of (4.20) with $k_{int} > 0$ and $\tilde{N}(t) = N(t)$ (with values for $N(t)$ taken from the Wang data) gives even worse results than the purely renal elimination case. The problem with this model is that for the first few hours while the neutrophil concentration is low, the elimination of the G-CSF is mainly renal and the solution closely tracks the results from the purely renal elimination simulation. But as soon as the circulating neutrophil concentrations get high enough the elimination of G-CSF by binding becomes dominant and quickly drives the G-CSF concentration to very low levels. Similar results are seen if our full neutrophil model (4.1)–(4.3) is coupled to (4.20) with $\tilde{N}(t) = [N_R(t) + N(t)]$.

The tendency of the internalisation term to quickly drive the G-CSF concentrations down, along with the propensity for parameter fitting with linear scales resulted in several previous models using versions of (4.20) to take kinetic parameters for which the elimination of G-CSF is always renal dominated. This is seen both when the G-CSF kinetics is coupled to physiological models as in [5, 11] and when using traditional empirical models as in [30, 69], which consequently all have elimination dynamics which are always renal dominated.

This is true in both the models of Craig [11], which used (4.20) with $\tilde{N}(t) = N(t)$, and Krzyzanski [30] which used an equation similar to (4.20) but taking account of binding to all available receptors. In both, elimination by internalisation is included in the mathematical models but occurs at an insignificant rate compared to the renal elimination, contrary to the clinical understanding that elimination of G-CSF by internalisation is the dominant removal mechanism at homeostasis.

From our numerical experiments it seems impossible to fit the single G-CSF equation (4.20) to data when $\tilde{N}(t)$ is taken to be $N(t)$. The mature marrow neutrophil reservoir is an order of magnitude larger than the total blood neutrophil pool, and the receptors on the mature neutrophils need to be taken into account in the kinetics as in (4.4),(4.5) to obtain a good fit to data. But taking account of all the receptors is not sufficient to obtain a model that fits the physiology closely. This is evidenced by the very poor fit obtained in Figure 4.2 when coupling our neutrophil model to the reduced G-CSF equation (4.20) with $\tilde{N}(t) = [N_R(t) + N(t)]$, and also from models such as that of Krzyzanski [30] that take account of the G-CSF receptors in marrow, but still obtain renal dominated kinetics.

The study of congenital diseases like cyclical neutropenia (CN)–an inherently oscilla-

tory and dynamic disease– and exogenous dosing regimens (such as during chemotherapy) necessitate that the dynamics of G-CSF be well-characterised. Hence we use the more realistic model (4.4),(4.5) for G-CSF pharmacokinetics rather than the single equation reduction (4.20).

4.3.3 Modelling Granulopoiesis

The first term on the right hand side of (4.2) gives the rate that mature neutrophils enter the bone marrow reservoir at time t, and is obtained by modelling the differentiation of stem cells at time $t-\tau_N(t)$ through mitosis of neutrophil precursors to time $t-\tau_N(t)+\tau_{N_P} = t-\tau_{N_M}(t)$ followed by maturation of the cells until time t. The time variation of $\tau_N(t)$ and $\tau_{N_M}(t)$ is solution dependent so this term involves state-dependent delays. Granulopoiesis models incorporating state-dependent delay have been employed before in [5, 19, 20], but the derivation of those models was inaccurate and they missed the important $V_{N_M}(G_1(t))/V_{N_M}(G_1(t-\tau_{N_M}(t)))$ term. Here we will show in detail how the mitotic and maturation stages of the neutrophil precursors can be modelled by age-structured PDE models, whose solution by the method of characteristics leads to the state-dependent delay terms in (4.2).

We do not model the cell-cycle process during mitosis, nor do we differentiate between the different maturation stages of dividing cells (myeloblasts, promyelocytes, myelocytes). Rather, to simplify the modelling and the resulting differential equations we model mitosis as an exponential process from the moment the HSC commits to differentiate to the end of the mitosis. The proliferation rate η_{N_P} is assumed to be independent of which stage in mitosis the cell has reached. There is evidence that the cytokine G-CSF affects the differentiation of HSCs and the effective proliferation rate during mitosis, as explained in [17], and so we allow both the differentiation rate κ and the proliferation rate η_{N_P} to vary with G_1, the circulating G-CSF, as seen in equations (4.8),(4.9), and explained in Section 4.3.4.

We let $n_p(t,a)$ be the cell density as a function of time t and age a during proliferation. We assume that cells age at a constant rate, $\dot{a}=1$, from age 0 to age τ_{N_P}, so τ_{N_P} is also the time period that cells spend in proliferation, and the proliferation rate is $\tau_{N_P}(G_1(t))$.

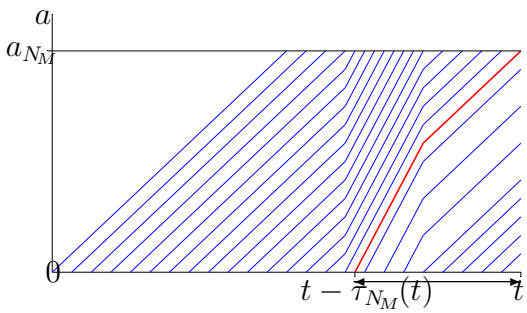

Figure 4.3 – During maturation the aging rate is variable with $\dot{a}(t) = V_{N_M}(G_1(t))$, so age is not trivially related to time, and the maturation time $\tau_{N_M}(t)$ is variable.

Then, differentiating,

$$\eta_{N_P}(G_1(t))n_p(t,a) = \frac{dn_p}{dt} = \frac{\partial n_p}{\partial t} + \frac{da}{dt}\frac{\partial n_p}{\partial a} = \frac{\partial n_p}{\partial t} + \frac{\partial n_p}{\partial a}$$

so the age-structured PDE model for proliferation is

$$\frac{\partial n_p}{\partial t} + \frac{\partial n_p}{\partial a} = \eta_{N_P}(G_1(t))n_p(t,a), \qquad t \geqslant 0, \quad a \in [0, \tau_{N_P}], \tag{4.21}$$

which, by the method of characteristics has solution

$$n_p(t,a) = n_p(t-a,0)\exp\left[\int_{t-a}^{t} \eta_{N_P}(G_1(s))ds\right], \; t \geqslant 0, \; a \in [0, \min\{t, \tau_{N_P}\}]. \tag{4.22}$$

If $\tau_{N_P} \geqslant a > t > 0$ the solution depends on the initial condition $n_p(0, a-t)$, but a similar expression applies. Here we have taken homeostasis as the initial condition throughout and so the solution in (4.22) is all that is required.

We model the maturing neutrophil precursors (metamyelocytes and bands) as a single homogeneous compartment. There is evidence that G-CSF affects the time that cells spend in maturation [3, 63] and the speed up in maturation has been measured experimentally [44]. Since the exact mechanism by which G-CSF affects maturation time is unknown, we will model this process by decoupling time from age and demanding that cells age by an amount a_{N_M}, but allowing them to mature at a variable aging rate $\dot{a}(t) = V_{N_M}(G_1(t))$ where $V_{N_M}(G_1)$ is a monotonically increasing function with $V_{N_M}(0) > 0$ and $\lim_{G_1 \to \infty} V_{N_M}(G_1) =$

$V_{max} < \infty$.

See Section 4.3.4 for further discussion of the function $V_{N_M}(G_1)$. We assume that the rate of cell death, γ_{N_M}, during maturation is constant independent of the concentration of G-CSF.

We let $n_m(t,a)$ be the cell density as a function of time t and age a during maturation for $t \geqslant 0$ and $a \in [0, a_{N_M}]$. Then the age-structured maturation model is

$$\frac{\partial n_m}{\partial t} + V_{N_M}(G_1(t))\frac{\partial n_m}{\partial a} = \frac{\partial n_m}{\partial t} + \frac{da}{dt}\frac{\partial n_m}{\partial a} = \frac{dn_m}{dt} = -\gamma_{N_M} n_m(t,a). \tag{4.23}$$

The characteristics are defined by $\dot{a} = V_{N_M}(G_1(t))$, and along characteristics for $t \geqslant \tau_{N_M}(t)$ we obtain

$$n_m(t, a_{N_M}) = n_m(t - \tau_{N_M}(t), 0)e^{-\gamma_{N_M}\tau_{N_M}(t)}. \tag{4.24}$$

Age-structured PDE models have been used in hematopoiesis models many times previously [9, 11, 20, 33], but special care needs to be taken to interpret $n_m(t,a)$ when the maturation has variable velocity, or an incorrect solution will be obtained.

Cells which mature at time t enter maturation at time $t - \tau_{N_M}(t)$ and so differentiated from HSCs at time $t - \tau_{N_M}(t) - \tau_{N_P} = t - \tau_N(t)$. The rate at which cells differentiate at time $t - \tau_N(t)$ is $\kappa(G_1(t - \tau_N(t)))Q(t - \tau_N(t))$, and hence

$$n_p(t - \tau_N(t), 0) = \kappa(G_1(t - \tau_N(t)))Q(t - \tau_N(t)).$$

Then by (4.22)

$$\begin{aligned} n_p(t - \tau_{N_M}(t), a_{N_M}) &= n_p(t - \tau_N(t), 0)\exp\left[\int_{t-a_{N_M}}^{t} \eta_{N_P}(G_1(s))ds\right] \\ &= \kappa(G_1(t - \tau_N(t)))Q(t - \tau_N(t))\exp\left[\int_{t-a_{N_M}}^{t} \eta_{N_P}(G_1(s))ds\right]. \end{aligned} \tag{4.25}$$

To obtain the boundary condition for the maturation phase, note that $n_p(t, \tau_{N_P})$ is the rate at which cells leave proliferation and enter maturation. Hence, to leading order, $n_p(t, \tau_{N_P})\delta t$ cells enter maturation in the time interval $[t, t+\delta t]$. Cells that enter maturation at time t will already have age $V_{N_M}(G_1(t))\delta t$ by time $t + \delta t$. Since $n_p(t,a)$ and $n_m(t,a)$ describe the density of cells in the proliferation and maturation phases, to avoid the

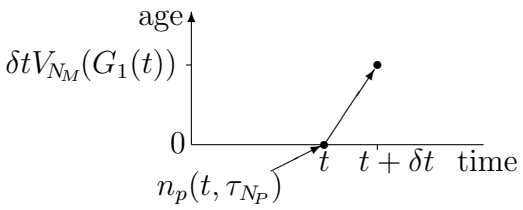

Figure 4.4 – Transition from proliferation to maturation.

spontaneous creation or destruction of cells at the transition between proliferation and maturation we require

$$\int_0^{V_{N_M}(G_1(t))\delta t} n_m(t+\delta t, a)da - \int_t^{t+\delta t} n_p(t, \tau_{N_P})dt = \mathcal{O}(\delta t^2).$$

Then

$$\begin{aligned} V_{N_M}(G_1(t))n_m(t,0) &= \lim_{\delta t\to 0}\frac{1}{\delta t}\int_0^{V_{N_M}(G_1(t))\delta t} n_m(t+\delta t, a)da \\ &= \lim_{\delta t\to 0}\frac{1}{\delta t}\int_t^{t+\delta t} n_p(t, \tau_{N_P})dt = n_p(t, \tau_{N_P}), \end{aligned} \tag{4.26}$$

and hence the boundary condition for the maturation compartment is

$$n_m(t-\tau_{N_M}(t), 0) = n_p(t-\tau_{N_M}(t), \tau_{N_P})/V_{N_M}(G_1(t-\tau_{N_M}(t))). \tag{4.27}$$

Combining (4.24), (4.25), (4.27) and (4.14) we obtain

$$\begin{aligned} n_m(t,a_{N_M}) &= \frac{n_p(t-\tau_{N_M}(t), \tau_{N_P})}{V_{N_M}(G_1(t-\tau_{N_M}(t)))}e^{-\gamma_{N_M}\tau_{N_M}(t)} \\ &= \frac{\kappa(G_1(t-\tau_N(t))Q(t-\tau_N(t))}{V_{N_M}(G_1(t-\tau_{N_M}(t)))}\exp\left[\int_{t-\tau_N(t)}^{t-\tau_{N_M}(t)}\eta_{N_P}(G_1(s))ds - \gamma_{N_M}\tau_{N_M}(t)\right] \\ &= \frac{\kappa(G_1(t-\tau_N(t)))Q(t-\tau_N(t))}{V_{N_M}(G_1(t-\tau_{N_M}(t)))}A_N(t). \end{aligned} \tag{4.28}$$

Again because of the variable aging-rate there is a correction factor to apply to $n_m(t, a_{N_M})$ to obtain the rate that cells leave maturation. To calculate this rate notice that cells which reach age a_{N_M} at time t have age $a_{N_M} - V_{N_M}(G_1(t))\delta t + \mathcal{O}(\delta t^2)$ at time $t-\delta t$. Thus the

number of neutrophils that mature in the time interval $[t-\delta t, t]$ is

$$\int_{a_{N_M}-V_{N_M}(G_1(t))\delta t}^{a_{N_M}} n_m(t-\delta t, a)da + \mathcal{O}(\delta t^2) = V_{N_M}(G_1(t))n_m(t, a_{N_M})\delta t + \mathcal{O}(\delta t^2).$$

Hence, the rate that cells leave maturation is $V_{N_M}(G_1(t))n_m(t, a_{N_M})$, which using (4.28) can be written as

$$\kappa(G_1(t-\tau_N(t)))Q(t-\tau_N(t))A_N(t)\frac{V_{N_M}(G_1(t))}{V_{N_M}(G_1(t-\tau_{N_M}(t)))}, \tag{4.29}$$

which is the first term on the right-hand side of (4.2). The correction factor $V_{N_M}(G_1(t))/V_{N_M}(G_1(t-\tau_{N_M}(t)))$ was omitted from the state-dependent DDE models in [5, 20].

4.3.4 G-CSF Pharmacodynamics

G-CSF in concert with many other cytokines regulates important parts of granulopoiesis. The precise mechanisms by which it does this are not fully understood (and would probably be beyond the level of detail that we would want to model mathematically even if they were) but it is known that G-CSF acts along several signalling pathways in complex processes which activate and generate secondary signals that regulate neutrophil production [23, 59, 70].

The initiation of signalling pathways and the transfer of the resulting signals responsible for the various effects of a given drug may be driven directly by receptor binding and/or the internalisation of the drug. Assuming the rate at which a drug is internalised is proportional to its bound concentration, we do not need to distinguish between the different possible pathways and will use the concentration of the bound drug to drive the pharmacodynamics and produce the effects in the body.

Many previous models applied the cytokine paradigm mentioned in the introduction to model cytokine effects directly from the circulating neutrophil concentrations. For example in [5, 8, 9, 11, 20, 33], the differentiation function was taken to be a monotonically decreasing function of the circulating neutrophil concentration. Some authors preferred instead to introduce simplified pharmacodynamic models using direct and indirect PD effects related to the concentration of unbound G-CSF [60, 69] while other more detailed

approaches have also been studied [58, 65, 66].

The cytokine paradigm breaks down when G-CSF is given exogenously. Immediate responses of the hematopoietic system to G-CSF administration include releasing neutrophils from the marrow reservoir into circulation, and increasing the maturation speed of neutrophils, so the circulating concentration of neutrophils and the total number of neutrophils in the reservoir and circulation both increase, which results in G-CSF and neutrophil concentrations being high concurrently. Consequently we will use G-CSF concentrations from (4.4),(4.5) to directly model the pharmacodynamic effects of G-CSF on the differentiation rate of HSCs κ, the effective proliferation rate of neutrophil precursors in mitosis η_{N_P}, the aging rate of maturing neutrophils V_{N_M}, and the release rate of neutrophils from the bone marrow reservoir φ_{N_R}.

We use Hill and Michaelis-Menten functions to model the G-CSF dependency of these effects. There is some disagreement in the literature over exactly which cytokines are important in different parts of the process, and we may be assigning some effects to G-CSF that are actually due to GM-CSF or one of the other myriad of cytokines that regulate granulopoiesis. If these other cytokines are mostly in quasi-equilibrium with G-CSF, using G-CSF as a cipher for all the cytokines should produce very similar effects without the extraordinary complexity that would be inherent in modelling each one of the cytokines.

Mammalian studies [6, 24, 34] reveal that neutrophils are still produced even in the absence of G-CSF, presumably because other cytokines are acting. Accordingly, we will construct our effects functions to have non-zero activity even in the complete absence of G-CSF. Moreover, in Section 4.4.3 we will consider the case of G-CSF knockout mathematically with our model to derive a parameter constraint to reduce the number of unknown parameters.

Recall that the concentration of G-CSF bound to mature neutrophils satisfies the inequality $G_2(t) \leqslant V[N_R(t) + N(t)]$ with equality only if every G-CSF receptor were bound to two G-CSF molecules. We suppose that the rate that mature neutrophils are released from the marrow reservoir into circulation is dependent on the fraction $G_{BF}(t) = G_2(t)/(V[N_R(t) + N(t)])$ of their receptors which are bound to G-CSF. The

rate is then given by the Michaelis-Menten function $\varphi_{N_R}(G_1)$ defined by (4.17). Letting

$$\varphi_{N_R}^{ratio} = \frac{\varphi_{N_R}^{max}}{\varphi_{N_R}^{*}} > 1, \tag{4.30}$$

this function is also similar to the one used by Shochat [60] that was adapted in Craig [11] except that we use the fraction of bound receptors to drive the function. At homeostasis (4.16) and (4.17) imply that

$$\varphi_{N_R}(G_{BF}^{*}) = \varphi_{N_R}(G_2^{*}/[V(N^{*} + N_R^{*})]) = \varphi_{N_R}^{*}.$$

The parameter b_G defines the half-effect concentration with

$$\varphi_{N_R}(G_{BF}^{*} + b_G) = \frac{1}{2}(\varphi_{N_R}^{*} + \varphi_{N_R}^{max}),$$

while the condition $\varphi_{N_R}(0) > 0$ implies the constraint

$$b_G > \varphi_{N_R}^{ratio} G_{BF}^{*} = \frac{G_2^{*}\varphi_{N_R}^{ratio}}{V(N_R^{*} + N^{*})}. \tag{4.31}$$

To model the effects of G-CSF on the differentiation, proliferation and maturation some care must be taken. We posit that it is cytokine signalling that drives these processes, and $G_2(t)$ denotes the concentration of bound G-CSF, which is proportional to the rate that G-CSF is internalised. So it would be tempting to use $G_2(t)$ to govern these processes, and indeed initially we tried this without success. The problem is that $G_2(t)$ models the concentration of G-CSF bound to mature neutrophils in the marrow reservoir and circulation. Through (4.4) and (4.5) this gives a very good model of the removal of G-CSF from circulation because although the neutrophil progenitor cells also have G-CSF receptors, these cells are relatively few in number and have relatively few receptors, hence they can be ignored when modelling the G-CSF kinetics. However, when modelling the pharmacodynamic effects of G-CSF it appears to be crucial to take account of the binding of G-CSF to the neutrophil precursors, and it is the freely circulating G-CSF which is available to bind to the G-CSF receptors on the immature neutrophils and precursors. Consequently, we should use $G_1(t)$ to govern the cytokine dependent differentiation, proliferation, and maturation.

Another way to see that it should be the circulating G-CSF $G_1(t)$, and not the G-CSF bound to mature neutrophils $G_2(t)$ that should govern these processes is as follows. If the concentration of mature neutrophils is decreased then the concentration of bound G-CSF will also decrease because the number of receptors available to bind to will be decreased, but the concentration of unbound G-CSF will increase because the rate the G-CSF is removed by internalisation is reduced. However, with a reduced concentration of neutrophils, an elevated cytokine concentration is needed to increase differentiation, proliferation and maturation speed.

We model the differentiation rate from HSCs to neutrophil precursors using the Hill function (4.8). Very little is known about how the differentiation rate changes in function of G-CSF, but we suppose that it will not vary by orders of magnitude, since this would lead to instability in the HSC population, while the HSC population is observed to be very stable in healthy subjects [48]. It is then convenient to assume that the homeostatic rate is at the midpoint of the range of possible differentiation rates so

$$\kappa^* = \frac{1}{2}(\kappa^{min} + \kappa^{max}). \tag{4.32}$$

With this assumption (4.8) is a standard sigmoidal Hill function with minimum differentiation rate $\kappa(0) = \kappa^{min}$, and with $\kappa(G_1)$ increasing monotonically with G_1 and such that at homeostasis $\kappa(G_1^*) = \kappa^*$, while for large concentrations $\lim_{G_1\to\infty} \kappa(G_1) = \kappa^* + (\kappa^* - \kappa^{min}) = \kappa^{max}$. To ensure that neutrophils are still produced in the complete absence of G-CSF we will require that $\kappa^{min} > 0$.

G-CSF is believed to increase the effective rate of mitosis during proliferation by reducing apoptosis. Thus we use a monotonically increasing Michaelis-Menten function $\eta_{N_P}(G_1(t))$ defined by (4.9) to describe the G-CSF dependent effective proliferation rate (which measures the difference between actual proliferation and apoptosis). This function looks a little different than the other Michaelis-Menten functions we will use, but this is simply because it has been scaled to give the correct minimal and homeostasis effects with $\eta_{N_P}(0) = \eta_{N_P}^{min} > 0$ and $\eta_{N_P}(G_1^*) = \eta_{N_P}^*$, with $\eta_{N_P}(G_1)$ a monotonically increasing function of G_1.

Letting

$$\eta_{N_P}^{max} = \lim_{G_1 \to \infty} \eta_{N_P}(G_1) = \eta_{N_P}^* + \frac{b_{N_P}}{G_1^*}(\eta_{N_P}^* - \eta_{N_P}^{min}),$$

we see that

$$\frac{b_{N_P}}{G_1^*} = \frac{\eta_{N_P}^{max} - \eta_{N_P}^*}{\eta_{N_P}^* - \eta_{N_P}^{min}},$$

so the parameter $b_{N_P} > 0$ determines the relative position of $\eta_{N_P}^* \in [\eta_{N_P}^{min}, \eta_{N_P}^{max}]$ with $\eta_{N_P}^* > (\eta_{N_P}^{min} + \eta_{N_P}^{max})/2$ when $b_{N_P} \in (0, G_1^*)$ and $\eta_{N_P}^* < (\eta_{N_P}^{min} + \eta_{N_P}^{max})/2$ when $b_{N_P} > G_1^*$.

G-CSF is known to affect the time that neutrophils spend in maturation [3, 63], an acceleration in maturation that Price [44] measured experimentally, but the mechanism by which G-CSF speeds up maturation is not well understood. We choose to model this process by decoupling time from age and demanding that cells age by an amount a_{N_M}, but allowing them to mature at a variable aging rate $\dot{a}(t) = V_{N_M}(G_1(t))$ where $V_{N_M}(G_1)$ is a monotonically increasing Michaelis-Menten function given in (4.10). This is similar to the form used in Craig [11] which was adopted from Foley [20], and is also functionally equivalent to (4.17).

b_V is the half effect parameter for the aging velocity with $V_{N_M}(G_1^* + b_V) = (1 + V_{max})/2$. We require that $V_{N_M}(0) > 0$, which from (4.10) is equivalent to

$$b_V > G_1^* V_{max}. \tag{4.33}$$

This constraint ensures that the aging velocity $V_{N_M}(G_1)$ is strictly positive for all $G_1 \geqslant 0$. The function $V_{N_M}(G_1)$ also satisfies the homeostasis condition $V_{N_M}(G_1^*) = 1$, so that at homeostasis the aging rate is 1. The aging rate saturates with $\lim_{G_1 \to \infty} V_{N_M}(G_1) = V_{max} < \infty$.

Notice that, using (4.13)

$$\tfrac{d}{dt}(t - \tau_{N_M}(t)) = 1 - \tfrac{d}{dt}\tau_{N_M}(t) = \frac{V_{N_M}(G_1(t))}{V_{N_M}(G_1(t - \tau_{N_M}(t)))}, \tag{4.34}$$

and positivity of $V_{N_M}(G_1)$ assures that $t - \tau_{N_M}(t)$, and similarly $t - \tau_N(t)$, are monotonically increasing functions of t. This is important in state-dependent DDE theory for existence and uniqueness of solutions. Physiologically, it assures that cells which have exited proliferation or maturation never re-enter those phases.

The responses of our new model and the model of Craig [11] to exogenous administration of G-CSF are very different. With our new model both differentiation and proliferation are increased with increased G-CSF so that after some time delay the marrow reservoir gets replenished. In the previous model, the G-CSF triggered an immediate release of neutrophils from the marrow reservoir into circulation and the resulting high circulating neutrophil count would cause differentiation and proliferation to be decreased. This meant the the marrow reservoir would suffer a double depletion with increased release into circulation combined with reduced production of new mature neutrophils, which could lead to instabilities in the model that ought not to be occurring in the granulopoiesis of healthy subjects.

Since the four functions (4.8),(4.9),(4.10) and (4.17) describe the effects of G-CSF on granulopoiesis, rather than modelling the processes that lead to the effects, the parameters in these functions do not correspond to physiological quantities that can be measured directly. Nevertheless these parameters can be determined by fitting the response of the system to experimental data as described in Section 4.4.4.

4.3.5 Modelling exogenous drug administration

As noted following (4.4), $I_G(t)$ denotes the input of exogenous G-CSF. The administration of rhG-CSF (in our case filgrastim) typically takes two forms: IV infusion (where the drug is given intravenously over a period of time) or subcutaneously (injection under the skin). In the former case, the drug passes directly into the bloodstream meaning the bioavailable fraction (the percentage of the administered dose that enters the blood) is 100%. In this case, we express the single exogenous administration as

$$I_G(t) = \begin{cases} \frac{Do}{t_{inf}V_d}, & t_0 \leqslant t \leqslant t_{inf} \\ 0 & \text{otherwise,} \end{cases} \tag{4.35}$$

where Do is the administered dose, t_0 is the start of the infusion, t_{inf} is the time of infusion and V_d is the volume of distribution. The volume of distribution is a pharmacokinetic parameter which relates the hypothetical volume a drug would occupy to the concentration it is observed in the plasma. It is typically calculated for a drug by dividing the administered

dose by the concentration in the blood immediately following an administration for the simplest case of IV bolus administration (instantaneous administration into the blood). Drugs given subcutaneously do not immediately reach the bloodstream. Instead, a certain proportion of the medication remains in the subcutaneous tissue pool before diffusing into the plasma. Some previous studies, notably [5, 20] used an extra transition compartment to model the administered G-CSF concentration in the tissues before reaching the blood and allowed for the free exchange between this central (blood) compartment and the tissue compartment. Owing to the specifics of the pharmacokinetics of filgrastim, we will instead use the following direct input functions from [30] and [11] to model subcutaneous administration as

$$I_G(t) = \begin{cases} \frac{k_a DoF}{V_d} e^{k_a t}, & t \geqslant t_0 \\ 0 & t < t_0, \end{cases} \tag{4.36}$$

where k_a is the constant of absorption, and F is the bioavailable fraction (the fraction of non-metabolised dose which enters the system). This direct form is preferred over the two compartment method previously employed in [5, 20] because of the relatively small volume of distribution exhibited by filgrastim (the bio-similar exogenous form of G-CSF), which is to say that V_d is less than the standard 70L measure of highly distributed drugs [11] and that the drug does not have a strong tendency to redistribute into the tissues.

The pharmacokinetic model of the chemotherapeutic drug (Zalypsis®) used in this paper is the same as in [11]. Briefly, the concentration of chemotherapeutic drug in the system is modelled using a set of four ordinary differential equations which was determined to be suitable through population pharmacokinetic analysis [41]. The PK model of Zalypsis® is given by

$$\begin{gathered} \tfrac{d}{dt}C_p(t) = I_C(t) + k_{fp}C_f(t) + k_{sl_1 p}C_{sl_1}(t) - (k_{pf} + k_{psl_1} + k_{el_C})C_p(t) \\ \tfrac{d}{dt}C_f(t) = k_{pf}C_p(t) + k_{sl_2 f}C_{sl_2}(t) - (k_{fp} + k_{fsl_2})C_f(t) \\ \tfrac{d}{dt}C_{sl_1}(t) = k_{psl_1}C_p(t) - k_{sl_1 p}C_{sl_1}(t), \quad \tfrac{d}{dt}C_{sl_2}(t) = k_{fsl_2}C_f(t) - k_{sl_2 f}C_{sl_2}(t), \end{gathered} \tag{4.37}$$

where C_p is the concentration in the central (blood) compartment, C_f is the concentration in the fast-exchange tissues, and C_{sl_1} and C_{sl_2} are the concentrations in the slow-exchange tissues, k_{ij} are traditional rate constants between the i^{th} and j^{th} compartments ($i, j =$

p, f, sl_1, sl_2), and k_{el_C} is the rate of elimination from the central compartment. We consider the chemotherapeutic drug to be administered by IV infusion, so $I_C(t) = Dose_{Zal}/\Delta_t$, where $Dose_{Zal}$ is the administered dose and Δ_t is the time of infusion.

In contrast to the pharmacodynamic effects of G-CSF, chemotherapy has negative effects on the neutrophil (and other blood) lineages. Chemotherapy (and radiotherapy) works by disrupting the cell-cycle of tumours [37] but this interference also affects all cells which are dividing, including the neutrophil progenitors. The cytotoxic side effects chemotherapeutic treatment has on the neutrophils is called myelosuppression and it is a leading cause of treatment adaptation and/or cessation for patients undergoing chemotherapy [11]. Since chemotherapy's myelosuppressive action only affects cells capable of division, we model the pharmacodynamic effects of chemotherapy on the HSCs, which rarely divide, and the neutrophil progenitors in the proliferative phase, which divide regularly until they exit the mitotic phase.

Since the effects of chemotherapy on the HSCs are not clear, we model the antiproliferative effect as a simple linear decrease of the rate of apoptosis experienced by these cells by replacing γ_Q in equation (4.18) by $\gamma_Q + h_Q C_p(t)$ where $C_p(t)$ is the concentration of the chemotherapeutic drug in the central blood compartment given by (4.37), and h_Q is a factor to be determined (as outlined in Section 4.4.5). Then (4.18) gives

$$A_Q(t) = 2e^{-\gamma_Q \tau_Q - h_Q \int_{t-\tau_Q}^{t} C_p(s)ds}. \tag{4.38}$$

It is convenient to numerically implement (4.38) as a differential equation, and applying Leibniz's Rule to (4.38), similar to the derivation of (4.15), we obtain

$$\tfrac{d}{dt} A_Q(t) = (h_Q(C_p(t-\tau_Q) - C_p(t)))A_Q(t), \tag{4.39}$$

and we replace (4.7) by (4.39) when chemotherapy is administered.

The second effect of chemotherapeutic drugs is to reduce the effective proliferation rate of the mitotic neutrophil progenitors. We model this by replacing η_{N_P} of (4.9) by

$$\eta_{N_P}^{chemo}(G_1(t), C_p(t)) = \eta_{N_P}^{inf} + \frac{\eta_{N_P}(G_1(t)) - \eta_{N_P}^{inf}}{1 + (C_p(t)/EC_{50})^{s_c}}, \tag{4.40}$$

which is a modification of the model used in [11]. Here $\eta_{N_P}^{inf}$ corresponds to the effective proliferation rate in the presence of an infinite dose of the drug. We require $\eta_{N_P}^{inf} < \eta_{N_P}^{min}$ to ensure that effective proliferation is reduced, so $\eta_{N_P}^{chemo}(G_1(t), C_p(t)) < \eta_{N_P}^{chemo}(G_1(t))$ whenever $C_p(t) > 0$. We will allow the possibility of $\eta_{N_P}^{inf} < 0$, which would correspond to negative effective proliferation (more death than division in the mitotic phase) in the presence of very large concentrations of the chemotherapeutic drug, though we note that because the drug is cleared from circulation relatively quickly we will have $\eta_{N_P}^{chemo}(G_1(t), C_p(t)) > 0$ most of the time even if $\eta_{N_P}^{inf} < 0$. If $\eta_{N_P}^{inf} \in (0, \eta_{N_P}^{min})$ then effective cell division is reduced but never completely halted however large the concentration of the chemotherapeutic drug. EC_{50} is the concentration of chemotherapeutic drug which gives the half-maximal effect, and s_c is a Hill coefficient. The parameters h_Q, $\eta_{N_P}^{inf}$, EC_{50}, and s_c will all be estimated using fitting techniques described in Section 4.4.5.

4.4 Parameter Estimation and Equation Constraints

In this section we show how our mathematical model imposes constraints on its own parameters to be self-consistent, and how experimental data can be used to determine model parameters. We begin in Section 4.4.1 by studying the model at homeostasis and deriving inequalities that the parameters must satisfy, as well as showing how experimentally measured quantities can be used to directly determine some parameters in the model. In Section 4.4.2 we show how the G-CSF pharmacokinetic parameters can be determined using a combination of model equation constraints and parameter fitting to experimental data from single administrations of G-CSF. In Section 4.4.3, G-CSF knockout is used to derive further parameter constraints and relationships. Finally in Section 4.4.4 we show how the pharmacodynamic parameters in the neutrophil equations can be determined by fitting the model to experimental data for the circulating neutrophil concentrations after a single IV or subcutaneous administration of G-CSF.

4.4.1 Neutrophil Steady-State Parameter Determination and Constraints

At homeostasis let Q^* be the stem cell concentration and denote the sizes of the four neutrophil compartments at homeostasis by N_P^* (proliferation) , N_M^* (maturation), N_R^* (marrow reservoir), N^* (total blood neutrophil pool), and the average time that a cell

spends in one of these stages at homeostasis by τ_{N_P}, a_{N_M}, $\tau^*_{N_R}$ and $\tau^*_{N_C}$, respectively. With the exception of τ_{N_P}, all of these quantities have been determined experimentally, but unfortunately only τ_{N_P} and a_{N_M} actually appear in our model. In this section we show that our model imposes some constraints on the values of these parameters, and also how the values of κ^*, N^*_P, N^*_M, N^*_R, N^*, a_{N_M}, $\tau^*_{N_R}$ and $\tau^*_{N_C}$ can be used through the model to determine values for the parameters τ_{N_P}, $\eta^*_{N_P}$, γ_{N_M}, γ_{N_R}, γ_N and $\varphi^*_{N_R}$ which do appear in the model in Section 4.2.

At homeostasis equations (4.1)–(4.3) become

$$0 = -\big(\kappa^* + \kappa_\delta + \beta(Q^*)\big)Q^* + A^*_Q\beta(Q^*)Q^*, \tag{4.41}$$

$$\kappa^* Q^* A^*_N = (\varphi^*_{N_R} + \gamma_{N_R})N^*_R, \tag{4.42}$$

$$\varphi^*_{N_R} N^*_R = \gamma_N N^*. \tag{4.43}$$

Equation (4.41) has the trivial solution $Q^* = 0$ with other solutions given by

$$\kappa^* + \kappa_\delta = (A^*_Q - 1)\beta(Q^*) \tag{4.44}$$

To the best of our knowledge, there is no experimental data to determine the relative rates of differentiation to the three cell lines (erythrocytes, neutrophils, thrombocytes) at homeostasis. In the absence of any evidence to the contrary, we will assume that these are all equal. Since κ^* denotes the differentiation rate to the neutrophil line and κ_δ differentiation to erythrocyte and thrombocyte precursors we obtain

$$\kappa^* = \tfrac{1}{2}\kappa_\delta = \tfrac{1}{3}(A^*_Q - 1)\beta(Q^*). \tag{4.45}$$

At homeostasis neutrophil precursors are assumed to enter the mitotic phase at rate κ^*Q^*. They then proliferate at a rate $\eta^*_{N_P}$ for a time τ_{N_P}. The total number of cells in the proliferative phase at homeostasis is thus

$$N^*_P = \int_0^{\tau_{N_P}} \kappa^* Q^* e^{\eta^*_{N_P} s} ds = \kappa^* Q^* \frac{e^{\eta^*_{N_P}\tau_{N_P}} - 1}{\eta^*_{N_P}}, \tag{4.46}$$

and cells leave proliferation and enter maturation at a rate R_P^* given by

$$R_P^* = \kappa^* Q^* e^{\eta_{N_P}^* \tau_{N_P}}. \tag{4.47}$$

At homeostasis from (4.10) we have $V_{N_M}(G_2^*) = 1$, and thus from (4.11), the time spent in maturation at homeostasis is a_{N_M}. The number of cells of age s for $s \in [0, a_{N_M}]$ in the maturation phase is then $\kappa^* Q^* \exp(\eta_{N_P}^* \tau_{N_P} - \gamma_{N_M} s)$, and the total number of cells in the maturation phase is

$$N_M^* = \int_0^{a_{N_M}} \kappa^* Q^* e^{\eta_{N_P}^* \tau_{N_P} - \gamma_{N_M} s} ds = \kappa^* Q^* e^{\eta_{N_P}^* \tau_{N_P}} \frac{1 - e^{-\gamma_{N_M} a_{N_M}}}{\gamma_{N_M}}. \tag{4.48}$$

Writing

$$A_N^* = \exp\left(\eta_{N_P}^* \tau_{N_P} - \gamma_{N_M} a_{N_M}\right), \tag{4.49}$$

which corresponds to (4.14) at homeostasis, we can rewrite (4.48) as

$$N_M^* = \kappa^* Q^* A_N^* \frac{e^{\gamma_{N_M} a_{N_M}} - 1}{\gamma_{N_M}}. \tag{4.50}$$

Now the rate at which cells leave the maturation phase is

$$\kappa^* Q^* e^{\eta_{N_P}^* \tau_{N_P} - \gamma_{N_M} a_{N_M}} = \kappa^* Q^* A_N^*.$$

The average time, $\tau_{N_C}^*$, that neutrophils spend in circulation in the blood (in the total blood neutrophil pool) has been measured a number of times. However, what is actually measured is the half removal time, $\tau_{1/2}$, which gives γ_N, the removal rate from circulation by

$$\gamma_N = \frac{1}{\tau_{N_C}^*} = \frac{\ln 2}{\tau_{1/2}}. \tag{4.51}$$

Equation (4.43) ensures that at homeostasis the rate neutrophils leave the reservoir and enter circulation equals the rate at which they are removed from circulation. From this we obtain

$$\varphi_{N_R}^* = \frac{\gamma_N N^*}{N_R^*}. \tag{4.52}$$

The rate at which neutrophils exit the mature marrow reservoir is given by $(\varphi_{N_R}^* + \gamma_{N_R}) N_R^*$

where $\varphi^*_{N_R}$ is the transition rate constant for cells entering circulation and γ_{N_R} is the random death rate. Thus the average time that cells spend in the reservoir at homeostasis is

$$\tau^*_{N_R} = \frac{1}{\varphi^*_{N_R} + \gamma_{N_R}}. \tag{4.53}$$

Hence the random death rate in the reservoir, $\gamma_{N_R} \geqslant 0$, is given by

$$\gamma_{N_R} = \frac{1}{\tau^*_{N_R}} - \varphi^*_{N_R}, \tag{4.54}$$

and we require that

$$\tau^*_{N_R}\varphi^*_{N_R} \leqslant 1 \tag{4.55}$$

to ensure that $\gamma_{N_R} \geqslant 0$. That said, using (4.51) and (4.52), we can rewrite (4.55) as

$$\frac{\tau^*_{N_R}}{\tau^*_{N_C}} \leqslant \frac{N^*_R}{N^*}. \tag{4.56}$$

The apoptosis rate during the maturation phase, $\gamma_{N_M} \geqslant 0$, is calculated by eliminating $\kappa^* Q^* A^*_N$ from (4.42) and (4.50). Also making use of (4.54), we obtain

$$F_M(\gamma_{N_M}) := N^*_R(e^{\gamma_{N_M} a_{N_M}} - 1) - \gamma_{N_M}\tau^*_{N_R}N^*_M = 0. \tag{4.57}$$

It is easy to see that $F_M(0) = 0$ and hence $\gamma_{N_M} = 0$ is one solution of (4.57). Since $F''_M(\gamma) > 0$ for all $\gamma \geqslant 0$, if $F'_M(0) < 0$ there is a unique $\gamma_{N_M} > 0$ such that $F_M(\gamma_{N_M}) = 0$, and no positive value of γ such that $F_M(\gamma) = 0$ if $F'_M(0) \geqslant 0$. Since cell death is known to occur in the maturation compartment (see [36]), we should choose our parameters so that (4.57) admits a solution $\gamma_{N_M} > 0$. The condition $F'_M(0) > 0$ is equivalent to

$$\frac{N^*_R}{N^*_M} < \frac{\tau^*_{N_R}}{a_{N_M}}, \tag{4.58}$$

and to include apoptosis in the maturation compartment our parameters must be chosen to satisfy (4.58).

Equation (4.56) can be interpreted as a lower bound on $\tau^*_{N_R}$, and (4.58) as an upper

bound. Eliminating $\tau^*_{N_R}$ from these two bounds we find that the parameters must satisfy

$$\frac{a_{N_M}}{\tau^*_{N_C}} < \frac{N^*_M}{N^*} \tag{4.59}$$

for the constraints (4.56) and (4.58) to be consistent. Then $\tau^*_{N_R}$ must satisfy

$$\tau^*_{N_R} \in \left(a_{N_M} \frac{N^*_R}{N^*_M}, \tau^*_{N_C} \frac{N^*_R}{N^*} \right) \tag{4.60}$$

for both (4.56) and (4.58) to be satisfied as strict inequalities. All the quantities in (4.60) have been estimated experimentally. To be consistent with our model the values must satisfy both (4.59) and (4.60). In Section 4.5 we state parameters that satisfy these constraints. With those parameters we take $\gamma_{N_M} > 0$ to be the unique strictly positive solution to (4.57).

Equation (4.42) ensures that the rate cells enter and leave the reservoir are equal at homeostasis. Rearranging and using (4.52) we obtain

$$A^*_N = \frac{N^*_R}{\kappa^* Q^* \tau^*_{N_R}}, \tag{4.61}$$

which determines A^*_N. Now from (4.49) we have

$$e^{\eta^*_{N_P} \tau_{N_P}} = A^*_N e^{\gamma_{N_M} a_{N_M}}, \tag{4.62}$$

which determines $e^{\eta^*_{N_P} \tau_{N_P}}$, and it remains to determine one of $\eta^*_{N_P}$ or τ_{N_P} in order to be able to find the other. However (4.46) implies that

$$\eta^*_{N_P} = \kappa^* Q^* \frac{e^{\eta^*_{N_P} \tau_{N_P}} - 1}{N^*_P} = \kappa^* Q^* \frac{A^*_N e^{\gamma_{N_M} a_{N_M}} - 1}{N^*_P} \tag{4.63}$$

and now from (4.62) we have

$$\tau_{N_P} = \frac{1}{\eta^*_{N_P}} \ln\left(A^*_N e^{\gamma_{N_M} a_{N_M}} \right). \tag{4.64}$$

In Section 4.5 we use the equations of this section to determine parameter values for our model.

4.4.2 Estimation of G-CSF Pharmacokinetic Parameters

Following [2, 26, 30, 71] we take the homeostasis concentration of the free circulating G-CSF to be $G_1^* = 0.025\,\text{ng/mL}$. The parameter V in (4.5) is the same parameter V as appears in (4.20). But V is difficult to interpret directly from (4.20), and although published values are available, they vary widely between sources. For the pharmacokinetic G-CSF model (4.4),(4.5) the meaning of V is clear; its simply the conversion factor that converts a neutrophil concentration N in units of 10^9 cells per kilogram of body mass, into the corresponding G-CSF concentration VN in units of nanograms per millilitre when every receptor on the neutrophils is bound.

To compute V, we first note that the molecular mass of G-CSF is $18.8\,\text{kDa} = 18800\,\text{g/mol}$ [30] or dividing by Avogadro's constant, the equivalent weight of G-CSF is $G_{mw} = 3.12 \times 10^{-11}\,\text{ng/molecule}$. We take the number of receptors per neutrophil to be $R = 600$, which is in the middle of the range that Barreda [2] cites, though we note that both smaller and larger numbers can be found in the literature. Then given N, the number of receptors per millilitre is

$$R \times \frac{70}{5000} \times 10^9 \times N,$$

where we assume body mass of 70 kg and 5000 mL of blood. Since two molecules bind to each receptor the maximum concentration of bound G-CSF is

$$VN = 2 \times G_{mw} \times R \times \frac{70}{5000} \times 10^9 \times N = 0.525N\,\text{ng/mL}$$

and hence

$$V = 0.525\,(\text{ng/mL})/(10^9\text{cells/kg}). \tag{4.65}$$

Values have been published for several of the other parameters in the G-CSF equations (4.4),(4.5), but these have been largely based on *in vitro* experiments and/or simpler G-CSF models using mixed-effects estimation techniques, and so are not directly applicable to our model [30, 52, 58, 69].

At homeostasis, equations (4.4),(4.5) give

$$G_2^* = \frac{(G_1^*)^{Pow}}{(G_1^*)^{Pow} + (k_{int} + k_{21})/k_{12}} V[N_R^* + N^*], \tag{4.66}$$

and

$$\begin{aligned} G_{prod} &= k_{ren}G_1^* + k_{int}G_2^* \\ &= k_{ren}G_1^* + k_{int}V[N_R^* + N^*]\frac{(G_1^*)^{Pow}}{(G_1^*)^{Pow} + (k_{int} + k_{21})/k_{12}}. \end{aligned} \tag{4.67}$$

Once values of k_{int}, k_{12}, k_{21}, k_{ren} and Pow are determined as we describe below, (4.66) and (4.67) determine values for G_2^* and G_{prod}.

The remaining parameters might be determined by simulating the full model with exogenous G-CSF administration and fitting the response of the model to published data for such experiments. However, that would involve also fitting the as yet undetermined pharmacodynamic parameters in equations (4.1)–(4.17) which would create a very large optimisation problem, with the potential for interactions between the pharmacokinetic and pharmacodynamic parameters to create a complicated functional with many local minima. To avoid this, we prefer to determine the pharmacokinetic and pharmacodynamic parameters separately. Here we determine the PK parameters by decoupling the G-CSF equations (4.4)-(4.5) from the neutrophil dynamics.

There have been a number of studies tracking the response of the hematopoietic system to a single administration of exogenous G-CSF including Wang [69] and Krzyzanski [30]. If data were available for circulating neutrophil and marrow reservoir neutrophil concentrations as functions of time it would be possible to treat equations (4.4)-(4.5) separately from the rest of the model as a system of two ordinary differential equations with $[N_R(t) + N(t)]$ treated as a known non-autonomous forcing term determined by the data. But unfortunately it is not known how to directly measure either marrow neutrophil reservoir or bound G-CSF concentrations, and such values are not reported in the literature.

In the absence of marrow neutrophil data we will decouple the G-CSF kinetic equations (4.4)-(4.5) from the rest of the model by replacing the time dependent term $[N_R(t) + N(t)]$ by the constant N_{tot} to obtain

$$\begin{aligned} \tfrac{d}{dt}G_1(t) &= I_G(t) + G_{prod} - k_{ren}G_1(t) \\ &\quad - k_{12}(N_{tot}V - G_2(t))G_1(t)^{Pow} + k_{21}G_2(t) \end{aligned} \tag{4.68}$$

$$\tfrac{d}{dt}G_2(t) = -k_{int}G_2(t) + k_{12}\big(N_{tot}V - G_2(t)\big)G_1(t)^{Pow} - k_{21}G_2(t). \tag{4.69}$$

In (4.68) and (4.69) the constant N_{tot} represents the constant total number of neutrophils available for G-CSF binding, and will be treated as an extra parameter to be determined during the fitting. It should correspond approximately to an average value of $[N_R(t)+N(t)]$ across the time course of the data.

With data for bound G-CSF unavailable we are constrained to fit (4.68),(4.69) to data for the unbound G-CSF. To do this we use digitisations of two sets of data from Wang [69] from a 750 μg intravenous (IV) administration of G-CSF and from a subcutaneous (SC) administration of the same dose. SC administrations necessarily include the absorption kinetics of a drug, as outlined in equation (4.36), whereas IV administrations reach the blood directly and can be modelled more simply as in (4.35). For these reasons, both IV and SC data were used simultaneously during the fitting procedure to best characterise the parameters. Rather than fitting directly to the data from Wang [69], to obtain robust parameter fits we took the G-CSF data from the SC and IV administrations and fit a spline through each to define functions $G^{SC}_{dat}(t)$ and $G^{IV}_{dat}(t)$ over the time intervals $0 \leqslant t \leqslant 2$ days for which the data were taken. With postulated parameter values we then use the Matlab [38] ordinary differential equation solver *ode45* to simulate (4.68),(4.69) over the same time interval to define functions $G^{SC}_1(t)$ and $G^{IV}_1(t)$. We measure the error between the simulated solutions and the data using the L^2 function norm defined by

$$\|G\|_2^2 = \int_0^T G(t)^2 dt. \tag{4.70}$$

For the IV data which varies over orders of magnitude, as seen in Figure 4.2, we use a log scale, while for the SC data a linear scale is appropriate. We define a combined error function for both simulations by

$$Err = \| \log(G^{IV}_1) - \log(G^{IV}_{dat})\|_2^2 + \chi^{0.95} \|G^{SC}_1 - G^{SC}_{dat}\|_2^2, \tag{4.71}$$

where the scale factor χ defined by

$$\chi = \frac{\max_{t\in[0,T]} \log(G^{IV}_{dat}(t)) - \min_{t\in[0,T]} \log(G^{IV}_{dat}(t))}{\max_{t\in[0,T]} G^{SC}_{dat}(t) - \min_{t\in[0,T]} G^{SC}_{dat}(t)}, \tag{4.72}$$

effectively rescales the data so that both data sets have equal weight. (Since $\chi < 1$ the

power 0.95 in (4.71) works to give slightly more weight to the SC data).

Fitting was performed using the Matlab [38] *lsqcurvefit* least squares solver, with the error function *Err* evaluated numerically by sampling the functions at a thousand equally spaced points. It is convenient to define the constant

$$N_{elim} = 1 - \frac{k_{ren} G_1^*}{G_{prod}} \tag{4.73}$$

where N_{elim} is the fraction of G-CSF clearance performed through internalisation at homeostasis (obtained in (4.73) as one minus the fraction of renal clearance at homeostasis). The estimation was performed for the G-CSF parameters: k_{12}, k_{21}, Pow, k_{int}, the neutrophil constant N_{elim}, and the pharmacokinetic drug parameters k_a, and F. The elimination fraction N_{elim} was either fixed ($N_{elim} = 0.6$ and 0.8 in Table 4.I) or fitted (the other entries in Table 4.I). At each step of the optimisation the candidate k_{12}, k_{21}, Pow, k_{int} and N_{elim} are used to determine the dependent parameters G_2^*, k_{ren}, and G_{prod}, which from (4.68),(4.69) and (4.73) are given by

$$G_2^* = V N_{tot} \frac{(G_1^*)^{Pow}}{(G_1^*)^{Pow} + (k_{21} + k_{int})/k_{12}} \tag{4.74}$$

$$k_{ren} = \left(-1 + \frac{1}{N_{elim}}\right) V k_{int} (G_1^*)^{(Pow-1)} \frac{N_{tot}}{(G_1^*)^{Pow} + (k_{21} + k_{int})/k_{12}} \tag{4.75}$$

$$G_{prod} = k_{int} G_2^* + k_{ren} G_1^*. \tag{4.76}$$

The following fitting procedure was employed. First parameters were fit from IV data for a 750 μg administration [69] on the log scale to ensure that behaviour at both high and low concentrations were properly characterised. Next initial SC parameters were fit from 750 μg SC data in linear scale. Using the parameters from these two fits as seed values, we next obtain final parameter values by fitting both log-concentration IV and linear SC data simultaneously using the norm defined in (4.71). Finally, as the pharmacokinetic parameters related to the SC administration have been shown to be dose-dependent [58], we re-estimate F and k_a for lower doses of 300 μg and 375 μg [30, 69]. Since V_d is typically calculated by the ratio of the dose to the initial concentration in the blood for IV administrations [15], we have applied the same calculation here to scale the G-CSF prediction to the first measured data point. Accordingly, the volume of distribution was recalculated

Name	Value 1	Value 2	Value 3	Value 4	Value 5	Units
N_{elim}	0.097478	0.6	0.71678	0.8	0.87358	–
k_{ren}	1.3142	0.45064	0.2456	0.16139	0.094597	days^{-1}
k_{12}	2.3004	2.2519	2.1342	2.2423	2.878	days^{-1}
k_{21}	407.1641	198.2403	168.2588	184.8658	259.8087	days^{-1}
k_{int}	394.5111	459.2721	275.2744	462.4209	632.0636	days^{-1}
Pow	1.7355	1.4418	1.4631	1.4608	1.4815	–
N_{tot}	3.9496	4.1767	4.1457	4.2009	3.606	10^9 cells/kg
$Do = 750\,\mu$g, $V_d = 2178.0$ mL						
F	0.99752	0.75	0.75	0.75	0.98271	–
k_a	3.8154	5.2142	5.0574	5.143	4.1931	days^{-1}
Err	0.16352	0.15716	0.17901	0.18543	0.21130	–
$Do = 300\,\mu$g, $V_d = 4754.7$ mL						
F	1	0.63361	0.62299	0.64466	0.71424	–
k_a	6.3783	8.0804	8.0628	8.0236	7.4367	days^{-1}
$Do = 375\,\mu$g, $V_d = 2322.9$ mL						
F	0.89831	0.4801	0.48549	0.49964	0.57618	–
k_a	4.18161	6.7326	6.6324	6.6133	6.1259	days^{-1}

Table 4.I – Pharmacokinetic parameter estimates from the simplified G-CSF model (4.68),(4.69) for different homeostasis elimination fractions of N_{elim}. Err is defined by (4.71) for the 750 μg dose. As described in the text, dose-dependent drug parameters were only recalculated for the lower doses.

to fit the administered dose. The resulting parameters are reported in Table 4.I.

Figure 4.5 compares the solutions from the fitting procedure of the simplified model (4.68) (4.69) for the parameter set with $N_{elim} = 0.80$ from Table 4.I to the Wang [69] data for 750 μg IV and SC doses in log and linear scales, respectively.

Figure 4.6(a-b) gives linear and log scale plots of the simulations of (4.68),(4.69) with the $N_{elim} = 0.80$ parameter set from Table 4.I for an IV administration from Krzyzanski [30]. In this case no fitting was performed; the Krzyzanski [30] protocol is simulated using parameters obtained from fitting to the Wang data, and a good fit to the data is still obtained. Figure 4.6(c) shows another simulation for a slightly larger SC dose, with the same G-CSF parameters (only the the dose-dependent drug parameters k_a and F were fit, as already noted), and we again obtain good agreement with the data.

Figure 4.6(d) validates the use of the N_{tot} simplification used for (4.68),(4.69) by comparing N_{tot} to $N_R(t)+N(t)$ from the solution of the full model (4.1)-(4.17) and to $N_R^*+N^*$.

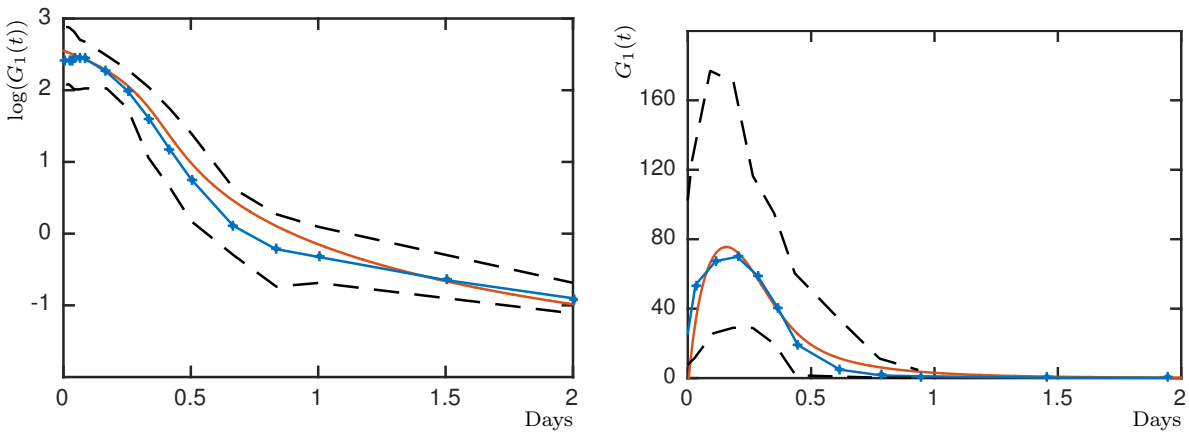

(a) 25 minute IV infusion

(b) Subcutaneous injection

Figure 4.5 – G-CSF PK parameter fitting results of (4.68),(4.69) with parameter values taken from Table 4.I with $N_{elim} = 0.80$. In both panels, a 750 μg dose is administered following the protocol described in Wang [69]. Blue lines with data: digitised data median values, red solid lines: model solution with estimated parameters, black dashed lines: maximum and minimum values of the digitised data.

This demonstrates how N_{tot} effectively averages $N_R(t) + N(t)$ over most of the simulation.

We characterize the parameter sets found for the simplified G-CSF model (4.68),(4.69) by the fraction N_{elim} of the G-CSF that is cleared by binding and internalisation at homeostasis. For $0 \leqslant N_{elim} < 1/2$ the elimination is renal dominated at homeostasis, while for $1/2 < N_{elim} \leqslant 1$ the pharmacokinetics are internalisation dominant. As already mentioned in Section 4.3.2, from a clinical standpoint, it is believed that $N_{elim} > 1/2$, while a number of previously published models including [11, 30, 69] have N_{elim} close to zero.

When we included N_{elim} as a parameter to be fit the results were very sensitive to the seed values used to start the optimisation and had a tendency to produce parameter sets with very low or very high N_{elim} (see the $N_{elim} = 0.097$ and $N_{elim} = 0.87358$ parameter sets in Table 4.I), but we also found a good fit with $N_{elim} = 0.71678$ and were able to find good fits for any fixed value of N_{elim}, as seen in Figure 4.5 (see Table 4.I for parameter sets with $N_{elim} = 0.6$ and 0.8). Our results seem to indicate that there is at least a one parameter family of plausible parameter sets with each set characterised by the value of N_{elim}. This arises because we are fitting the simplified model (4.68),(4.69) without any data for the bound G-CSF concentrations. If the model (4.68),(4.69) were linear then

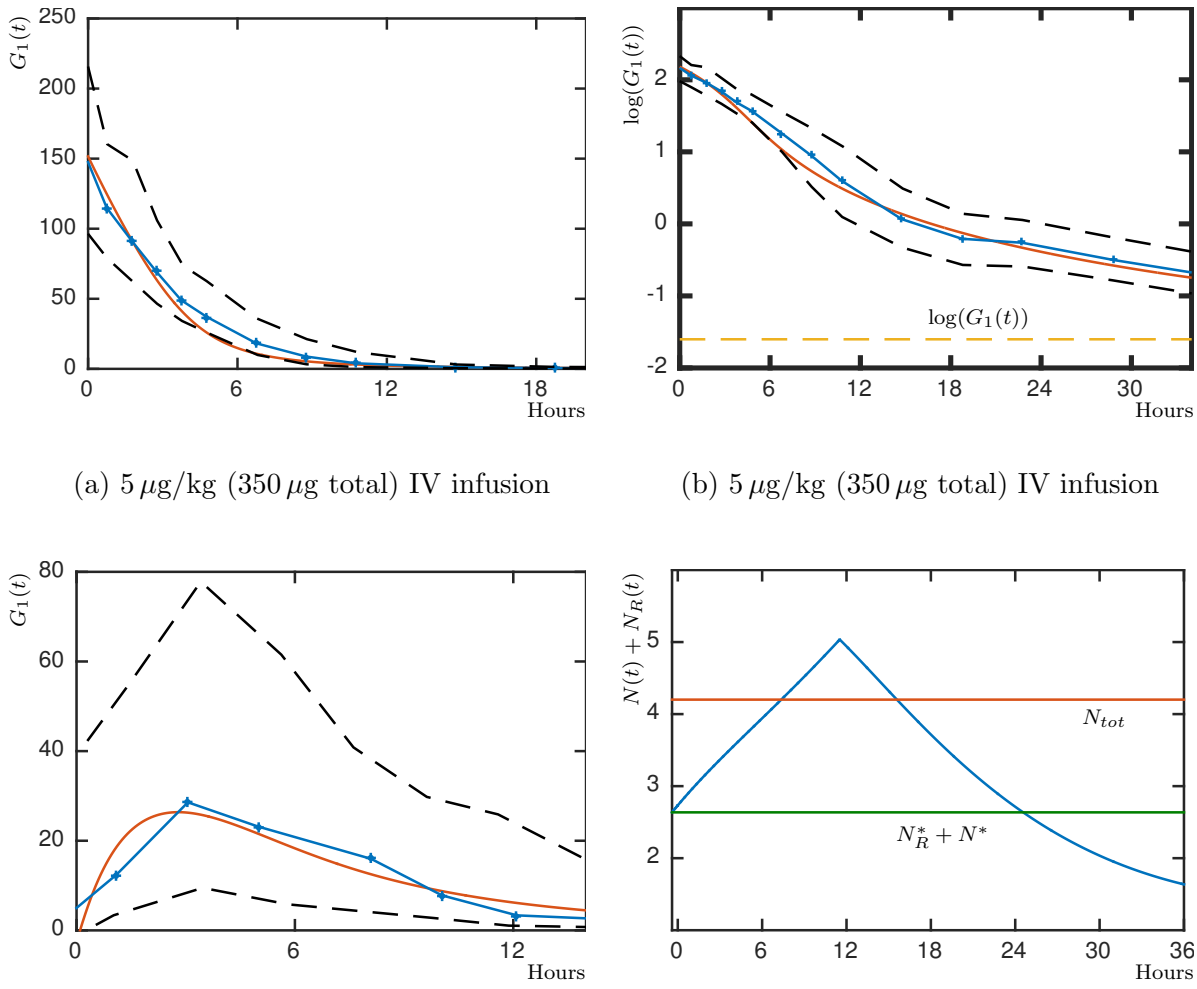

(a) 5 μg/kg (350 μg total) IV infusion

(b) 5 μg/kg (350 μg total) IV infusion

(c) 375 μg subcutaneous administration

(d) 750 μg IV infusion

Figure 4.6 – G-CSF pharmacokinetic parameter fitting results of (4.68),(4.69) with parameter values taken from Table 4.I with $N_{elim} = 0.80$ compared for different administration types, doses, and datasets. a) & b) A simulation of (4.68),(4.69) is compared to data from [30] in linear and log scales. c) A simulation compared to data from [69]. d) Neutrophil concentrations (blue line) of the full neutrophil model (4.1)-(4.17) compared to the value of N_{tot} and $N_R^* + N^*$. For a to c: blue line with data: digitised data median values, red solid line: model solution from estimated parameters, black dashed lines–digitised data maximum and minimum values.

parameter identifiability theory would require data from both components of the solution in order to identify unique parameters in the model. Even though (4.68),(4.69) is nonlinear, the lack of any bound G-CSF data allows us to fit the unbound G-CSF concentrations with different parameter sets, which will result in different solutions for the unmeasured bound G-CSF concentrations. In Section 4.4.4 we will see that different G-CSF kinetic parameter sets will result in similar G-CSF responses, but markedly different neutrophil dynamics. The small differences in the reported errors Err in Table 4.I are not sufficient alone to make a definitive judgement of which is the optimal parameter set. In the following sections we will study the response of the full system (4.1)-(4.17) not just to exogenous G-CSF but also chemotherapeutic treatment (both alone and with prophylactic exogenous G-CSF) which will lead us to conclude that the PK parameters from Table 4.I with $N_{elim} = 0.80$ produce the best model responses to a variety of scenarios.

As seen in Table 4.I, the estimates obtained for N_{tot} are significantly larger than $[N_R^* + N^*]$. However as Figure 4.6(d) shows for a 750 μg dose administered by a 25 minute IV infusion, N_{tot} is an approximate average for $[N_R(t) + N(t)]$ over the initial part of the simulation. This, along with the similarity between the results given by (4.4)-(4.5) and the full model (as illustrated in Figure 4.2) gives us confidence not only in the simplified model (4.68)-(4.69) for estimating the G-CSF kinetic parameters, but also provides additional confirmation that the marrow reservoir neutrophils $N_R(t)$ must be included along with the total blood neutrophil pool $N(t)$ in the full kinetic G-CSF model (4.4)-(4.5) in order to reproduce the observed physiological response.

4.4.3 Parameter estimates from G-CSF knockout

Several murine studies [6, 34] have looked at the effects of G-CSF knockout by producing mice lacking G-CSF receptors and measuring the differences in circulating neutrophil counts compared to wild type mice. The conclusion of these studies is that even in the case of complete incapacity of the neutrophils to bind with G-CSF, neutrophil counts were still between 20 and 30% of normal levels. This is consistent with G-CSF not being the sole cytokine to regulate neutrophil production. Consequently we will ensure that our model produces reduced but non-zero circulating neutrophil concentrations in the complete absence of G-CSF, and so in this section we consider the behaviour of the equations

defining neutrophil production when $G_1 \equiv G_2 \equiv 0$. In that case the four G-CSF dependent functions take values $\kappa(0) = \kappa^{min}$, $\eta_{N_P}(0) = \eta_{N_P}^{min}$, $V_{N_M}(0) \in (0,1)$ (by (4.33)), and $\varphi_{N_R}(0) \in (0, \varphi_{N_R}^*)$ (by (4.31)).

We let N_{ko}^* denote the total blood neutrophil pool under G-CSF knockout and define the ratio

$$C_{ko} = N_{ko}^*/N^*. \tag{4.77}$$

Let $\theta = R_{Pko}/R_P^*$ be the ratio of the rate of cells leaving proliferation in the absence of G-CSF to the rate of cells leaving proliferation at homeostasis. Using (4.47) and a similar calculation for R_{Pko} we obtain

$$\theta = \frac{R_{Pko}}{R_P^*} = \frac{\kappa^{min} Q^* e^{\tau_{N_P} \eta_{N_P}^{min}}}{\kappa^* Q^* e^{\tau_{N_P} \eta_{N_P}^*}} = \frac{\kappa^{min}}{\kappa^*} e^{\tau_{N_P} \eta_{N_P}^* (\mu - 1)}, \tag{4.78}$$

where we also introduce the second auxiliary parameter

$$\mu = \eta_{N_P}^{min}/\eta_{N_P}^* \leqslant 1, \tag{4.79}$$

which measures the fractional reduction in the proliferation rate at knockout. In (4.78) we have assumed that the number of stem cells is unchanged at knockout. Since the differentiation rate to neutrophils will be decreased from κ^* to κ^{min} in the absence of G-CSF, the number of stem cells will actually increase, but using (4.44) and (4.6) this increase can be calculated and is found to be less than 1% for our model parameters.

For given values of θ, μ and $e^{\tau_{N_P} \eta_{N_P}^*}$ we will use (4.78) to determine the ratio κ^{min}/κ^*. Since $\kappa^{min} \leqslant \kappa^*$ (see (4.32)), (4.78) implies that $\theta \leqslant e^{\tau_{N_P} \eta_{N_P}^* (\mu - 1)}$. Rearranging this gives a lower bound for μ, from which obtain the constraint

$$\mu \in \left(1 + \frac{\ln(\theta)}{\tau_{N_P} \eta_{N_P}^*}, 1\right). \tag{4.80}$$

Here $\mu = 1$ corresponds to a constant proliferation rate independent of G-CSF, with the reduced production of neutrophils at knockout caused by a reduction of the differentiation rate κ. If μ is equal to its lower bound then κ is constant independent of G-CSF concentration, and the reduced production of neutrophils is caused by the reduced effective proliferation rate η_{N_P}. For intermediate values of μ, both κ^{min} and $\eta_{N_P}^{min}$ are reduced from

their homeostasis values, and μ acts as a tuning parameter to weight the relative contribution of each mechanism with κ^{min}/κ^* a monotonically decreasing function of $\mu = \eta_{N_P}^{min}/\eta_{N_P}^*$.

A value for θ can be computed by studying the dynamics in the absence of G-CSF after the proliferation stage. Letting N_{ko}^* and N_{Rko}^* denote the number of neutrophils at knockout in the total blood pool and in the marrow reservoir respectively, the rate that cells enter and leave circulation should be equal implying that $\gamma_N N_{ko}^* = \varphi_{N_R}(0) N_{Rko}^*$, or

$$N_{Rko}^* = \frac{1}{\varphi_{N_R}(0)} \gamma_N N_{ko}^*. \tag{4.81}$$

The rate R_{Mko} that mature neutrophils are created at knockout is then equal to the rate that neutrophils enter and leave the marrow reservoir, and hence

$$R_{Mko} = (\varphi_{N_R}(0) + \gamma_{N_R}) N_{Rko}^* = \gamma_N N_{ko}^* \left(1 + \frac{\gamma_{N_R}}{\varphi_{N_R}(0)}\right). \tag{4.82}$$

During G-CSF knockout, the maturation time is given by $a_{N_M}/V_{N_M}(0)$, during which cells die at a constant rate γ_{N_M} (which is not affected by G-CSF). Hence the rate R_{Pko} that cells exit proliferation in the absence of G-CSF is related to R_{Mko} by

$$R_{Pko} e^{-\gamma_{N_M} \frac{a_{N_M}}{V_{N_M}(0)}} = R_{Mko}.$$

Thus,

$$R_{Pko} = e^{\gamma_{N_M} \frac{a_{N_M}}{V_{N_M}(0)}} R_{Mko} = \gamma_N N_{ko}^* \left(1 + \frac{\gamma_{N_R}}{\varphi_{N_R}(0)}\right) e^{\gamma_{N_M} \frac{a_{N_M}}{V_{N_M}(0)}}. \tag{4.83}$$

A similar calculation yields R_P^*, the rate that cells leave proliferation at homeostasis (with G-CSF), as

$$R_P^* = \gamma_N N^* \left(1 + \frac{\gamma_{N_R}}{\varphi_{N_R}^*}\right) e^{\gamma_{N_M} a_{N_M}}. \tag{4.84}$$

Then

$$\theta = \frac{R_{Pko}}{R_P^*} = C_{ko} \frac{\varphi_{N_R}(0) + \gamma_{N_R}}{\varphi_{N_R}^* + \gamma_{N_R}} \exp\left[a_{N_M} \gamma_{N_M} \left(\frac{1}{V_{N_M}(0)} - 1\right)\right], \tag{4.85}$$

where C_{ko} is defined by (4.77).

4.4.4 Estimating the Pharmacodynamic Parameters

We still require estimates for six parameters, μ, b_{N_P}, V_{max}, b_V, b_G and $\varphi_{N_R}^{max}$ in the functions defining the pharmacodynamic effects of G-CSF on the neutrophil production and mobilisation.

We digitised data from Wang [69] for average circulating neutrophil concentrations for three days following a 375 μg and a 750 μg 25-minute IV infusion. The data also contained circulating G-CSF concentrations, but we did not use the G-CSF concentrations for fitting. As in Section 4.4.2, instead of fitting directly to the data points we used it to to define two continuous functions $N_{dat}^{375}(t)$ and $N_{dat}^{750}(t)$, one for each dose, and fit the response of the full model (4.1)-(4.17) to these functions.

The fitting is difficult because no data is available for reservoir or stem cell concentrations, and the circulating neutrophil concentrations are only measured for three days after the infusion. Since the proliferation time for neutrophil precursors is about a week, this data cannot be used to fit any stem cell parameters, as no cells that commit to differentiate to the neutrophil line after the infusion will reach circulation during this time (which is why we do not re-estimate any stem cell parameters in the current work). Although at homeostasis it also takes about a week for cells to traverse maturation and the marrow reservoir, these processes are greatly sped up after G-CSF administration, and cells that are in proliferation at the time of the infusion can reach circulation within a day, enabling us to estimate relevant parameters.

After three days the neutrophil concentrations have not returned to their homeostatic values. If parameters are fit just using this short interval of data, we found parameters which gave good fits to the circulating neutrophil concentrations over the first three days, but for which the neutrophil concentrations then under went very large deviations from homeostasis values lasting months or more. There is no evidence of a single G-CSF administration destabilising granulopoiesis [39]. Accordingly, we will require that the fit parameters result in stable dynamics. We do this by adding artificial data points for $7 \leqslant t \leqslant 21$ days. Accordingly we construct $N_{dat}^{375}(t)$ and $N_{dat}^{750}(t)$ over two disjoint time intervals as splines through the data points for $t \in [0, 3]$ and as constant functions $N_{dat}^{dose}(t) = N^*$ for $t \in [7, 21]$. Since we have no data for t between 3 and 7 days describing how the neutrophils return to homeostasis, we do not define values for $N_{dat}^{dose}(t)$ for this

time interval.

For candidate parameter values, we then used Matlab's [38] delay differential equation solver *ddesd* to simulate (4.1)-(4.17) over the full 21-day time interval. This defined the functions $N^{375}(t)$ and $N^{750}(t)$, from which we were able to measure the error between the data and the simulated solutions using an L^2 function norm similar to the one defined in (4.70). For the disjoint time intervals, we have two integrals to perform, and rescale them to carry equal weight and hence define

$$\|N\|_2^2 = \frac{1}{3}\int_0^3 N(t)^2 dt + \frac{1}{14}\int_7^{21} N(t)^2 dt, \tag{4.86}$$

with corresponding fitting error

$$Err = \|N_{dat}^{375}(t) - N^{375}(t)\|_2^2 + \|N_{dat}^{750}(t) - N^{750}(t)\|_2^2. \tag{4.87}$$

Parameter estimation was performed using the *fmincon* function in Matlab [38]. As in the G-CSF fitting described in Section 4.4.2, the error was evaluated by sampling the functions at one thousand points (with 500 in each time interval because of the scaling in (4.86)).

Instead of directly fitting the six parameters specified at the start of this section, we let $\tilde{b}_V = b_V/V_{max}$ and fit to the six parameters μ, b_{N_P}, V_{max}, $\tilde{b}_V$, $\varphi_{N_R}(0)$ and $\varphi_{N_R}^{ratio}$. This set of parameters is easier to fit to because the constraints (4.31) and (4.33) then become simply $\varphi_{N_R}(0) > 0$ and $\tilde{b}_V > G_1^*$, while the original constraints both involve more than one of the unknown parameters. From (4.17),(4.30) and (4.78), at each step of the optimisation the six fitting parameters define the remaining parameters via

$$\begin{aligned} \eta_{N_P}^{min} &= \mu\,\eta_{N_P}^*, \qquad \varphi_{N_R}^{max} = \varphi_{N_R}^{ratio}\varphi_{N_R}^*, \qquad b_V = \tilde{b}_V V_{max}, \\ \kappa^{min} &= \theta\kappa^* e^{(\tau_{N_P}\eta_{N_P}^*(1-\mu))}, \qquad b_G = G_{BF}^* \frac{\varphi_{N_R}^{max} - \varphi_{N_R}(0)}{\varphi_{N_R}^* - \varphi_{N_R}(0)}. \end{aligned} \tag{4.88}$$

where θ itself is calculated from (4.85). The Hill coefficient of (4.8) was set to be $s_1 = 1.5$, midway within its plausible range of values, as explained in Section 4.5.

The estimation of μ requires some caution as its lower bound in (4.80) changes at each iteration of the optimisation as θ varies, and we see from (4.85) that θ itself depends on

three of the parameters to which we are fitting. Nonsensical results are obtained if the model is simulated with μ outside its bounds. Since the constraint is difficult to apply, to ensure that (4.80) is respected we use a penalty method. Consequently, (4.80) is checked at each iteration of the optimisation and if μ is outside of its bounds μ is reset to the bound and after the simulation is computed Err is multiplied by the penalty factor $e^{|\mu-\mu_{bound}|^{1/2}}$ which is larger than 1 when $\mu \neq \mu_{bound}$. The error function thus penalised cannot have a minimum with μ outside of its bounds, and so the optimisation routine is forced to find values for μ within the permissible range.

A family of G-CSF kinetic parameter sets was reported in Table 4.I in Section 4.4.2. Estimates for the pharmacodynamic parameters were performed for every parameter set in Table 4.I. The resulting pharmacodynamic parameters are reported in Table 4.II.

Name	Value 1	Value 2	Value 3	Value 4	Value 5	Units
N_{elim}^{simp}	0.097478	0.6	0.71678	0.8	0.87358	–
N_{elim}	0.3631	0.4508	0.6204	0.7033	0.8153	–
μ	0.96381	0.86303	0.85482	0.84458	0.90768	–
b_{N_P}	0.125	0.026182	0.025994	0.022868	0.024908	ng/mL
V_{max}	7.9932	7.9881	7.9697	7.867	7.994	–
$\tilde{b}_V$	0.031250	0.031251	0.031255	0.031283	0.031261	ng/mL
$\varphi_{N_R}(0)$	0.072801	0.026753	0.023154	0.020056	0.049852	days^{-1}
$\varphi_{N_R}^{ratio}$	10.9606	11.7257	11.9442	11.3556	11.9706	–
$\eta_{N_P}^{min}$	1.6045	1.4367	1.4231	1.406	1.5111	days^{-1}
$\varphi_{N_R}^{max}$	3.9897	4.2682	4.3478	4.1335	4.3574	days^{-1}
b_V	0.24979	0.24964	0.24909	0.24611	0.2499	ng/mL
b_G	6.3999×10^{-5}	0.0002107	0.00019058	0.00018924	0.00018725	–
θ	0.45978	0.18895	0.17099	0.15096	0.32529	–
κ^{min}	0.0052359	0.0073325	0.0073325	0.0073325	0.0073325	days^{-1}
Err	0.3482	0.3153	0.2928	0.2843	0.3762	–

Table 4.II – Parameter estimation results for the pharmacodynamic parameters. N_{elim}^{simp} refers to N_{elim} value of the corresponding kinetic parameters for the simplified G-CSF model given in Table 4.I. N_{elim} is the corresponding value for the full model, then stated are the six fit parameters, followed by the dependent parameters. The approximation error to the data is found by integrating (4.3) as in (4.87) and comparing to Wang's data [69] for a 375 μg and 750 μg IV infusion of 25 minutes.

Since G_2^* in the full model (4.1)-(4.17) is given by (4.66) which differs from the value given by (4.74) for the simplified model (4.68),(4.69), the values of G_{prod} and N_{elim} derived

for the two models will also be different. In Table 4.II the values from Section 4.4.2 for the simplified model are referred to as N_{elim}^{simp}, and we also state the corresponding value of N_{elim} for the full model from (4.73) using (4.67).

It is important to note that if μ were close to 1 and far from its lower bound, then $\kappa^{min}/\kappa^* \ll 1$, and the wide variation in possible differentiation rates could have potentially destabilising effects on the stem cells. However, for most of the investigated parameter sets (except for $N_{elim}^{simp} = 0.097478$) with the added 'stabilising' data, μ was found to be essentially equal to its lower bound. In this case κ^{min} is almost equal to κ^*, and the rate of differentiation out of the stem cell compartment is essentially constant and (4.8) is virtually independent of the influence of G-CSF. For the current model with the imposed stabilising data, this implies that any change in production is produced by variations in the effective proliferation rate of (4.9). Without the additional data points, we found parameter estimates where μ was far from its lower bound and κ^{min} was similarly lower than κ^* but these led to unstable dynamics. As seen in Sections 4.4.5 and 4.6, the parameter estimates obtained are shown to successfully reproduce protocols for chemotherapy-alone and chemotherapy with adjuvant G-CSF. Accordingly, differentiation from the hematopoietic stem cells is likely close to constant in reality but from our results, we cannot conclude that differentiation is independent of G-CSF.

Figure 4.7, compares the resulting model solutions for three different values of N_{elim}, two of which are shown to be less optimal. Also included are the corresponding G-CSF predictions without any re-estimation from the values obtained in Section 4.4.2. For $N_{elim} = 0.097478$, the G-CSF response is well predicted as seen in Figure 4.7b but because of the renal domination of these parameters, the cytokine paradigm fails in the endogenous-only case. Moreover, repeated administrations of exogenous G-CSF will not accumulate per clinical observations. The G-CSF response seems to be well characterised by the $N_{elim}^{simp} = 0.87358$ parameters in Figure 4.7f however the dynamics of the neutrophil response in Figure 4.7e do not stay within the data bounds, and so are not a good fit. Using $N_{elim}^{simp} = 0.80$, both the neutrophil and G-CSF responses are successfully predicted in Figures 4.7c and 4.7d. The two sets with the lowest errors ($N_{elim}^{simp} = 0.71678$ and $N_{elim}^{simp} = 0.8$) were used to determine parameters relating to the pharmacodynamic effects of chemotherapy, which is discussed in Section 4.4.5.

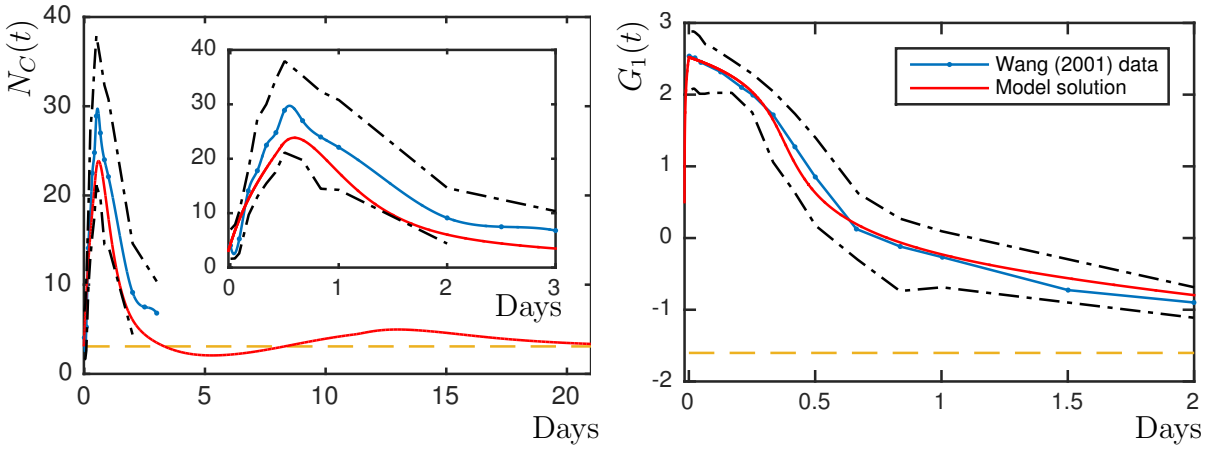

(a) $N_{elim}^{simp} = 0.097478$ (b) $N_{elim}^{simp} = 0.097478$

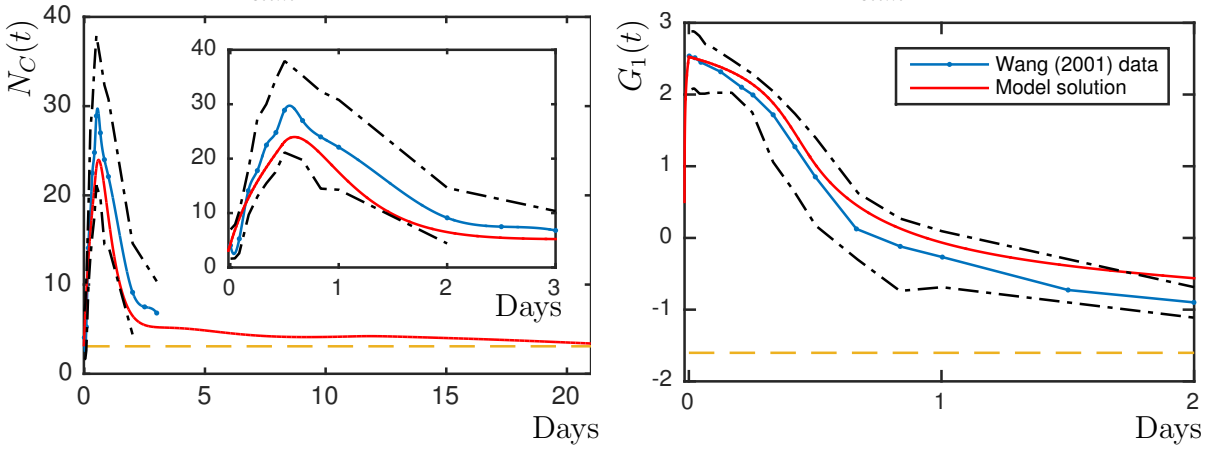

(c) $N_{elim}^{simp} = 0.80$ (d) $N_{elim}^{simp} = 0.80$

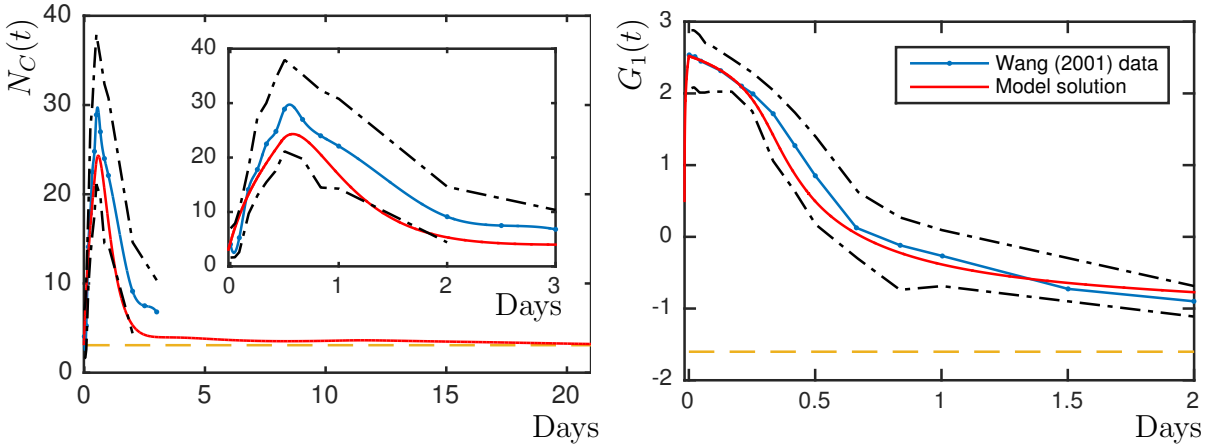

(e) $N_{elim}^{simp} = 0.87358$ (f) $N_{elim}^{simp} = 0.87358$

Figure 4.7 – Simulations of the full model (4.1)-(4.17) for various parameter sets with different N_{elim} values. Left: Circulating neutrophil concentrations in 10^9cells/kg over 21 days, with the first three days shown as an inset. Right: The corresponding circulating G-CSF concentrations. Blue lines with data: digitised data from Figure 7 (neutrophil concentrations) and Figure 6 (G-CSF concentrations) of Wang [69], red solid lines: model solution, black dashed lines: maximum and minimum digitised data values from Figure 7 and Figure 6 of [69], yellow dashed lines: respective homeostatic values.

4.4.5 Estimation of Chemotherapy Related Parameters

To estimate parameters in (4.38) and (4.40), data from the results of the Phase I clinical trial of Zalypsis® were digitised from González-Sales [22]. Unlike the data used for fitting in Sections 4.4.2 and 4.4.4, here the protocols differ from one subject to the next and are reported per patient. All dosing regimens were as stated [22] with doses scaled by body surface area (BSA). Since the subjects were patients undergoing anti-cancer treatments, deviations from the prescribed protocols were frequent. Thus only subjects in the top row (A, B) and bottom row (D, E) of Figure 3 in [22] were retained for our analyses.

As with the parameter estimation of the two previous sections, we define the function $N_{dat}^{ch_j}(t)$ from a spline fit to the data, where $j = A, B, D, E$ corresponds to each of the retained subjects. Likewise, the function $N^{ch_j}(t)$ was defined from the solution from the DDE solver *ddesd* in Matlab [38] for each patient. When the subject was administered two or more cycles of chemotherapy, we took time intervals corresponding to the first two cycles. Thus, the time spans differed for each subject-specific fitting procedure and were: $t_{span_A} = [0, 43]$, $t_{span_B} = [0, 41]$, $t_{span_C} = [0, 47]$, and $t_{span_D} = [0, 61]$. As explained in Section 4.5, to account for each subject's baseline ANC, we adjust a scaling factor so our homeostasis N^* value matches each individual's. We have previously shown the robustness of a similar model to pharmacokinetic interindividual and interoccasion variability which substantiates this adjustment and the use of average values in physiological models [10]. For each of the four patients, we define the integrals

$$\frac{1}{|t_{span_j}|}\int_{\min(t_{span_j})}^{\max(t_{span_j})} N(t)^2 dt, \tag{4.89}$$

where $j = A, B, D, E$. To find average parameter values which fit to all four patients together, we further defined the average error in the L^2 function norm of (4.70) between the simulated solutions and the data by

$$Err = \frac{1}{4}\sum_j \|N^{ch_j}(t) - N_{dat}^{ch_j(t)}\|_2^2. \tag{4.90}$$

Parameters h_Q, $\eta_{N_P}^{inf}$, s_c, and EC_{50} were then estimated using the *lsqcurvefit* optimisation routine in Matlab [38] and similarly averaged. These values are reported in Table 4.III

Name	Value 1	Value 2	Units
N_{elim}^{simp}	0.71678	0.8	–
N_{elim}	0.6204	0.7033	–
h_Q	0.0071122	0.0079657	–
EC_{50}	0.78235	0.72545	ng/mL
s_c	0.90568	0.89816	–
$\eta_{N_P}^{inf}$	0	0	days^{-1}
Err	0.17068	0.16965	–

Table 4.III – Results of the parameter estimation of chemotherapy effects values.

and the results of Figure 4.8 were obtained from simulations using these parameters. For each of h_Q, EC_{50}, s_c, and $\eta_{N_P}^{inf}$, similar estimates were obtained for $N_{elim}^{simp} = 0.71578$ and $N_{elim}^{simp} = 0.8$, although the average error of $N_{elim}^{simp} = 0.8$ is slightly smaller and was accordingly retained as optimal.

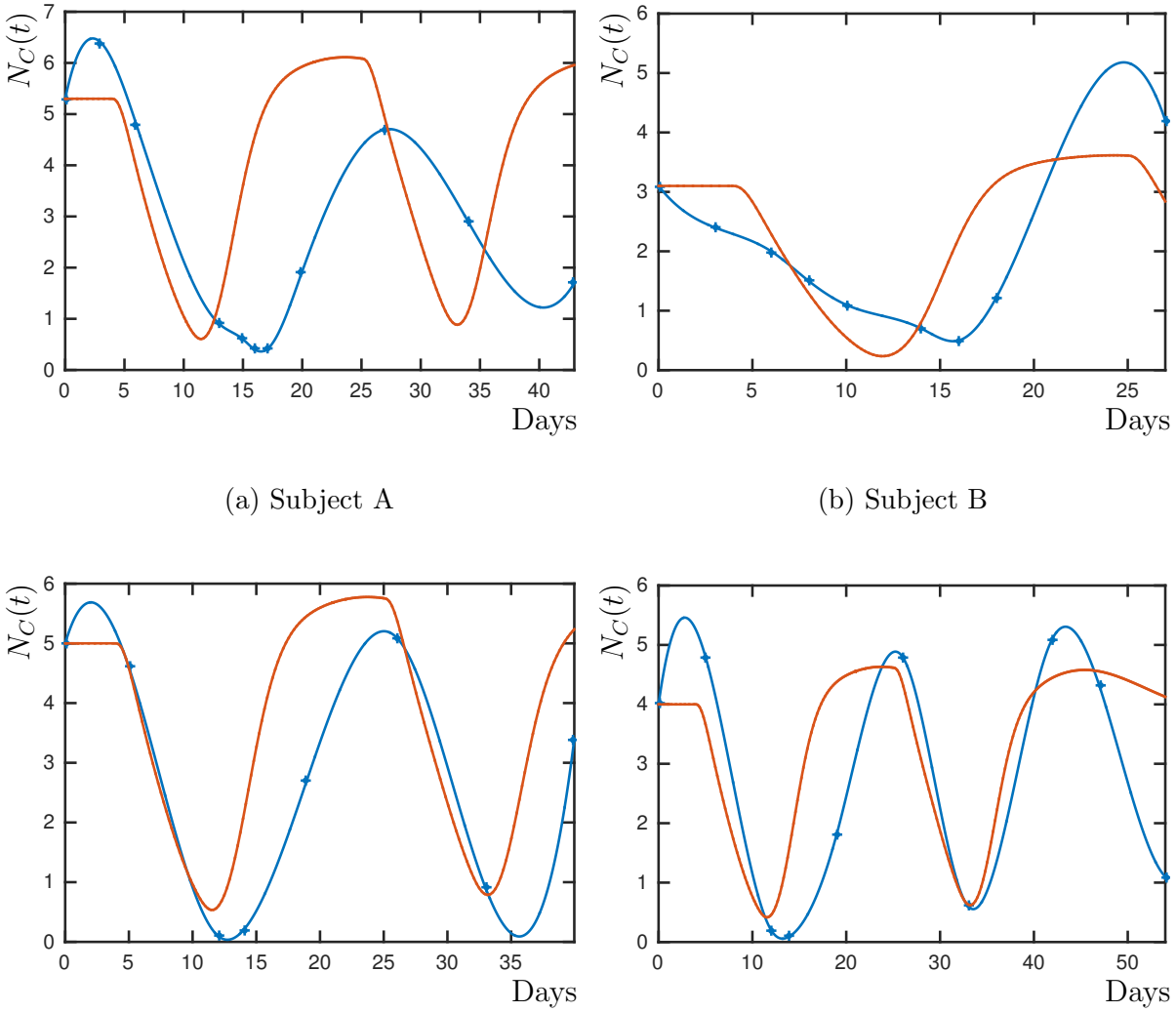

(a) Subject A

(b) Subject B

(c) Subject D

(d) Subject E

Figure 4.8 – Results from the chemotherapy parameter fitting for $N_{elim}^{simp} = 0.80$ parameters over two chemotherapy cycles. Model solutions were obtained using the parameters given in Table 4.II and by simulating the full model (4.1)-(4.17). Chemotherapeutic concentrations are obtained via (4.37) and (4.40). Equation (4.18) is replaced by (4.38) and solved by using (4.39) Data and experimental protocols from Figure 3 of Gonzàlez-Sales [22]. Blue lines with data: digitised data, red solid lines: model solution.

4.5 Parameter Values

Here we summarise the parameter values we use in the full model taken from experimental results and the fitting procedures described in Section 4.4. For the model to be self-consistent these parameters must be positive and satisfy the parameter constraints that we derived above, namely: (4.30), (4.31), (4.33), (4.59), (4.60) and (4.80).

The main model parameters are stated in Table 4.IV. For the stem cells we reuse parameter values for Q^*, γ_Q, τ_Q, f_Q, s_2 and $\beta(Q^*)$ from previous modelling (sometimes rounding them to fewer significant figures). The value of θ_2 is obtained by evaluating (4.6) at homeostasis and rearranging to obtain

$$\theta_2 = \left[\frac{(Q^*)^{s_2}\beta(Q^*)}{f_Q - \beta(Q^*)}\right]^{\frac{1}{s_2}}. \tag{4.91}$$

In Table 4.IV we quote a value of θ_2 to five significant figures, but in our computations all parameters defined by formulae are evaluated to full machine precision. This ensures that our differential equation model has a steady state exactly at the stated homeostasis values.

For the neutrophil parameters we mainly take experimental values from the work of Dancey [14] and use the formulae of Section 4.4.1 to determine the related model parameter values. However, some choices and adjustments need to be made to ensure that the values are consistent with the model. Dancey [14] measured the circulating neutrophil pool to be 0.22×10^9cells/kg and the recovery rate to be 0.585 from which we obtain the total blood neutrophil pool N^* (including the marginated pool) to be

$$N^* = \frac{0.22}{0.585} \approx 0.3761 \times 10^9 \text{cells/kg}. \tag{4.92}$$

Since $N(t)$ measures the total blood neutrophil pool in units of 10^9cells/kg some care needs to be taken when comparing to data, where absolute neutrophil counts (ANC) measure the circulating neutrophil pool in units of cell/μL. Based on 70 kg of body mass and 5 litres of blood we have the default conversion factor for healthy subjects of

$$ANC = 0.585 \times \frac{70}{5} \times 1000 \times N(t) = 8190\, N(t)\, \text{cell}/\mu\text{L}. \tag{4.93}$$

Name	Interpretation	Value	Units	Source
γ_Q	HSC apoptosis rate	0.1	days^{-1}	[5, 11]
τ_Q	Time for HSC re-entry	2.8	days	[4, 11, 33, 35]
A_Q^*	HSC Amplification Factor	$1.5116^\dagger$	–	Eq. (4.7)
f_Q	Maximal HSC re-entry rate	8	days^{-1}	[4, 5, 11]
s_2	HSC re-entry Hill coefficient	2	–	[4, 5, 11]
θ_2	Half-effect HSC concentration	$0.080863^\dagger$	10^6cells/kg	Eq. (4.91)
κ_δ	HSC differentiation rate to other lines	$0.014665^\dagger$	days^{-1}	Eq. (4.45)
κ^{min}	HSC-neutrophil minimal differentiation rate	$0.0073325^\dagger$	days^{-1}	Eq. (4.88)
κ^*	HSC-neutrophil homeo differentiation rate	$0.0073325^\dagger$	days^{-1}	Eq. (4.45)
s_1	HSC-neutrophil differentiation Hill coefficient	1.5	–	Eq. (4.96)
$\eta_{N_P}^*$	Neutrophil homeostasis effective proliferation rate	$1.6647^\dagger$	days^{-1}	Eq. (4.63)
b_{N_P}	Neutrophil proliferation M-M constant	0.022868	ng/mL	Fit Table 4.II
$\eta_{N_P}^{min}$	Neutrophil minimal proliferation rate	1.4060	days^{-1}	Eq. (4.88)
τ_{N_P}	Neutrophil proliferation time	$7.3074^\dagger$	days	Eq. (4.64)
V_{max}	Maximal neutrophil maturation velocity	7.8670	–	Fit Table 4.II
b_V	maturation velocity half-effect concentration	0.24611	ng/mL	Eq. (4.88)
a_{N_M}	Homeostasis neutrophil maturation time	3.9	days	[14, 25] & (4.95)
γ_{N_M}	Neutrophil death rate in maturation	$0.15769^\dagger$	days^{-1}	Eq. (4.57)
$\varphi_{N_R}^*$	Homeostasis Reservoir Release rate	$0.36400^\dagger$	days^{-1}	Eq. (4.52)
$\varphi_{N_R}^{max}$	Maximal Reservoir Release rate	$4.1335^\dagger$	days^{-1}	Eq. (4.88)
b_G	Reservoir Release half-effect concentration	1.8924×10^{-4}	–	Eq. (4.88)
γ_{N_R}	Neutrophil death rate in reservoir	$0.0063661^\dagger$	days^{-1}	Eq. (4.54)
γ_N	Neutrophil Removal Rate from Circulation	35/16	days^{-1}	Eq. (4.51)
G_1^*	Homeostasis Free G-CSF Concentration	0.025	ng/mL	[2, 26, 30, 71]
G_{BF}^*	Homeostasis neutrophil receptor bound fraction	1.5823×10^{-5}	–	Eq. (4.16)
G_{prod}	Endogenous G-CSF production rate	$0.014161^\dagger$	ng/mL/day	Eq. (4.67)
V	Bound G-CSF conversion factor	0.525	$\frac{\text{ng/mL}}{10^9\text{cells/kg}}$	Eq. (4.65)
k_{ren}	G-CSF renal elimination rate	0.16139	days^{-1}	Fit Table 4.I
k_{int}	G-CSF effective internalisation rate	462.42	days^{-1}	Fit Table 4.I
k_{12}	G-CSF Receptor binding coefficient	2.2423	$(\text{ng/mL})^{-\text{Pow}}\text{days}^{-1}$	Fit Table 4.I
k_{21}	G-CSF Receptor unbinding rate	184.87	days^{-1}	Fit Table 4.I
Pow	Effective G-CSF binding coefficient	1.4608	–	Fit Table 4.I

Table 4.IV – Model Parameters. † – these parameters are displayed to 5 significant figures here, but the value is actually defined by the stated equation, and in simulations/computations we use the stated formula to define the value to machine precision.

This gives a baseline homeostasis ANC of $8190N^* = 3080\,\text{cell}/\mu\text{L}$, well within the accepted normal range of $1800 - 7000\,\text{cells}/\mu\text{L}$ [50]. When comparing our model to data for individuals with different baseline ANCs (as in Section 4.4.5) we adjust the conversion factor (4.93), but not the parameter values in our model, so that N^* gives the homeostasis ANC

Name	Interpretation	Value	Units	Source
Q^*	HSC homeostasis concentration	1.1	10^6cells/kg	[4, 11, 33]
$\beta(Q^*)$	HSC re-entry rate	0.043	days^{-1}	[11, 35]
N^*	Homeostasis Total Blood Neutrophil Pool	0.22/0.585	10^9cells/kg	Eq. (4.92)
N_R^*	Homeostasis Neutrophil Reservoir Concentration	2.26	10^9cells/kg	[14]
N_P^*	Homeostasis Neutrophil Proliferation Concentration	0.93	10^9cells/kg	Eq. (4.94)
N_M^*	Homeostasis Neutrophil Maturation Concentration	4.51	10^9cells/kg	Eq. (4.94)
G_2^*	Homeostasis bound G-CSF concentration	2.1899×10^{-5}	ng/mL	Eq. (4.66)
$\tau_{N_R}^*$	Homoeostasis Neutrophil mean time in reservoir	2.7	days	[14, 25] & (4.95)
$\tau_{N_C}^*$	Homoeostasis Neutrophil mean time in circulation	16/35	days	[14]
$\tau_{1/2}$	Circulating Neutrophil half-removal time	7.6	hours	[14]
A_N^*	Homeostasis neutrophil proliferation+maturation amplification	$1.0378 \times 10^{5\dagger}$	–	Eq. (4.61)
$\tilde{b}_V$	scaled maturation half-effect concentration	0.031283	ng/mL	Fit Table 4.II
$\varphi_{N_R}^{ratio}$	Ratio of maximal and homeostasis reservoir release rates	11.356	–	Fit Table 4.II
$\varphi_{N_R}(0)$	Minimal reservoir release rate	0.020056	days^{-1}	Fit Table 4.II
θ	Ratio of rate cells leave proliferation at knockout to homeostasis	0.15096	–	Eq. (4.85)
C_{ko}	Knockout total blood neutrophil pool fraction	0.25	–	[6, 34]
μ	Ratio of minimal and homeostasis proliferation rates	0.84458	–	Fit Table 4.II

Table 4.V – Auxiliary Parameters which are not in the model in Section 4.2, but whose values are used to define other parameters. † – these parameters are displayed to 5 significant figures here, but the value is actually defined by the stated equation, and in simulations/-computations we use the stated formula to define the value to machine precision.

of the data.

Dancey [14] measures the proliferation and maturation phases at homeostasis to be $N_P^* = 2.11 \times 10^9$cells/kg (mainly promyelocytes and myelocytes) and $N_M^* = 3.33 \times 10^9$cells/kg (metamyelocytes and bands). Using these numbers in the calculations in Section 4.4.1 results in a proliferation time τ_{N_P} defined by (4.64) of about 26 days. In our model τ_{N_P} is the time from when the HSC first commits to differentiate to the neutrophil line to the end of proliferation of the neutrophil precursors. Although this time has never been definitively measured, 26 days seems to be too long. This is confirmed by the time to neutrophil replenishment in the blood after both allogenic and autologous stem cell transplantation [1, 7], where circulating neutrophils are seen two weeks after the transplant. We suspect that this overly long proliferation time results from the simplification in our model of considering proliferation as a single homogenous process as detailed in Section 4.3.3.

To obtain a more realistic proliferation time of around a week, close to the 6.3 days that Smith [62] states, we keep the total of $N_P^* + N_M^* = 5.44 \times 10^9$cells/kg as found by

Dancey [14], but redistribute cells between proliferation and maturation and set

$$N_P^* = 0.93 \times 10^9 \text{cells/kg}, \qquad N_M^* = 4.51 \times 10^9 \text{cells/kg}. \tag{4.94}$$

Dancey [14] measured the half removal time of neutrophils from circulation to be $t_{1/2} = 7.6\,\text{hrs}$. Accordingly, using (4.51) and rounding, we set $\gamma_N = 35/16 = 2.1875\,\text{days}^{-1}$ and obtain $\tau_{N_C}^*$ as the reciprocal of this. Then equation (4.58) imposes the constraint that $a_{N_M} < 5.4823\,\text{days}$. If we set $a_{N_M} = 3.9\,\text{days}$ close to the value of 3.8 days found by Hearn [25], then (4.60) imposes the constraint that $\tau_{N_R}^* \in (1.9543, 2.7472)$. Hence we take

$$a_{N_M} = 3.9\,\text{days}, \qquad \tau_{N_R}^* = 2.7\,\text{days}, \tag{4.95}$$

so that both constraints are satisfied, and $a_{N_M} + \tau_{N_R}^* = 6.6\,\text{days}$, the value given in [14]. The rest of the neutrophil homeostasis parameters are calculated using the formulae of Section 4.4.1, paying attention in (4.61) to multiply Q^* by 10^{-3} to convert it to the same units as N_R^*.

The G-CSF pharmacokinetic parameters are fit using the simplified G-CSF model (4.68),(4.69) as described in Section 4.4.2. This produces multiple, but equally plausible, parameter sets but as described in subsequent sections not all of these result in good fits to data when we consider the neutrophil response of the full model (4.1)-(4.17) to administrations of G-CSF or of chemotherapy. Consequently as stated in Section 4.4.5, to obtain the best responses of the system to these scenarios we use the fourth set of pharmacokinetic parameters from Table 4.I which for the simplified G-CSF model have $N_{elim}^{simp} = 0.8$ to define k_{ren}, k_{12}, k_{21}, k_{int} and Pow, as well as the exogenous G-CSF parameters V_d, F, k_a (where the last three are dose dependent). Equations (4.66), (4.67) and (4.73) then define G_2^*, G_{prod} and $N_{elim} = 0.7033$ for the full model.

At G-CSF knockout, from [6, 34] we have $C_{ko} \in [0.2, 0.3]$, so it is natural to set $C_{ko} = 0.25$.

For the pharmacodynamic parameters, similar to Pow, arguments could be made for choosing $s_1 = 1$ or $s_1 = 2$, but having fit Pow and finding it close to 1.5, we will simply set

$$s_1 = 1.5 \tag{4.96}$$

to reduce the number of parameters that need to be fit by one. The remaining pharmacodynamic parameters μ, b_{N_P}, V_{max}, $\tilde{b}_V$, $\varphi_{N_R}(0)$ and $\varphi_{N_R}^{ratio}$ were then fit as described in Section 4.4.4, with these parameters defining values of the dependent parameters $\eta_{N_P}^{min}$, $\varphi_{N_R}^{max}$, b_V and b_G via (4.88). From Section 4.4.3 we also obtain values for θ from (4.85) and κ^{min} from (4.88). Each set of kinetic parameters from Table 4.I defines a different set of pharmacodynamic parameters as reported in Table 4.II, but as noted already we prefer the parameter set for $N_{elim}^{simp} = 0.80$ which corresponds to $N_{elim} = 0.7033$.

The full set of parameter values for our combined neutrophil and G-CSF model (4.1)-(4.17) are given in Table 4.IV, along with their units, interpretation and source. Since some of these parameters are defined by equations involving auxiliary parameters that do not explicitly appear in the full model we state these parameters and their source in Table 4.V. Parameters related to the pharmacokinetics and pharmacodynamics of both of the exogenous drugs which have not previously been stated are given in Table 4.VI.

4.6 Model evaluation and functional responses

Having estimated the G-CSF pharmacokinetic, homeostasis related, and chemotherapy pharmacodynamic parameters individually as described in Sections 4.4.2, 4.4.4, and 4.4.5, a convincing evaluation of the ability of the model is to successfully predict data obtained during the concurrent administration of both exogenous drugs. For this, as in [11], we simulated the CHOP14 protocol described in [43] and [42] which includes the administration of both chemotherapy and exogenous G-CSF. Although the chemotherapeutic drug modelled in Section 4.3.5 is not part of the combination therapy of the CHOP14 regimen, the cytotoxic effects of the anticancer drugs are presumed to be similar. To compare to the CHOP14 data published in [29], we simulated a regimen of six cycles of 14-day periodic chemotherapeutic treatment with rhG-CSF treatment beginning four days after the administration of chemotherapy and continuing for ten administrations per cycle. As in [11], the simulated dose of 4 μg of Zalypsis® was selected from the optimal regimens identified in [22] and per the CHOP14 protocol outlined in [42, 43], ten 300 μg doses of subcutaneous G-CSF were simulated per cycle. The lower dose of 300 μg was selected since we assumed an average weight of 70kg per patient throughout.

Figure 4.9 shows the result of the neutrophil response comparison of the model's predic-

Name	Interpretation	Value	Units	Source
	Filgrastim			
	300 mcg dose			
V_d	Volume of distribution	4754.7	mL	Fit Table 4.I
F	Bioavailable fraction	0.64466	–	Fit Table 4.I
k_a	Subcutaneous rate of absorption	8.0236	days^{-1}	Fit Table 4.I
	375 mcg dose			
V_d	Volume of distribution	2322.9	mL	Fit Table 4.I
F	Bioavailable fraction	0.49964	–	Fit Table 4.I
k_a	Subcutaneous rate of absorption	6.6133	days^{-1}	Fit Table 4.I
	750 mcg dose			
V_d	Volume of distribution	2178.0	mL	Fit Table 4.I
F	Bioavailable fraction	0.75	–	Fit Table 4.I
k_a	Subcutaneous rate of absorption	5.143	days^{-1}	Fit Table 4.I
	Zalypsis®			
k_{fp}	Rate of exchange from compartment f to p	18.222	days^{-1}	[41]
k_{sl_1p}	Rate of exchange from compartment sl_1 to p	0.6990	days^{-1}	[41]
k_{pf}	Rate of exchange from compartment p to f	90.2752	days^{-1}	[41]
k_{psl_1}	Rate of exchange from compartment p to sl_1	8.2936	days^{-1}	[41]
k_{el_C}	Rate of elimination	132.0734	days^{-1}	[41]
k_{sl_2f}	Rate of exchange from compartment sl_2 to f	62.5607	days^{-1}	[41]
k_{fsl_2}	Rate of exchange from compartment f to sl_2	9.2296	days^{-1}	[41]
BSA	Body surface area	1.723	m^2	[41]
h_Q	Effect of chemotherapy on $Q(t)$	0.0079657	–	Fit Table 4.III
EC_{50}	Half-maximal effect of chemotherapy on η_{N_P}	0.75390	–	Fit Table 4.III
s_c	Chemotherapy effect Hill coefficient	0.89816	–	Fit Table 4.III
$\eta_{N_P}^{inf}$	Proliferation rate with infinite chemotherapy dose	0	days^{-1}	Fit Table 4.III

Table 4.VI – Exogenous drug administration parameters determined by parameter fitting as explained in Sections 4.4.2 and 4.4.5. For Zalpysis®, p: plasma/central compartment, f: fast-exchange tissues, sl_1: first slow-exchange tissues, sl_2: second slow-exchange tissues.

tion to the clinical data. Unlike experimental settings where information on the HSCs, the marrow neutrophils, and the bound G-CSF concentrations are unavailable, the model's solutions for $Q(t)$, $N_R(t)$, and $G_2(t)$ are easily obtainable and provide insight into not only the mechanisms responsible for myelosuppression during chemotherapy, but also ways in which this toxicity might be avoided. In Figure 4.10, the HSCs, neutrophils in the marrow reservoir, and bound and unbound G-CSF are all seen to converge to periodic responses. However, while the reduction in HSC concentrations is minimal (Figure 4.10a)

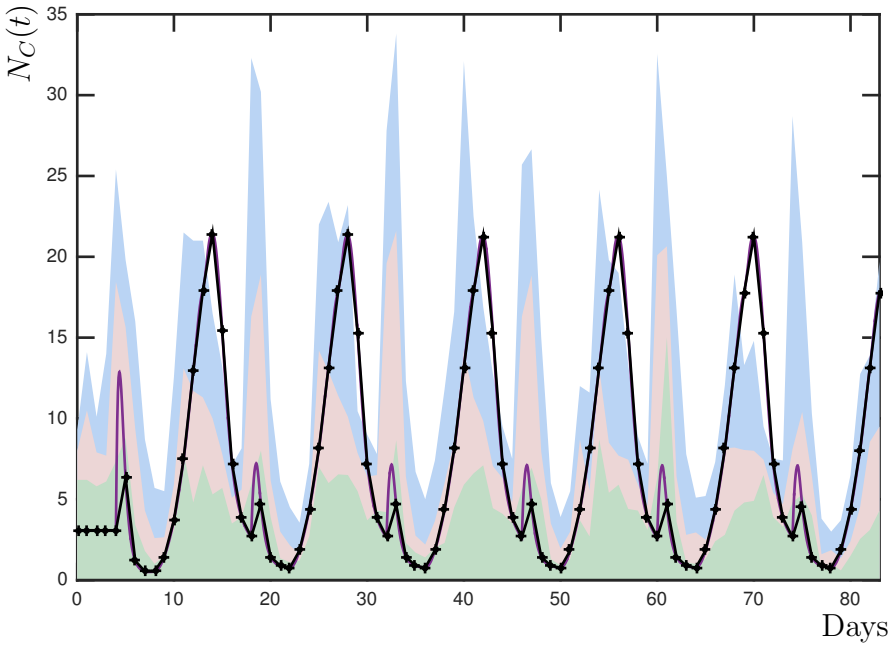

Figure 4.9 – Comparison of the predicted neutrophil response to the CHOP14 protocol [42, 43] for $N_{elim}^{simp} = 0.80$. In this regimen, 4 μg of Zalypsis® given by a 1 hour IV infusion is administered 14 days apart, beginning on day 0, for 6 cycles (84 days total). Per cycle, ten administrations of 300 μg subcutaneous doses of filgrastim are given beginning four days after the start of the chemotherapeutic cycle and continuing to day 13 post-chemotherapy. The simulation is compared to data from [29], presented in quartiles. In pale green: the first quartile, in pale pink: median range, in pale blue: third quartile. Black line with sampling points: model prediction sampled every day at clinical sampling points, solid purple line: full model prediction.

the neutrophil marrow reservoir is seen in Figure 4.10b to become severely depleted. This depletion is caused by the delayed effects of the administration of chemotherapy but also the rapid transit of cells from the reservoir into the blood caused by the introduction of exogenous G-CSF four days post-chemotherapy (see Figure 4.11e below). This in turn prevents ANC recoveries from depressed values, despite the administration of G-CSF. As in [66] and [11], it is likely that delaying the beginning of prophylactic G-CSF support during chemotherapy would help to combat myelosuppression, but this will is a future avenue of investigation.

It can also be illuminating to study how each of the model's functions correspond to the estimated parameters to obtain further insight on the mechanisms of granulopoiesis. Figure 4.11 shows the functions $\kappa(G_1)$, $\eta_{N_P}(G_1)$, $\eta_{N_P}^{chemo}(G_1)$, $V_{N_M}(G_1)$, and $\varphi_{N_R}(G_{BF})$ and

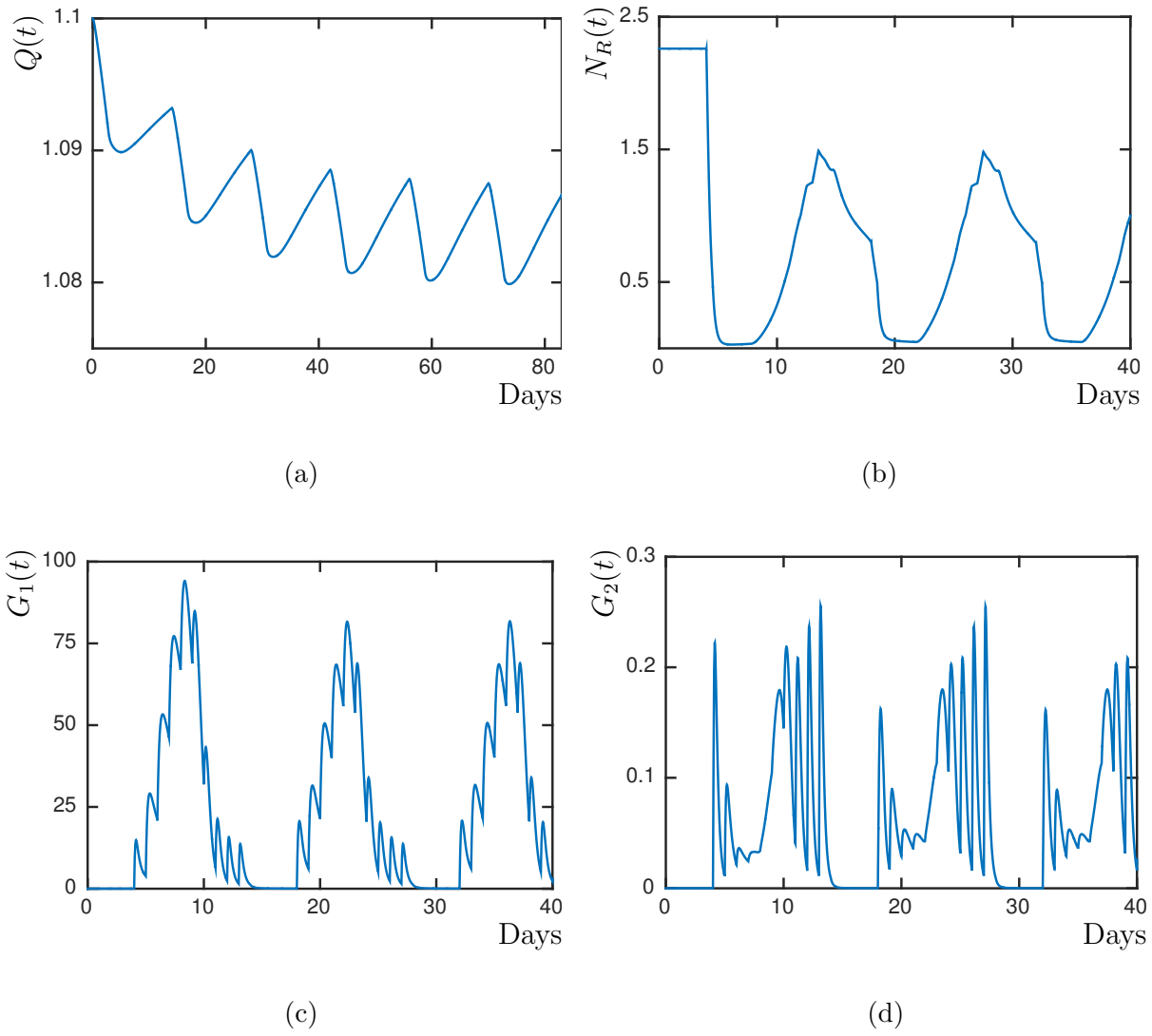

Figure 4.10 – Model responses to the CHOP14 protocol as described in Section 4.6. In a) $Q(t)$ over the six CHOP cycles detailed above, b), c), and d) $N_R(t)$, $G_1(t)$, and $G_2(t)$ over three CHOP cycles.

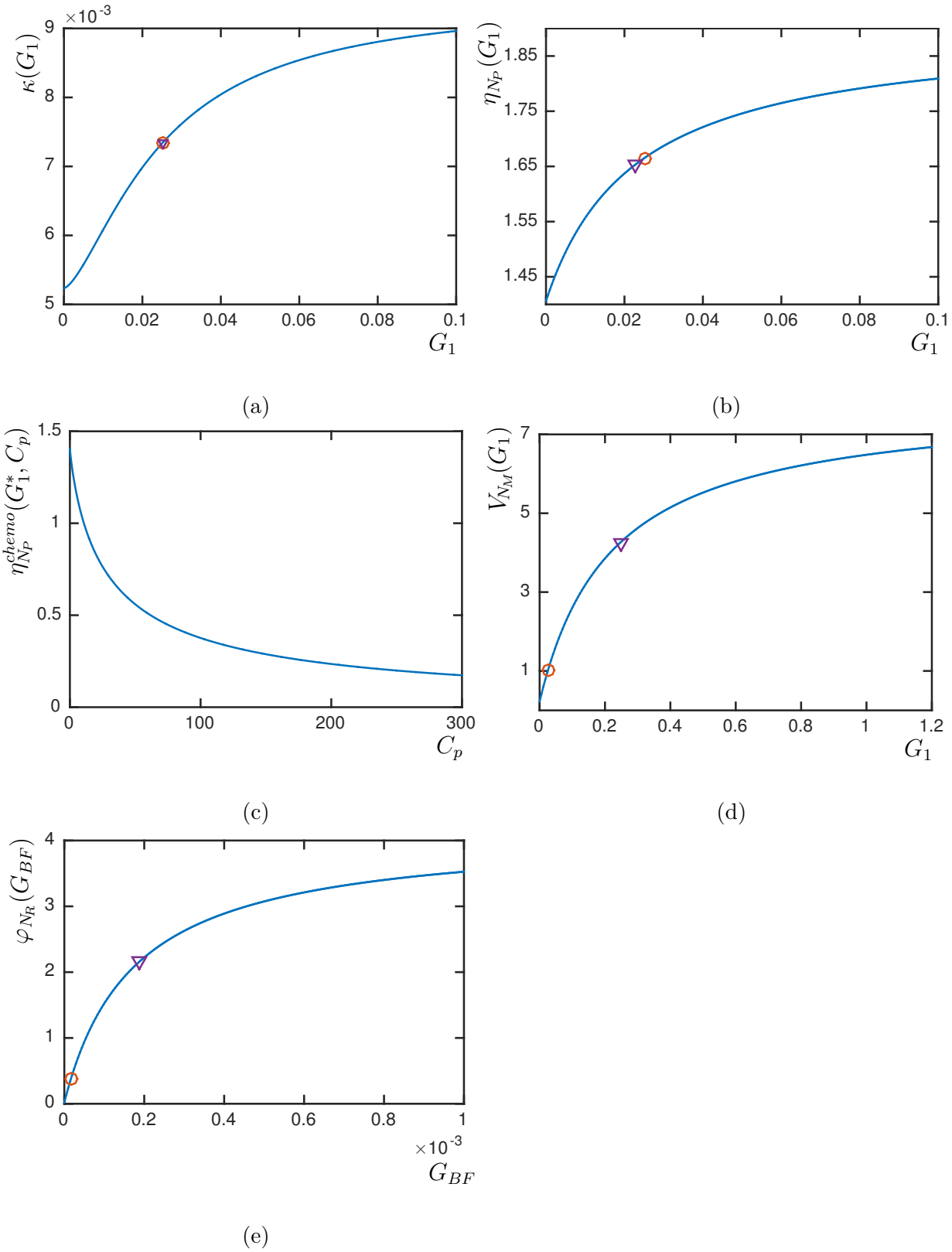

Figure 4.11 – Visualisation of the granulopoiesis model's mechanisms as functions of their variables (solid blue lines) with their respective homeostatic and half-effect values (purple triangles), when relevant. Red circles: homeostasis values.

identifies their respective homeostatic levels. We can see that $\varphi_{N_R}(G_{BF})$ in Figure 4.11e, has a homeostasis concentration $\varphi_{N_R}(G^*_{BF})$ very close to $\varphi_{N_R}(0)$. This reflects the ability of the granulopoietic system to respond rapidly in the case of emergencies [47] but also supports the hypothesis that early prophylactic support with G-CSF during chemotherapy may hasten the emptying of the reservoir due to the responsiveness of $\varphi_{N_R}(G_{BF}(t))$ in particular.

4.7 Discussion

Clinically relevant translational models in medicine must not only accurately depict different and independent treatment regimes [66], they must also be able to reconstruct homeostatic and pathological cases which may be intervention independent. The granulopoiesis model we have developed is physiologically-relevant and, perhaps most importantly, provides insight beyond that which is clinically measurable. The updated pharmacokinetic model of G-CSF, novel in that it explicitly accounts for unbound and bound concentrations, correctly accounts for G-CSF dynamics whereas previous one compartment models all resulted in renal dominated dynamics. The new pharmacokinetic model also further allows us to comment on the principle mechanisms driving the production of neutrophils. Although the relatively small number of neutrophil progenitors do not have a significant effect on G-CSF kinetics, our results suggest that differentiation, proliferation and maturation speed are driven primarily by signalling from G-CSF bound to neutrophil progenitors, and not from signalling of G-CSF bound to mature neutrophils. We can further characterise the principle processes governing myelosuppression during the concurrent administration of chemotherapy and prophylactic G-CSF, which we have determined lies in the simultaneous depletion of the marrow reservoir by high doses of exogenous G-CSF combined with fewer neutrophils reaching the reservoir due to the cytotoxicity of the anti-cancer drug.

The modelling reported here combines a number of original approaches to the conceptualisation of physiological, pharmacokinetic, and pharmacodynamics models and to the estimation of parameters and model verification. For example, traditional least squares estimation was redefined using functions which ensured robustness and allowed for comparisons of predictions to data over richly sampled intervals instead of at fewer data points.

Moreover, the model's physiological realism served as a means of evaluating the suitability of optimised parameter values so we were not relying solely on goodness-of-fit, which can obfuscate the biological relevance of results [67]. The inclusion of the detailed characterisations of physiological mechanisms in our model therefore serves as a litmus test of suitability in addition to providing intuition about the processes driving granulopoiesis.

The broader implications of the approaches outlined in this work extend into various domains. The derivation of a delay differential equation model with variable ageing rate from an age-structured PDE, as described in Section 4.3.3, is mathematically significant and its intricate nature has previously led to previous modelling errors. As mentioned, the fitting procedures outlined in Sections 4.4.2, 4.4.4, and 4.4.5 motivate the development of more refined least squares methods and parameter estimation techniques. Additionally, the novel pharmacokinetic model of G-CSF has ramifications with respect to the usual approaches used by PK/PD modellers. The mischaracterisation of the elimination dynamics, despite the inclusion of internalisation terms, has led to models which contradict what is known of the physiology. While they can characterise certain clinical situations, like the single administration of exogenous G-CSF, they fail when applied to more complex scenarios. Without accounting for the entire process of neutrophil development or using physiological rationale for a model's parameters, one is unable to judge whether a model captures the complicated dynamics of granulopoiesis. In the model we have developed, we have ensured the accuracy of its predictions and the appropriateness of its parameters through careful construction. In turn, this rational approach has implications for the clinical practice where it can serve to optimise dosing regimens in oncological settings and also serve to pinpoint the origins of dynamical neutrophil disorders like cyclic neutropenia, ultimately contributing to the improvement of patient care and outcomes.

Acknowledgements

ARH and MCM are grateful to the National Science and Engineering Research Council (NSERC), Canada for funding through the Discovery Grant program. MC wishes to thank NSERC for funding from the PGS-D program. We are grateful to Fahima Nekka, Jun Li, Jacques Bélair, and David Dale for their insight and support.

References

[1] G. Baiocci, G. Scambia, P. Benedetti, G. Menichella, U. Testa, L. Pierelli, R. Martucci, M.L. Foddai, B. Bizzi, S. Mancuso, and C. Peschle. Autologous stem cell transplantation: Sequential production of hematopoietic cytokines underlying granulocyte recovery. *Cancer Research*, 53:1297–1303, 1993.

[2] Daniel R Barreda, Patrick C Hanington, and Miodrag Belosevic. Regulation of myeloid development and function by colony stimulating factors. *Developmental and Comparative Immunology*, 28(5):509 – 554, 2004.

[3] S. Basu, G. Hodgson, M. Katz, and A.R. Dunn. Evaluation of role of G-CSF in the production, survival, and release of neutrophils from bone marrow into circulation. *Blood*, 100:854–861, 2002.

[4] S. Bernard, J. Bélair, and M.C. Mackey. Oscillations in cyclical neutropenia: New evidence based on mathematical modeling. *Journal of Clinical Investigation*, 228:1–16, 2015.

[5] G. Brooks, G.P. Langlois, J. Lei, and M.C. Mackey. Neutrophil dynamics after chemotherapy and G-CSF: The role of pharmacokinetics in shaping the response. *Journal of Theoretical Biology*, 315:97–109, 2012.

[6] S. Bugl, S. Wirths, M.R. Müller, and M.P. Radsak. Current insights into neutrophil homeostasis. *Annals of the New York Academy of Sciences: Hematopoietic Stem CellsVIII*, 1266:171–178, 2012.

[7] M.S. Cairo, Y. Suen, L. Sender, E.R. Gillan, W. Ho, J.M. Plunkett, and C. van de Ven. Circulating granulocyte colony-stimulating factor (G-CSF) levels after allogenic and autologous bone marrow transplantation: Endogenous G-CSF production correlates with myeloid engraftment. *Blood*, 79:1869–1873, 1992.

[8] C. Colijn and M.C. Mackey. A mathematical model of hematopoiesis: I. Periodic chronic mylogenous leukemia. *Journal of Theoretical Biology*, 237:117–132, 2005.

[9] C. Colijn and M.C. Mackey. A mathematical model of hematopoiesis: II. Cyclical neutropenia. *Journal of Theoretical Biology*, 237:133–146, 2005.

[10] M. Craig, M. González-Sales, J. Li, and F. Nekka. Impact of pharmacokinetic variability on a mechanistic physiological pharmacokinetic/pharmacodynamic model: A case study of neutrophil development, PM00104, and filgrastim. In B. Toni, editor, *Interdisciplinary Mathematical Research and Applications*. Springer, New York, 2015 (to appear).

[11] M. Craig, A.R. Humphries, J. Bélair, J. Li, F. Nekka, and M.C. Mackey. Neutrophil dynamics during concurrent chemotherapy and G-CSF administration: Mathematical modelling guides dose optimisation to minimise neutropenia. *Journal of Theoretical Biology*, 385:77–89, 2015.

[12] D.C. Dale and M.C. Mackey. Understanding, treating and avoiding hematological disease: Better medicine through mathematics? *Bulletin of Mathematical Biology*, 77:739–757, 2015.

[13] D.C. Dale and K. Welte. Cyclic and chronic neutropenia. In G.H. Lyman and D.C. Dale, editors, *Hematopoietic Growth Factors in Oncology*. Springer, 2011.

[14] J.T. Dancey, K.A. Deubelbeiss, L.A. Harker, and C.A. Finch. Neutrophil kinetics in man. *The Journal of Clinical Investigation*, 58:705–715, 1976.

[15] J.T. DiPiro, W.J. Spruill, W.E. Wade, R.A. Blouin, and J.M. Pruemer, editors. *Concepts in Clinical Pharmacokinetics*, volume 5. American Society of Health-System Pharmacists, Bethesda, MA, 2010.

[16] C. Durand and P. Charbord. *Stem Cell Biology and Regenerative Medicine*, volume 3. River Publishers, Aalborg, Denmark, 2010.

[17] M. Endele, M. Etzrodt, and T. Schroeder. Instruction of hematopoietic lineage choice by cytokine signaling. *Experimental Cell Research*, 329:207–213, 2014.

[18] C. Foley, S. Bernard, and M.C. Mackey. Cost-effective G-CSF therapy strategies for cyclical neutropenia: Mathematical modelling based hypotheses. *Journal of Theoretical Biology*, 238:756–763, 2006.

[19] C. Foley and M.C. Mackey. Dynamic hematological disease: A review. *Journal of Mathematical Biology*, 58:285–322, 2009.

[20] C. Foley and M.C. Mackey. Mathematical model for G-CSF administration after chemotherapy. *Journal of Theoretical Biology*, 257:27–44, 2009.

[21] L.E. Friberg and M.O. Karlsson. Mechanistic models for myelosuppression. *Investigational New Drugs*, 21:183–194, 2003.

[22] M. González-Sales, B. Valenzuela, C. Pérez-Ruixo, C. Fernández Teruel, B. Miguel-Lillo, Soto Matos A., et al. Population pharmacokinetic-pharmacodynamic analysis of neutropenia in cancer patients receiving PM00104 (Zalypsis®). *Clinical Pharmacokinetics*, 51:751–764, 2012.

[23] A.M. Greeenbaum and D.C. Link. Mechanisms of G-CSF-mediated hematopoietic stem and progenitor mobilization. *Leukemia*, 25:211–217, 2011.

[24] W.P. Hammond, E. Csiba, A. Canin, H. Hockman, L.M. Souza, J.E. Layton, and D.C. Dale. Chronic neutropenia. A new canine model induced by human granulocyte colony-stimulating factor. *Journal of Clinical Investigation*, 87:704–710, 2 1991.

[25] T. Hearn, C. Haurie, and M.C. Mackey. Cyclical neutropenia and the peripherial control of white blood cell production. *Journal of Theoretical Biology*, 192:167–181, 1998.

[26] M Kawakami, H Tsutsumi, T Kumakawa, H Abe, M Hirai, S Kurosawa, M Mori, and M Fukushima. Levels of serum granulocyte colony-stimulating factor in patients with infections. *Blood*, 76(10):1962–1964, 1990.

[27] N. D. Kazarinoff and P. van den Driessche. Control of oscillations in hematopoiesis. *Science*, **203**:1348–1350, 1979.

[28] E. A. King-Smith and A. Morley. Computer simulation of granulopoiesis: Normal and impaired granulopoiesis. *Blood*, **36**:254–262, 1970.

[29] A. Krinner, I. Roeder, M. Loeffler, and M. Scholz. Merging concepts - coupling an agent-based model of hematopoietic stem cells with an ODE model of granulopoiesis. *BMC Systems Biology*, 7:117, 2013.

[30] W. Krzyzanski, P. Wiczling, P. Lowe, E. Pigeolet, M. Fink, A. Berghout, and S. Balser. Population modeling of filgrastim PK-PD in healthy adults following intravenous and subcutaneous administrations. *Journal of Clinical Pharmacology*, 9 Suppl:101S–112S, 2010.

[31] T. Kuwabara, Y. Kato, S. Kobayashi, H. Suzuki, and Y. Sugiyama. Nonlinear pharmacokinetics of a recombinant human granulocyte colony-stimulating factor derivative (Nartograstim): Species differences among rats, monkeys and humans. *Journal of Pharmacology and Experimental Therapeutics*, 271:1535–1543, 1994.

[32] J.E. Layton and N.E. Hall. The interaction of G-CSF with its receptor. *Frontiers in Bioscience*, 31:177–199, 2006.

[33] J. Lei and M.C. Mackey. Multistability in an age-structured model of hematopoiesis: Cyclical neutropenia. *Journal of Theoretical Biology*, 270:143–153, 2011.

[34] G. Lui, H. Yang, X. Wang, and Y. Chu. Modulation of neutrophil development and homeostasis. *Current Molecular Medicine*, 13:1270–1283, 2013.

[35] M.C. Mackey. Cell kinetic status of hematopoietic stem cells. *Cell Proliferation*, 34:71–83, 2001.

[36] M.C. Mackey, A.A.G. Aprikyan, and D.C. Dale. The rate of apoptosis in post mitotic neutrophil precursors of normal and neutropenic humans. *Cell Proliferation*, 36:27–34, 2003.

[37] V. Maholtra and M.C. Perry. Models of anti-cancer therapy. Classical chemotherapy: Mechanism, toxicities, and the therapeutic window. *Cancer Biology and Therapy*, 2:S2–S4, 2003.

[38] Mathworks. *MATLAB 2013a*. Mathworks, Natick, Massachusetts, 2013.

[39] G.. Molineux. Granulocyte colony-stimulating factors. In G.H. Lyman and D.C. Dale, editors, *Hematopoietic Growth Factors in Oncology*. Springer, 2011.

[40] G. Molineux, T. Arvedson, and M. Foote. *Twenty years of G-CSF Clinical and Nonclinical Discoveries*. Springer Basel AG, Basel, Switzerland, 2012.

[41] C. Pérez-Ruixo, B. Valenzuela, C. Fernández Teruel, M. González-Sales, B. Miguel-Lillo, A. Soto-Matos, et al. Population pharmacokinetics of PM00104 (Zalypsis®) in cancer patients. *Cancer Chemotherapy and Pharmacology*, 69:15–24, 2012.

[42] M. Pfreundschuh, L. Trümper, M. Kloess, R. Schmits, A.C. Feller, C. Rudolph, et al. Two-weekly or 3-weekly CHOP chemotherapy with our without etoposide for the treatment of elderly patients with aggressive lymphomas: Results of the NHL-B2 trial of the DSHNHL. *Blood*, 104:634–641, 2004.

[43] M. Pfreundschuh, L. Trümper, M. Kloess, R. Schmits, A.C. Feller, C. Rudolph, et al. Two-weekly or 3-weekly CHOP chemotherapy with our without etoposide for the treatment of young patients with good prognosis (normal LDH) aggressive lymphomas: Results of the NHL-B1 trial of the DSHNHL. *Blood*, 104:626–633, 2004.

[44] T.H. Price, G.S. Chatta, and D.C. Dale. Effect of recombinant granulocyte colony-stimulating factor on neutrophil kinetics in normal young and elderly humans. *Blood*, 88:335–340, 1996.

[45] L. Pujo-Menjouet, S. Bernard, and M.C. Mackey. Long period oscillations in a g_0 model of hematopoietic stem cells. *SIAM J Applied Dynamical Systems*, 4:312–332, 2005.

[46] A.L. Quartino, L.E. Friberg, and M.O. Karlsson. A simultaneous analysis of the time-course of leukocytes and neutrophils following docetaxel administration using a semi-mechanisitic myelosuppression model. *Investigational New Drugs*, 30:833–845, 2012.

[47] S.M. Rankin. The bone marrow: A site of neutrophil clearance. *Journal of Leukocyte Biology*, 88:241–251, 2010.

[48] C. Riether, C.M. Schürch, and A.F. Ochsenbein. Regulation of hematopoietic and leukemic stem cells by the immune system. *Cell Death and Differentiation*, 22:187–198, 2015.

[49] S. Rubinow and J. Lebowitz. A mathematical model of neutrophil production and control in normal man. *Journal of Mathematical Biology*, 1:187–225, 1975.

[50] D.H. Ryan. Examination of blood cells. In K. Kaushansky, M.A. Lichtman, J.T. Prchal, M.M. Levi, O.W. Press, L.J. Burns, and M. Caligiuri, editors, *Williams Hematology*, volume 9. McGraw-Hill Companies, Inc., 2016.

[51] M. Santillán. On the use of the Hill functions in mathematical models of gene regulatory networks. *Mathematical Modelling of Natural Phenomena*, 3:85–97, 2008.

[52] C.A. Sarkar, K. Lowenhaupt, P.J. Wang, T. Horan, and D.A. Lauffenburger. Parsing the effects of binding, signaling, and trafficking on the mitogenic potencies of granulocyte colony-stimulating factor analogues. *Biotechnology Progress*, 35:3–186, 2015.

[53] S. Schirm, C. Engel, M. Loeffler, and M. Scholz. Modelling chemotherapy effects on granulopoiesis. *BMC Systems Biology*, 8:138, 2014.

[54] S. Schmitz. *Ein mathematisches Modell der zyklischen Haemopoese.* PhD thesis, Universitat Koln, 1988.

[55] S. Schmitz, H. Franke, M. Löffler, H.E. Wichmann, and V. Diehl. Model analysis of the contrasting effects of GM-CSF and G-CSF treatment on peripheral blood neutrophils observed in three patients with childhood-onset cyclic neutropenia. *British Journal of Haematology*, 95:616–625, 1996.

[56] S. Schmitz, M. Loeffler, J. B. Jones, R. D. Lange, and H. E. Wichmann. Synchrony of bone marrow proliferation and maturation as the origin of cyclic haemopoiesis. *Cell Tissue Kinetics*, **23**:425–441, 1990.

[57] M. Scholz, C. Engel, and M. Loeffler. Modelling human granulopoiesis under polychemotherapy with G-CSF support. *Journal of Mathematical Biology*, 50:397–439, 2005.

[58] M. Scholz, S. Schirm, M. Wetzler, C. Engel, and M. Loeffler. Pharmacokinetic and -dynamic modelling of G-CSF derivatives in humans. *Theoretical Biology and Medical Modelling*, 9:1497–1502, 2012.

[59] C.L. Semerad, F. Liu, A.D. Gregory, K. Stumpf, and D.C. Link. G-CSF is an essential regulator of neutrophil trafficking from the bone marrow to the blood. *Immunity*, 17:413–423, 2002.

[60] E. Shochat, V. Rom-Kedar, and L.A. Segel. G-CSF control of neutrophils dynamics in the blood. *Bulletin of Mathematical Biology*, 69:2299–2338, 2007.

[61] D. Shvitra, R. Laugalys, and Y. S. Kolesov. Mathematical modeling of the production of white blood cells. In G. Marchuk and L.N. Belykh, editors, *Mathematical Modeling in Immunology and Medicine*, pages 211–223, Amsterdam, 1983. North-Holland.

[62] C.W. Smith. Production, distribution, and fate of neutrophils. In K. Kaushansky, M.A. Lichtman, J.T. Prchal, M.M. Levi, O.W. Press, L.J. Burns, and M. Caligiuri, editors, *Williams Hematology*, volume 9. McGraw-Hill Companies, Inc., 2016.

[63] K. Spiekermann, J. Roesler, A. Emmendoerffer, J. Elsner, and K. Welte. Functional features of neutrophils induced by g-csf and gm-csf treatment: Differential effects and clinical implications. *Leukemia*, 11:466–478, 1997.

[64] K. Terashi, M. Oka, S. Ohdo, T. Furukubo, C. Ikeda, M. Fukuda, H. Soda, S. Higuchi, and S. Kohno. Close association between clearance of recombinant human granulocyte colony-stimulating factore (G-CSF) and G-CSF receptor on neutrophils in cancer patients. *Antimicrobian Agents and Chemotherapy*, 43:21–24, 1999.

[65] O. Vainas, S. Ariad, O. Amir, W. Mermershtain, V. Vainstein, M. Kleiman, O. Inbar, R. Ben-Av, A. Mukherjee, S. Chan, and Z. Agur. Personalising docetaxel and G-CSF schedules in cancer patients by a clinically validated computational model. *British Journal of Cancer*, 107:814–822, 2012.

[66] V. Vainstein, Y. Ginosar, M. Shoham, D.O. Ranmar, A. Ianovski, and Z. Agur. The complex effect of granulocyte colony-stimulating factor on human granulopoiesis

analyzed by a new physiologically-based mathematical model. *Journal of Theoretical Biology*, 235:311–327, 2005.

[67] P. van der Graaf and N. Benson. Systems pharmacology: Bridging systems biology and pharmacokinetics-pharmacodynamics (PKPD) in drug discovery and development. *Pharmaceutical Research*, 28:1460–1464, 2011.

[68] G. K. von Schulthess and N. A. Mazer. Cyclic neutropenia (CN): A clue to the control of granulopoiesis. *Blood*, **59**:27–37, 1982.

[69] B. Wang, T.M. Ludden, E.N. Cheung, G.G. Schwab, and L.K. Roskos. Population pharmacokinetic-pharmacodynamic modeling of filgrastim (r-metHuG-CSF) in healthy volunteers. *Journal of Pharmacokinetics and Pharmacodynamics*, 28:321–342, 2001.

[70] A.C. Ward, J.L. Monkhouse, X.F. Csar, I.P. Touw, and P.B. Bello. The Src-like tyrosine kinase Hck is activated by granulocyte colony-stimulating factor (G-CSF) and docks to the activated G-CSF receptor. *Biochemical and Biophysical Research Communications*, 251(1):117–123, 1998.

[71] K Watari, S Asano, N Shirafuji, H Kodo, K Ozawa, F Takaku, and S Kamachi. Serum granulocyte colony-stimulating factor levels in healthy volunteers and patients with various disorders as estimated by enzyme immunoassay. *Blood*, 73(1):117–122, 1989.

[72] H.E. Wichmann and M. Loffler. *Mathematical Modeling of Cell Proliferation: Stem Cell Regulation in Hemopoiesis*. CRC Press, Boca Raton, 1988.

[73] X. Wu, F. Nekka, and J. Li. Steady-state volume of distribution of some two compartmental models with immediate linear and saturated eliminations., Under review.

Chapters 2 to 4 have demonstrated the translational applicability of our physiological model of granulopoiesis and also introduced novel concepts in PK model construction. The final article of this dissertation takes a methodological look at model design and conception by situating physiological modelling within quantitative systems pharmacology. The following paper is accepted for publication in *CPT: Pharmacometrics and Systems Pharmacology* (date of acceptance: February 16, 2016. PSP-2015-0207DR).

Chapter 5

Approaching Pharmacometrics as a Palaeontologist Would: Recovering the Links Between Drugs and the Body Through Reconstruction

Morgan Craig[1], Mario González-Sales[1,2], Jun Li[1], Fahima Nekka[1]

[1]Faculté de Pharmacie, Université de Montréal, Montréal, QC, Canada H3T 1J4, [2] InVentiv Health Clinical, 5260 Boulevard Décarie, Montréal, QC H3X 2H9

Keywords

systems biology; pharmacokinetic variability; physiological modelling; mathematical modelling

Introduction

Our knowledge of dinosaurs comes primarily from the fossil record. Notwithstanding the condition of these vestiges, palaeontologists reconstruct early reptilian life by comparison to previously discovered specimens. When relics are missing, reasonable deductions are used to fill in the gaps.

Likewise, one can draw parallels to systems pharmacology/mechanistic modelling–the explicit depiction of the causality between drug exposure and response [5]–which gives a more complete picture of drugs in the human body.

Modelling and the Systems Pharmacology

Mathematical modelling in pharmacokinetics/pharmacodynamics (PK/PD) continues to become increasingly refined, in step with improvements to both computational and mathematical analytical techniques and our understanding of human physiology. In that vein, mechanistic models, which offer phenomenological insights absent from traditional empirical, data driven modelling techniques, are a useful tool for subsequent pharmacometric research [2]. The parameters involved in systems models bear a direct correspondence to the physiological system of interest and have a "fundamental basis in our understanding of the biological/pharmacological system" [7]. In practice, these models are constructed in consortium with clinicians and other scientists to ensure a rational and realistic construction to improve their reliability. Generally, given the specificity of each of the model's parameters and the paucity of available datasets, parameters are identified through established sources (deemed the prior method [9]). Models are then evaluated and refined by comparison to published experiments and can be used to predict the behaviour of the system in a variety of scenarios. As a result of the generic nature of the model's construction, their application to a diverse range of patients and pathologies is possible.

It is well recognised that drug concentrations act as surrogates for their action in the body and that plasma concentrations are only proxies for drug effect sites that are located outside the blood [2]. Physiological modelling replies directly to this issue by taking the whole system into account. With the aim to recreate the processes underlying drug effects as faithfully as possible, physiological models are able to better represent the true action of xenobiotics and are therefore well-positioned for hypothesis generation and verification [7].

Despite the increasing use of physiological modelling in systems pharmacology, the approach is under represented in the literature when compared to traditional approaches where the main goal is to successfully mimic the data. This can be attributed to the relative mathematical complexity of the techniques involved in physiological modelling, which require time to understand the system, construct the model, and determine parameters. Further, as is the case with the more common physiologically-based pharmacokinetic (PBPK) model, the role of PK and PD variability upon systems-level models has not been fully addressed [7]. In response, using a physiological model of granulopoiesis we devel-

oped for the optimisation of chemotherapy [3], we have recently shown that when the physiology is sufficiently detailed, the model inherently explains and reduces the previously estimated population PK variability [4]. This is likely attributable to its bottom-up construction since development from first principles suggests that variability is explicated and incorporated into the minute details of the resulting models and their parameters [2]. Incertitude, included by design, is thereby progressively reduced throughout the model's construction [10]. Nevertheless, we maintain that an ideology-free methodology should be adopted when addressing the quantification of drug-effects to best balance the feasibility and benefits of any given approach. Calls for the integration of quantitative systems pharmacology (QSP) along the drug discovery pathway have come from scientific bodies as the recognition of the indispensability of translational models increases [2, 10]. Several authors have previously highlighted numerous applications of QSP from early discovery to late stage drug development [1, 2]. Publishing such case studies is important to both situate QSP in the current scientific environment and to highlight their essentiality to the future of translational drug discovery.

A Physiological Model of Granulopoiesis Applied to Chemotherapeutic Dose Optimisation

An illustrative example of the use of mechanistic modelling in systems pharmacology is in applications to hematology where there is a need to predict the neutrophil response to chemotherapeutic treatment ([3] and references therein). In a PK/PD setting, the most common strategy to study myelosuppression-related neutropenia is to relate dose or concentrations to neutrophil numbers using mixed effects modelling techniques and transit compartment modelling [6]. These semi-mechanistic models estimate the transit time from progenitor neutrophil cells to circulating neutrophils from clinical data and mimic the developmental stages of neutrophils in the bone marrow. Since the underlying model structure is fairly straightforward, parameter estimates from data are available in a reasonable timeframe and can be used early in the drug development pipeline. Crucially, a downside to using data to estimate the model structure and its parameters is the disconnect from the physiology.

Indeed, while we can easily register patient blood counts, measuring the proliferation,

the cytokine-dependent rate of maturation, and reservation within the marrow is more complicated and rarely performed. As in the case of mixed effects modelling applied to PKs, blood counts (concentrations) reflect the upstream marrow processes and the interaction of the regulatory cytokines with the blood system [2]. To advance our understanding of granulopoiesis for applications to both different pathologies and to different experimental conditions, physiological models developed with systems biology approaches are warranted [7].

Underlying the physiological model of neutrophil development is a particular attention to first principles modelling and the translation of the current knowledge of the system's inner workings mathematically [8]. These physiological models are flexible in that they do not rely on empirical data for their construction and can be applied to various experimental models [7]. Their development can take longer than the data driven approaches since in-depth mathematical and physiological knowledge is required. Accordingly, here we do not make the case for the abolishment of empirical methods. Instead, we caution against discounting the power of mechanistic modelling in pharmacology altogether in favour of quicker or more direct methods. We recently refined a physiological model for granulopoiesis and applied it to the problem of dose optimisation in oncological settings [3]. The basis of our approach was a physiological model of marrow neutrophil development that accounts for hematopoietic stem cells, proliferating and maturing neutrophils, the marrow neutrophil reservoir, circulating neutrophils, and the marginal pool. The complete model is comprised of three delay differential equations with state-dependent delays and a variable aging rate (see the model schematic in Figure 1 of [3]). Together with the physiological model, we incorporated validated PK models of a chemotherapeutic drug (PM00104) and filgrastim, a recombinant-human form of granulocyte colony-stimulating factor (G-CSF) and predicted clinical data of 172 patients undergoing the CHOP14 protocol, a 14-day periodic chemotherapeutic treatment. In the original protocol, filgrastim was administered 10 times, from day 4 to day 13 of each chemotherapy cycle. We were able to demonstrate that delaying the first dose of filgrastim post-chemotherapy administration to day 7 reduced the number of doses of filgrastim necessary to mitigate neutropenia from 10 to four or even three, which is supported by the physiology of neutrophil marrow development since the delayed response to chemotherapeutic drugs and to G-CSF are di-

rectly related to the time it takes for cells to reach and subsequently be released from the marrow reservoir. In this model, parameters were estimated from a broad swath of the literature for an individual patient and no data fitting was undertaken. Additionally, the myelosuppression model was shown to be generalisable across different chemotherapy regimens (PM00104 vs combination chemotherapy in the CHOP14 protocol), highlighting the flexibility presented by QSP modelling developed using first-principles. The robustness of the model's prediction was demonstrated by incorporating the full PK variability profiles of both drugs and checking for statistical differences in the model's output [4]. Despite the presence of variability in the PKs, we found no statistically significant change in the model's prediction with reference to three critical clinical endpoints.

Perspectives

The debates and advances of the naturalists in the early nineteenth century subsequently reimagined our understanding of the species that walked our planet. These early scientists' capacities for abstraction and their appeal to a systems-level organisational structure filled in the gaps in not only the knowledge of the day, but the missing pieces in the records left behind. QSP, which exists at the confluence of systems biology and pharmacometrics, provides a return to this macroscopic examination of drugs and their interactions with the body. Systems pharmacology is increasingly recognised for its dual impact on drug development and patient care and models of adverse drug reactions have been identified as a crucial goal of QSP [10]. The field does and will play an increasingly important role as drug targets become progressively complex and elusive and as we seek to not just explain data, but to understand the fundamentals of physiology that drive the response to drugs. The model discussed in this manuscript serves as an example of the application of systems-level modelling to translational medicine and is demonstrative of the influence of systems modelling on both drug development and on the means with which we respond to patient needs. Broadly, it is important to recognise that physiological modelling is not applicable in all settings or for all problems due to the more complex nature of model construction and the difficulty of estimating and identifying parameters. Nevertheless, there is room within the pharmacometrics community to develop both empirical and mechanistic models in concert as they respond to different philosophical questions: how do we explain our data

(traditional PK/PD) and what drives the response observed within patient populations (systems pharmacology)? Acknowledging and making use of approaches outside of those traditionally used in PK/PD modelling will allow pharmacometricians to answer elemental questions about drugs and improve patient care, which remains the ultimate task of our discipline.

Acknowledgments

This work was supported by the Natural Sciences and Engineering Research Council (NSERC, Canada) PGS-D program (MC), the MITACS ELEVATE program (MGS), and the NSERC Industrial Research Chair in Pharmacometrics (FN/JL), jointly supported by Novartis, Pfizer and inVentiv Health Clinical. We wish to thank Université de Montréal, inVentiv Health Clinical and our collaborators M. Mackey (McGill University), Tony Humphries (McGill University), and Jacques Bélair (Université de Montréal) for their insight and support during this project. We gratefully acknowledge the comments of the anonymous reviewers that significantly improved this manuscript.

Conflicts of Interest/Disclosure

The authors have no conflict of interest to declare.

References

[1] B.M. Agoram and O. Demin. Integration not isolation: arguing the case for quantitative and systems pharmacology in drug discovery and development. *Drug Discovery Today*, 16:1031–1036, 2011.

[2] B.M. Agoram, S.W. Martin, and P.H. van der Graaf. The role of mechanism-based pharmacokinetic/pharmacodynamic (PK/PD) modelling in translational research of biologics. *Drug Discovery Today*, 12:1018–1024, 2007.

[3] M. Craig, A.R. Humphries, J. Bélair, J. Li, F. Nekka, and M.C. Mackey. Neutrophil dynamics during concurrent chemotherapy and G-CSF administration: Mathematical modelling guides dose optimisation to minimise neutropenia. *Journal of Theoretical Biology*, 385:77–89, 2015.

[4] M. Craig, M. González-Sales, J. Li, and F. Nekka. Impact of pharmacokinetic variability on a mechanistic physiological pharmacokinetic/pharmacodynamic model: A case study of neutrophil development, PM00104, and filgrastim. In B. Toni, editor, *Interdisciplinary Mathematical Research and Applications*. Springer, New York, 2015 (to appear).

[5] M. Danhof, E.C.M. de Lange, O.E. Della Pasqua, B.A. Ploeger, and R.A. Voskuyl. Mechanism-based pharmacokinetic-pharmacodynamic (PK-PD) modeling in translational drug research. *Trends in Pharmacogical Sciences*, 29:186–191, 2008.

[6] L. Friberg, A. Henningsson, H. Maas, L. Nguyen, and M. Karlsson. Model of chemotherapy-induced myelosuppression with parameter consistency across drugs. *Journal of Clinical Oncology*, 20:4713–4721, 2002.

[7] T.A. Leil. A Bayesian perspective on estimation of variability and uncertainty in mechanism-based models. *Clinical Pharmacology and Therapeutics: Pharmacometrics and Systems Pharmacology*, 3:e121, 2014.

[8] M.C. Mackey. Dynamic haematological disorders of stem cell origin. In J.G. Vassileva-Popova and E.V. Jensen, editors, *Biophysical and Biochemical Information Transfer in Recognition*. Plenum Publishing Corporation, New York, 1979.

[9] B.A. Ploeger, P.H. van der Graaf, and M. Danhof. Incorporating receptor theory in mechanism-based pharmacokinetic-pharmacodynamic (PK-PD) modeling. *Drug Metabolism and Pharmacokinetics*, 24:3–15, 2009.

[10] D.R. Sorger, S.R.B. Allerheiligen, R.B. Abernethy, K.L.R. Altman, A.C. Brouwer, A. Califano, D.Z. D'Argenio, R. Iyengar, W.J. Jusko, R. Lalonde, D.A. Lauffenburger, B. Shoichet, J.L. Stevens, P. Subramaniam, S. van der Graaf, and P. Vincini. Quantitative and Systems Pharmacology in the Post-genomic era: New Approaches to Discovering Drugs and Understanding Therapeutic Mechanisms. An NIH white paper by the QSP Workshop Group. Technical report, National Institutes of Health of the United States of America, Bethesda, Maryland, USA, 2011.

Chapter 6

Discussion

The work presented in this dissertation had the primary goal of adapting the use of rhG-CSF during concurrent anticancer treatment to reduce the incidences of neutropenia during periodic chemotherapy. For this, a physiological DDE model of granulopoiesis derived from an age-structured PDE was constructed and PK/PD models of filgrastim and PM001014 (Zalypsis®) were incorporated. Resulting from the initial project were supplemental investigations that emphasise the selected modelling philosophy. Ultimately, this thesis has the double implication of developing a translational model that could impact patients' prognoses and advancing methodological considerations in the pharmaceutical sciences.

Chapter 2 of this thesis focussed on the construction of the physiological model of granulopoiesis with detailed PK/PD models and demonstrated its predictive ability through comparison to clinical data. Regimen optimisation during the concurrent chemotherapeutic treatment with rhG-CSF prophylactic administration was ensured by analysis of the physiological principles driving the neutrophil response to cytotoxic drugs and myelostimulation as well as numerical simulations. Using *in silico* simulations of 500 individuals in five different variability scenarios, this dose adaptation was validated in Chapter 3 when PopPK models were added to the physiological PK/PD model and no statistically significant differences between typical patients and the population in predictions were found with regards to three important clinical endpoints. In Chapter 4, a novel physiologically-motivated PK model of filgrastim with updated pharmacodynamic models further refined the granulopoiesis model. Detailed overviews of the derivation of the DDE model and of parameter estimation approaches for physiological models were outlined and can serve as representative cases for others wishing to adopt a similar approach. Crucially, we also demonstrated that the mass-action equilibrium hypothesis for unbound and bound drugs does not hold for G-CSF in homeostatic conditions, a finding with potential consequences for a variety of PK approaches. In Chapter 5, a methodological survey of physiological approaches in systems pharmacology was addressed using the granulopoiesis model as a

case study. A call for a balanced approach to PK/PD modelling was presented.

The use of physiological models to study hematopoiesis has an extensive history in mathematical biology, but is perhaps just beginning to gain recognition in pharmacometrics and systems pharmacology. While the approach may yet to have found traction within the pharmaceutical sciences community, the advantages it offers should solidify its use. Most notably, physiological models constructed from first principles are flexible across pathologies, requiring only minor parameter re-estimation and not a complete model restructuring due to the separation of system-specific and drug-specific parameters [1]. As we tend towards a personalised view of medicine, the identification of the mechanisms at the heart of patient-specific reactions becomes increasingly significant [4]. Consequently, a purely empirical approach is no longer warranted and, indeed, is likely to fail when one wishes to provide rationale for the diversity of observed drug responses. Increasingly, based both on translational and drug development factors, there is a recognition of the necessity to account for physiological mechanisms underlying drug responses [1, 4, 5]. The model studied here, which has been demonstrated to be predictive and robust, is a prime example of fulfilling these dual roles and underscores the evolving approach to PK/PD modelling in translational drug analysis. Further, the conceptual philosophies highlighted herein stress the importance of interdisciplinary research for modelling xenobiotics since approaches incorporating mechanistic understandings of the system of interest afford unparalleled insight into the physiological principles driving the body's response to drugs.

Even so, there remain much to address in quantitative systems pharmacology approaches to granulopoiesis and beyond. As described in the preceding sections, we have already studied the regimen adaptation of the use of G-CSF during chemotherapy by minimising cytotoxicity. To this study, it would also be compelling to include a model for tumour growth. In this combined model, the adaptation of both the chemotherapeutic and rhG-CSF regimens would simultaneously weigh treatment benefits (tumour reduction) with the limitation of the undesired effects (myelosuppression) which, in turn, would give a more complete view of such concomitant administration protocols. Additionally, as eluded to in Chapter 1, the stochastic influences on HSC differentiation which have not yet fully been elucidated likely warrant further investigation [3]. It has been suggested that these random effects may lie at the heart of hematopoietic stem cell pathologies like chronic

myeloid leukaemia (CML) and cyclical neutropenia [2]. The granulopoiesis model developed herein is well-positioned to respond to further investigations of stem cell and neutrophil pathologies but there remains room for the incorporation of stochastic elements and the investigation of their impact. The physiological model could also be applied to stem cell transplant treatments to better delineate the mechanisms governing the success or failure of allogenic or autologous transplantations. For this, it will be important to have a more global model of the hematopoietic system which includes the principle lineages and their respective cytokines, and this is work we are currently undertaking. The complete model of hematopoiesis is complicated by cellular cross-talk and the non-specificity of certain cytokines acting on various cell types. Accordingly, both bench science and modelling work must be relied upon to address the complex interplay of the blood system as a whole. As always, mathematical modelling must remain informed by laboratory and clinical work. However, ultimately there also needs to be recognition of the inverse relationship and an increasing acceptance that models and their predictions can instruct both experimental and clinical approaches.

Although comparative discussions on modelling philosophies may seem to be purely academic, the establishment of quantitative systems pharmacology departments at the major pharmaceutical companies indicates otherwise. It could even be argued that, outside of a handful of scholarly groups working on the advancement of the field, industry is driving the push towards increasingly mechanistic approaches in PK/PD in their efforts to discover new molecules addressing complex pathologies. Recognition of the role systems pharmacology modellers have to play, not only early in the drug development pipeline but perhaps more principally as integrative translational researchers, will positively influence the quality of research and ameliorate the predictive strengths of the resulting modelling work. Ultimately, the central interest underlying improvements in pharmaceutical modelling remains bettering patient care. As such, regardless of the philosophical motivations we make as researchers, care should be taken to ensure that the preeminent concern is invariably addressing patients' needs.

References

[1] M. Danhof, E.C.M. de Lange, O.E. Della Pasqua, B.A. Ploeger, and R.A. Voskuyl. Mechanism-based pharmacokinetic-pharmacodynamic (PK-PD) modeling in translational drug research. *Trends in Pharmacogical Sciences*, 29:186–191, 2008.

[2] D. Peixoto, D. Dingli, and J.M. Pacheco. Modelling hematopoiesis in health and diseaase. *Mathematical and Computer Modelling*, 53:1546–1557, 2011.

[3] C.W. Smith. Regulation of neutrophil homeostasis. In K. Kaushansky, M.A. Lichtman, E. Beutler, T.J. Kipps, U. Sligsohn, and J.T. Prchal, editors, *Williams Hematology*, volume 8. McGraw-Hill Companies, Inc., 2010.

[4] D.R. Sorger, S.R.B. Allerheiligen, R.B. Abernethy, K.L.R. Altman, A.C. Brouwer, A. Califano, D.Z. D'Argenio, R. Iyengar, W.J. Jusko, R. Lalonde, D.A. Lauffenburger, B. Shoichet, J.L. Stevens, P. Subramaniam, S. van der Graaf, and P. Vincini. Quantitative and Systems Pharmacology in the Post-genomic era: New Approaches to Discovering Drugs and Understanding Therapeutic Mechanisms. An NIH white paper by the QSP Workshop Group. Technical report, National Institutes of Health of the United States of America, Bethesda, Maryland, USA, 2011.

[5] P. van der Graaf and N. Benson. Systems pharmacology: Bridging systems biology and pharmacokinetics-pharmacodynamics (PKPD) in drug discovery and development. *Pharmaceutical Research*, 28:1460–1464, 2011.

Appendix I

Simulation Code for the Physiological PK/PD Neutrophil Model with Exogenous Drug Administration

```
1  NeutrophilCode2016.m
2  %This is the driver for the full system as described in the
       manuscript submitted to BMB in December 2015.
3
4  close all
5  clear all
6
7  %y(1)=Stem cells
8  %y(2)=Neutrophils
9  %y(3)=G-CSF (unbound)
10 %y(4)=ODE expression of tau_NM(t)
11 %y(5)=Central compartment of Zalypsis
12 %y(6)=ODE expression of A_Q (stem cell amplification)
13 %y(7)=ODE expression of A_N (neutrophil amplification)
14 %y(8)=Second compartment of Zalypsis (fast-exchange with
       blood)
15 %y(9)=Third compartment of Zalypsis (slow-exchange with blood
       )
16 %y(10)=Neutrophils in the reservoir
17 %y(11)=Fourth compartment of Zalypsis (another slow-exchange
       with blood)
18 %y(12)=G-CSF (G2-bound)
19
```

```
20 tic %Times the simulation time
21 datestr(now) %Displays the actual time
22
23 %Parameters for stem-cells
24
25 PA.Qstar=1.1;%Homeostasis concentration of HSCs
26 PA.gamma_s=0.1;%Apoptosis of HSCs
27 PA.tau_s=2.8; %Stem-cell maturation time
28 PA.AQstar=2*exp(-PA.gamma_s*PA.tau_s);
29 PA.fQ=8;%Maximal rate of HSC self-renewal THIS VALUE IS FROM
      SUSPECT SOURCES AND HAS NOT BEEN RATIFIED
30 PA.s2=2;%Hill coefficient for self-renewal rate of stem-cells
31 PA.BetaQstar=0.043;%HSC self-renewal rate at homeostasis
32 PA.theta2=((PA.Qstar^(PA.s2)*PA.BetaQstar)/(PA.fQ-PA.
      BetaQstar))^(1/PA.s2);%Measures differentiation rate of
      stem-cells
33
34 %Parameters related to neutrophils
35
36 %Set population sizes at homeoestasis for neutrophil stages
37
38 PA.Np=0.93;%Steady-state mitotic neutrophil concentration
39 PA.Nm=4.51;%Steady-state maturing neutrophil concentration
40 PA.Nrstar=2.26;%Steady-state marrow reservoir concentration
41 PA.Nstar=(0.22/0.585);%Circulating neutrophil count at
      homeostasis
42
43 %Calculate gamma_N
44
45 PA.gamma_N=35/16;%Circulating neutrophil apoptosis rate
46
```

```
%Find average time spent in circulation

PA.tauNC=1/PA.gamma_N;

%Calculate the homeostatic transition rate (pool to
   circulation)

PA.trans_homeo=(PA.gamma_N*PA.Nstar)/(PA.Nrstar);

%Set maturation time and time spent in reservoir

PA.aNM=3.9;%Maturation time
PA.tauNR=2.7;%Time spent in reservoir

%Calculate apoptosis rate out of the reservoir

PA.gammaNr=(1/PA.tauNR)-PA.trans_homeo;

%Solve transcendental equation for maturation apoptosis rate

fgam = @(x) PA.Nrstar*(exp(x*PA.aNM)-1)-x*PA.tauNR*PA.Nm;

%Approximate root (truncating exponential to quadratic)

gamapprox=2*((PA.tauNR*PA.Nm)/(PA.aNM*PA.Nrstar)-1)/PA.aNM;
PA.gammaNM=fzero(fgam,gamapprox);

%Calculate homeostatic differentiation rate

%PA.kappaNstar=(PA.gammabarN*PA.Npoolstar+PA.gamma_N*PA.Nstar
   )/(PA.Qstar*1E-3*PA.ANstar);
```

```
76 PA.kappaNstar=(1/3)*(PA.AQstar-1)*PA.BetaQstar;
77
78 %Calculate the differentiation rates to other cell lines
79
80 PA.kappa_delta=(-(PA.kappaNstar+PA.BetaQstar)*PA.Qstar+(PA.
      AQstar*PA.BetaQstar*PA.Qstar))/PA.Qstar;
81 PA.kappa_delta1=(2/3)*(PA.AQstar-1)*PA.BetaQstar;
82
83 %Calculate amplification rate
84
85 %PA.ANstar=exp(PA.etaNP_0*PA.tauNP-PA.gamma0_0*PA.tauNM);
86 PA.ANstar=PA.Nrstar/(PA.kappaNstar*PA.Qstar*1E-3*PA.tauNR);
87
88 %Calculate amplification in proliferative phase
89
90 PA.etaNPTAU=PA.ANstar*exp(PA.gammaNM*PA.aNM);
91
92 %Calculate proliferation rate
93
94 PA.etaNP_h=PA.kappaNstar*PA.Qstar*1E-3*((PA.etaNPTAU-1)/PA.Np
      );
95
96 %Calculate time in proliferative phase
97
98 PA.tauNP=(1/PA.etaNP_h)*log(PA.ANstar*exp(PA.gammaNM*PA.aNM))
      ;
99
100 %Check the conditions on parameters
101
102 %Bounds on time spent in pool from Equation 1.68
103
```

```
104 PA.tauNRlessthan=PA.tauNC*PA.Nrstar/PA.Nstar;
105 PA.tauNRgreaterthan=PA.aNM*PA.Nrstar/PA.Nm;
106
107 if PA.tauNR > PA.tauNRlessthan
108     disp(PA.tauNR)
109     disp(PA.tauNC)
110     disp(PA.Nrstar)
111     disp(PA.Nstar)
112     error('tauNR > tauNC*Nr/N')
113 elseif PA.tauNR < PA.tauNRgreaterthan
114     error('tauNR < aNM*Nr/Nm')
115 end
116
117 %Three conditions of Equations 1.64, 1.66, and 1.67
118
119 disp(['Bound 1: Need ',num2str(PA.tauNR/PA.tauNC),' less than
        ',num2str(PA.Nrstar/PA.Nstar)])
120 disp(['Bound 2: Need ',num2str(PA.aNM/PA.tauNR),' less than '
       ,num2str(PA.Nm/PA.Nrstar)])
121 disp(['Bound 3: Sufficient that ',num2str(PA.tauNR/PA.tauNP),
       ' less than ',num2str(PA.Nrstar/PA.Np)])
122
123 disp('Effective number of divisions in proliferative phase is
       ')
124 disp(num2str(log2(exp(PA.etaNP_h*PA.tauNP))))
125 disp('Effective number of divisions in proliferative and
       maturation phase is')
126 disp(num2str(log2(exp(PA.etaNP_h*PA.tauNP-PA.gammaNM*PA.aNM))
       ))
127 disp('These numbers should be about 18 and 15')
128
```

```
129 %Checks for steady-state in equations
130
131 disp('Stem-cell equation at homeostasis')
132 disp(num2str(-(PA.kappaNstar+PA.BetaQstar+PA.kappa_delta)*PA.
       Qstar+PA.AQstar*PA.BetaQstar*PA.Qstar))
133 disp('Circulating neutrophil equation at homeostasis')
134 disp(num2str(PA.trans_homeo*PA.Nrstar-PA.gamma_N*PA.Nstar))
135 disp('Neutrophil reservoir equation at homeostasis')
136 disp(num2str(PA.ANstar*PA.kappaNstar*1E-3*PA.Qstar-(PA.
       gammaNr+PA.trans_homeo)*PA.Nrstar))
137
138 %PK parameters for the G-CSF
139
140 PA.kren=0.16139;%Rate of renal elimination of G-CSF (linear)
141 PA.kint=462.4209;%Rate of G-CSF internalisation
142 PA.k12G=2.2423;%Rate of binding
143 PA.k21G=184.8658;%Rate of unbinding
144 PA.Gstar=0.025;%Concentration of G-CSF at homeostasis
145 PA.V=0.525;%Bound G-CSF conversion factor
146 PA.pow=1.4608;%Hill coefficient of G-CSF binding relationship
147
148 %Calculate G2 homeostasis concentration
149 PA.G2_h=(PA.k12G*PA.Gstar^PA.pow*PA.V*(PA.Nstar+PA.Nrstar))/(
       PA.kint+PA.k12G*PA.Gstar^PA.pow+PA.k21G);
150 %Calculate production rate of G1 (unbound G-CSF)
151 PA.Gprod=PA.kren*PA.Gstar+PA.k12G*PA.Gstar^PA.pow*PA.V*(PA.
       Nstar+PA.Nrstar)-PA.k12G*PA.Gstar^PA.pow*PA.G2_h-PA.k21G*PA
       .G2_h;
152
153 %Check for steady state
154
```

```
disp('Unbound G-CSF at homeostasis')
disp(num2str(PA.Gprod-PA.kren*PA.Gstar-PA.k12G*((PA.Nstar+PA.Nrstar)*PA.V-PA.G2_h)*PA.Gstar^PA.pow+PA.k21G*PA.G2_h))
disp('Bound G-CSF at homeostasis')
disp(num2str(-PA.kint*PA.G2_h+PA.k12G*((PA.Nstar+PA.Nrstar)*PA.V-PA.G2_h)*PA.Gstar^PA.pow-PA.k21G*PA.G2_h))

%Parameters for the chemotherapy (Zalypsis)

PA.Cl=43.7*24;%Rate of clearance
PA.V1=32.7;%Volume in central compartment
PA.Q2=123*24;%Amount of transit (second compartment)
PA.V2=162;%Volume of second compartment
PA.Q3=11.3*24;%Amount of transit (third compartment)
PA.V3=388;%Volume of third compartment
PA.Q4=62.3*24;%Amount of transit (fourth compartment)
PA.V4=23.9;%Volume of fourth compartment
PA.k10=PA.Cl/PA.V1;%Rate of elimination
PA.k12=PA.Q2/PA.V1;%Rate of transit from compartment 1 to 2
PA.k21=PA.Q2/PA.V2;%Rate of transit from compartment 2 to 1
PA.k13=PA.Q3/PA.V1;%Rate of transit from compartment 1 to 3
PA.k31=PA.Q3/PA.V3;%Rate of transit from compartment 3 to 1
PA.k24=PA.Q4/PA.V2;%Rate of transit from compartment 2 to 4
PA.k42=PA.Q4/PA.V4;%Rate of transit from compartment 4 to 2
PA.BSA=1.723;%Average body surface area

% Neutrophil parameters that need to be determined

%Parameters determined through fitting
PA.Ntot=4.2009;%Constant accounting for average N+Nr (for reduced G-CSF model)
```

```
183 PA.muval=0.844575731873359;%Ratio of minimal and homeostasis
    proliferation rates
184 PA.bNP=0.022867963747985;%Neutrophil proliferation Michaelis-
    Menten constant
185 PA.Vmax=7.866997674083609;%Maximal neutrophil maturation
    velocity
186 PA.trans_ratio=11.355614184371277;%Ratio of maximal and
    homeostasis reservoir release rates
187 PA.ftrans0=0.020055920452792;%Minimal reservoir release rate
188 PA.bvtilde=0.031283425611887;%Scaled maturation half-effect
    concentration
189
190 PA.bv=PA.bvtilde*PA.Vmax;%Maturation velocity half-effect
    concentration
191
192 %Set parameters
193
194 Cko=0.25;%Knockout total blood neutrophil pool fraction
195 VN0=1+(PA.Vmax-1)*(-PA.Gstar/(PA.bv-PA.Gstar));%Maturation
    velocity at knockout
196 theta=(Cko*(PA.ftrans0+PA.gammaNr)/(PA.trans_homeo+PA.gammaNr
    ))*exp(PA.aNM*(PA.gammaNM/VN0-PA.gammaNM));%Ratio of rate
    cells leave proliferation at knockout to homeostasis
197 PA.s1=1.5;%HSC-neutrophil differentiation Hill coefficient
198
199 %Parameters calculated from fit parameters
200
201 %Calculate neutrophil minimal proliferation rate
202 PA.etaNP_min=PA.muval*PA.etaNP_h;
203 %Calculate HSC-neutrophil minimal differentiation rate
```

```
204 PA.kappaN_min=theta*PA.kappaNstar*exp(PA.tauNP*PA.etaNP_h*(1-
       PA.muval));%
205 %Calculate homeostasis neutrophil receptor bound fraction
206 GBFstar=PA.G2_h/(PA.V*(PA.Nstar+PA.Nrstar));
207 %Calculate reservoir Release half-effect concentration
208 PA.bG=GBFstar*((PA.trans_ratio*PA.trans_homeo-PA.ftrans0)/(PA
       .trans_homeo-PA.ftrans0));
209 %Calculate maximal Reservoir Release rate
210 PA.trans_max=PA.trans_ratio*PA.trans_homeo;
211
212 %Chemotherapy PD parameters
213
214 PA.EC50=0.75390;%Half-maximal effect of chemotherapy on etaNP
215 PA.sc=0.89816;%Chemotherapy effect Hill coeffcient
216 PA.hQ=0.0079657;%Effect of chemotherapy on HSCs
217 PA.eta_NPneg=0;%Proliferation rate with infinite chemotherapy
        dose
218
219 %The next two if statements administer the doses of
       chemotherapy and G-CSF over a given infusion time (Delta_C
       for chemo and s for G-CSF).
220
221 %Administer chemo (0=no, 1=yes)
222 PA.AdminChemo=0;
223
224 %Administration parameters
225
226 PA.DoseChemo=4000;%Chemotherapy dose (mcg/m^2)
227 PA.TotalDose=PA.DoseChemo*PA.BSA;%Chemotherapy dose (mcg)
228 PA.DeltaC=1/24;%Duration of chemotherapy infusion (IV
       infusion)
```

```
229
230 %Administer SC-dose of G-CSF (0=no, 1=yes; if IV G-CSF
       administered automatically)
231 PA.AdminGCSF=1;
232
233 PA.Dose=375000;%G-CSF dose
234
235 %Dose-dependent SC parameters
236
237 if PA.Dose==300000
238
239     %Dose=300mcg
240
241     PA.F=0.64466;
242     PA.ka=8.0236;
243     PA.Vd=2322.9;
244
245 elseif PA.Dose==375000
246
247     %Dose=375mcg
248
249     PA.F=0.49964;
250     PA.ka=6.6133;
251     PA.Vd=4754.7;
252
253 elseif PA.Dose==750000
254
255     %Dose=750mcg
256
257     PA.F=0.75;
258     PA.ka=5.143;
```

```
259     PA.Vd=2178.0;
260
261 else
262
263     disp('No PK parameters for this SC dose')
264     return
265
266 end
267
268 %Parameters defining the IV administration of G-CSF
269
270 PA.ivt0=-25/60/24;%Time IV infusion begins (in days)
271 PA.tinf=25/60/24;%Duration of IV infusion (in days)
272
273 %Determine chemotherapy and G-CSF administration regimens
274
275 PA.Period=21;%Period of chemotherapy treatment
276 PA.DayAdminChemo=0;%Day chemotherapy is administered
277 PA.NumAdminsChemo=1;%Number of chemotherapy administrations
278
279 PA.GCSFPeriod=1;%Time between G-CSF repeated doses
280 PA.AdminsGCSF=1;%Number of G-CSF administrations post-chemo
281 days=1;%The number of days post-chemotherapy after which
       exogenous G-CSF is administered
282
283 % Define integration time interval & initial conditions
284
285 % Integration time interval (in days)
286 totaltime=[0 PA.Period*(PA.NumAdminsChemo+4)];
287
288 %Define initial conditions
```

```
289 IC=[PA.Qstar,PA.Nstar,PA.Gstar,PA.aNM,0,PA.AQstar,PA.ANstar
    ,0,0,PA.Nrstar,0,PA.G2_h];
290
291 %Solve the DDEs (choose either subcutaneous G-CSF or IV
    infusion)
292
293 %If G-CSF is given subcutaneously
294 [sol]=Main_Chemo4(totaltime,IC,PA,days);%zalypsis chemo
    regimen
295
296 %If G-CSF is given by IV
297
298 %[sol]=Main_Chemo4IV(totaltime,IC,PA,days);%zalypsis chemo
    regimen
299
300 toc %Displays simulation time
301
302 %Various plots
303
304 figure(1); g1=plot(sol.x,sol.y(1,:),'r');hold on;
305 g2=plot([0 max(totaltime)],[PA.Qstar PA.Qstar],'--');
306 xlabel('Time (days)','FontSize',10)
307 ylabel('HSC Concentration (10^9 cells/kg)','FontSize',10)
308 legend([g1 g2],'Model solution','Homeostastic Concentration')
309
310 figure(2); g1=plot(sol.x,sol.y(2,:).*0.585.*(70/5),'r');hold
    on;
311 g2=plot([0 max(totaltime)],[PA.Nstar*0.585*(70/5) PA.Nstar
    *0.585*(70/5)],'--');
312 xlabel('Time (days)','FontSize',10)
```

```
313 ylabel('Circulating neutrophils (10^9 cells/kg)','FontSize'
       ,10)
314 legend([g1 g2],'Model solution','Homeostastic Concentration')
315
316 figure(3); g1=plot(sol.x,sol.y(2,:),'r');hold on;
317 g2=plot([0 max(totaltime)],[PA.Nstar PA.Nstar],'--');
318 xlabel('Time (days)','FontSize',10)
319 ylabel('Neutrophil Concentration (10^9 cells/L)','FontSize'
       ,10)
320 legend([g1 g2],'Model solution','Homeostastic Concentration')
321
322 figure(4); g1=plot(sol.x,sol.y(3,:),'r');hold on;
323 g2=plot([0 max(totaltime)],[PA.Gstar PA.Gstar],'--');
324 xlabel('Time (days)','FontSize',10)
325 ylabel('Unbound G-CSF concentration (ng/mL)','FontSize',10)
326 legend([g1 g2],'Model solution','Homeostastic Concentration')
327
328 GBF=(sol.y(3,:).^PA.pow)./(sol.y(3,:).^PA.pow+(PA.kint+PA.
       k21G)/PA.k12G);
329 GBFstar=(PA.Gstar.^PA.pow)./(PA.Gstar.^PA.pow+(PA.kint+PA.
       k21G)/PA.k12G);
330
331 figure(5); g1=plot(sol.x,GBF,'r');hold on;
332 g2=plot([0 max(totaltime)],[GBFstar GBFstar],'--');
333 set(gca,'FontSize',10);
334 xlabel('Time (days)','FontSize',10)
335 ylabel('Bound Fraction GBF','FontSize',10)
336 legend([g1 g2],'Model solution','Homeostastic Concentration')
337
338 figure(6); g1=plot(sol.x,sol.y(10,:),'r');hold on;
339 g2=plot([0 max(totaltime)],[PA.Nrstar PA.Nrstar],'--');
```

```
340 xlabel('Time (days)','FontSize',10)
341 ylabel('Neutrophil Concentration in Marrow Reservoir (10^9
       cells/kg)','FontSize',10)
342 legend([g1 g2],'Model solution','Homeostastic Concentration')
```

```
1  function [sol] = Main_Chemo4(totaltime,IC,PA,days)
2  %This function simulates the neutrophil model (as in the BMB
       paper submitted December 2015) for periodic chemotherapy
       and/or subcutaneous G-CSF
3
4  PA.AdminDay=days;%Define day the G-CSF treatment begins post-
       chemotherapy
5
6  %Call the DDE solver and set options
7
8  %Set solver options
9  opts = ddeset('RelTol',1e-6,'AbsTol',1e-6,'MaxStep',1e-2);
10 %Call solver (which calls RHS below)
11 sol = ddesd_f5(@Chemo4,@(t,y) delayP(t,y,PA),IC,totaltime,
       opts);
12
13 function dydt = Chemo4(t,y,Z)
14
15 %Initialise history function vectors
16
17 ylag1 = Z(:,1); %Creates solution vector with lag tau_S
18 ylag2 = Z(:,2); %Creates solution vector with lag tau_N
19 ylag3 = Z(:,3); %Creates solution vector with lag tau_N+
       tau_NP
20 ylag4 = Z(:,4); %Creates solution vector with lag tau_NM
21
22 %Initialise administration parameters
```

```
23 Infusion=0;%Chemotherapy infusion parameter
24 GCSF_Dose=0;%G-CSF administration parameter
25
26 if PA.DayAdminChemo <= t && t <= PA.DayAdminChemo + (PA.
   Period*PA.NumAdminsChemo)%If time is within chemo infusion
   time
27
28     tchemomod=mod(t-PA.DayAdminChemo,PA.Period);%Calculate
          modulo start of infusion time
29
30     if PA.AdminChemo==0
31
32         Infusion=0;%Infusion=0 since no chemotherapy is
              administered (PA.AdminChemo=0)
33
34     elseif PA.AdminChemo==1 && tchemomod < PA.DeltaC
35
36         Infusion=PA.TotalDose/PA.DeltaC;%Administer
              chemotherapy and calculate dose over infusion time
37
38     end
39
40    tgcsfmod=mod(tchemomod-PA.AdminDay,PA.GCSFPeriod);%
         Calculate time since chemotherapy admin began
41    tGCSFend=PA.AdminDay+PA.GCSFPeriod*PA.AdminsGCSF;%
         Calculate time when G-CSF administrations will end
42
43     if PA.AdminDay <= tchemomod && tchemomod <= tGCSFend
44
45         if PA.AdminGCSF == 0
46
```

```
47              GCSF_Dose=0;%Administer no G-CSF (PA.AdminGCSF=0)
48
49          else
50
51              GCSF_Dose=PA.ka*PA.F*(PA.Dose/PA.Vd)*exp(-PA.ka*
                    tgcsfmod);%Calculate G-CSF dose to administer (
                    subcutaneous)
52
53          end;
54
55      end;
56
57  end;
58
59
60  %Calculate maturation velocity at current time and with delay
61  V_n=((PA.Vmax-1)*(y(3)-PA.Gstar)/(y(3)-PA.Gstar+PA.bv))+1;%
        Used to calculate V_n(t)
62  V_n_lag=((PA.Vmax-1)*(ylag4(3)-PA.Gstar)/(ylag4(3)-PA.Gstar+
        PA.bv))+1;%Used to calculate V_n(t-tau_NM(t))
63
64  %Calculate proliferation rate at current time and with delay
65  eta_NPlag2=eta_NP_chemo(PA,ylag2(3),ylag2(5));%Value of
        neutrophil proliferation rate with lag tau_N(t)
66  eta_NPlag3=eta_NP_chemo(PA,ylag3(3),ylag3(5));%Value of
        neutrophil proliferation rate with lag tau_N(t)-tau_NP
67
68  %Expression for the derivative of AN (used in RHS of solver)
69  Deriv=y(7)*((V_n/V_n_lag)*(eta_NPlag3-eta_NPlag2)-(1-(V_n/
        V_n_lag))*PA.gammaNM);
70
```

```
71 %Differential equations for chemo model
72
73 %RHS of model with Ntot (use for reduced G-CSF model)
74
75 % dydt =   [ -(Beta(y(1),PA)+kappaN(y(3),PA)+PA.kappa_delta)*
   y(1)+(2*exp(-(PA.gamma_s+PA.hS*(y(5)./PA.V1))*PA.tau_s)*
   Beta(ylag1(1),PA))*ylag1(1)%Stem-cell differential equation
76 %          f_trans(PA,y(12),PA.Ntot/2,PA.Ntot/2)*y(10)-PA.
   gamma_N*y(2)%Neutrophils differential equation
77 %          GCSF_Dose+PA.Gprod-PA.kren*y(3)-PA.k12G*y(3)^PA.
   pow*PA.V*(PA.Ntot)+PA.k12G*y(3)^PA.pow*y(12)+PA.k21G*y(12)%
   DE for unbound G-CSF (G1)
78 %          1-(V_n/V_n_lag)%DE for tau_N=tau_NM
79 %          Infusion-(PA.k10+PA.k12+PA.k13)*y(5)+PA.k21*y(8)+
   PA.k31*y(9)%Chemo 1 compartment DE
80 %          0
81 %          Deriv%DE for amplification of neutrophils
82 %          -(PA.k21+PA.k24)*y(8)+PA.k12*y(5)+PA.k42*y(11)%
   Chemo 2 compartment
83 %          -PA.k31*y(9)+PA.k13*y(5)%Chemo 3 compartment
84 %          (y(7)*1E-3*kappaN(ylag2(3),PA))*ylag2(1)*(V_n/
   V_n_lag)-y(10)*(f_trans(PA,y(12),y(2),y(10))+PA.gammaNr)%
   Pool
85 %          -PA.k42*y(11)+PA.k24*y(8);%Chemo 4 compartment
86 %          -PA.kint*y(12)+PA.k12G*(PA.Ntot*PA.V-y(12))*y(3)^
   PA.pow-PA.k21G*y(12)];%DE for bound G-CSF (G2)
87
88
89 %RHS of full model
90 dydt =   [ -(Beta(y(1),PA)+kappaN(y(3),PA)+PA.kappa_delta)*y
   (1)+(y(6)*Beta(ylag1(1),PA))*ylag1(1)%Stem-cell
```

```
   differential equation
91          f_trans(PA,y(12),y(2),y(10))*y(10)-PA.gamma_N*y(2)%
               Neutrophils differential equation
92          GCSF_Dose+PA.Gprod-PA.kren*y(3)-PA.k12G*y(3)^PA.pow*
               PA.V*(y(2)+y(10))+PA.k12G*y(3)^PA.pow*y(12)+PA.
               k21G*y(12)%DE for unbound G-CSF (G1)
93          1-(V_n/V_n_lag)%DE for tau_N=tau_NM
94          Infusion-(PA.k10+PA.k12+PA.k13)*y(5)+PA.k21*y(8)+PA.
               k31*y(9)%Chemo 1 compartment DE
95          y(6)*(PA.hQ*(ylag1(5)/PA.V1-y(5)/PA.V1))
96          Deriv%DE for amplification of neutrophils
97          -(PA.k21+PA.k24)*y(8)+PA.k12*y(5)+PA.k42*y(11)%Chemo
               2 compartment
98          -PA.k31*y(9)+PA.k13*y(5)%Chemo 3 compartment
99          (y(7)*1E-3*kappaN(ylag2(3),PA))*ylag2(1)*(V_n/
               V_n_lag)-y(10)*(f_trans(PA,y(12),y(2),y(10))+PA.
               gammaNr)%Pool
100         -PA.k42*y(11)+PA.k24*y(8);%Chemo 4 compartment
101         -PA.kint*y(12)+PA.k12G*((y(2)+y(10))*PA.V-y(12))*y
               (3)^PA.pow-PA.k21G*y(12)];%DE for bound G-CSF (G2)
102
103 end
104
105 end
```

```
1  function [sol] = Main_Chemo4IV(totaltime,IC,PA,days)
2  %This function simulates the neutrophil model (as in the BMB
      paper submitted December 2015) for an IV infusion of G-CSF
      with NO chemotherapy
3
4  PA.AdminDay=days;
5
```

```
%Call the DDE solver and set options

opts = ddeset('RelTol',1e-6,'AbsTol',1e-6,'MaxStep',1e-2);
sol = ddesd_f5(@Chemo4,@(t,y) delayP(t,y,PA),IC,totaltime,
   opts);

function dydt = Chemo4(t,y,Z)

%Initialise history function vectors

%Create lag solution vectors
ylag1 = Z(:,1); %Creates solution vector with lag tau_S
ylag2 = Z(:,2); %Creates solution vector with lag tau_N
ylag3 = Z(:,3); %Creates solution vector with lag tau_N+
   tau_NP
ylag4 = Z(:,4); %Creates solution vector with lag tau_NM

%Initialise administration parameters
Infusion=0;%Chemotherapy infusion parameter
GCSF_Dose=0;%G-CSF administration parameter

%Statements for IV infusion administration (G-CSF only)
if t<PA.ivt0 || t > PA.ivt0+PA.tinf

   GCSF_Dose=0;%Administer no G-CSF since outside of infusion
       time

else

   GCSF_Dose=PA.Dose/PA.Vd/PA.tinf;%Calculate administered
      dose
```

```
33
34 end
35
36 %Calculate maturation velocity at current time and with delay
37 V_n=((PA.Vmax-1)*(y(3)-PA.Gstar)/(y(3)-PA.Gstar+PA.bv))+1;%
   Used to calculate V_n(t)
38 V_n_lag=((PA.Vmax-1)*(ylag4(3)-PA.Gstar)/(ylag4(3)-PA.Gstar+
   PA.bv))+1;%Used to calculate V_n(t-tau_NM(t))
39
40 %Calculate proliferation rate at current time and with delay
41 eta_NPlag2=eta_NP_chemo(PA,ylag2(3),ylag2(5));%Value of
   neutrophil proliferation rate with lag tau_N(t)
42 eta_NPlag3=eta_NP_chemo(PA,ylag3(3),ylag3(5));%Value of
   neutrophil proliferation rate with lag tau_N(t)-tau_NP
43
44 %Expression for the derivative of AN (used in RHS of solver)
45 Deriv=y(7)*((V_n/V_n_lag)*(eta_NPlag3-eta_NPlag2)-(1-(V_n/
   V_n_lag))*PA.gammaNM);%Derivative of A_N
46
47 %Differential equations for ChemoX model
48
49 %RHS of full model
50 dydt =    [-(Beta(y(1),PA)+kappaN(y(3),PA)+PA.kappa_delta)*y
   (1)+(y(6)*Beta(ylag1(1),PA))*ylag1(1)%Stem-cell
   differential equation
51          f_trans(PA,y(12),y(2),y(10))*y(10)-PA.gamma_N*y(2)%
              Neutrophils differential equation
52          GCSF_Dose+PA.Gprod-PA.kren*y(3)-PA.k12G*y(3)^PA.pow*
              PA.V*(y(2)+y(10))+PA.k12G*y(3)^PA.pow*y(12)+PA.
              k21G*y(12)%DE for unbound G-CSF (G1)
53          1-(V_n/V_n_lag)%DE for tau_N=tau_NM
```

```
54          Infusion-(PA.k10+PA.k12+PA.k13)*y(5)+PA.k21*y(8)+PA.
               k31*y(9)%Chemo 1 compartment DE
55          y(6)*(PA.hQ*(ylag1(5)/PA.V1-y(5)/PA.V1))
56          Deriv%DE for amplification of neutrophils
57          -(PA.k21+PA.k24)*y(8)+PA.k12*y(5)+PA.k42*y(11)%Chemo
                2 compartment
58          -PA.k31*y(9)+PA.k13*y(5)%Chemo 3 compartment
59          (y(7)*1E-3*kappaN(ylag2(3),PA))*ylag2(1)*(V_n/
               V_n_lag)-y(10)*(f_trans(PA,y(12),y(2),y(10))+PA.
               gammaNr)%Pool
60          -PA.k42*y(11)+PA.k24*y(8);%Chemo 4 compartment
61          -PA.kint*y(12)+PA.k12G*((y(2)+y(10))*PA.V-y(12))*y
               (3)^PA.pow-PA.k21G*y(12)];%DE for bound G-CSF (G2)
62
63  end
64
65  end
```

```
1   function Beta=Beta(y,PA)
2   %This function calculates the rate of self-renewal (beta) in
       the HSC compartment
3   Beta=PA.fQ*(PA.theta2^PA.s2)/(PA.theta2^PA.s2+y^PA.s2);
```

```
1   function d = delayP(t,y,PA)
2   %This function sets up the delay vectors necessary for the
       DDE solver.
3
4   %Delays in order are: tau_S, tau_N, tau_N+tau_NP, and tau_NM
5
6   d = [t-PA.tau_s,t-tauN(PA,y(4)),t-tauN(PA,y(4))+PA.tauNP,t-y
       (4)];
7
```

```
end
```

```
function eta_NP_chemo=eta_NP_chemo(PA,y,C)
%This function calculates the effect of chemotherapy on the
   rate of proliferation eta_Np

eta_NP_chemo=PA.eta_NPneg+(eta_NP(PA,y)-PA.eta_NPneg).*(PA.
   EC50^(PA.sc)./(PA.EC50^(PA.sc)+(C./PA.V1).^(PA.sc)));
```

```
function eta_NP=eta_NP(PA,y)
%This function calculates the rate of proliferation eta_Np

eta_NP=PA.etaNP_h+PA.bNP*((PA.etaNP_h-PA.etaNP_min).*(y/PA.
   Gstar-1))./(y+PA.bNP);
```

```
function f_trans=f_trans(PA,y,N,NR)
%This function calculates nu_Nr (formerly ftrans) which is
   the rate of release out of the marrow reservoir into
   circulation.

%Model with Ntot
% fact1=y./(PA.V*PA.Ntot);
% fact2=PA.G2_h/(PA.V*PA.Ntot);
% f_trans=PA.trans_homeo.*(PA.trans_ratio.*(fact1-fact2)+PA.
   bG)./(fact1-fact2+PA.bG);

%Full model
fact1=y./(PA.V*(N+NR));
fact2=PA.G2_h/(PA.V*(PA.Nstar+PA.Nrstar));
f_trans=PA.trans_homeo.*(PA.trans_ratio.*(fact1-fact2)+PA.bG)
   ./(fact1-fact2+PA.bG);
```

```
function gamma_s_chemo=gamma_s_chemo(PA,C)
%This function calculates the effect of chemotherapy on the rate of apoptosis in the HSC compartment (gammaS is now expressed as gammaQ)

gamma_s_chemo=PA.gamma_s+PA.hQ.*(C./PA.V1);
```

```
function gamma_s=gamma_s(PA,G,C)
%This function calculates gammaQ (formerly gammaS)

gamma_s=PA.gamma_s+(gamma_s_chemo(PA,C)-PA.gamma_s);
```

```
function kappaN=kappaN(y,PA)
%This function calculates the differentiation rate kappaN out of the HSC compartment

kappaN=PA.kappaN_min+(2.*(PA.kappaNstar-PA.kappaN_min).*y.^PA.s1)./(y.^PA.s1+PA.Gstar.^PA.s1);
```

```
function tauN=tauN(PA,tauNM)
%This function calculates tauN=tauNp+tauNm

tauN=PA.tauNP+tauNM;
```